USAAML TECHNICAL REPORT 65-25

EXPLORATION OF HIGH-SPEED FLIGHT WITH THE XH-51A RIGID ROTOR HELICOPTER

L. R. 18374

By

William K. Foulke

June 1965

U. S. ARMY AVIATION MATERIEL LABORATORIES
FORT EUSTIS, VIRGINIA

CONTRACT DA 44-177-AMC-150(T)
LOCKHEED-CALIFORNIA COMPANY
BURBANK, CALIFORNIA

BLANK PAGES
IN THIS
DOCUMENT
WERE NOT
FILMED

DDC Availability Notice

Qualified requesters may obtain copies of this report from DDC.

This report has been furnished to the Department of Commerce for sale to the public.

Disclaimer

The findings in this report are not to be construed as an official Department of the Army position, unless so designated by other authorized documents.

When Government drawings, specifications, or other data are used for any purpose other than in connection with a definitely related Government procurement operation, the United States Government thereby incurs no responsibility nor any obligation whatsoever; and the fact that the Government may have formulated, furnished, or in any way supplied the said drawings, specifications, or other data is not to be regarded by implication or otherwise as in any manner licensing the holder or any other person or corporation, or conveying any rights or permission, to manufacture, use, or sell any patented invention that may in any way be related thereto.

Disposition Instructions

Destroy this report when it is no longer needed. Do not return it to the originator.

HEADQUARTERS
U S ARMY TRANSPORTATION RESEARCH COMMAND
FORT EUSTIS, VIRGINIA 23604

This report has been reviewed by the U. S. Army Transportation Research Command and is considered to be technically sound. The work was performed under Contract DA 44-177-AMC-150(T) as part of the Exploratory Development Program. This program was undertaken in order to investigate the high-speed potential of rotary-wing aircraft.

The Army is currently sponsoring other high-speed rotary-wing flight research programs similar to this in order to provide the basic technology required for future designs of high-performance rotary-wing aircraft.

NOTE

On 1 March 1965, *after this report had been prepared,* the name of this command was changed from U.S. Army Transportation Research Command to:

U.S. ARMY AVIATION MATERIEL LABORATORIES

Task 1P121401A14311
Contract DA 44-177-AMC-150(T)
USAAML Technical Report 65-25
June 1965

EXPLORATION OF HIGH-SPEED FLIGHT WITH THE XH-51A RIGID ROTOR HELICOPTER

L. R. 18374

By
William K. Foulke

Prepared by
Lockheed-California Company
Burbank, California

for
U. S. ARMY AVIATION MATERIEL LABORATORIES
FORT EUSTIS, VIRGINIA

ABSTRACT

A systematic research program to investigate the capability of the Lockheed-developed "rigid" rotor system in the XH-51A helicopters is discussed in this report.

The primary objective of the research program was to attain level flight performance at a true airspeed of 200 knots; 210 knots true airspeed was actually attained with the Compound XH-51A.

Analytical studies, design, fabrication and modification, laboratory tests, wind tunnel and ground tests, and research flight tests of two rotor configurations and a "compound" version of the helicopter were performed. This work is described and the data obtained with their analyses are presented in this report.

PREFACE

This report describes a program of research in high speed flight with the XH-51A Rigid Rotor helicopter. The research program was conducted by the Lockheed-California Company under contract to the U. S. Army Transportation Research Command (USATRECOM), Fort Eustis, Virginia.

The research program was started in April 1964 and was completed in November 1964. Technical monitoring of the program for USATRECOM was by Major L. R. Riesterer, Messrs. LeRoy Ludi, Robert Berrisford, John Crigler, and Andrew Connor. The Lockheed program was under the technical direction of Mr. A. W. Turner, Flight Test Division Engineer. Additional Lockheed personnel associated with the program included Messrs. R. A. Berry, C. J. Buzzetti, R. H. Cotton, W. K. Foulke, R. J. Goudey, L. F. Hauck, D. P. Hegg, J. F. Johnston, D. W. Lodge, F. D. Pfeiffer, D. R. Segner, J. E. Rhodes, R. F. Stanton, D. R. Wyrick, and others.

Appreciation is due to USATRECOM for help in obtaining various items of hardware, such as jet engines, and for providing assistance and advice in planning and executing the entire research program.

CONTENTS

ILLUSTRATIONS

ILLUSTRATIONS (Cont'd.)

ILLUSTRATIONS (Cont'd.)

ILLUSTRATIONS (Cont'd.)

ILLUSTRATIONS (Cont'd.)

ILLUSTRATIONS (Cont'd.)

ILLUSTRATIONS (Cont'd.)

TABLES

SYMBOLS

BUNO	Bureau of Naval Weapons Number (Abbr.)
B.L.	buttline, left or right of aircraft longitudinal centerline
b	wingspan
°C	temperature, degrees centigrade
C_D	total drag coefficient $C_D = \frac{\text{Drag}}{q\ S_w}$
C_L	lift coefficient $C_L = \frac{\text{Lift}}{q\ S_w}$
$C_{L_{max}}$	maximum attainable lift coefficient
C_{l_R}	rolling moment coefficient about the rotor mast $C_{l_R} = \frac{l_R}{q\ S_w\ b}$
C_{m_R}	pitching moment coefficient $C_{m_R} = \frac{M_R}{q\ S_w\ \bar{c}}$
C_{m_α}	longitudinal stability derivative, $\frac{dC_m}{d\alpha}$
C_Δ	jet thrust coefficient $C_\Delta = \frac{\text{jet thrust}}{q\ S_w}$
$\bar{c}$	length of the mean aerodynamic chord
c.g., C.G.	center of gravity referenced to rotor mast centerline
cps	cycles per second
Deg., ( )°	angular degrees
EAS	equivalent airspeed

FAA	Federal Aviation Agency (abbr.)
FRL	fuselage reference line, an arbitrary longitudinal line parallel to fore and aft centerline and waterline
F.S.	fuselage station, plus inches aft of datum
F_6	flapwise bending moment at rotor station 6
F_{6_p}	helicopter pitching component of F_6
F_{6_R}	helicopter rolling component of F_6
g	acceleration of gravity; also flight load factor, multiples of g
HP	horsepower
IAS	indicated airspeed
i	incidence angle
i_G	gyro arm incidence angle relative to gyro plane, + leading edge up
i_t	tailplane incidence angle relative to FRL, + leading edge up
i_w	wing incidence angle relative to FRL, + leading edge up
K	constant term, defined where used
Kn, Kts	knots, nautical miles per hour
l_R	rolling moment about rotor mast
M	Mach number
M	moment, foot-pounds or inch-pounds
M_{hub}	moment produced by a blade acting on the hub
M_R	pitching moment about rotor mast
M_{shaft}	moment produced by entire rotor acting on the rotor mast
MAC	mean aerodynamic chord

mph	statute miles per hour
N. Dn	nose down
N. Up	nose up
n	flight load factor, multiples of g where noted, adjusted to a standard gross weight by the ratio $n = n(\text{test}) \frac{\text{gross weight (test)}}{\text{gross weight (standard)}}$
P	notation for per revolution when relating frequencies to rotor rotating frequency; e.g., 1P, one per revolution 3P, three per revolution
psi	pounds per square inch
psf	pounds per square foot
q	dynamic pressure $q = \frac{\rho V_T^2}{2}$
R	rotor radius
RPM, rpm	revolutions per minute
S	surface area
S_{HT}	horizontal tail area
S_W	wing area
SHP	shaft horsepower
TAS	true airspeed
V_c	calibrated airspeed
V_D	dive speed
V_{ip}	equivalent airspeed
V_H	maximum speed in level flight

V_{in}	indicated airspeed
V_L	design limit speed
V_{max}	maximum speed
V_T	true airspeed
W	weight
W_{AVG}	average weight
WL	waterline, + above datum - below datum
α	angle of attack
σ	air density ratio $\sigma = \frac{\rho}{\rho_0}$
σ	rotor solidity, ratio of blade area to disc area
ρ	test condition air density
ρ_0	sea level standard day air density
θ_0	collective blade angle at blade station zero, hub centerline + leading edge up

SUMMARY

The program outlined in this report included research objectives to expand the maneuvering envelope of the three-blade rotor system, to explore large offsets in center of gravity, to establish base line data with the newly designed four-blade rotor, and to investigate the characteristics of the compound mode of flight. These objectives were attained, and at the same time, the store of rotary-wing technology was enriched.

As an indication of the flight regimes explored during this research program, the maneuvering envelopes which were demonstrated with each of the three vehicle configurations tested are shown in Figure 1, below.

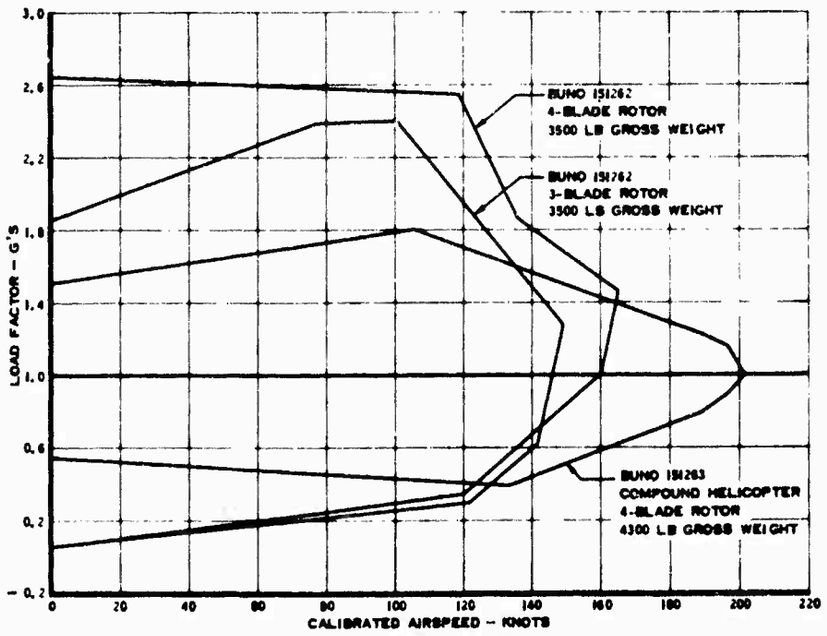

Figure 1. Speed and Load Factor Diagram.

CONCLUSIONS

A. LABORATORY, WIND TUNNEL, AND GROUND TESTS

1. Laboratory fatigue tests of the helicopter primary dynamic components extended the safe fatigue life of these components to 150 hours. Two components failed in fatigue during the test. The titanium tail rotor blade cuff was redesigned in steel as a result of its failure, and new parts to this design were installed for the remainder of the flight tests. One strap of the main rotor blade tension-torsion pack failed, but the unit continued through its test spectrum without additional failure.

2. Wind tunnel tests defined and verified a compound helicopter configuration which was suitable for the research flight tests.

3. Ground whirl, shake, structural proof, and operational tests verified the structural adequacy, dynamic stability and functional capability of the flight articles prior to the start of the research flight tests.

B. THREE-BLADE-ROTOR FLIGHT TESTS

1. Large offsets in the center-of-gravity location, up to 17,000 inch-pounds, can be accommodated with adequate structural margins. There were no undesirable effects on control power or control response at these large offsets.

2. The mid-center-of-gravity maneuvering envelope was expanded to its practical limits: extreme attitude at low speed, engine rpm droop as a function of rapid collective pitch change in hover, and vibration and power limits at high speed.

3. Maneuvering stability, although having adequate gradients at low and moderate speeds, becomes less pronounced at high speed and load factor with indications of a trend toward neutral or negative maneuvering stability at still higher speeds or load factors.

C. FOUR-BLADE-ROTOR FLIGHT TESTS

1. Control power and response of the XH-51A helicopter with the four-blade rotor was essentially the same as with the three-blade rotor.

2. Maneuvering stability remained positive with adequate gradients, relatively unaffected by high speed or load factor.

3. Rotor system structural loads were reduced to levels lower than those existing with the three-blade rotor system.

4. Cabin vibration levels were excessive with the four-blade rotor system in high-speed forward flight. The vibration was reduced during the program but it still remained above acceptable limits at the conclusion of the program. Temporary modifications to the rotor blades showed how the vibration levels could be further reduced but this would require changes beyond the scope of the research program.

5. Hover performance was less than with the three-blade system, because of the additional profile drag of the fourth blade. Comparative performance in forward flight was not obtained because of the nonstandard blade configuration.

6. The selection of the four-blade rotor for the compound helicopter was verified by the results of the flight program.

D. COMPOUND HELICOPTER FLIGHT TESTS

1. The speed objective of 200 knots was exceeded with adequate structural, performance, and control margins.

2. Vibration levels, although excessive in the pure helicopter mode and with low auxiliary thrust level, are reduced to very low levels in compound flight.

3. Structural loads were very satisfactorily low. There was no indication of sharply increasing structural loads with high speeds, even though the main rotor blades were penetrating the critical Mach number range.

4. Positive static longitudinal and maneuvering stability was demonstrated throughout the flight envelope of the helicopter.

5. Techniques were developed for entry to autorotation at flight speeds far in excess of normal rotary wing capability. Qualitative evaluation of the effect of either rotor drive power loss or auxiliary thrust loss was conducted.

6. Performance tests and data obtained in three modes of operation (i.e., pure helicopter, helicopter with low

auxiliary thrust, and compound) indicate that with little or no jet thrust, the performance is limited; but in the compound mode, adequate performance will be available for further expansion of the flight envelope.

7. Rotor lift loading was reduced to less than 5% of the helicopter gross weight in level flight.

RECOMMENDATIONS

Based on the results of the work performed under the contract, several important areas are worthy of continued study and additional flight research.

1. Higher forward flight speeds can and should be explored. The next logical increment in speed should be to 230 knots. This speed can be attained with a minimum of modification to the XH-51A compound helicopter and adequate performance is available.

2. The maneuvering capability of the compound helicopter should be explored. Load factor sharing between the rotor and the wing offers interesting possibilities. Flight operating techniques require study and development in order to exploit this configuration and to disclose its possibilities and capabilities in tactical situations.

3. Autorotation, entry to autorotation, and sustained level flight autorotation should be further explored to define the vehicle characteristics in this flight mode and to develop optimum procedures and piloting techniques.

4. The capabilities of the compound helicopter as a weapon platform should be explored. This would include simulated and actual operation with various weapon systems which are now in general use and also with systems now proposed or in development.

INTRODUCTION

As early as 1958, the dynamics and characteristics of rigid rotor systems were being investigated by the Lockheed-California Company through analytical studies, wind tunnel tests, and free flight and radio controlled flying scale models. This work resulted in the design and construction of a full scale research vehicle, the CL-475, in which various configurations of the rigid rotor system were tested in flight.

Following the Lockheed-sponsored flight development work with the CL-475, two XH-51A research helicopters were designed, constructed, and flown under a contract funded jointly by the U. S. Army and U. S. Navy. This research culminated in a Military Research Evaluation at the U. S. Naval Air Test Center, Patuxent River, Maryland in late 1963. This evaluation was conducted by pilots and engineers of the Army and Navy and was supported by the Lockheed-California Company.

Following the completion of the Military Research Evaluation, the U. S. Army Transportation Research Command, Fort Eustis, Virginia, and the Lockheed-California Company entered into a contract (reference 1) for further research and exploration of high speed flight with the XH-51A rigid rotor helicopters. Four phases of work were outlined in the contract.

PHASE I - SPARES AND SUPPORTING DATA

Certain dynamic components with unexpired life were interchanged between the two helicopters to make available a limited amount of flight time on one helicopter.

A complete inspection was conducted on the second helicopter and all dynamic components requiring replacement due to condition or expired life time were replaced.

Data resulting from separately funded laboratory fatigue tests to extend the safe fatigue life of the primary dynamic components to 150 hours were submitted.

PHASE II - THREE-BLADE-ROTOR FLIGHT TESTS

Flight tests to expand the maneuvering envelope and to explore the effect of large center-of-gravity offsets were conducted with the three-blade-rotor helicopter, utilizing the flight time made available under Phase I.

PHASE III - FOUR-BLADE-ROTOR BASE LINE

Following the Phase II work, a four-blade rotor system designed and fabricated under Lockheed funding was installed on the XH-51A helicopter. Ground and flight tests were conducted to establish base line data on the four-blade system for comparison with the three-blade system and to verify the selection of the four-blade configuration for the compound vehicle.

PHASE IV - COMPOUND HELICOPTER

The analysis and design, fabrication, and incorporation of modifications to the second XH-51A helicopter resulting in the compound configuration were part of this phase of work. Wind tunnel tests, ground tests and flight tests were conducted in a program to explore high speed flight and to investigate the interaction between rotor, wing, and auxiliary jet thrust and the resulting effects on general flying qualities, performance, vibration, and structural loads.

Figure 2, 3, and 4 are photographs showing the three basic helicopter configurations which were flown during the research program.

This report presents the results of the work performed by the Lockheed-California Company under contract DA 44-177-AMC-150(T). The work is discussed in several broad categories: analytical studies and design work; detailed descriptions of the test articles, laboratory, wind tunnel and ground tests; and the research flight tests.

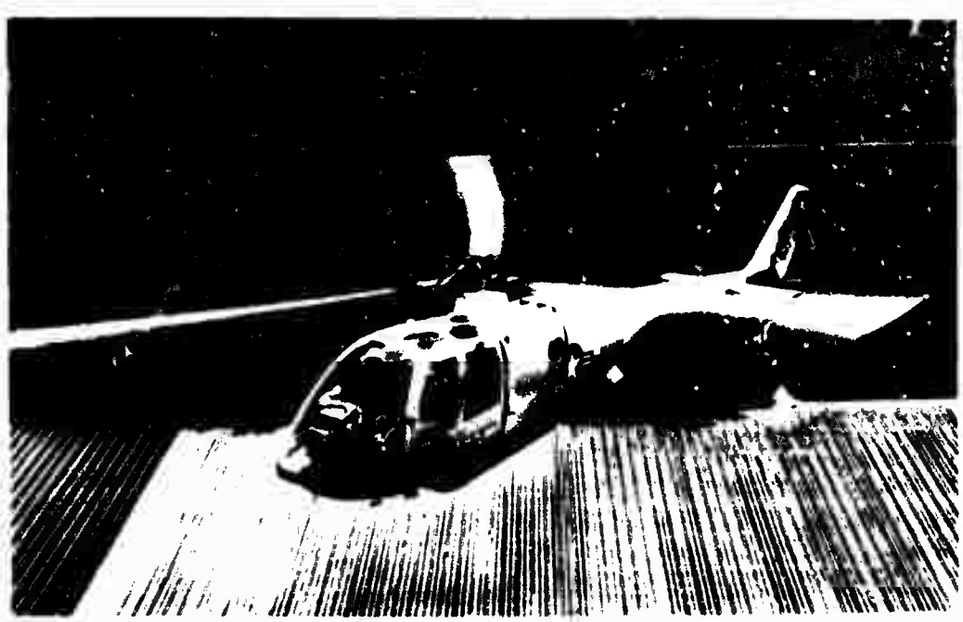

Figure 2. XH-51A Helicopter, BUNO 151262, Three-Blade Rotor.

Figure 3. XH-51A Helicopter BUNO 151262, Four-Blade Rotor.

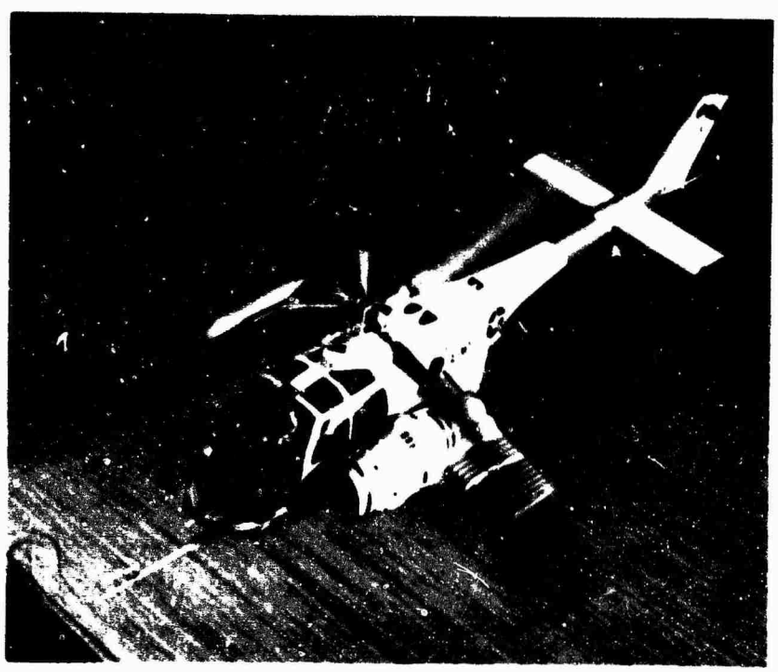

Figure 4. XH-51A BUNO 151263, Compound Helicopter

ANALYTICAL STUDIES AND DESIGN

Previously conducted analytical studies under a joint Army/Navy research program established the three-blade rotor as optimum for the pure helicopter mode. To expand the performance to a speed objective of 200 knots under the current program, extensive analytical research was directed toward a four-blade rotor configuration as a possible means of reducing blade loads anticipated at the higher speeds. Also under analytical consideration during this phase of the program was the addition of stub wings to provide lift and permit unloading of the main rotor in forward flight, and the addition of a jet engine to provide auxiliary propulsion.

A. COMPARISON OF THE THREE- AND FOUR-BLADE ROTOR CONFIGURATIONS

Design Characteristics

The basic empty weight of the vehicle is increased 139 pounds due to the extra blade. The other prime difference involves overall rotor stiffness and control power. The individual blade stiffness is essentially the same as that used on the three-blade rotor. The overall rotor stiffness, as seen by the rotor drive shaft, is proportional to the individual blade stiffness times the number of blades over 2. Therefore, for the same blade stiffness or same cyclic angle, the moment seen by the shaft or body is 4 over 3 times that for the three-blade rotor. The extra blade weight increases the body inertia. The overall effect is an increase in frequency and an increase in shaft moment per degree of transient cyclic pitch change.

Basic Loads for Level Flight

By use of appropriate factors, a reasonable first approximation of the chordwise and flapwise loads at speeds above transition from hover (i.e., above approximately 40 knots) can be obtained. These loads can be obtained for the four-blade rotor using three-blade rotor test data and for the ratios between blade thrust and blade angles of the three- and four-blade systems. Figure 5 shows a comparison of 1g level flight loads on the three-blade rotor and calculated loads on the four-blade rotor using the above approach.

Structural Description

The four-blade main rotor hub detail, as shown in Figure 6, is similar in constructional detail to the three-blade configuration. A four-armed hub is substituted for the three-armed hub, and an additional blade is added, the blade being the same as that used on the three-blade installation.

The basic geometry of the three- and four-arm hubs is essentially the same except as follows:

1. Increase in hub pre-cone from 2.8 degrees to 3.2 degrees.
2. Removal of holes in the maximum stress area to reduce the stress level and stress concentration.

Blade natural frequencies on the three-blade and four-blade rotors are essentially the same.

Basic Loads - Transients

The rotor shaft moment for a given transient condition, i.e., stick pulse, will increase due to the increase in rotor stiffness. The loads on the hub and blade will not increase, however, because the ratio of increased stiffness is the same ratio by which the shaft moment is divided to obtain the hub moment as shown below.

Transient maximum shaft moment

$$\frac{\text{4-blade rotor stiffness}}{\text{3-blade rotor stiffness}} = 1.33$$

$$M_{hub} \quad \text{3-blade} = \frac{M_{shaft}}{1.5}$$

$$M_{hub} \quad \text{4-blade} = \frac{M_{shaft}}{2.0}$$

The following additional modifications were incorporated in the helicopter to convert from the three- to the four-blade rotor.

1. A new control gyro with four arms was installed and connected to the existing control push rods in the center of the mast. The new gyro has the same polar inertia as the three-blade rotor gyro (7.5 slug ft^2).

2. The transmission vertical motion was locked out by installation of solid links in place of the 9,000-pounds-per-inch springs utilized in the three-blade system. The transmission pitch rate of 14,400 pounds per inch for the three-blade system is retained with the four-blade system.

3. The cabin suspension system, which was set at 1,200 pounds per inch for the three-blade system, was removed, and the cabin is now rigidly attached to the fuselage centerbody.

B. COMPOUND HELICOPTER PRELIMINARY STUDY

Jet Engine Selection

A trade-off study was made of existing jet engines pertinent to the subject installation. The evaluation included the J-69-T-25 with a sea level military thrust of 895 pounds at 200 knots, the J-85-5 with a

sea level military thrust of 1820 pounds at 200 knots, and the J-60-P-2 with a military thrust of 2490 pounds at 200 knots. The required jet thrust was calculated to be 1200 pounds at 200 knots and 2200 pounds at 250 knots.

The selection of the J-60 was made on the following basis.

1. It was better matched to a speed goal of 250 knots than the other jet engines.

2. A single engine would allow one side of the fuselage to be uncluttered for an emergency exit.

3. A nacelle complete with structural attachments was available from a T-39A and could be used with a minimum of modification.

4. J-60 engines were available through Army sources.

5. A single J-60 is lighter than either two J-85's or three J-69's.

Jet Engine Location

The J-60 is located on the left side, in a forward position opposite the pilot in order to allow the pilot free egress in any emergency, to keep the lateral and longitudinal center-of-gravity locations within allowable limits, and to balance the yawing moment caused by the cambered tail rotor pylon at high speeds. The vertical location of the jet engine was selected such that the jet thrust vector provides minimum pitching moment about the vehicle's center of gravity while, at the same time, providing reasonable isolation of the horizontal tail and tail rotor from the jet exhaust.

This position is approximately 20 inches higher than that shown in the proposal and incorporates a bent-down tailpipe to satisfy the thrust vector and exhaust clearance restrictions.

Wing Selection and Location

During the preliminary design phase leading to the configuration shown in the proposal, it was assumed that it was permissible to require the rotor to support approximately one-third of the gross weight at 250 knots. Later studies, substantiated by flight test results, indicated the advisability of requiring the rotor to carry a portion of the load, although less than that originally assumed. This change resulted in a wing area of 70 square feet being selected instead of the 44 square feet shown in the proposal. In the interest of obtaining a lightweight

wing structure and of minimizing the wing download in hover, an aspect ratio of 4.05 and a taper ratio of 0.5 were selected.

Since the jet engine is located about half way up on the fuselage instead of near the bottom, as shown in the proposal drawing, the original high position of the wing placed it too close to the engine nacelle for a low drag configuration. For this reason, a low wing position was selected with the wing spar passing under the engine, and with the wing root incorporated in the nacelle.

Tail Rotor Loads

In the original XH-51A configuration, a cambered tail rotor pylon was included to help provide the required antitorque yawing moment in forward flight and thus to relieve the loads on the tail rotor. This cambered tail rotor pylon is retained on the XH-51 compound configuration and the fin area is increased by 6-inch chord extension aft. At high speeds, the torque of the main rotor is low, because this rotor is unloaded, so that the major unbalanced yawing moment will be due to the jet thrust multiplied by its lateral offset. At 250 knots, the yawing moment due to the offset jet engine is almost exactly balanced by the cambered tail rotor pylon. For this condition, the tail rotor thrust requirement is only 68 pounds; the major load is on the tail rotor pylon.

C. STRUCTURAL DESIGN CRITERIA, COMPOUND HELICOPTER

The Military Specification MIL-S-8698 (ASG), "Structural Design Requirements, Helicopter" dated July 1, 1954, and Civil Aeronautics Manual 6, "Rotorcraft Airworthiness; Normal Category" dated October 1, 1959, are used as guides for the selection of the design criteria for the compound version of the Model XH-51A helicopter.

The structural design criteria and loads established herein are for the purpose of design only and are not intended as requirements to be demonstrated by the vehicles.

Loads are presented only for the new or modified components of the compound helicopter and for components previously designed but which have higher loads as a consequence of the increase in maximum forward speed. All other loads and criteria are as contained in reference 2. Unless otherwise specified, the criteria and loads presented are on a limit basis.

Design Strength Criteria

Design Weights

The weight data used for structural analysis are based on the preliminary estimates of the basic design gross weight.

	Weight	Horiz. Arm - F.S.	Vertical Arm - W.L.	Lateral Arm - B.L.
Weight Empty	3,605	108.58	56.92	4.49
Unusable Fuel and Oil	16			
Engine Oil	24			
Special Equipment	46			
Pilot	200			
Flight Test Equipment	169			
Zero Fuel Weight	4,060	104.42	55.45	.10
Fuel	440			
Basic Design Gross Weight	4,500	104.78	52.92	.19

The variation of the vehicle center-of-gravity, as gross weight varies from weight empty to maximum design gross weight, is shown in Figure 7. The variation is expressed as a resultant moment about the rotor shaft centerline, due to lateral and fore and aft travel of the center-of-gravity. The maximum permissible resultant moment is 20,000 inch-pounds.

Design Flight Speeds

The design forward flight speeds are defined as:

Helicopter Mode

V_L = 130 knots in level flight at sea level

Compound Mode

V_L = 250 knots in level flight at sea level.

Design Rotor Speeds

The design rotor speeds are the same as those outlined in reference 3 for the original vehicle. In the helicopter mode of flight, the normal rotor speed is 355 rpm and in the compound mode of flight, 327 rpm.

Design Load Factors

Figure 8 presents an envelope of design limit load factors versus rotor speed. Included is a plot of the estimated load factor variation with rotor speed based on a maximum mean rotor lift coefficient, $C_{L_{max}}$, of 1.0.

Figure 9 shows the design limit airload factor envelopes for rotor and wing. In order not to penalize aft body fuselage structure, which was previously designed to a maximum limit load factor of 3.0 for Model XH-51A, the rotorcraft center-of-gravity acceleration is restricted to not more than 3.0 in all combinations of rotor lift and wing lift in the compound mode, while the wing is designed to a maximum of 2.0g. Figure 9 shows variation of rotor lift and wing air load lift wi . forward flight speed. The maximum positive maneuver load factors are:

	Forward Speed	Load Factor
Main Rotor	0 to 109 kn.	3.0
	109 to 250 kn.	3.0 to 0.6 (linear)
Wing	109 to 168 kn.	1.0 to 2.0 (linear)
	168 to 250 kn.	2.0

The negative maneuver load factors are:

	Forward Speed	Load Factor
Main Rotor	0 to 250 kn.	-.5 to -.6 (linear)
Wing	78 to 250 kn.	-.5

The gust load factors are based on a 30-foot-per second gust and an arbitrary gust alleviation factor of 1.0. The gust level load factors include the level flight trim loading schedule between the wing and rotor.

Landing Conditions

Landing loads are based on the basic design gross weight in combination with the landing parameters shown below:

	Rotor Lift	Limit Sink Velocity	Reserve Energy Requirement - Sink Velocity	Ground Coefficient of Friction
Vertical	2W/3	4.57 ft/sec	5.60 ft/sec	.25 acting fwd
Vertical with Fwd. Speed.	2W/3	4.04 ft/sec	4.96 ft/sec	.50 acting aft

The limit sink velocities are based on the stiffness characteristics and ground loads for the original landing gear configuration of the XH-51A.

The load factor associated with the limit sink velocity is designated as the limit ground load factor. The load factor associated with the reserve energy requirement sink velocity is considered for ultimate design of the spring member. The landing gear (except for the spring member), the gear carry-through structure, and all structure affected by gear loads have been designed for ultimate loads resulting from 1.5 times the limit ground load factor.

The design ground load factors are determined from Figure 10.

D. STRUCTURAL DESCRIPTION, COMPOUND HELICOPTER

Detailed structural analysis for new or modified components pertinent to the compound helicopter are contained in the report of reference 4. The following is a structural description of the subject components.

Wing

The wing, shown in the sketch of Figure 11, is of semimonocoque design with a single beam designed to take the full shear and bending moment. The beam is sloped 26° to facilitate attachment to the existing aft canted bulkhead in the fuselage. The wing skin is beaded in the chordwise direction with 3/8 inch-high beads at 3.5 inches spacing and attached to the beam and additional spanwise stringers.

The spanwise stringers are supported by ribs at a maximum of 20-inch spacing. The beam web is designed to be nonbuckling at ultimate load to eliminate secondary beam cap bending. At the wing root, the beam is lapped onto the aft canted fuselage bulkhead, and the wing torsion

is transferred to the fuselage side by a continuous skate angle. Because the main beam is sloped 26°, a balancing chordwise bending moment is developed. This moment is taken by the upper and lower aft stringers onto a fuselage reinforcing ring segment.

At the nacelle, the wing beam curves down through the nacelle and is attached to the aft canted bulkhead, providing continuity through the fuselage to the right wing. The wing skin is attached to the nacelle side with a continuous skate angle which transfers the wing torsion into the nacelle. The nose-up torsion from the wing, combined with the nacelle nose-down inertia torsion, is taken by the forward nacelle attachment and the wing beam, resulting in a relief load on the wing beam. This relief load is conservatively neglected.

Nacelle and Engine Installation

The nacelle and engine installation is shown in Figure 12. The thrust engine (J-60-P-2), with the basic structural portion of the T-39A nacelle and pylon, is mounted to the fuselage with two primary supports and the pylon surface structure. The forward primary support consists of a fitting, located near the nacelle-engine center-of-gravity attached to the fuselage engine support structure. The aft primary support consists of attachments to the wing beam located at the aft end of the nacelle. The engine-nacelle fore and aft loads are carried by the pylon.

Since the T-39A nacelle was fully analyzed, only a comparison of maximum engine trunnion loads for several conditions is made to verify the structural integrity of the jet engine pod assembly in this application.

Vertical Tail

The vertical tail shown in Figure 13 is the basic XH-51A tail with a 6.0 inch trim tab added. The load is increased due to the higher speeds and the addition of the trim tab.

Horizontal Stabilizer

The initial stabilizer selected for the compound helicopter was the same as the basic configuration for the XH-51A except that the span was increased from 65 to 84 inches. The final configuration, established on the basis of flight test stability results, is approximately three times larger in area. Pertinent details of each configuration are contained in Section C.

Four-Blade Rigid Rotor

The four-blade-rotor system is similar in constructional detail to the three-blade system. A four-armed hub is substituted for the three-armed hub and an additional blade is added. The blades are the same as those used for the three-blade system. The hub is shown in the sketch on Figure 6. Each arm is the same as for the three-blade hub except for the built-in cone angle, changed from 2.8° to 3.2°, and an improved detail design removing holes in the maximum stress area to reduce stress level and stress concentration.

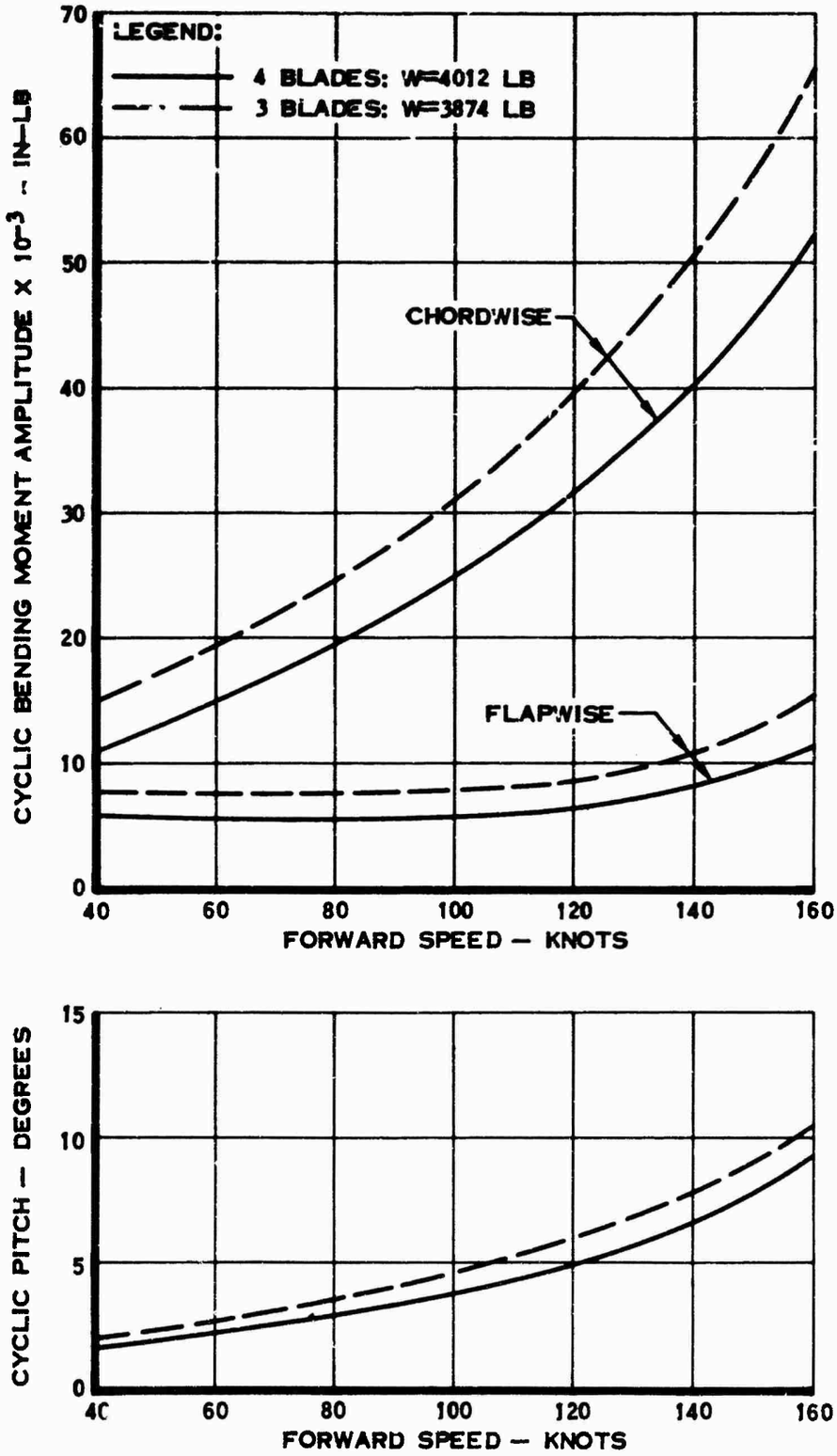

Figure 5. Comparison of Loads for a Three- and Four-Blade XH-51A, Hub Station 6.0.

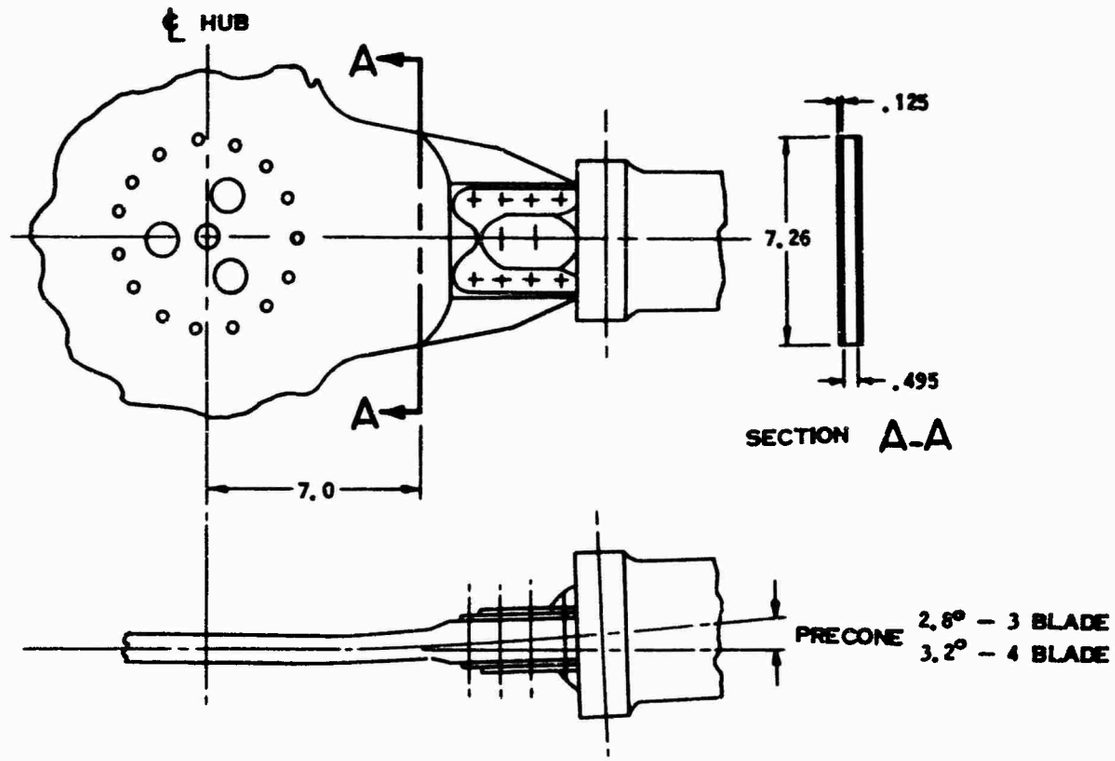

Figure 6. Main Rotor Hub Detail

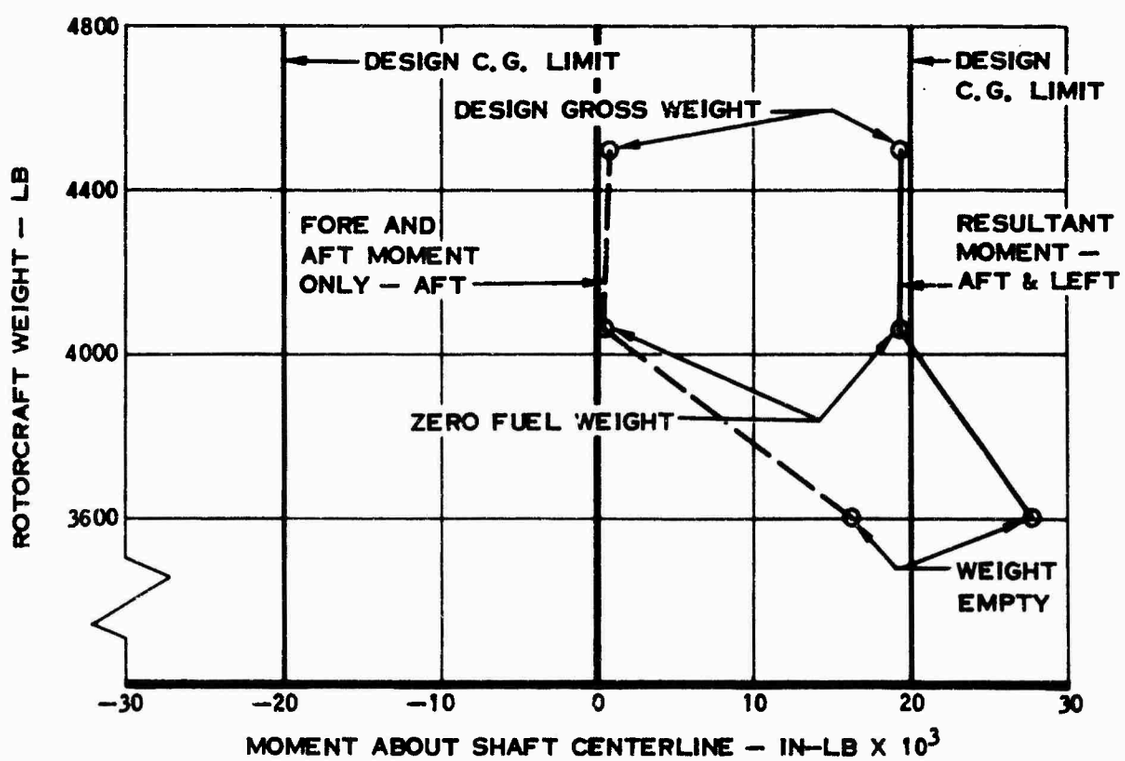

Figure 7. Center-of-Gravity Envelope

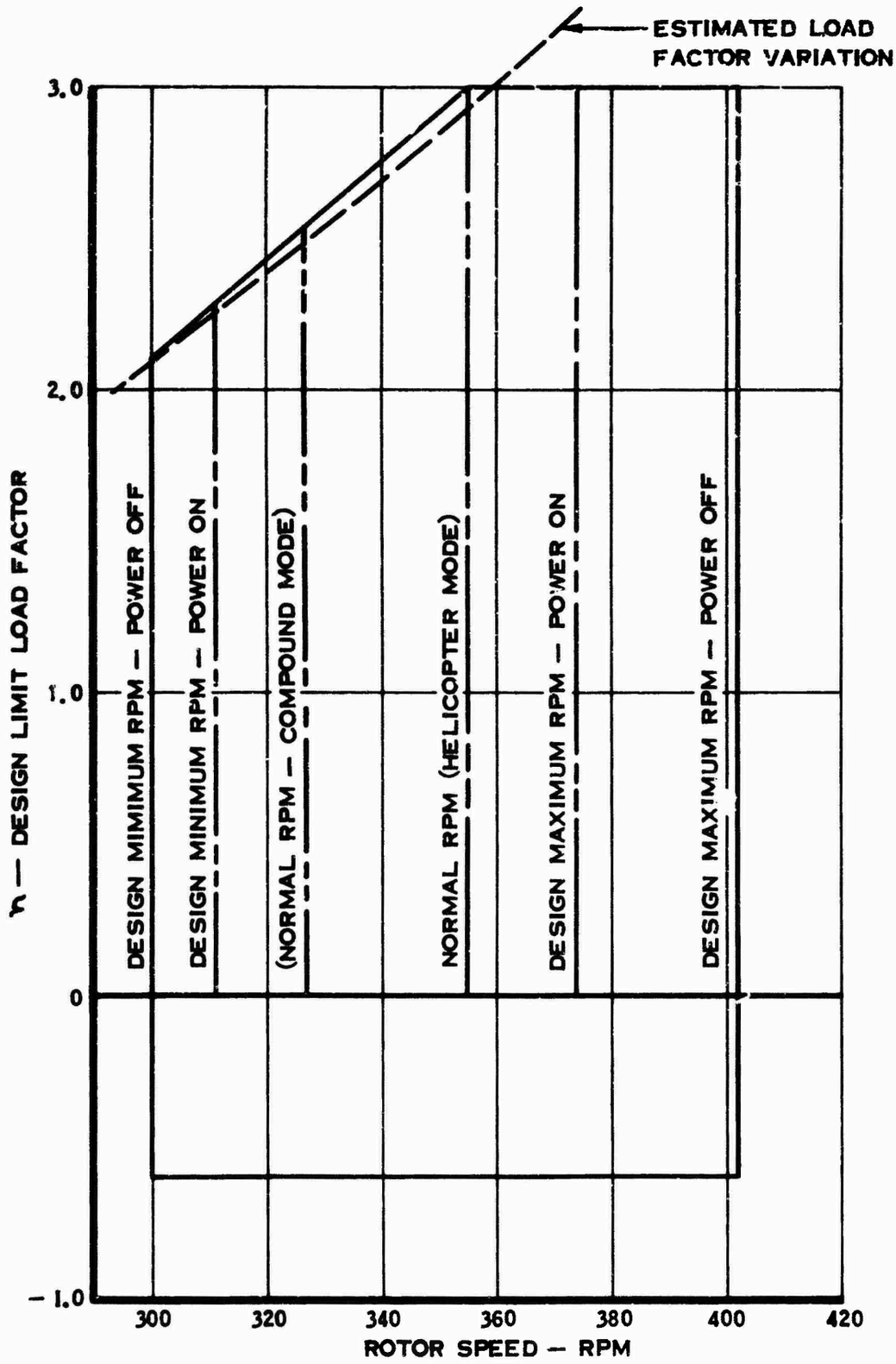

Figure 8. Design Limit Load Factor Versus RPM.

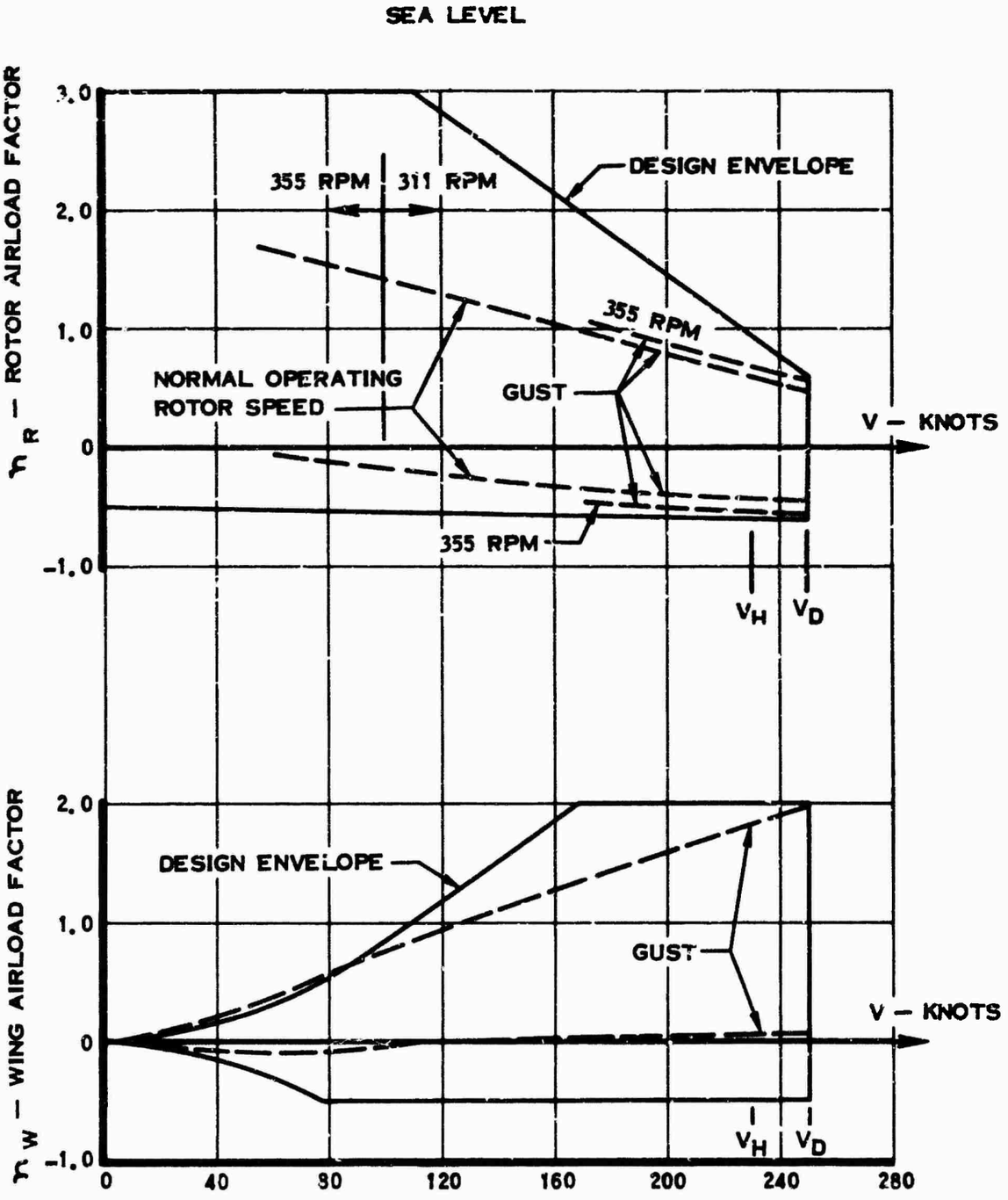

Figure 9. Design Limit Load Factor Envelopes Versus Flight Speed.

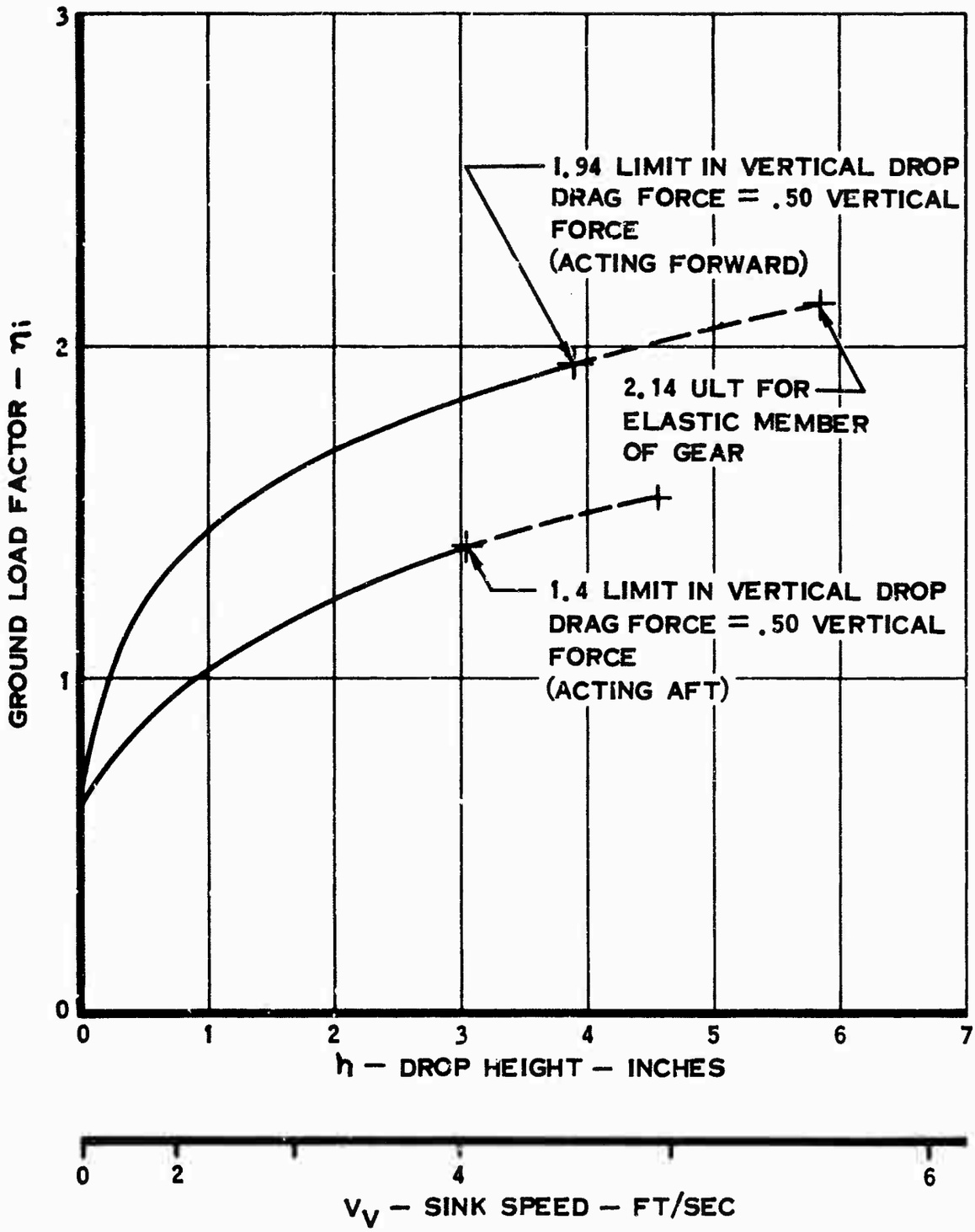

Figure 10. Ground Load Factor Versus Sinking Speed.

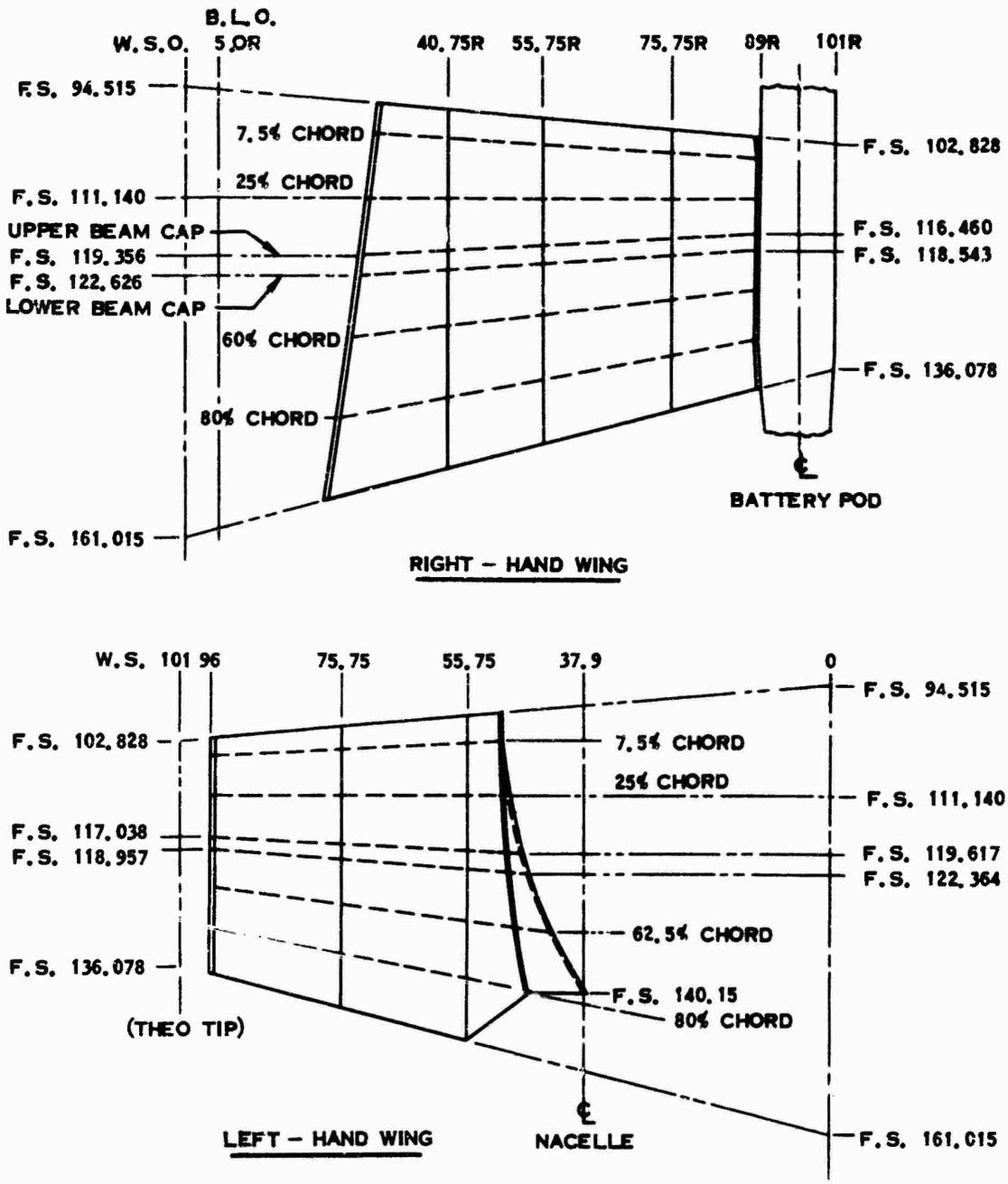

Figure 11. Wings

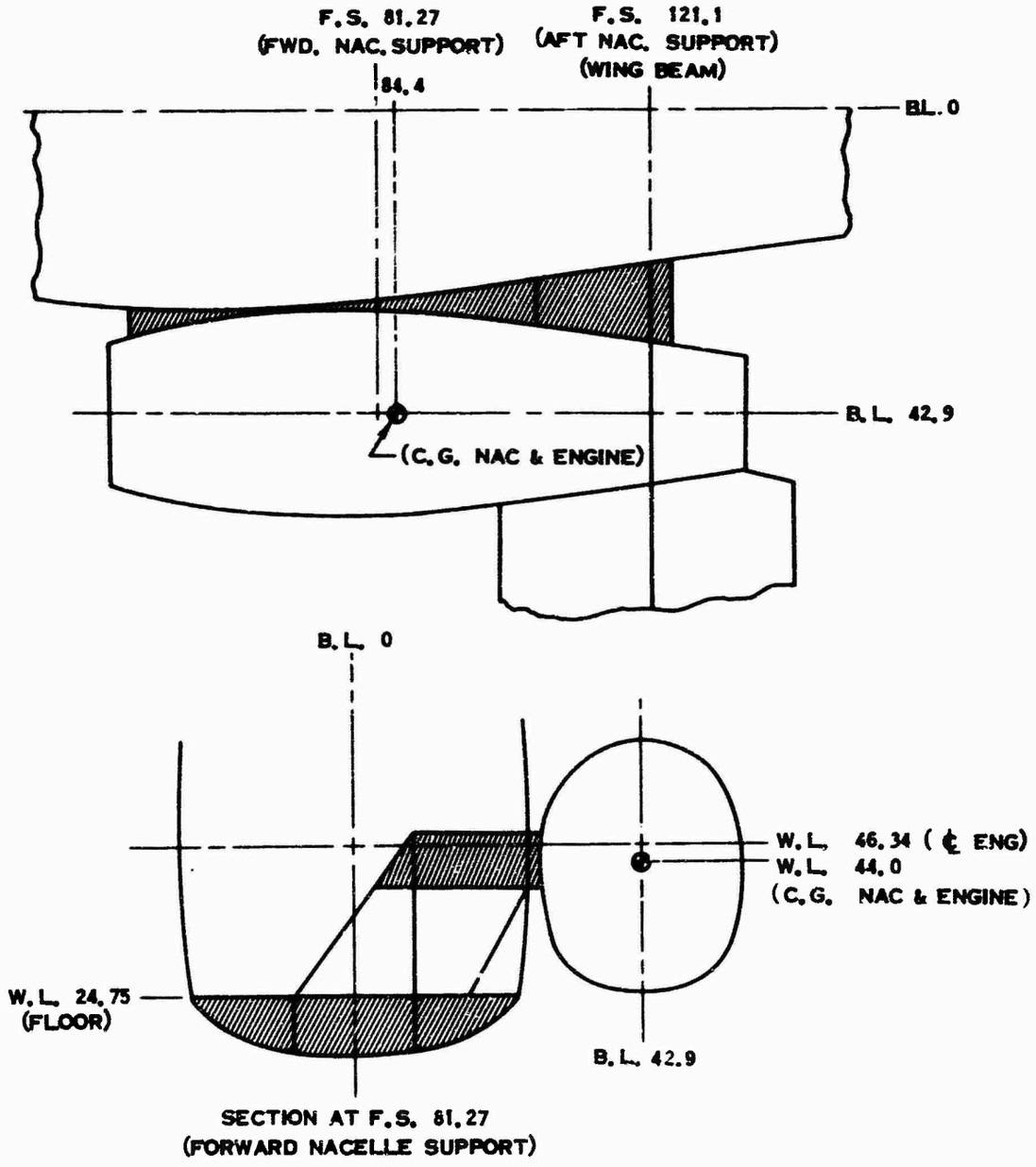

Figure 12. Nacelle and Engine Installation

NOTE:
THE VERTICAL TAIL IS THE BASIC XH-51A VERTICAL TAIL WITH A 6.0 IN. TRIM TAB ADDED. THE VERTICAL TAIL IS SWEPT APPROXIMATELY 45 DEGREES. THE SIDE SHEAR AND BENDING MOMENT ARE TAKEN BY THE FRONT BEAM.

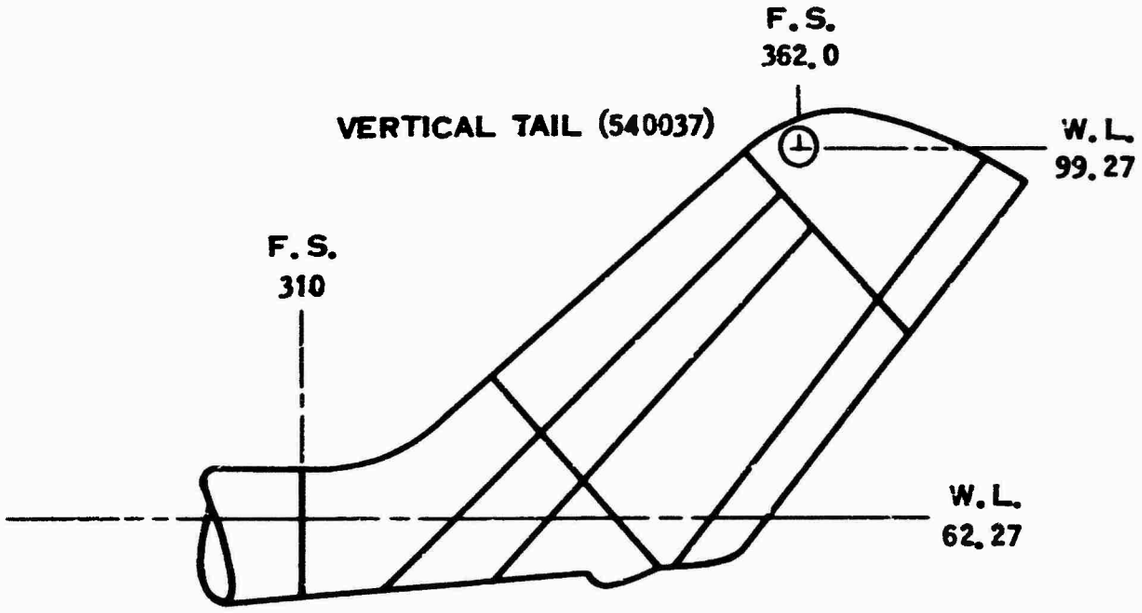

Figure 13. Vertical Tail

DESCRIPTION OF TEST ARTICLES

Three different vehicle configurations were tested during the subject program:

1. XH-51A three-blade rotor helicopter, Figure 2.

2. XH-51A four-blade rotor helicopter, Figure 3.

3. XH-51A compound helicopter. Figure 4.

Differences in the configurations are evident from a comparison of the various design parameters presented in Tables 1 through 3.

The photographs of Figures 14 through 19 show details of various components of each configuration.

TABLE 1
THREE-BLADE ROTOR HELICOPTER DESCRIPTION

General	
Design gross weight	3,950 lb
Fuel capacity	475 lb
Normal crew (plus research instrumentation)	2
Overall length	42.08 ft
Maximum ground attitude (tail low)	6°
Roll mass moment of inertia (including rotor)	1,023 slug ft^2
Pitch mass moment of inertia (including rotor)	3,046 slug ft^2
Yaw mass moment of inertia (including rotor)	3,055 slug ft^2
Cabin retention	floating
Main Rotor	
Type	rigid
Diameter	35 ft
Number of blades	3
Blade chord	13.5 inches
Blade weight	86 lb/blade
Airfoil section	modified NACA 0012
Blade taper	0
Blade twist (root to tip)	-5°
Rotational axis tilt	6° forward
Hub precone	+2.8°
Preset blade droop @ sta. 27.85	-1°
Disc area	962 ft^2
Disc loading	4.03 lb/ft^2
Solidity	.0613
Polar moment of inertia	760 slug ft^2
Normal operating speed	355 rpm

TABLE 1. (cont'd)	
Normal tip speed	650 ft/sec
Blade sweep	1.4° forward
Control Gyro	
Diameter	81 inches
Number of arms	3
Polar moment of inertia	7.5 slug ft^2
Tail Rotor	
Diameter	72 inches
Number of blades	2
Blade chord	8.5 inches
Hub type	teetering
Airfoil section	NACA 0012
Blade taper	0
Blade twist (root to tip)	-4.35°
Feathering moment balance weights:	
weight	2.25 lb/blade
arm	3.0 inches
Delta-three hinge	15°
Disc area	28.27 ft^2
Solidity	.1503
Pitch change travel	27° to -8°
Normal operating speed	2,085 rpm
Horizontal Stabilizer	
Span	84 inches
Chord	13 inches
Airfoil section	NACA 0015
Planform	rectangular
Aspect ratio	6.46
Area	7.58 ft^2
Incidence angle	-5.5°

TABLE 1. (cont'd)

Vertical Stabilizer	
Span	41.75 inches
Chord (tip) (root)	30 inches 45.5 inches
Area	10.95 ft^2
Taper ratio	.70
Aspect ratio	.95
Airfoil section	modified NACA 4424
Powerplant	
Type (PT6-B)	turboshaft
Max power (takeoff)	500 SHP @ sea level
MIL power (30 min)	450 SHP @ sea level
Fuel type	JP-4
Oil type	turbo 35

TABLE 2
FOUR-BLADE ROTOR HELICOPTER DESCRIPTION

The following design parameters primarily distinguish the four-blade rotor from the three-blade rotor helicopter configuration of Table 1.

General	
Design gross weight	4,100 lb
Roll mass moment of inertia (including rotor)	1,158 slug ft^2
Pitch mass moment of inertia (including rotor)	3,181 slug ft^2
Yaw mass moment of inertia (including rotor)	3,325 slug ft^2
Cabin retention	solid
Main Rotor	
Number of blades	4
Hub precone	+3.2°
Disc loading	4.17 lb/ft^2
Solidity	.0818
Polar moment of inertia	1013 slug ft^2
Control Gyro	
Diameter	72 inches
Number of arms	4
Polar moment of inertia	7.5 slug ft^2

TABLE 3
COMPOUND HELICOPTER DESCRIPTION

General	
Design gross weight	4,500 lb
Fuel capacity	475 lb
Normal crew (plus research instrumentation)	1 plus removable jump seat
Overall length	42.58 ft
Maximum ground attitude (tail low)	6°
Roll mass moment of inertia (including rotor)	1,500 slug ft^2
Pitch mass moment of inertia (including rotor)	3,180 slug ft^2
Yaw mass moment of inertia (including rotor)	3,800 slug ft^2
Cabin retention	solid
Main Rotor	
Type	rigid
Diameter	35 ft
Number of blades	4
Blade chord	13.5 inches
Blade weight	86 lb/blade
Airfoil section	modified NACA 0012
Blade taper	0
Blade twist (root to tip)	-5°
Rotational axis tilt	6° forward
Hub precone	+3.2°
Preset blade droop @ sta. 27.85	-1°
Disc area	962 ft^2
Solidity	.0818
Disc loading	4.68 lb/ft^2
Polar moment of inertia	1,013 slug ft^2
Normal operating speed	355 rpm
Blade sweep	1.4° forward

TABLE 3. (cont'd)

Control Gyro	
Diameter	72 inches
Number of arms	4
Polar moment of inertia	7.5 slug ft^2
Tail Rotor	
Diameter	72 inches
Number of blades	2
Blade chord	8.5 inches
Hub type	teetering
Airfoil section	NACA 0012
Blade taper	0
Blade twist (root to tip)	-4.35°
Feathering moment balance weights:	
weight	2.25 lb/blade
arm	3.0 inches
Delta-three hinge	15°
Disc area	28.27 ft^2
Solidity	.1503
Pitch change travel	27° to -8°
Normal operating speed	2,085 rpm
Wing	
Span (nominal)	16.83 ft
Taper ratio	.5
Area	70 ft^2
Aspect ratio	4.05
Sweepback (.25 C)	0
Chord (MAC)	51.72 inches
Airfoil	NACA 23012
Incidence (fixed)	-.9°

TABLE 3. (cont'd)

Horizontal Stabilizer	Initial Config.	Final Config.
Span	84 inches	132 inches
Chord (constant)	13 inches	26.4 inches
Area	7.58 ft^2	24.2 ft^2
Aspect ratio	6.46	5.0
Incidence	-1°	0°
Airfoil section	NACA 0015	NACA 0015

Vertical Stabilizer	
Span	41.75 inches
Chord (tip)	36 inches
Chord (root)	51.5 inches
Area	12.68 ft^2
Taper ratio	.70
Aspect ratio	.95
Airfoil section	modified NACA 4424

Powerplants	
Primary	
Type	turboshaft
Maximum power (takeoff)	500 SHP @ sea level
MIL power (30 minute limit)	450 SHP @ sea level
Fuel type	JP-4
Oil type	turbo 35
Auxiliary	
Type	turbojet
Military thrust @ 200K	2,490 lb @ sea level
Fuel type	JP-4
Oil type	turbo 35

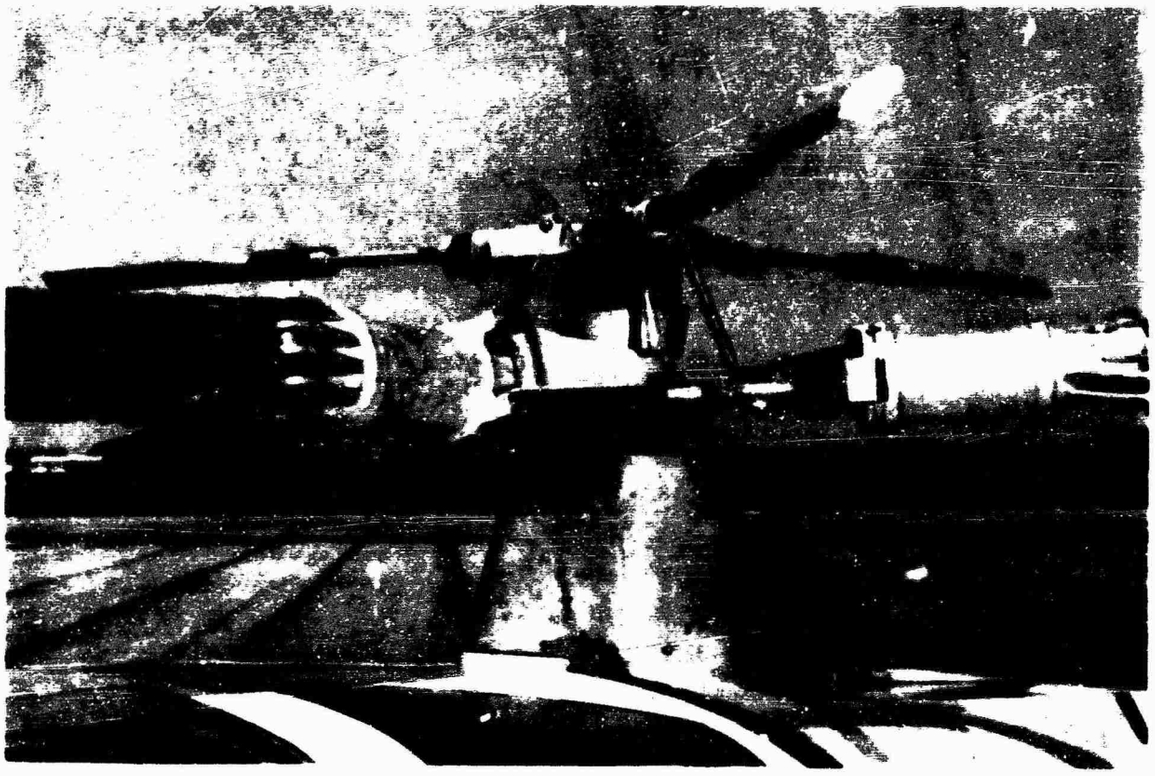

Figure 14. Three-Blade Hub Details

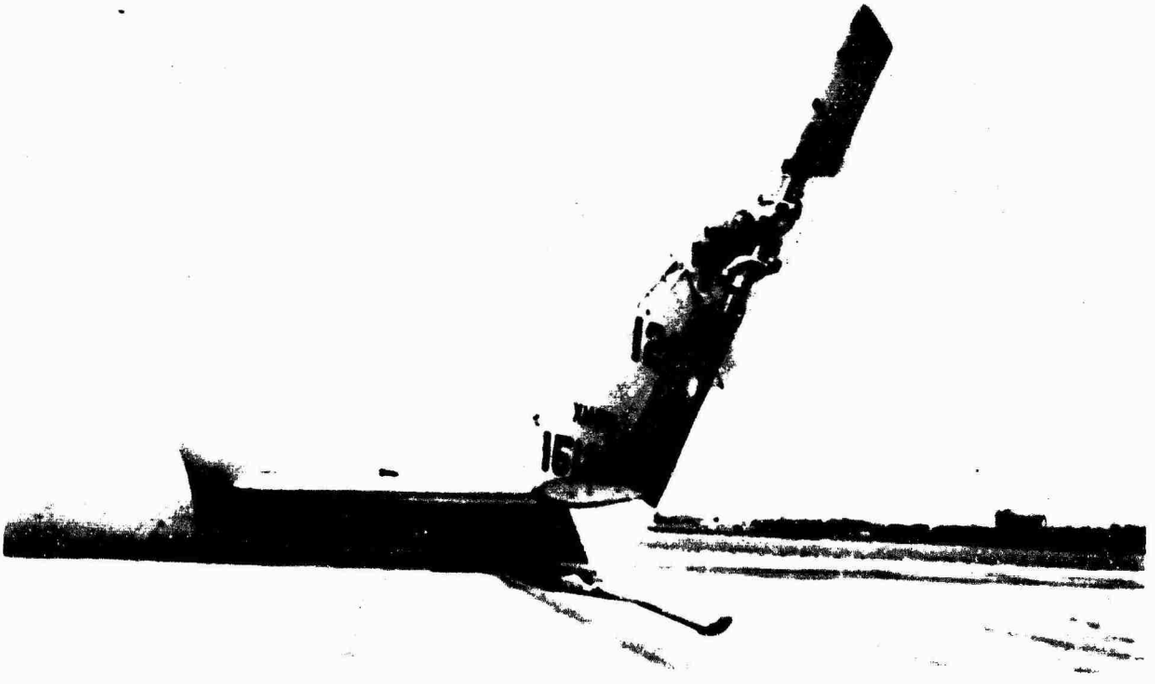

Figure 15. Tail Rotor, Horizontal Stabilizer, and Vertical Fin Details

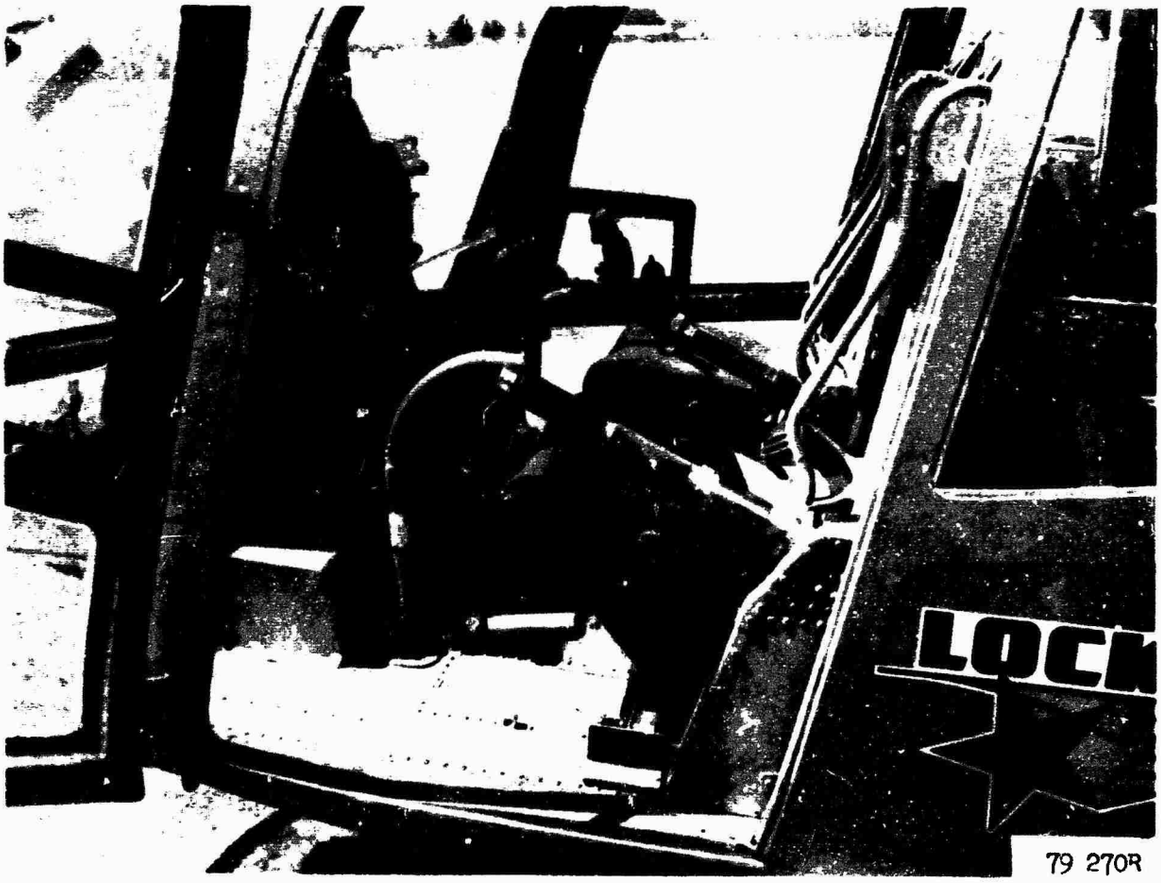

Figure 16. Cabin General Arrangemen.

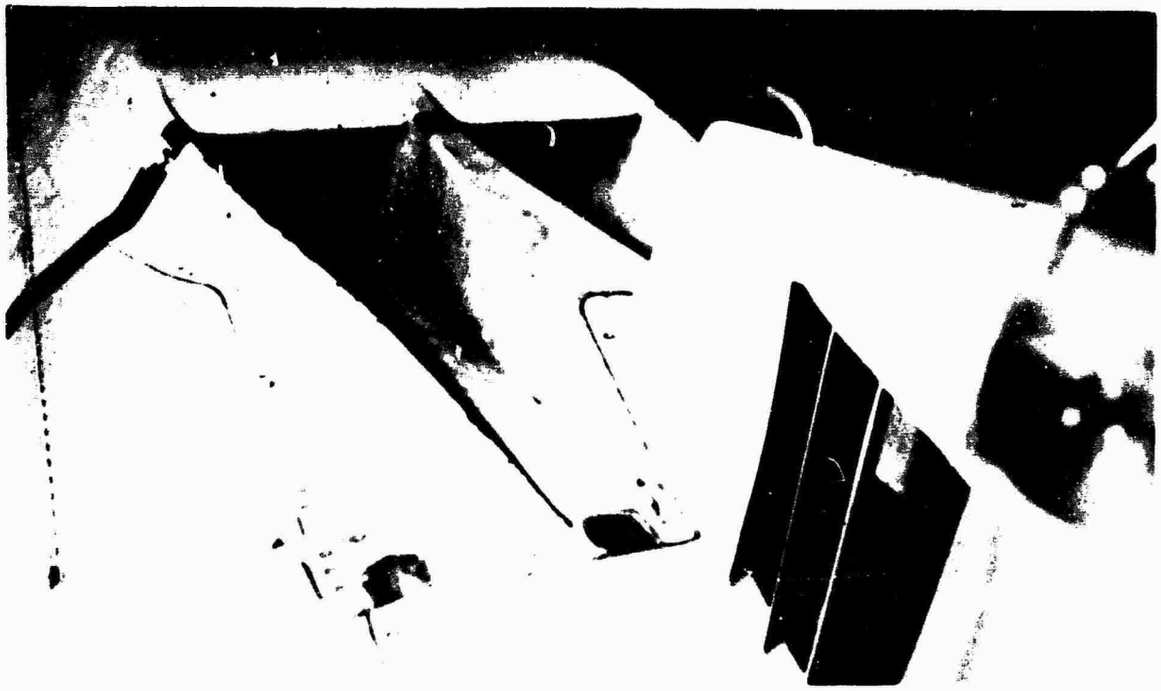

Figure 17. Details of Engine Air Inlet

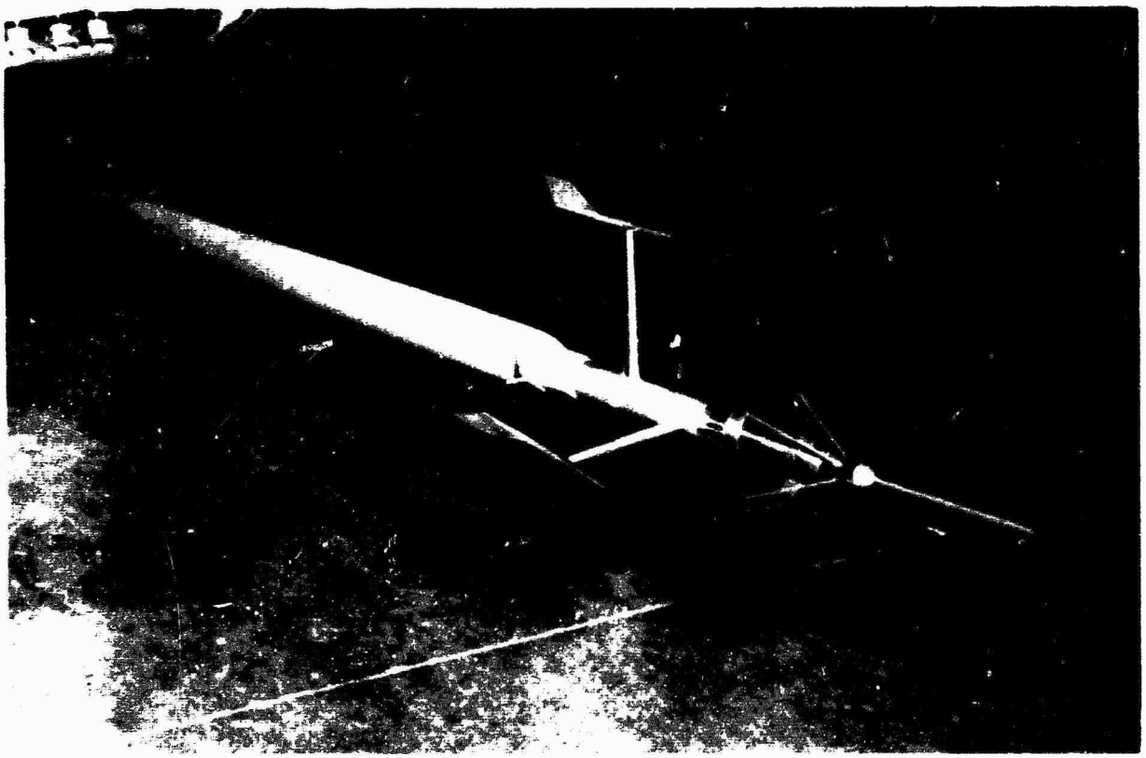

Figure 18. Detail of Nose Boom, Swiveling Airspeed Head, Sideslip Vane and Angle of Attack Vane

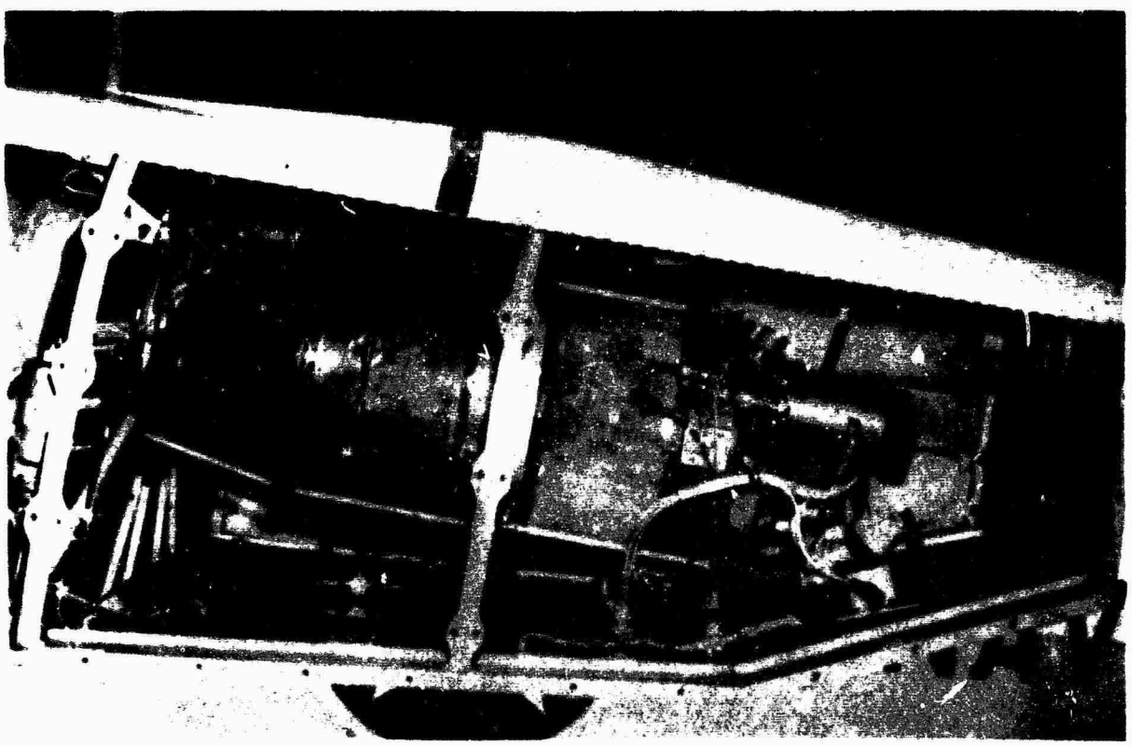

Figure 19. Engine Installation - Left Side

WIND TUNNEL, LABORATORY, AND GROUND TESTS

Extensive ground and laboratory tests were conducted to provide adequate information from which aerodynamic behavior could be predicted, dynamic characteristics determined, and 150-flight-hour structural integrity established.

A. WIND TUNNEL TEST

A brief wind tunnel test, using a quarter scale model of the compound helicopter without rotors, was conducted early in the program. The test had four objectives:

1. Develop low drag fillets between the nacelle and the fuselage and at the wing-nacelle junction.

2. Determine the horizontal stabilizer effectiveness.

3. Determine the effect of asymmetrical wing location on rolling moments.

4. Determine the effectiveness of spoilers on the wing.

All of the objectives were achieved. Relatively simple fillets were developed which resulted in half the parasite drag of the unfilleted configuration.

The equivalent flat plate area of the full-scale fuselage, wing, and nacelle is less than three square feet.

The horizontal stabilizer was tested at three incidence angles. The results permit a realistic analysis of the longitudinal stability of the aircraft and of the loads on the stabilizer.

Because of the unsymmetrical planform of the wing with the jet engine mounted on the left side, a rolling moment exists which must be balanced by the rotor during high-speed flight. As a result of the wind tunnel tests, the centerline of the full-scale wing was shifted 5 inches to the left of the fuselage centerline.

In the event of power failure at high speed, it is necessary to transfer the major portion of the lift from the wing to the rotor. The wind tunnel test indicated that spoilers are an effective means of reducing the wing lift, thereby permitting the rotor to assume the autorotative state.

B. STATIC PROOF TESTS

Airframe

The static proof test program was conducted on the model XH-51A BUNO 151263 compound helicopter which has been modified by the addition of wings, jet engine, and pod, and a four-blade rotor system as described earlier in this report. The vehicle was structurally complete including all doors and fairings. A dummy transmission was installed in place of the main rotor system, and an engine simulating jig was installed in place of the wing jet engine. One-hundred-percent scheduled proof loads, as outlined in the report of reference 2, were applied without residual buckling or excessive disformation.

The vehicle was supported above the floor by means of a steel frame which provided a rigid attachment at the simulated main rotor shaft flange.

Loads were applied to the forward fuselage and cabin structure with external belt type nylon straps and suitable wiffle tree beams. Aft body loads were applied at the tail rotor fitting by compression pads on the vertical stabilizer front beam and fuselage structure, and by both tension straps and pads at strategic locations along the fuselage.

Suitable felt-faced frames were used to apply loads to the wings and the horizontal stabilizer. A dummy engine was used to apply loads to the jet engine support structure.

Loads were also applied to the test vehicle by cabin air pressure contained by a plastic bag.

The static weight of the vehicle structure (1g loads) and the weight of all test jigs and loading devices on the structure were counter-balanced by means of cable-pulley-weight arrangements.

Hydraulic jacks were used to apply the test loads, acting through the straps, tension or compression pads, etc. Hydraulic pressure was supplied to the jacks by a "Hasket" pump and calibrated "Edison" pressure regulators. Calibrated pressure gauges were used to provide a visual check of the pressure regulator output to all hydraulic lines.

Vertical and lateral deflections were measured with ER804 electrical resistance deflection units.

Controls Proof Tests

The controls proof tests required that longitudinal forces, push and

pull, of 100 pounds be applied to the cyclic stick. Also required were lateral forces, left and right, of 67 pounds to be applied to the cyclic stick. The collective control handle forces required were pull-up and push-down at 100 pounds. The forces were to be applied with solid links in place of the positive springs, full boost-on pressure, and the control gyro locked to the hub in a level attitude at mid-collective position.

These forces were applied under the conditions stated, and no evidence of structural failure or deformation was present.

C. FATIGUE TESTS

Loading Spectra

To demonstrate that the primary dynamic components of the XH-51A helicopter and the XH-51A compound vehicle have a safe life potential of 150 hours of development flying, the anticipated use of the vehicle must first be described in detail. For this use, loading spectra can then be defined for components of the vehicle by employing histories of loadings recorded in flight. These loading histories were recorded on the XH-51A's flown with three-blade main rotors.

Outline of Operational Conditions: An essential step in the definition of loading spectra for fatigue tests is the selection of an adequately detailed description of the probable use of the vehicle. The anticipated service use of the vehicle covered by this report is presently limited to 150 hours of development flying. The description of this service is provided by the allocation of condition times the number of events which is presented in Table 4. The analysis leading to this selection was based on discussions with helicopter pilots and flight test engineers with experience in this type of service, supplemented by the experience with vehicle development flying at Lockheed.

Development of Loading Spectra: In the development of loading spectra for fatigue testing elements of the Lockheed rigid rotor helicopter, attention has largely been restricted to histories of flight and ground loadings recorded on oscillographs. The conditions for which records have been obtained include those listed in Table 4. These records were obtained during 1963 and 1964 for the three-blade version of the XH-51A helicopter, and they covered several modifications of the basic vehicle.

Table 5 lists the components and gauge locations for which reductions of flight data were undertaken. In addition, attention was focused on the tension-torsion pack and on the swash-plate lugs through which control link loads to the gyro arms are transmitted. For these

TABLE 4

ALLOCATION OF TIME AND NUMBER OF LOADING EVENTS FOR 150 HOURS OF DEVELOPMENT FLIGHT OF THE XH-51A.

Condition Description	Time in Hours	No. of Events in 150 Hours
Total Flight	150.0	360
Steady Flight Knots 0-30	34.5	
30-60	30.0	
60-90	36.0	
90-120	24.3	
120-140	6.9	
140-160	1.5	
160-180	.3	
Sideslip Flight	1.0	
Rearward Flight	.5	
Climb at Max. Continuous Power	6.0	
Descent at Partial Power	6.0	
Pull-ups Cyclic (.6-1.55g) at 30-60 Knots		58
Pull-ups Cyclic (.6-1.55g) at 60-90 Knots		192
Pull-ups Cyclic (.6-1.55g) at 90-120 Knots		97
Pull-ups Cyclic (.6-1.55g) at 120-140 Knots		28
Pull-ups Collective (.6-1.55g) at Hover		138
Pull-ups Collective (.6-1.55g) at 30-60 Knots		58
Phugoids		4
Pull-ups Cyclic (over 1.55g) at 30-60 Knots		13
Pull-ups Cyclic (over 1.55g) at 60-90 Knots		38
Pull-ups Cyclic (over 1.55g) at 90-120 Knots		19
Pull-ups Cyclic (over 1.55g) at 120-140 Knots		5
Pull-ups Collective (over 1.55g) at Hover		28
Pull-ups Collective (over 1.55g) at 30-60 Knots		12

TABLE 4 (cont'd)

Condition Description	Time in Hours	No. of Events in 150 Hours
Ground Conditions - Rotor Runup and Rundown		810
Ground Run	150.0	
Takeoffs		630
Landings		630
5° Slope Takeoffs		24
5° Slope Landings		24
10° Slope Takeoffs		12
10° Slope Landings		12
Flares		720
Control Pulses - Cyclic Roll Inputs		720
Cyclic Pitch Inputs		720
On-the-Spot Turns		120
Autorotation		180
Inadvertencies and Recoveries		12
Incidents of Vibratory Response #1		18
Incidents of Vibratory Response #2		72
Incidents of Vibratory Response #3		270

elements, the loadings were derived by analysis guided by selected reference load measurements.

To illustrate the scope of the data reduction program undertaken for the components listed in Table 5, the number of traces typically employed for each condition is shown in Table 6. For conditions not shown in these tables, flight records were not available and dependence was placed on analysis and other data. These conditions included landings and takeoffs on slopes, incidents of vibratory response at high speed, and other inadvertencies and recoveries. Care was taken to determine and account for the differences in loading response which are associated with differences in vehicle configuration.

The reduction of the loading trace histories for each structural component was carried out using the mean crossing peak count as a basis for spectrum definition. The unit spectra thus derived for particular flight conditions or events were combined to define the total loading history consistent with the vehicle use described in Table 4. In this work, many weighting factors had to be selected. The selections were made with the intention of developing a conservative representation of an extended period of development flying.

With the loading spectra defined for the components listed in Table 5, each component was examined to determine the most critical location in terms of calculated stress. Critical areas are noted in a later paragraph. By use of the stress load relations of reference 5, the load spectra were converted to stress spectra.

Definition of Test Loading Spectra: For the root region of the main rotor blade, multiple spectra covering a range of the phasings of flap and chord bending were specified. For other structural components, relatively simple unit spectra of test loadings were developed for repeated application.

Figure 20 illustrates a typical development of stress spectra for locations on the main rotor hub and blade. This figure includes definition of the anticipated flight stress spectrum from multiple bending moment spectra obtained from flight data. The spectrum so defined includes large numbers of small amplitude cycles. The need for such cycles in fatigue tests has been demonstrated but practical limitations on test time and cost usually prohibit the full representations of many millions of very small amplitude loadings. Consequently, only a portion of such small loadings are specified for test.

TABLE 5
COMPONENTS FROM WHICH FLIGHT RECORDS WERE REDUCED TO SPECTRA FORM - THREE-BLADE ROTOR

Main Rotor Hub and Blade		
	Station 6	Flap Bending
	Station 6	Chord Bending
	Station 45	Flap Bending
	Station 157	Flap Bending
Main Rotor Pitch Arm Control Link		
	Axial Load in Link	
Gyro Arm		
	Station 12.7	Flap Bending
	Station 12.7	Chord Bending
Tail Rotor Hub and Blade		
	Station 9.9	Chord Bending
	Station 19.5	Flap Bending
	Station 19.5	Chord Bending
Tail Rotor Pitch Arm Control Link and Cross Bar		
	Axial Load in Link	

Since the smaller loadings are believed to have particular significance in terms of crack propagation, their application is spread over the target test life rather than applying them all during the early stages of the test when their effect might be of negligible importance. This approach insures that a potentially important effect has not been ignored.

The particular scheme of spectrum truncation which is employed is based directly on established practice in the definition of test spectra. Figure 20 shows the truncation used for station 7, upper forward corner on the main rotor hub.

With a truncated stress spectrum defined, a set of discrete loading spectra, each representing one of the multiple spectra covering a range of phasings of flap and chord bending, must be developed. The summation of these multiple loading spectra must be made to fit the truncated spectrum defined in terms of stress.

Fatigue Test Results

The targeted test spectra of paragraph C (Loading Spectra), preceding, were applied in separate tests to the following components without visible evidence of structural damage:

Main Rotor Control Gyro Arm - 33 repetitive applications of a 15-hour unit block step-ordered spectrum.

Main Rotor Rotating Swash-plate Lug - 30 repetitive applications of a 15-hour unit block step-ordered spectrum.

Main Rotor Blade Pitch Control Arm - 30 repetitive applications of a 15-hour unit block step-ordered spectrum.

Main Rotor Blade and Hub - Three repetitive applications of a 150-hour basic flight-by-flight spectrum.

Tension-Torsion Pack - One of the tension-torsion pack straps failed during the twenty-third application of a 12-1/2-hour-unit block spectrum. Fifteen more applications of the unit spectrum were applied (making a total of 38 applications) without evidence of further fatigue damage.

Tail Rotor Assembly - One of the tail rotor assembly cuffs developed a fatigue crack during the fourth application of a 100-hour unit block spectrum.

Figures 21 through 30 show details of the fatigue tests listed above.

TABLE 6

LIST OF FLIGHT RECORDINGS EMPLOYED TO DEFINE SPECTRA FOR MAIN ROTOR SYSTEM (FINAL CONFIGURATION XH-51A)

Condition Description	Number of Samples				Total No. of Samples
	Fwd C.G.	Very Fwd. C.G.	Neutral C.G.	Aft C.G.	
Steady Flights Knots 0-30	17	2	1	2	22
30-60	4	1	4	4	13
60-90	5	2	3	3	13
90-120	5	3	6	3	17
120-140	7	1	3	7	18
140-160	2				2
Sideslip Flight	16				16
Rearward Flight	3				3
Climb at Max. Continuous Power			4		4
Descent at Partial Power	3				3
Pull-ups Cyclic (.6-1.55g) at 30-60 Knots		1	3	5	9
Pull-ups Cyclic (.6-1.55g) at 60-90 Knots		2	2	3	7
Pull-ups Cyclic (.6-1.55g) at 90-120 Knots	2		2	1	5
Pull-ups Cyclic (.6-1.55g) at 120-140 Knots	3		3	5	11
Pull-ups Collective (.6-1.55g) at Hover			1	1	2
Pull-ups Collective (.6-1.55g) at 30-60 Knots				2	2
Phugoids			3	3	6
Pull-ups Cyclic (over 1.55g) at 30-60 Knots		1	4	3	8
Pull-ups Cyclic (over 1.55g) at 60-90 Knots	2	1	3	2	8
Pull-ups Cyclic (over 1.55g) at 90-120 Knots			1	1	2
Pull-ups Collective (over 1.55g) at Hover			1	1	2

TABLE 6 (cont'd)

Condition Description		Number of Samples: Fwd. C.G.	Very Fwd. C.G.	Neutral C.G.	Aft C.G.	Total No. of Samples
Ground Conditions:	Rotor On-Off	1				1
	Ground Run	1		1		2
	Takeoffs			1	1	2
	Landings	2				2
Flares		4		1	1	6
Control Pulses - Cyclic Roll Inputs				6		6
Cyclic Pitch Inputs		1	3		4	8
On-the-Spot Turns		9				9
Autorotation		1	1	5	4	11

D. VIBRATION TESTS

The ground vibration tests were performed in two major test setups. The first setup determined the nonrotating blade natural frequencies. The second setup determined the natural frequencies of the compound helicopter including the forced response of the vehicle due to four-per-revolution excitation from the main rotor. The natural modes and frequencies of the wing systems were also examined.

These tests associated with the latter setup were performed in two phases. The first phase, with the aircraft resting on its skids and with the tail constrained, was specifically oriented to determine the natural frequencies and mode shapes of the wing system as added to the basic XH-51A. The second phase, with the aircraft hanging on a low-frequency suspension system, determined the free-free natural mode shapes and frequencies of the vehicle and forced response amplitudes due to four-per-revolution fore and aft excitation and lateral excitation of the hub.

Rotor

A ground vibration test of the four-blade-rotor system was conducted to determine the rotor system frequencies, Figure 31. Additionally, the system was checked to assure that there was no delta-three hinge effect, i.e., blade feathering due to hub bending.

The frequencies of the major modes of vibration are presented with corresponding data for the three-blade-rotor system for comparison purposes. No significant differences between the two systems were discovered as shown in Table 7.

TABLE 7
COMPARISON OF BLADE FREQUENCIES
NONROTATING

Mode	Frequency	
	3-Blade System	4-Blade System
First Flap Bending	1.50 cps	1.50 cps
Second Flap Bending	7.85 cps	8.23 cps
Third Flap Bending	19.80 cps	19.58 cps
First Inplane in Phase	7.03 cps	7.14 cps
First Inplane out of Phase	8.29 cps	8.01 cps
First Torsional	24.40 cps	25.60 cps

The airframe generally responded in the frequency range from 9 to 11 cps, which is well away from the main rotor operating speed of 355 rpm (5.92 cps). Unsymmetric wing bending occurred at 9.1, 9.53, and 9.64 cps with the aircraft resting on the skids and the shaker excitation on the left wing, symmetric on both wings, and on right wing, respectively. Left-wing first-bending frequency was measured at 15.7 cps and a coupled vertical bending and torsion of the left wing at 30.7 cps. The right-wing torsion was measured at 18.5 cps.

The wide frequency separation between left-wing vertical bending and torsion indicates freedom from flutter of the left wing; and the center-of-gravity of the right-wing pod's being forward and the separation between the right-wing vertical bending and torsion indicate that the right wing will also be free from flutter. There is no undue proximity of natural frequencies to the dominant harmonic frequencies of 1-P and 4-P of the main rotor, over its nominal operating range, except for the main engine pitch frequency which was close to 4-P. A summary of frequencies and modes of the compound helicopter is presented in Table 8.

TABLE 8
NATURAL MODES DESCRIPTION

Frequency (cps)	Wing Modes Description
9.10	Right-wing bending with fuselage roll, on skids
9.53	Unsymmetric wing bending with tips in phase
9.64	Unsymmetric wing bending with tips in phase
15.70	Left-wing bending
18.50	Right-wing torsion
30.70	Left-wing bending with engine nacelle pitch
	Miscellaneous Modes Description
4.50	Body pitch and plunge on skids
5.00	Fuselage roll on skids
6.40	Oscillograph lateral
8.52	Oscillograph mount frequency
11.10	Gyro arm vertical bending
12.00	Oscillograph frequency on mounts
12.70	Console lateral
14.70	Console lateral shear
21.70	Jet engine yaw
37.90	Tail rotor blade flap bending

An extensive shake test was also conducted to determine the natural frequencies and forced response characteristics of the large horizontal stabilizer (final configuration) on the compound helicopter. Two particularly active frequencies were found. The stabilizer has a primary antisymmetrical flapping response (roll) at 20.2 cps, and a primary symmetrical flapping response (out of phase with tail cone) at 30.2 cps. Both of the frequencies are sufficiently removed from the primary forcing functions, that is, 24 cps (main rotor blade passage) and 36 cps (1-P tail rotor), to indicate that excessive vibration would probably not be a problem in flight.

E. WHIRL TESTS

During the initial whirl tower runs with the four-blade rotor installed as shown in Figure 32, the spline clutch in the main power transmission shaft failed in such a manner that the clutch would not remain engaged.

Since it was determined that the necessary repairs would present an intolerable schedule hazard, the essential whirl checks were accomplished during tie-down tests of the flight article.

Vibration Characteristics

Rotating shake and rpm sweep tests were run to determine the blade frequencies of the rotating four-blade rotor on helicopter BUNO 151262.

For the rotating shake tests, symmetric excitation in plunge and antisymmetric excitation in roll were applied by the use of a pair of shakers attached to side booms. One shaker was used for the excitation in pitch through the fuselage at station 280. In addition to the shaker input, the rotating rotor always generates a four-revolution input caused by the aerodynamic loading condition of the rotor. The rotor input seems to be stronger than the shaker input. The presence of the four-revolution rotor input can be concluded from the fuselage and gearbox response which is almost independent from the shaker input frequency. The fuselage is responding to the shaker frequency only in the range of from 8 to 9 cps. In the case of roll excitation, some responses to higher frequencies were observed in the fuselage.

Tests were run at five discrete rotor speeds (75, 85, 91, 95, and 100% rpm) with a shaker input sweep through the frequency range from 7 to 50 cps. The blades responded primarily to the four-revolution translational motion of the gearbox in a three-revolution and a five-revolution flapping mode both of which are close to the natural frequencies of the second and third flapwise bending mode of the rotating cantilever beam.

The blade response at 75% and 85% rpm is predominant in three-revolution and above 90% rpm predominant in five-revolution as shown in Figure 33. The calculated second and third flapwise bending frequencies are shown for comparison on this figure.

For the rpm sweep tests, a record was taken during an acceleration and deceleration of the rotor because the blade response depends more on rotor speed than shaker input. The range from 62% rpm to 108% rpm was covered with a very low sweep rate, thus avoiding the effect of the

sweep rate. The aircraft was tied down on the skids, as in the shake test, and the tail rotor was disconnected. The results are shown in Figure 34. The response is predominant at three per revolution in the range between 75% and 87% rpm, at five per revolution above 90% rpm, and at six per revolution between 62% and 67% rpm.

Summarizing, it can be stated that the observed frequencies are very close to the calculated frequencies of the second and third flapwise bending modes of the rotating cantilever beam. In the rotor speed range below 70% rpm, the observed frequencies are slightly lower than the calculated frequencies.

When a roll degree of flexibility was added to the transmission mounting of helicopter BUNO 151262 (providing flexible mounting in pitch, roll and vertical translation), tests were conducted in an attempt to induce any possible rotor whirl mode in the tie-down rig, and with a slack in the tie-down cables. This initial test showed no indication of a rotor whirl mode.

An additional test was conducted by setting the ship on approximately two inches of die rubber which essentially reduced the stiffness of the gear system and allowed for more reaction if the whirl condition were to exist. The tie-down rig was also retained in a slack position. Again, no indication of a whirl condition was evident. The tests were essentially stick oscillation inputs of varied and increasing frequencies with the collective set at increasing increments of lift for each series. The aircraft was not allowed to lift off the ground even though the tie-down rig was slack.

Structural Loads

In general, the tie-down tests of BUNO 151262 served as an operational checkout of the rotor system stability and loads over a range of lift rpm, and body moments that encompassed planned flying of the four-blade rotor. Tests were conducted from essentially 1,000 pounds of lift up to 8,000 pounds (2.27g) at rotor speeds of 320 (90%), 355 (100%), and 370 (104%) and body moments from zero up to 30,000 inch-pounds.

The lift produced the high coning condition while the body moments introduced large cyclic bending moments. Rotor stability was checked at extreme coning by testing at 320 rpm (90%) and for flutter by operating at 370 rpm (104%).

Main rotor flapwise bending moment station 6, and main rotor chordwise bending moment station 6 were visually monitored during all tests. These two measurements were monitored because they were determined from previous test data to be the most representative loads of the overall

rotor system. Oscillograph records were taken for each test point during the tests.

To determine the effect of change in rpm on blade loads, tests were run at 320 rpm (low centrifugal force), 355 rpm (normal centrifugal force), and 370 rpm (high centrifugal force). Average and cyclic bending moments for flap and chord at station 6 are plotted versus rotor lift for the three speeds, Figure 35. This plot shows that the cyclic loads are not affected by lift. The average chord loads increased with the engine power input while the average flapwise bending moments decreased with increasing rpm due to the higher centrifugal force on the cone angle. The largest average flapwise bending down load at 370 rpm for 1,210 pounds of lift was 31,800 inch-pounds.

Cyclic flapwise bending moments were varied from zero to 10,400 inch-pounds to produce a body moment of 36,800 inch-pounds at 320 rpm. The maximum cyclic flapwise moment at 355 rpm was 11,100 inch-pounds to produce a body moment of 30,300 inch-pounds. At 370 rpm, the maximum cyclic flapwise moment was 10,300 inch-pounds to produce a body moment of 36,400 inch-pounds. The lift was varied from 1,000 pounds up to 8,000 pounds for each of the rpm's and body moment inputs. The maximum cyclic flapwise mending moment of 11,100 inch-pounds converts to a stress of 15,800 psi in the hub at the critical location which is rotor station 7.0.

Tests were run to check the dynamic response of the rotor system by pulsing the cyclic stick. These tests were run with 1,350 pounds of lift and 5,800 pounds of lift. The maximum cyclic flapwise bending moment was 20,000 inch-pounds producing a body moment of 70,800 inch-pounds. This 20,000 inch-pounds of flapwise bending moment produced a stress of 28,400 psi.

All structural loads from these tie-down tests were on or near those predicted for the four-blade-rotor system.

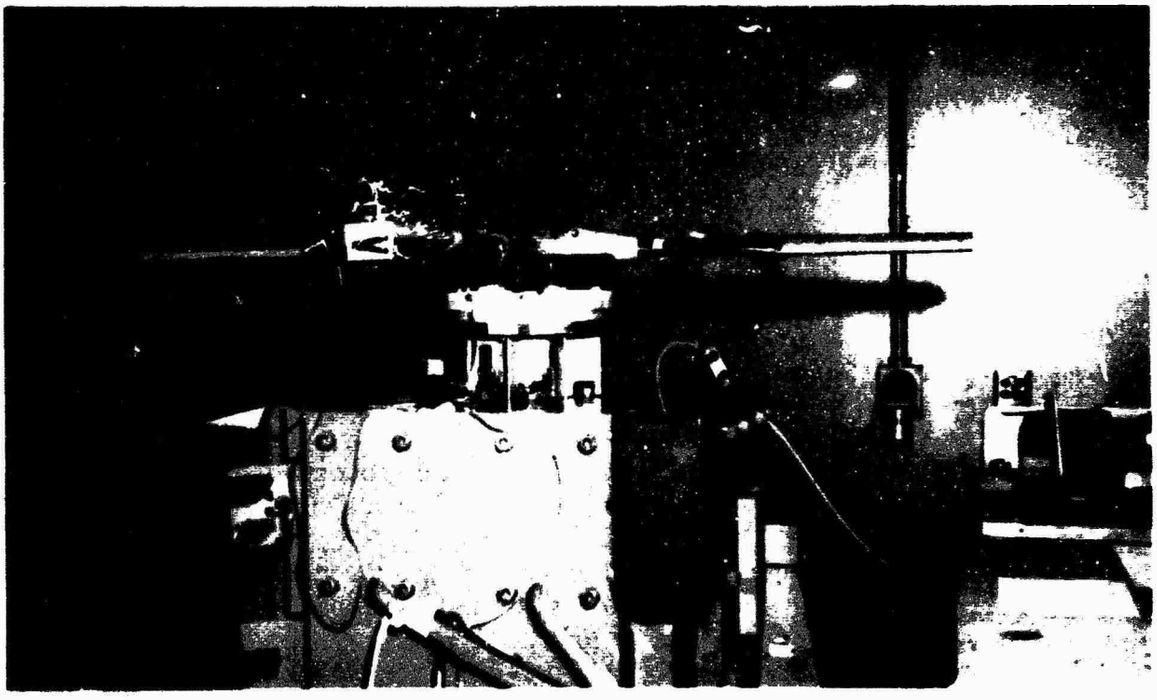

Figure 20. Development of Stress Spectra - Main Rotor Station 7 Upper Forward Corner.

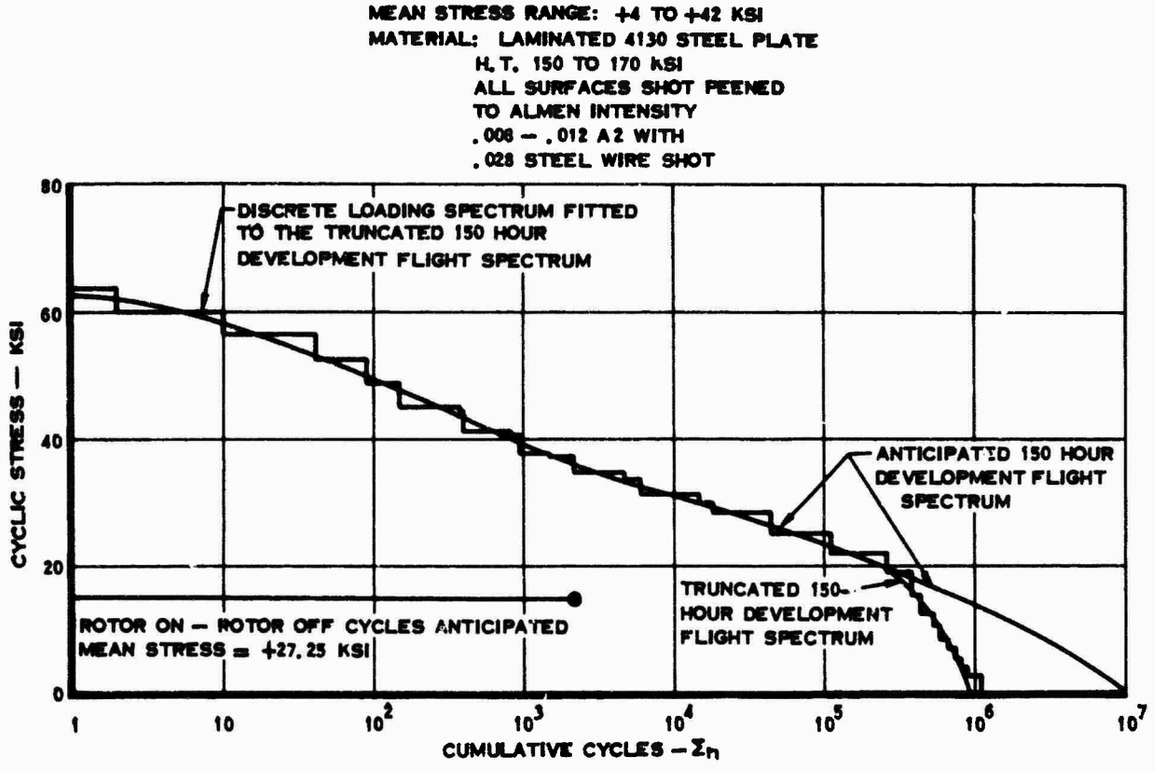

Figure 21. Gyro Arm Assembly on Shaker Table, Ready for Testing.

Figure 22. Swash-plate Lug Installed, Ready for Testing.

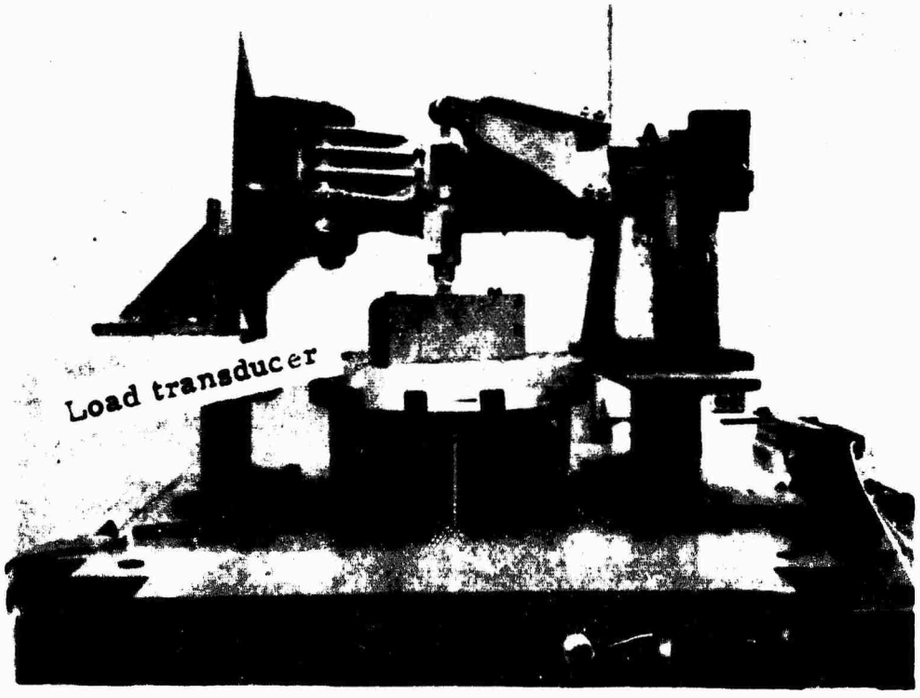

Figure 23. MRB Pitch Control Arm Installed, Ready for Testing.

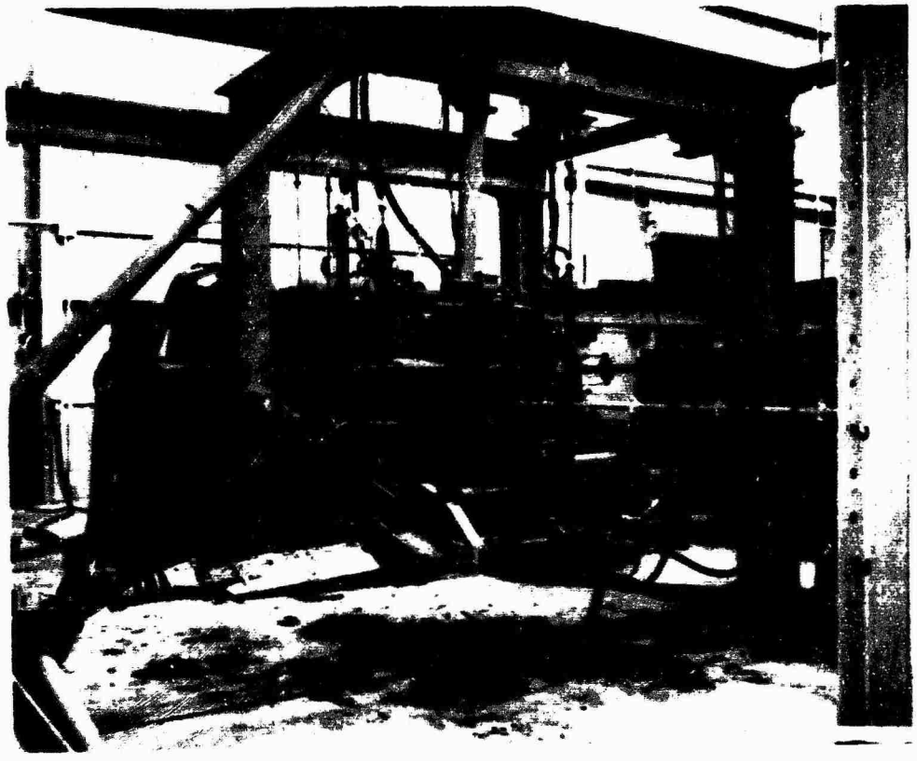

Figure 24. Installation of MRB Test Article and Hydraulic Loading Jacks in the Test Article.

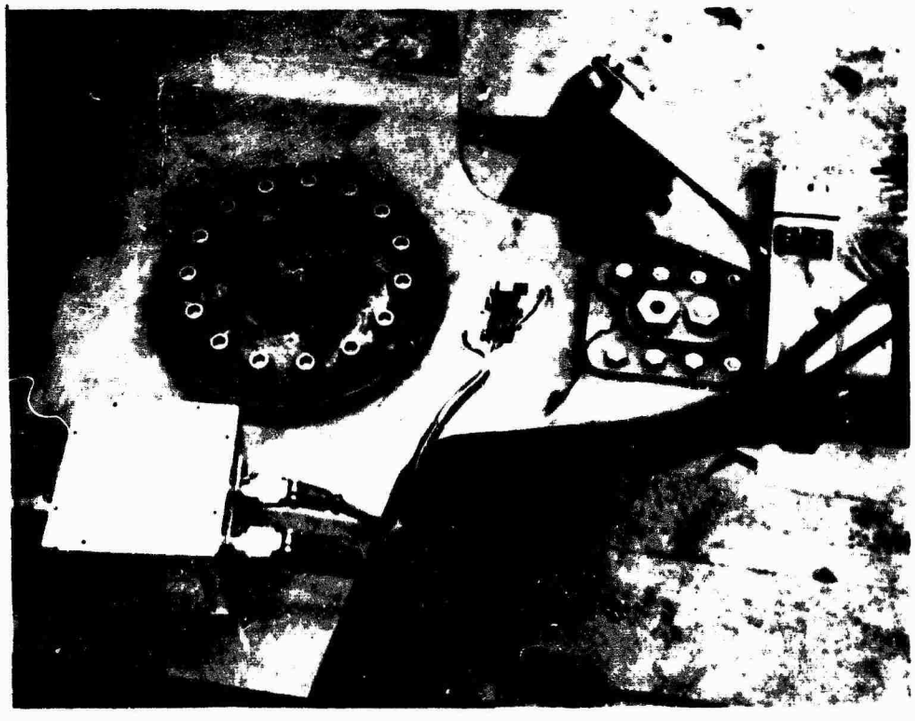

Figure 25. Closeup View Showing MRB Hub Installation. (Note Strain Gauge Bridge Installation at Station 6)

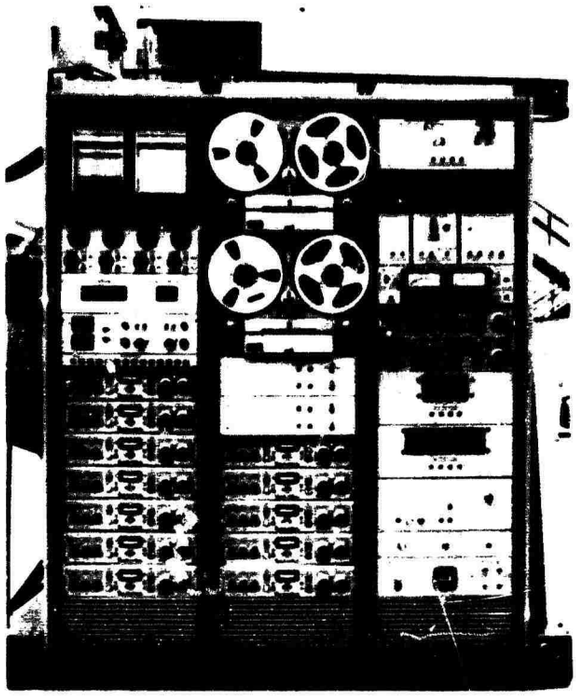

Figure 26. Load Programming System.

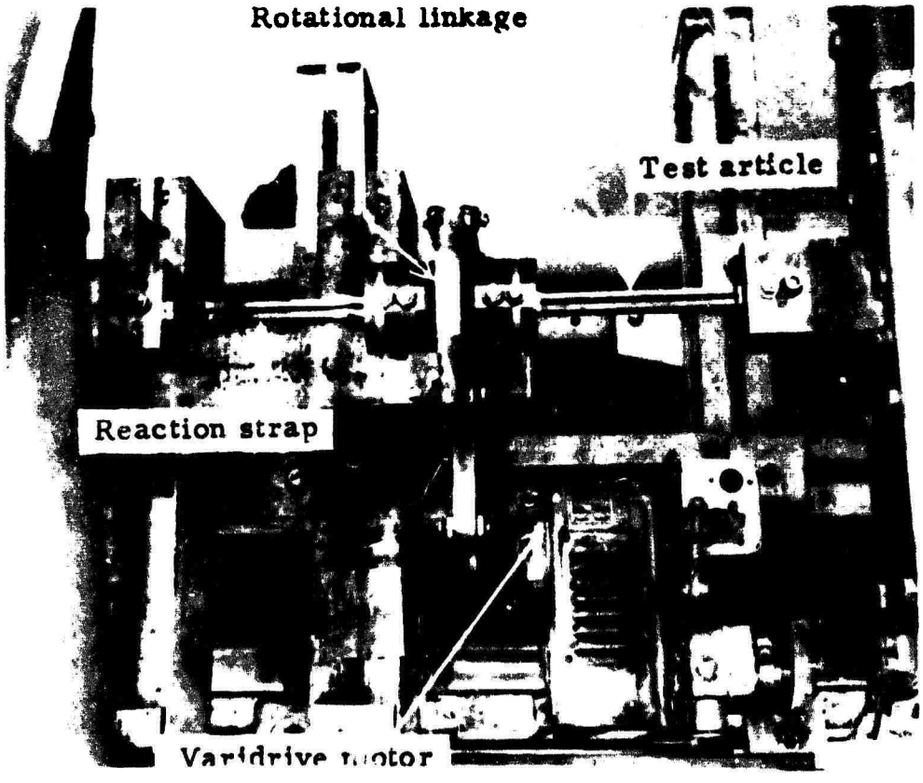

Figure 27. View Looking Down on Test Article Installation, Tension-Torsion Pack.

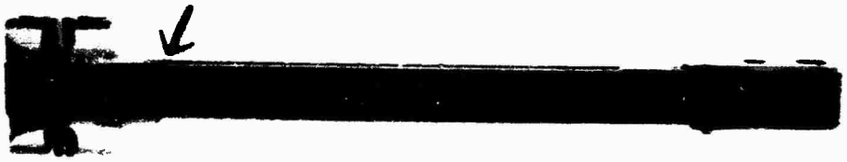

Figure 28. Strap Assembly, After Test, Showing Strap Failure.

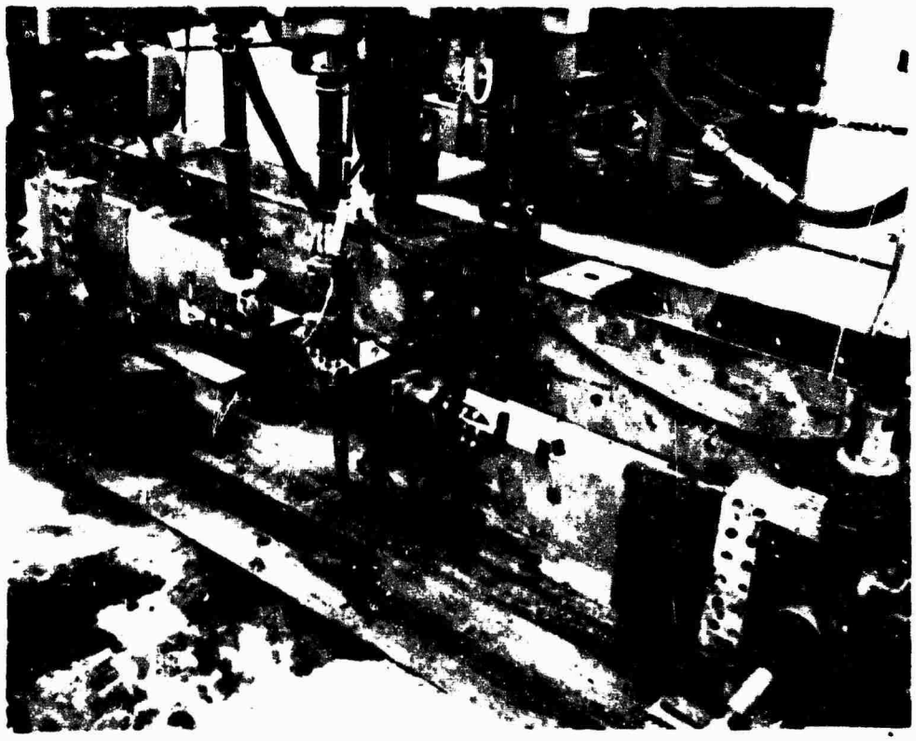

Figure 29. Closeup View of Test Installation Showing Attachment of Blade Loading Blocks and Pitch Link Loading Fixtures.

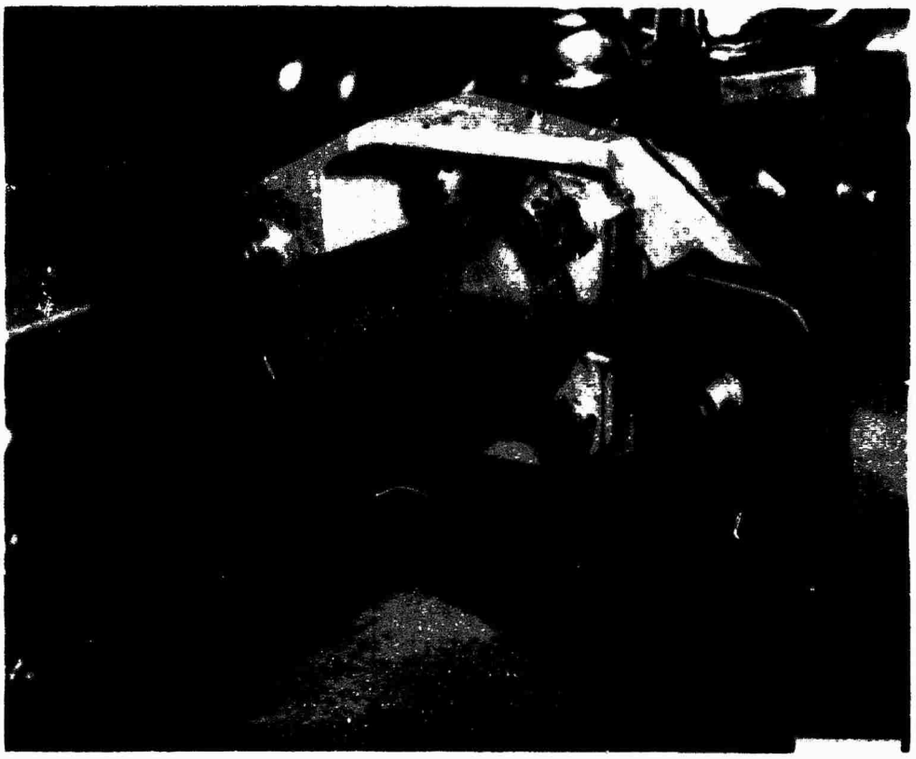

Figure 30. Bottom View of Damaged Hub Area.

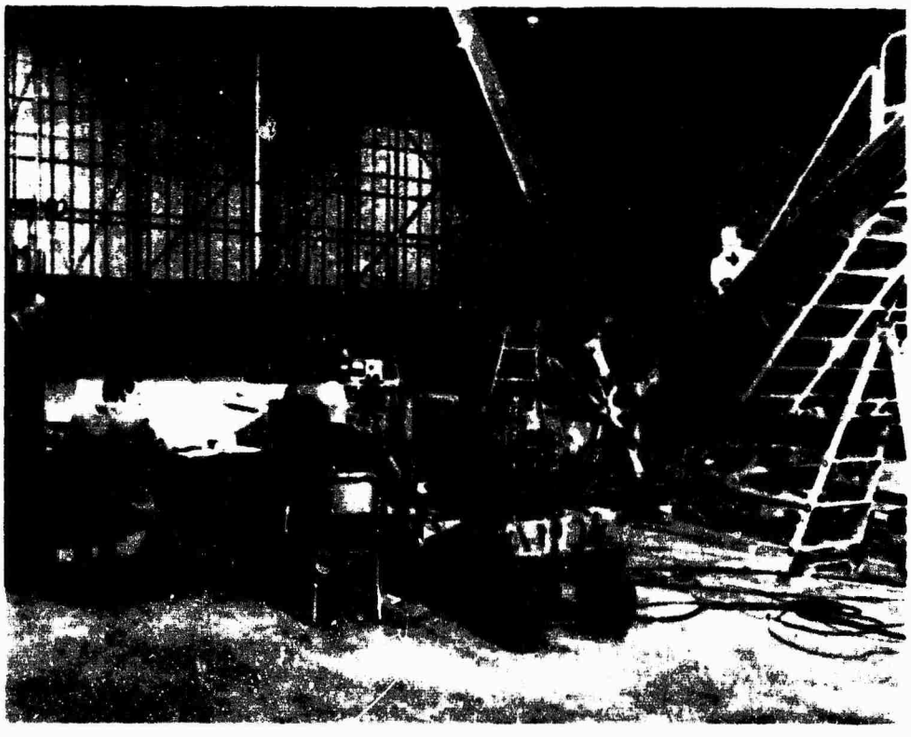

Figure 31. Four-Blade Rotor System - Nonrotating Frequency Response Test Setup.

Figure 32. Photo of Whirl Tower Run - Four-Blade Rotor.

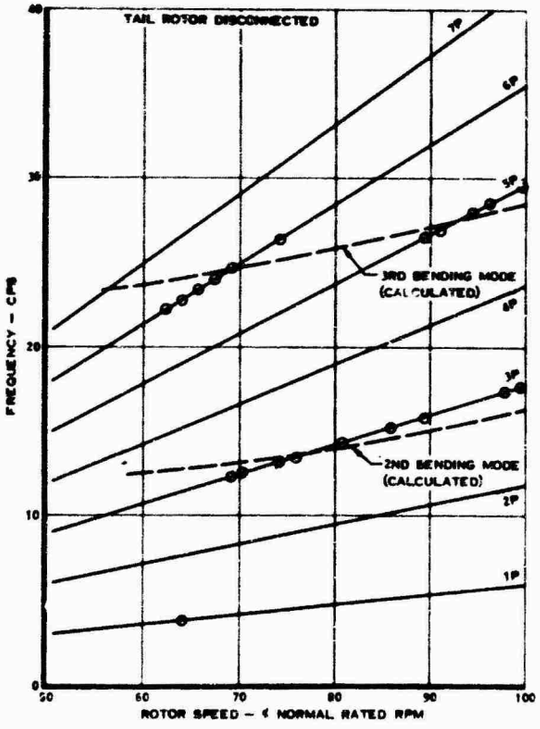

Figure 34. Main Rotor Blade Flapwise Bending Response at Station 6 with RPM Sweep.

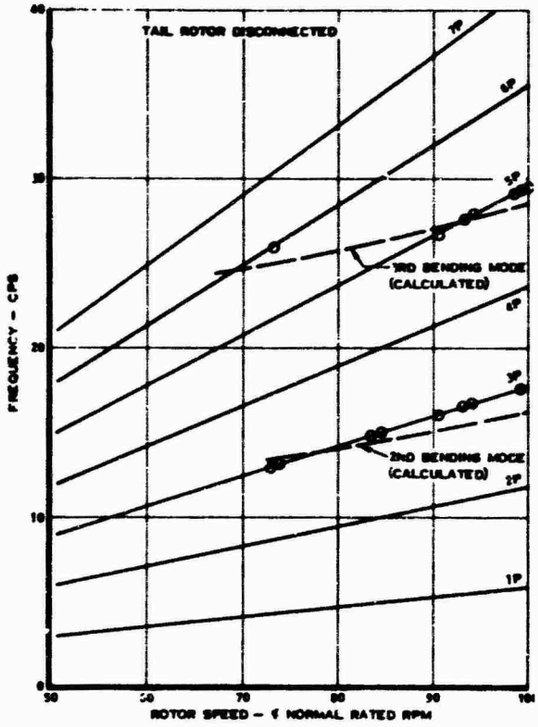

Figure 33. Main Rotor Blade Flapwise Bending Response at Station 6 with Shaker Input at Indicated RPM.

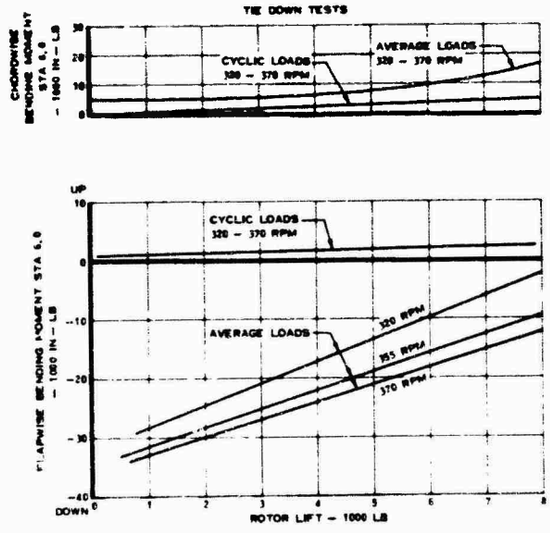

Figure 35. Four-Blade Main Rotor Loads at Station 6 Versus Rotor Lift.

RESEARCH FLIGHT TESTS

This section of the report describes the research flight tests which were conducted during the course of the contract with the three basic configurations of the XH-51A helicopter; namely, the three-blade rotor, the four-blade rotor, and the compound vehicle which had a wing and an auxiliary jet engine installed. Inasmuch as this report is primarily concerned with high-speed data, low speed data have not been plotted on many of the performance figures.

A. THREE-BLADE-ROTOR FLIGHT TESTS - PHASE II

As a result of the inspections and parts interchange between the two helicopters, a limited amount of flight time was made available for further exploration of the flight envelope with the three-blade rotor and for the determination of the effect of large offsets of the center-of-gravity. During these tests with XH-51A BUNO 151262, 39 flights were made for a total of 11.6 hours.

Test conditions and performance marks attained during the Phase II three-blade rotor flight tests are summarized in Table 9. Conditions which were newly attained during this phase of testing are marked with an asterisk. Higher levels than those shown have been previously demonstrated where the item is unmarked.

Performance

Performance testing was not one of the objectives of the Phase II program. A limited amount of performance data was obtained which verified that the helicopter performance level was unchanged. Figure 36 shows power required versus true airspeed for the three-blade rotor configuration.

During the offset center-of-gravity tests, installation of the lateral ballast boom increased the drag of the helicopter by an amount equivalent to approximately 4.5 square feet of flat plate area. The added drag of this configuration reduced the high-speed capability by approximately 15 knots at normal rated power. This did not seriously affect the ability of the helicopter to perform its primary test objectives; therefore, no attempt was made to reduce the drag.

The maximum speeds attained during the Phase II testing were 150 knots true airspeed at sea level and 113 knots true airspeed at a 7,900-foot density altitude. In both cases, available engine power was the limiting factor.

Flying Qualities

The principal research objective of the Phase II program was to extend the maneuvering flight envelope beyond previously demonstrated values.

TABLE 9
SUMMARY OF PHASE II TEST CONDITIONS

*Maximum True Airspeed (level flight)	150 kts
*Maximum True Airspeed (descent)	152.5 kts (175 mph)
*Maximum Calibrated Airspeed (level flight)	144.5 kts
Maximum Density Altitude	8000 ft
*Maximum Lateral C.G. Offset (L&R)	4.38"
Maximum Longitudinal C.G. Offset	0.2" aft, 1.29" fwd
*Maximum Bank Angle	69° @ 120 kts
	52° @ 140 kts
*Maximum Load Factor	1.9g (hover)
	2.42g (100 kts)
Maximum Gross Weight	4062 lb
Maximum Shaft Horsepower	474 hp

* For each of these items, the Phase II flight envelope exceeds what had previously been demonstrated.

This was accomplished in terms of higher speeds and larger lateral center-of-gravity offsets.

Figure 37 shows the basic maneuvering stability of the helicopter over a broad range of speeds at mid center-of-gravity. These data agree quite well with previously demonstrated characteristics, and the same general conclusion is reached. That is, with full longitudinal cyclic control sensitivity (100%), speeds greater than approximately 100 knots at a mid center-of-gravity result in less-than-optimum gradient of stick force per g. In lieu of any better definition, the minimum desired level, in this regard, is defined in Specification MIL-F-8785, paragraph 3.3.9, for fighter aircraft to be 14 pounds per g. As shown in Figure 38, the reduced maneuvering stability at high speed may be compensated to a degree by reducing the longitudinal cyclic control stick sensitivity. This modification results in a requirement for a larger cyclic stick input for the same output to the control gyro. Thus, higher pilot forces are required and the general level of stability is increased. At low speeds, the reduced sensitivity tends to reduce the response of the helicopter to longitudinal cyclic control inputs. The trade-off therefore lies somewhere between low response at low speeds and excessive response at high speeds. This problem was explored in some detail during previous test programs. These previous studies and the more recent testing in Phase II indicate that either of two configuration changes will provide an improvement in the level of maneuvering stability:

1. Incorporate a longitudinal cyclic control stick sensitivity shifting device, preferably automatic and speed-sensitive, or

2. Incorporate a four-blade-rotor system.

The improvements which can be anticipated from item 1 are shown in Figure 38. Here, speeds approaching 130-140 knots are possible before the stability reduces below the 14 pounds-per-g level. The improvements possible considering item 2 above are discussed under Phase III test results.

Maneuvering stability tests with lateral center-of-gravity offsets equivalent to 2.5 and 4.5 inches indicated that the stability decreased as the lateral moment was increased. Considering the magnitude of the lateral offset, the degree of stability change is not considered to be serious. The data shown on Figures 39 through 42 indicate that under the most adverse condition the maneuvering forces remain positive to speeds in excess of 100 knots.

Static longitudinal stability and trim characteristics were evaluated briefly during Phase II. Figure 43 shows the cyclic stick trim characteristics over the speed envelope of the helicopter. The effect of

large lateral center-of-gravity offset moments (16,000 inch-pounds) is also shown on this figure. The following results are indicated:

1. Stick-fixed stability (control motion versus speed) is positive.

2. Cyclic pitch control margins are adequate to the limits of the speed envelope.

3. The lateral trim requirement to balance the offset center-of-gravity moment does not seriously affect the lateral control power.

4. Cross-coupling characteristics between pitch and roll are negligible.

The basic static longitudinal stability of the helicopter is shown on Figure 44. This level of stability is approximately the same as previously demonstrated, and is slightly positive. The speed sensor was intentionally made inoperative for these tests so that a better base line could be established for subsequent test comparisons.

The effect of lateral center-of-gravity offset on longitudinal stability is shown on Figure 45. These data indicate that no adverse characteristics occur as a result of a large lateral center-of-gravity shift. Pilot comments during the course of testing confirmed this fact. It was noted, however, that a slight difference in stability existed between a right-hand and a left-hand offset. The results of a brief series of tests indicated that the reason for this was the asymmetric drag of the boom rather than the effect of the lateral moment itself. Since the boom is not representative of any reasonable operational installation, the subject was not investigated further.

Maneuvering envelopes developed during the three-blade rotor flight tests are shown on Figure 46 for the left lateral center-of-gravity offsets and Figure 47 for the right lateral offsets. The mid center-of-gravity maneuvering envelope is shown on both figures. The maneuvering envelopes representing the contract research objective have been indicated on these figures for comparison.

Structures

Structural loads were measured during the Phase II flight tests for the expansion of the maneuvering envelope with the three-blade rotor. In addition to defining the structural characteristics of the helicopter, the loads were monitored to assure continued flight safety.

Structural load measurements were made on the main rotor hub and blades,

control gyro arms, main rotor pitch links, tail rotor and horizontal stabilizer.

The results of the strain gauge program are presented here in terms of bending moments and stress. The calibrations were effected in terms of bending moment which are readily convertible into stresses from the known structural section properties along the span of any particular hub or blade design.

Preliminary measurements obtained on the main rotor early in the program indicated hub station 7.4 as the most critical area of the hub and blade. The primary objective of Phase II was the extension of the flight envelope, and the major effort during the program was, therefore, directed to the consideration of loads and stresses at the critical station. The stresses quoted for station 7.4 are calculated from the bending moments measured at station 6.0.

For the three-blade rotor, bending moments at station 6 can be converted to stress at station 7.4 by applying the conversion factors noted below:

Station 6 Flapwise Moment x 1.56 = Station 7.4 Flapwise Stress

Station 6 Chordwise Moment x 0.126 = Station 7.4 Chordwise Stress

In this report, the load measurements are divided into two components; cyclic load and average load. The sketch below indicates what these components mean.

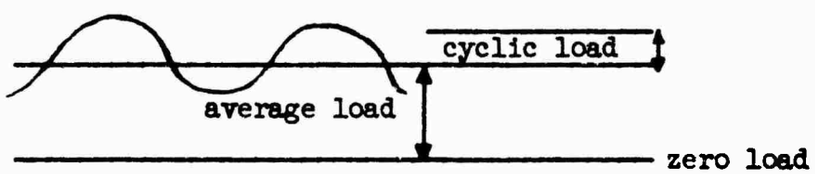

Average and cyclic main rotor bending moments, both flapwise and chordwise, are plotted against load factor and are shown for mid center-of-gravity in Figures 48 and 49. Data for a 10,000-inch-pound lateral center-of-gravity offset are shown on Figures 50 and 51 and for a 16,000-inch-pound offset on Figures 52 and 53.

Station 6 flapwise and chordwise bending moments plotted against calibrated airspeed are shown on Figure 54 for a 10,000-inch-pound center-of-gravity offset and on Figure 55 for a 16,000-inch-pound offset.

For convenience, a scale showing stress at station 7.4 is added to Figures 48 through 55.

Average Bending Stresses - Station 7.4

The highest values recorded were in the flapping plane. The average flapping stress variation was linear with load factor, being zero at 1.3g with a mid center-of-gravity offset and zero at 1.15g with a lateral center-of-gravity offset and increasing 32,000 psi for each 1.0g increment in load factor. The change of load factor for zero bending stress is due to the somewhat higher average test weight at the offset center-of-gravity. The maximum flap bending stresses were 37,000 psi at 0.07g and 34,000 psi at 2.3g. The average chordwise stresses were not significantly g sensitive; the level varied from 1,300 psi to 4,800 psi generally.

Cyclic Stresses - Station 7.4

A stress concentration factor of less than 3 has been estimated for station 7.4. The conservative use of a factor of 3 realizes an endurance stress of 26,000 psi. For average pull-up conditions, the cyclic flapping stress is around 20,000 psi and the cyclic chordwise stress around 9,000 psi. Assuming the moments are in phase, the average combined stress in maneuvers is about 29,000 psi which is only slightly above the estimated endurance stress of 26,000 psi. The number of cycles of stress above the endurance limit that would be accumulated due to maneuvers is relatively low compared to the ability to take millions of cycles at 26,000 psi; therefore, normal maneuvers should have very little damaging effect on the fatigue life. The highest combined cyclic stresses for the whole series of maneuvers were obtained in the pushover to 0.63g at 50 knots airspeed. Assuming the loads are in phase, the combined stress would be 44,000 psi. The combined stresses for the pull-up to 2.34g were 40,400 psi. These results illustrate that the cyclic stresses at the critical section are mainly a function of severity of pilot control input (which governs the blade flapping moment) rather than the load factor obtained (which has an effect mainly on the chordwise moments). The type of transient loads and stresses described above are included in the fatigue analysis (reference 2) and in the fatigue tests.

The lateral center-of-gravity displacements did not have a deleterious effect on the stresses obtained at the load factors flown. Each stress value shown on all curves versus load factor is the maximum value recorded during the maneuver and is not necessarily associated with the maximum load factor or the maximum average stress.

The stresses recorded line up well with the values anticipated for this hub design, and only minor design changes are required to reduce the levels should such a move be desired.

Vibration

Cabin vibration levels were recorded during Phase II flight testing and are shown in Figure 56. No effort was made to alter the vibration characteristics of the helicopter during this phase of the contract.

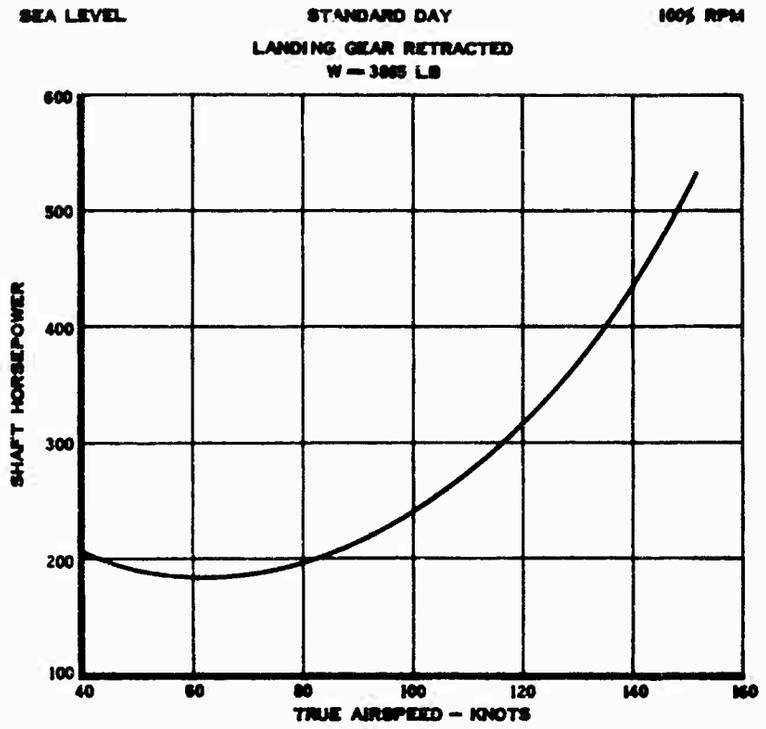

Figure 36. Level Flight Performance - Three-Blade Rotor.

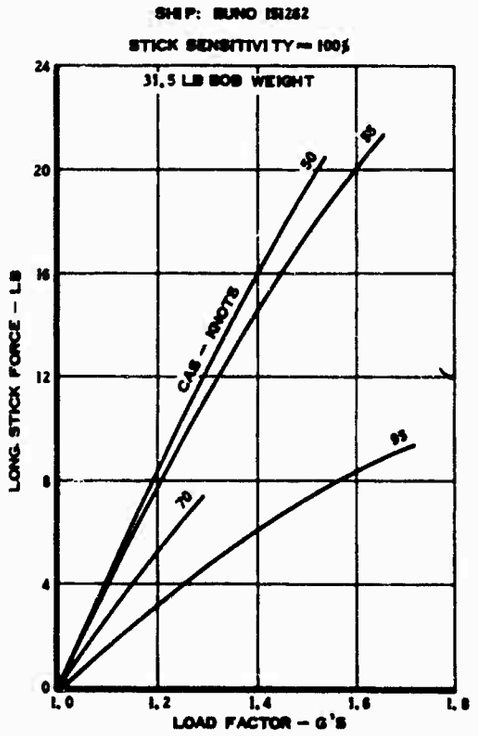

Figure 37. Maneuvering Stability - Three-Blade Rotor.

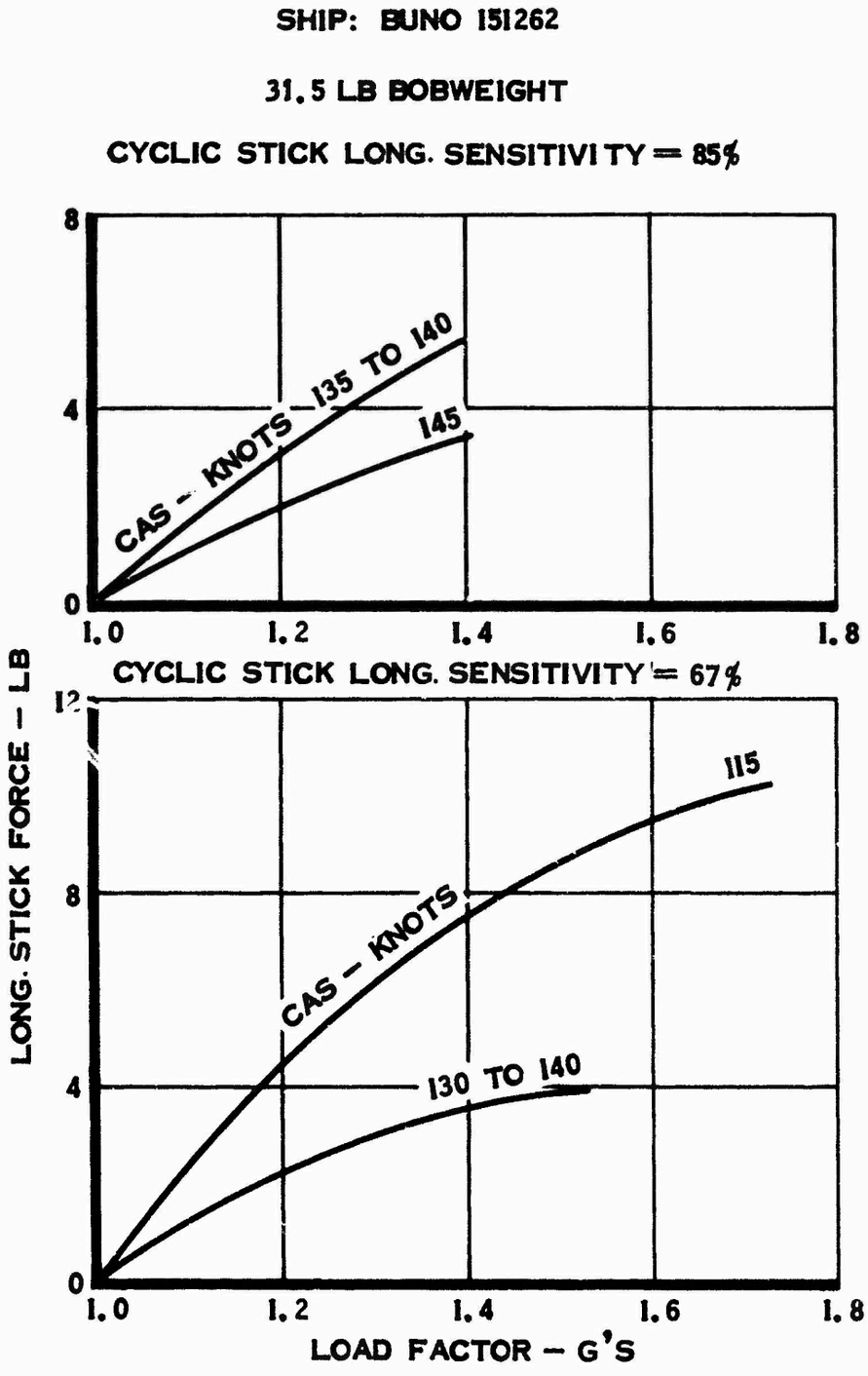

Figure 38. Maneuvering Stability, Mid Center-of-Gravity - Three-Blade Rotor.

RIGHT-HAND LATERAL OFFSET – 10,000 IN – LB

SHIP: BUNO 151262

31.5 LB BOBWEIGHT

CYCLIC STICK LONG. SENSITIVITY = 100%

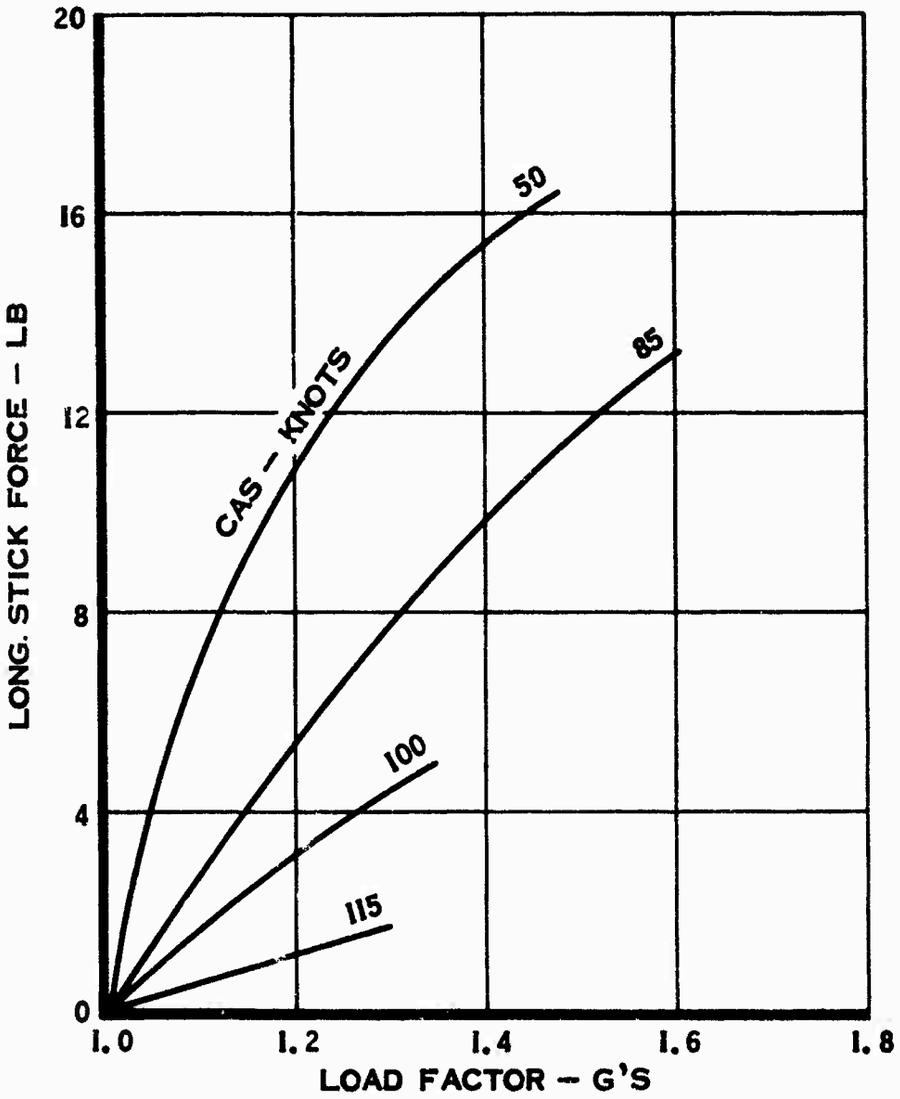

Figure 39. Maneuvering Stability, Mid Center-of-Gravity - Three-Blade Rotor.

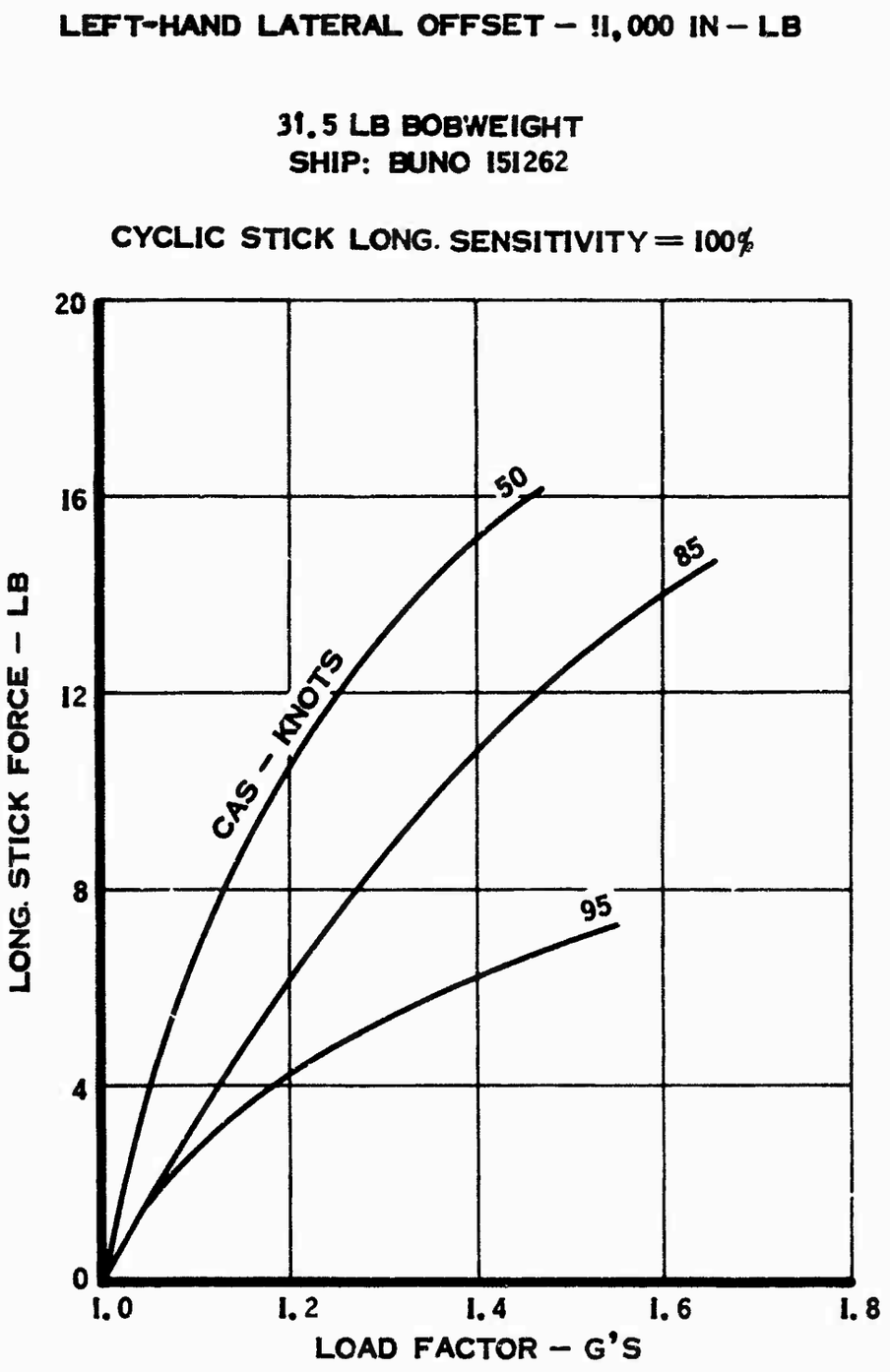

Figure 40. Maneuvering Stability - Three-Blade Rotor.

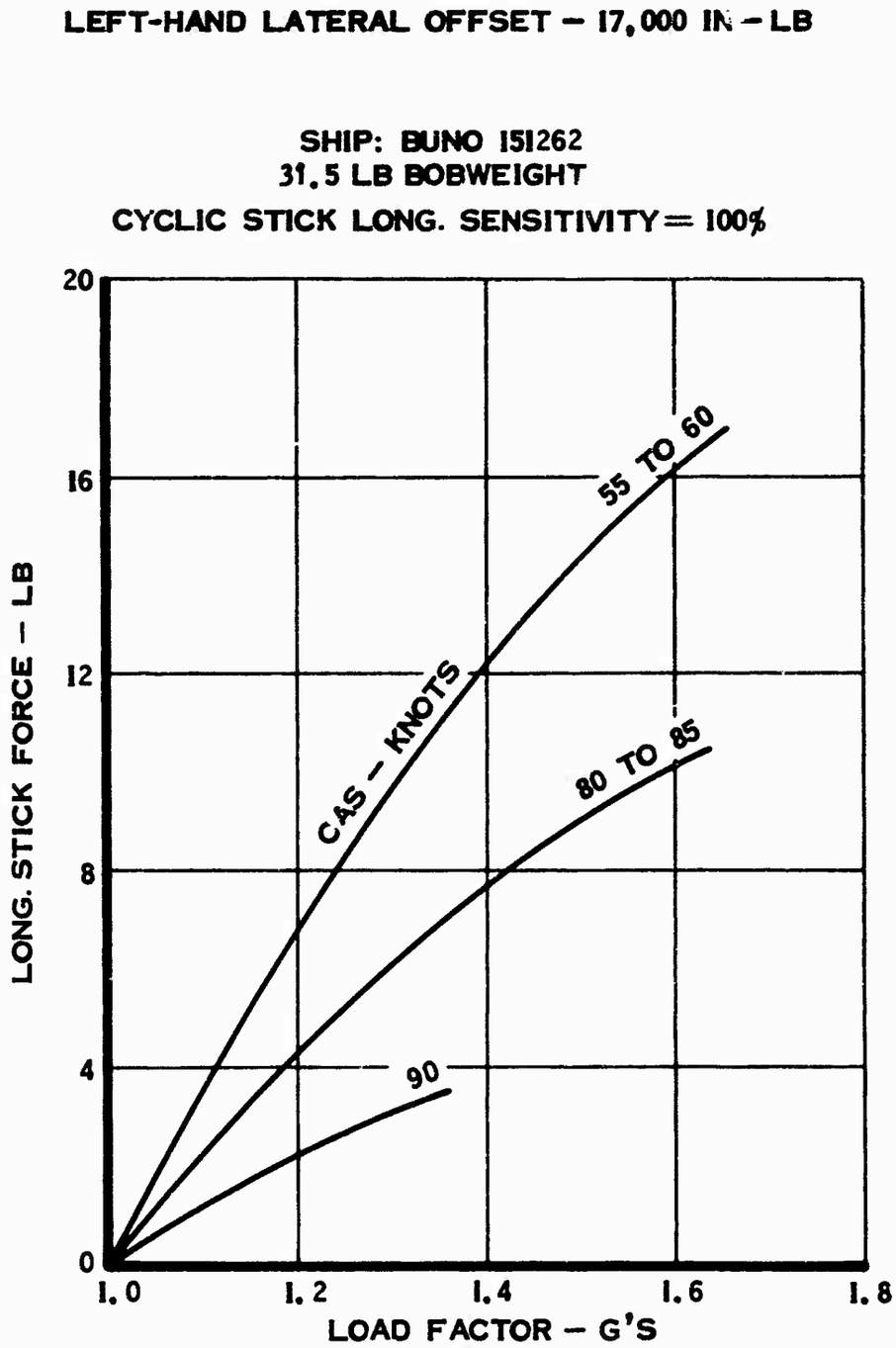

Figure 41. Maneuvering Stability - Three-Blade Rotor.

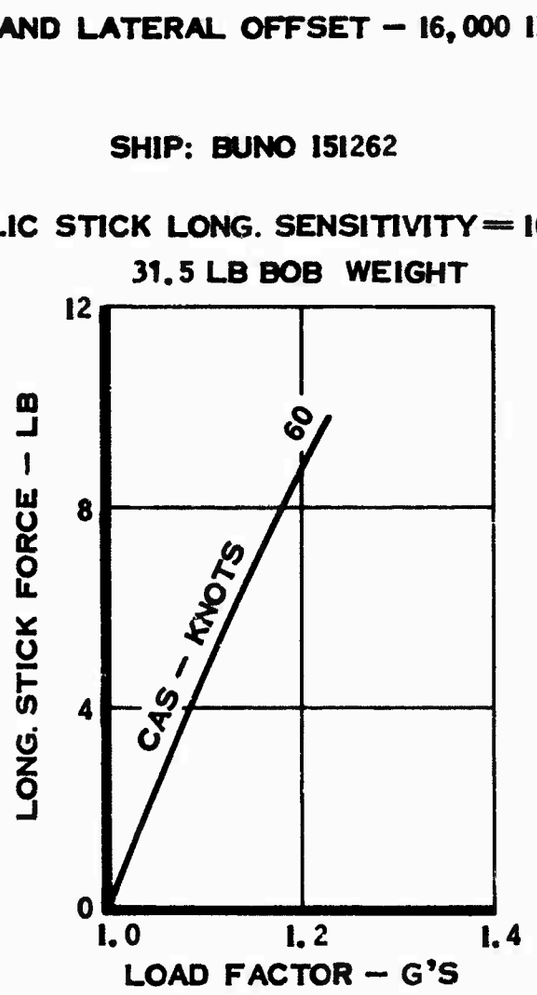

Figure 42. Maneuvering Stability - Three-Blade Rotor.

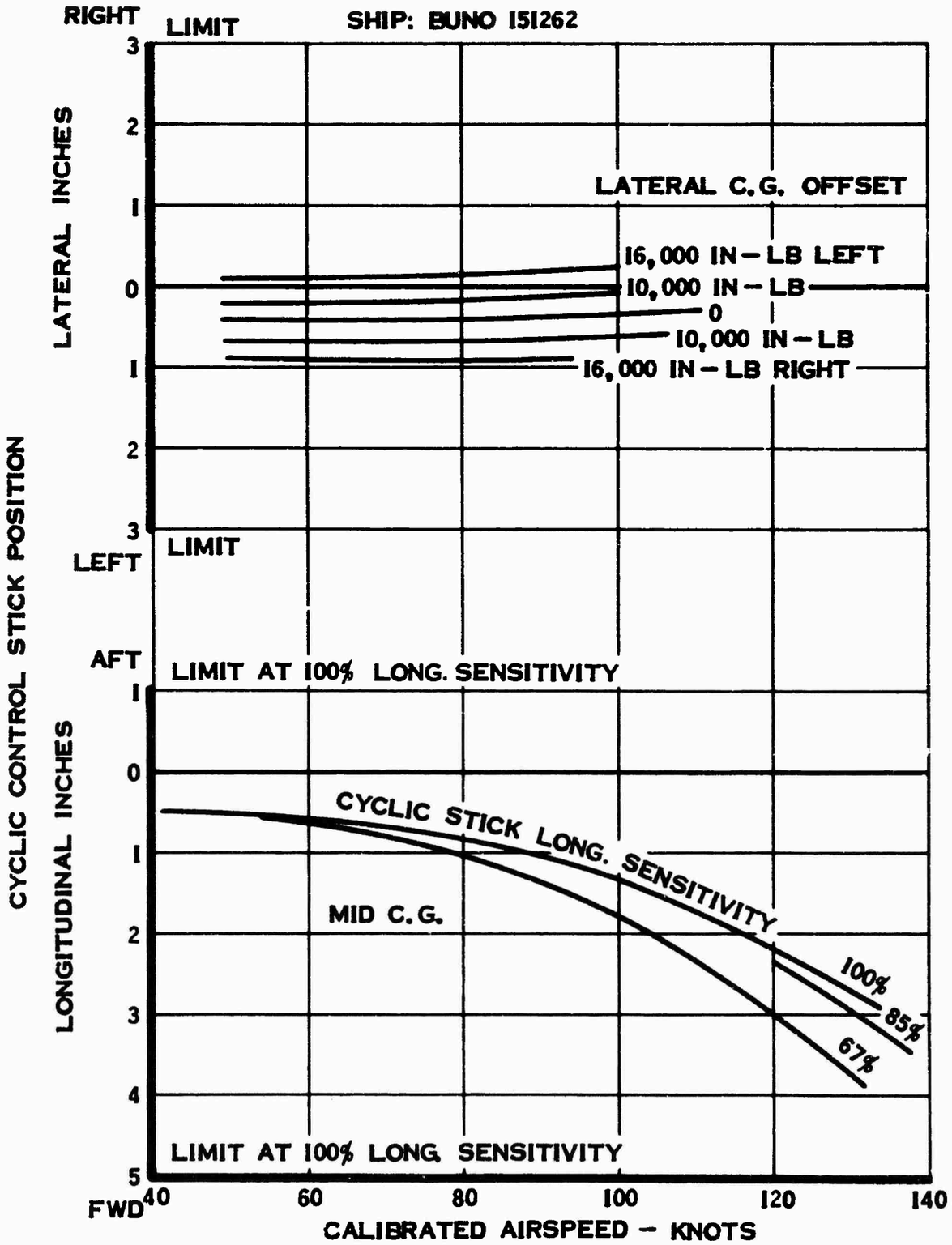

Figure 43. Cyclic Pitch Control to Trim - Level Flight - Three-Blade Rotor.

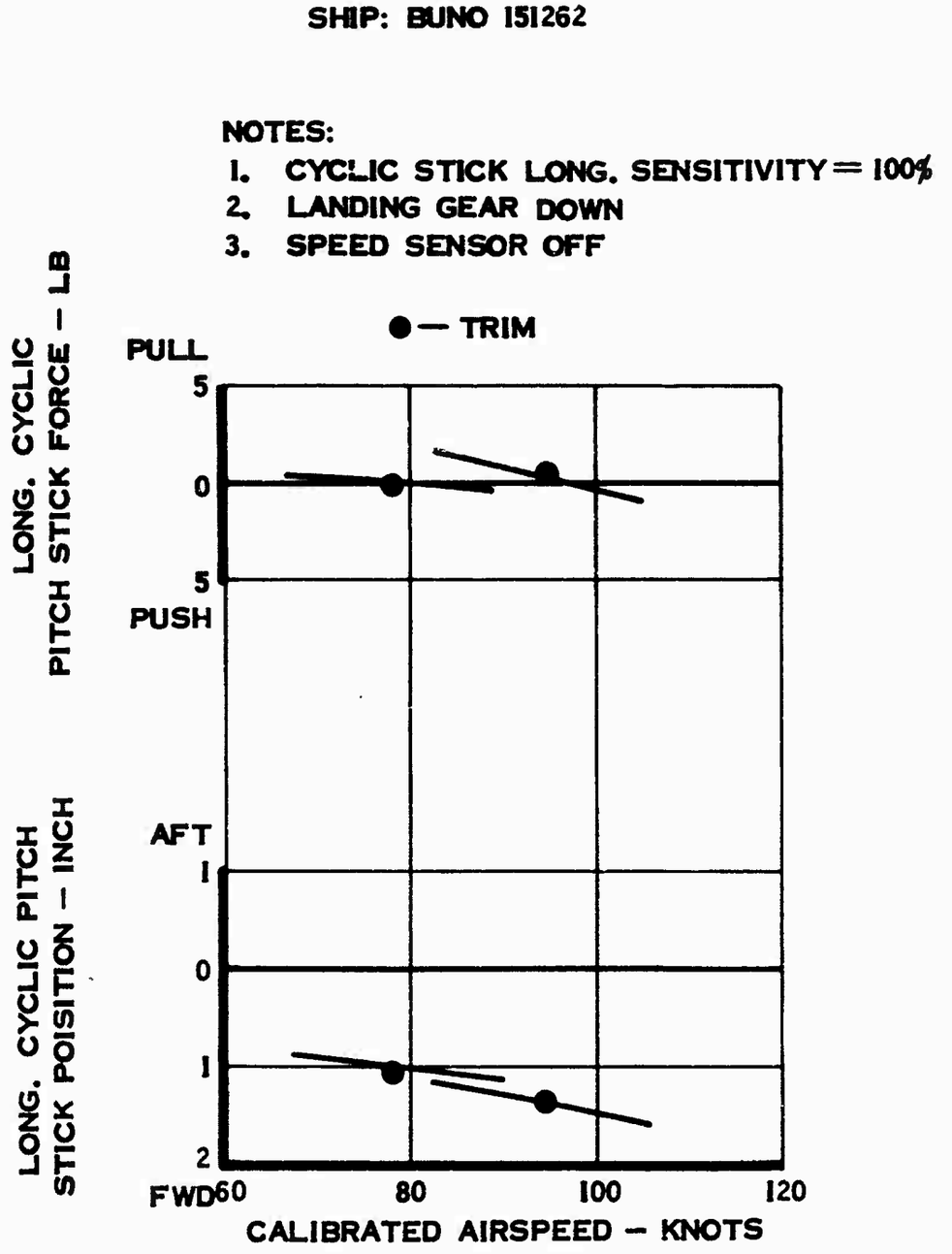

Figure 44. Static Longitudinal Stability - Three-Blade Rotor.

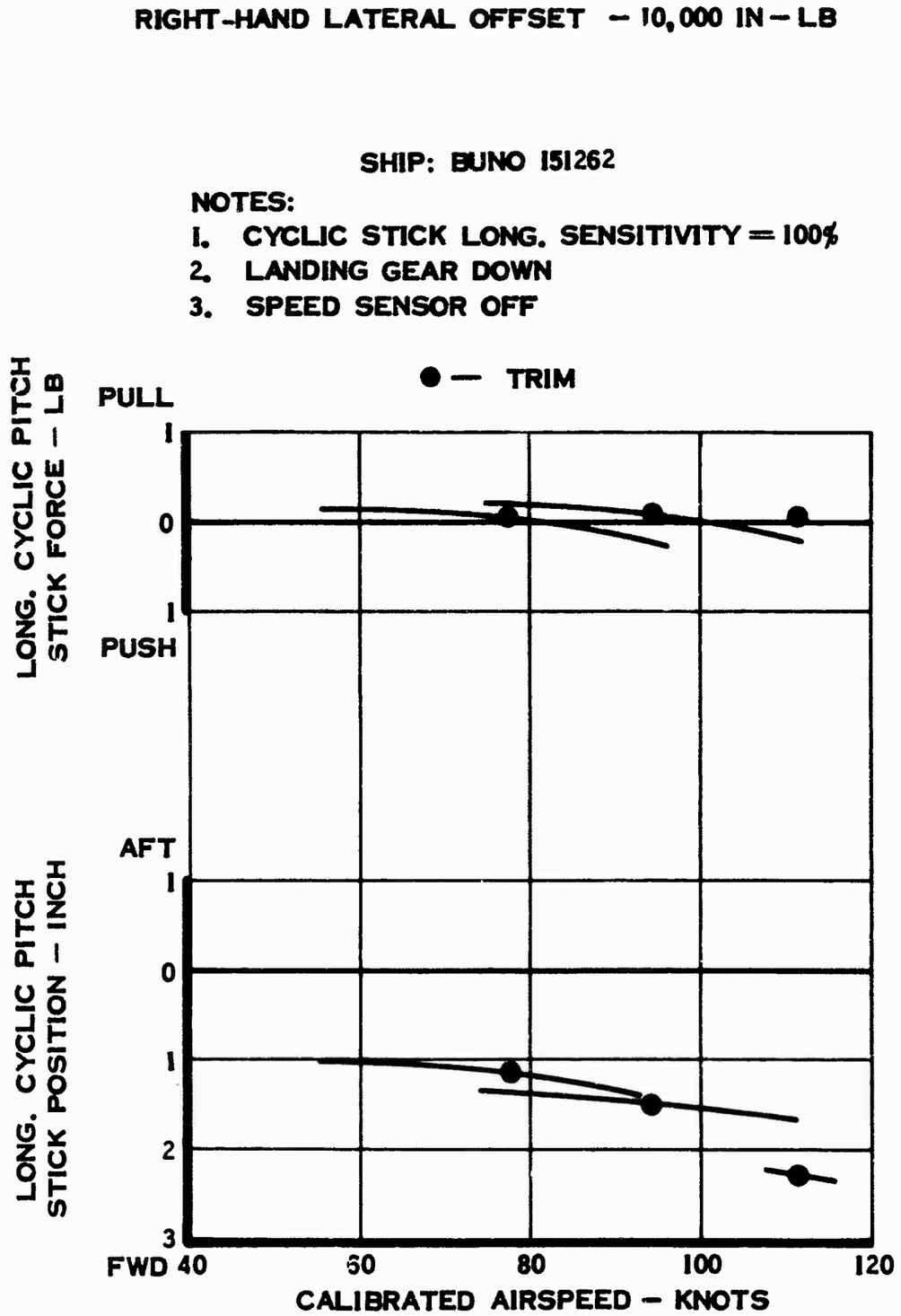

Figure 45. Static Longitudinal Stability - Three-Blade Rotor.

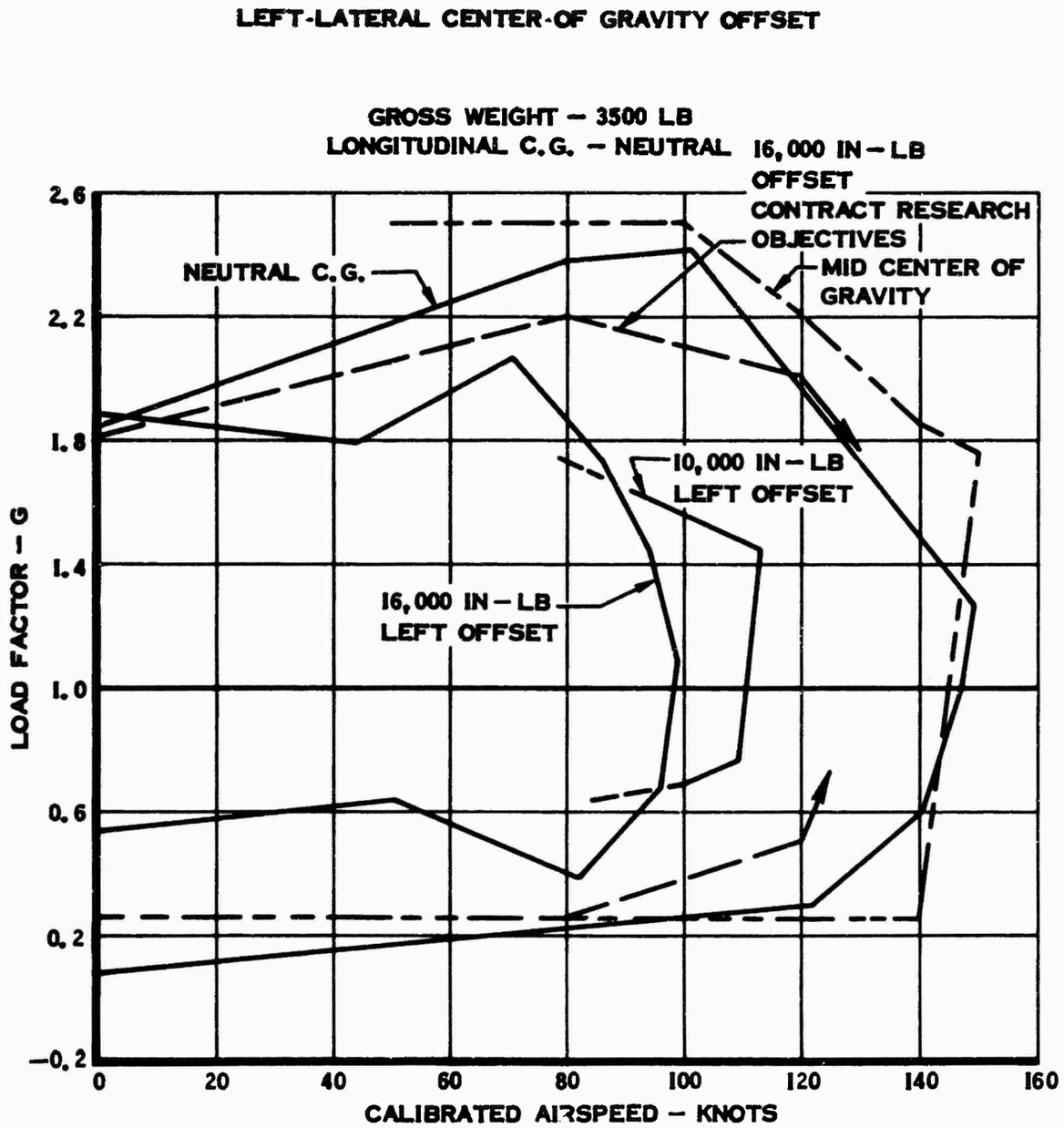

Figure 46. Maneuvering Envelope - Three-Blade Rotor.

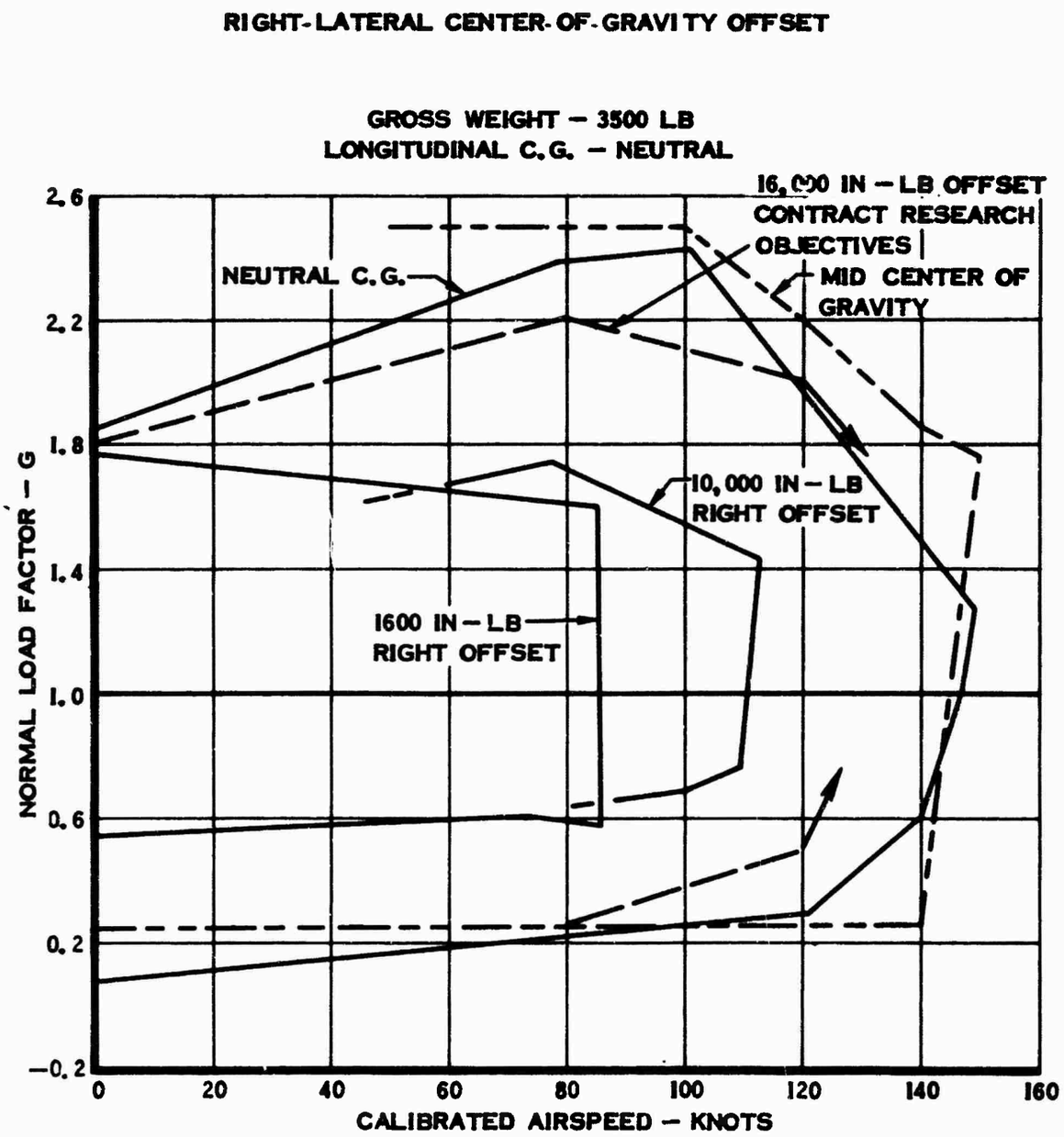

Figure 47. Maneuvering Envelope - Three-Blade Rotor.

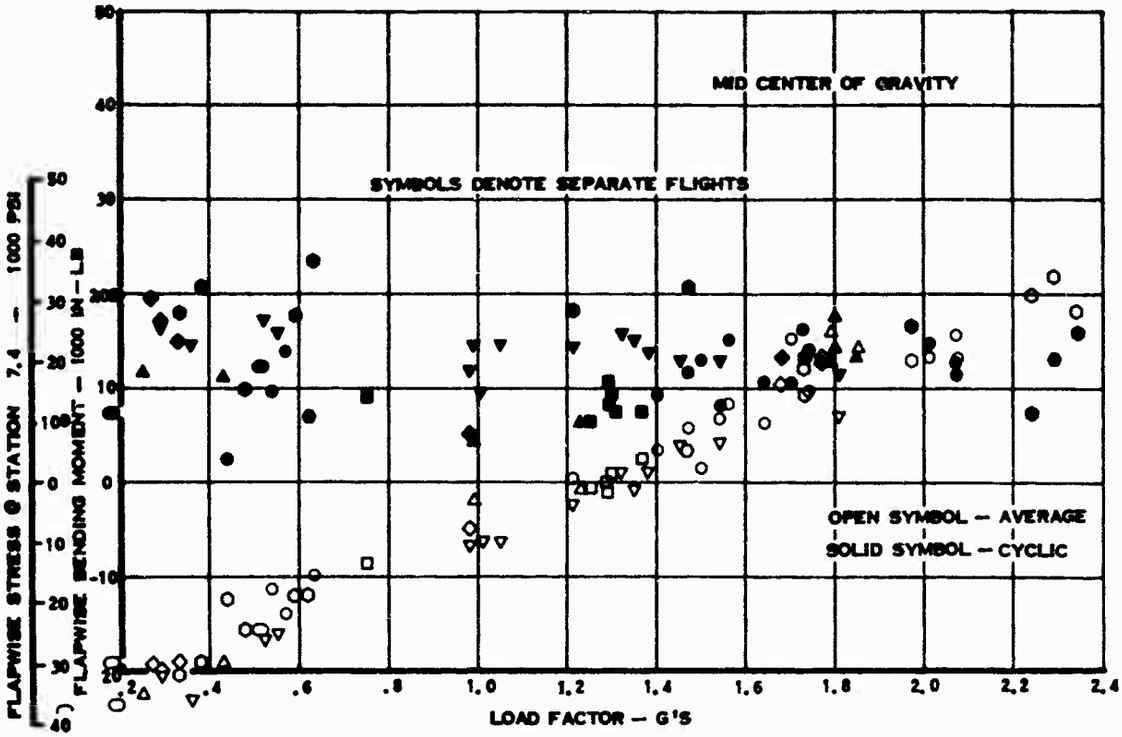

Figure 48. Flapwise Bending Moment at Station 6 Versus Load Factor - Three-Blade Rotor.

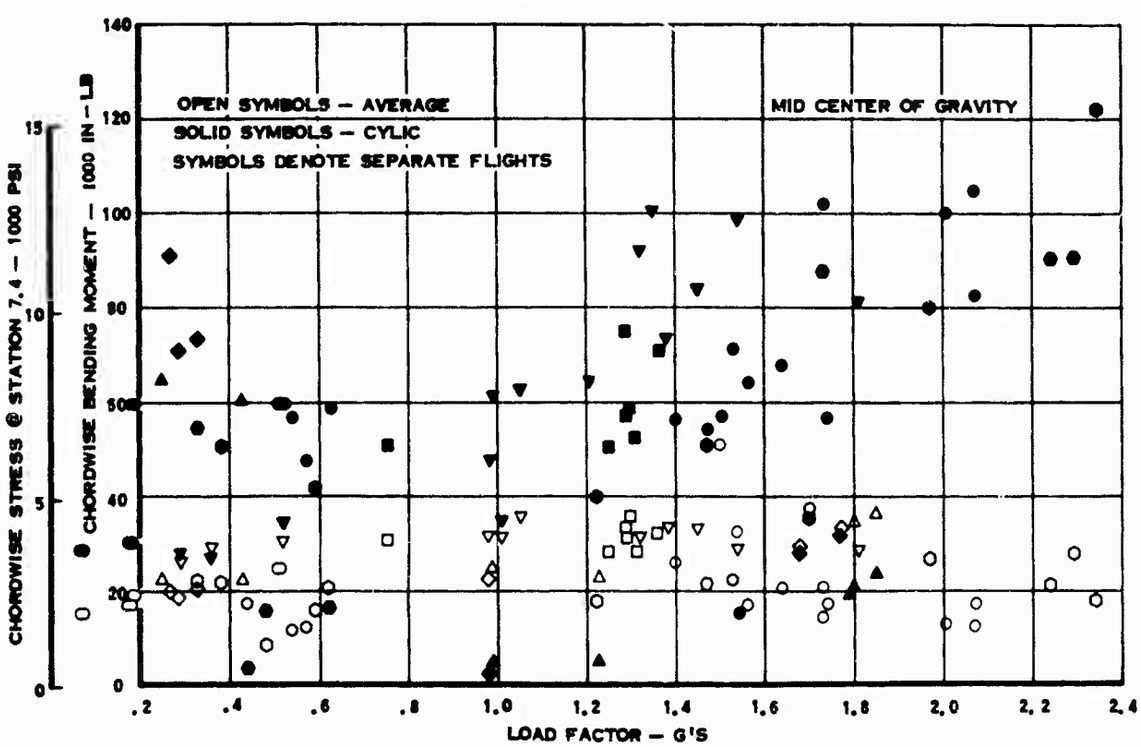

Figure 49. Chordwise Bending Moment at Station 6 Versus Load Factor - Three-Blade Rotor.

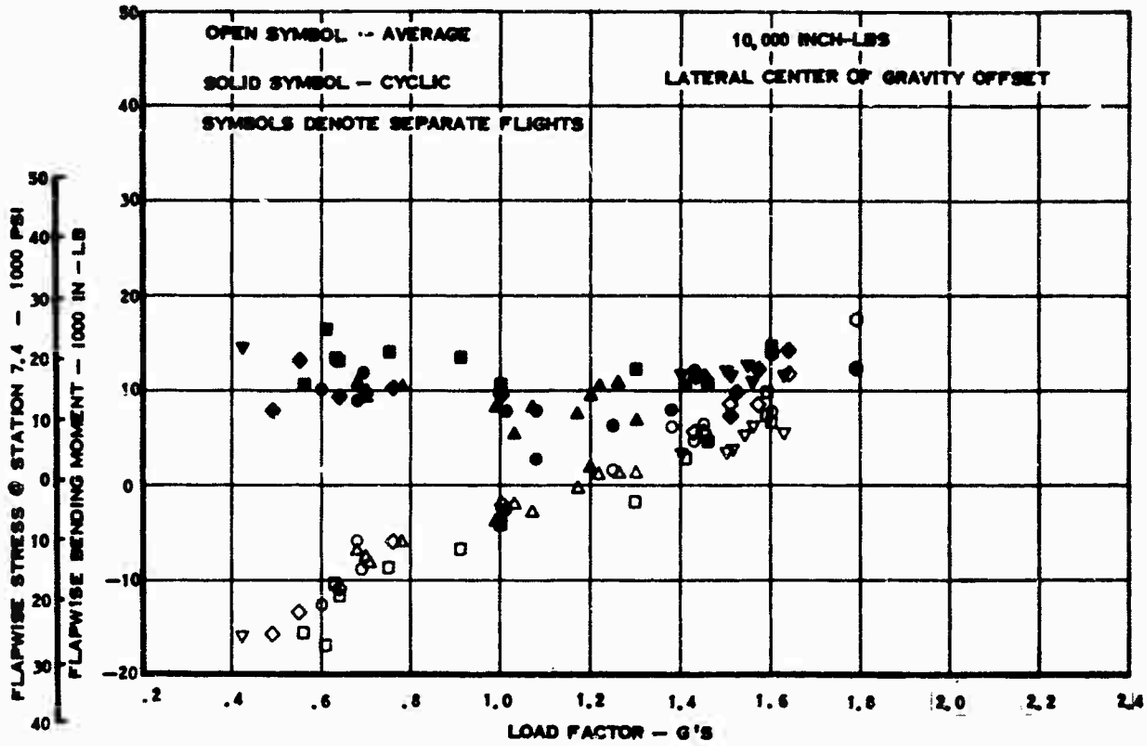

Figure 50. Flapwise Bending Moment at Station 6 Versus Load Factor - Three-Blade Rotor.

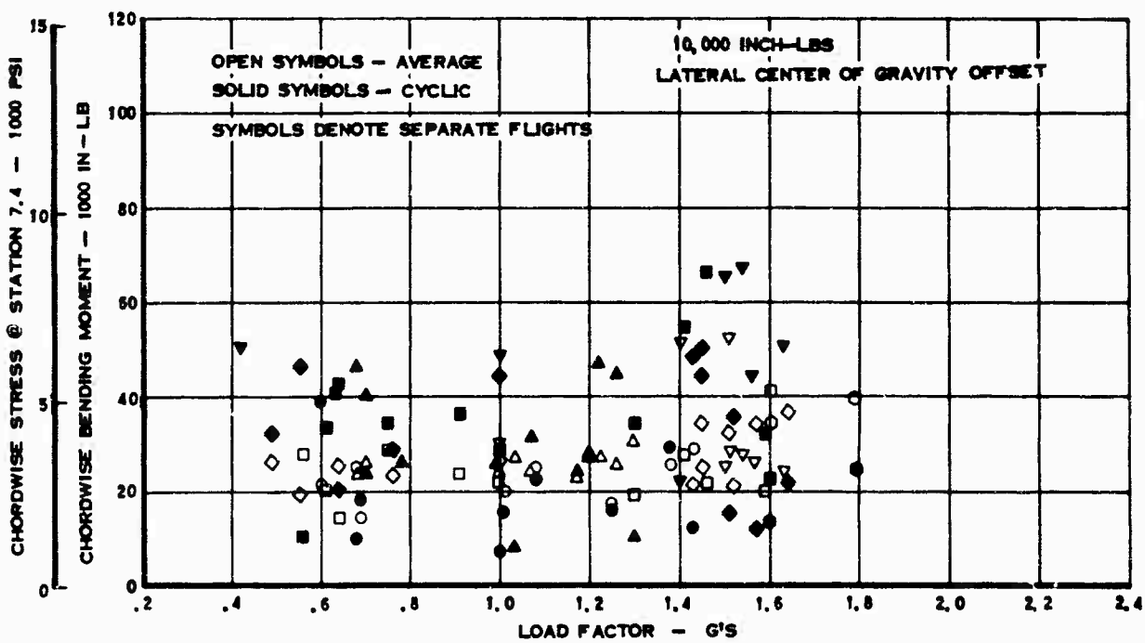

Figure 51. Chordwise Bending Moment at Station 6 Versus Load Factor - Three-Blade Rotor.

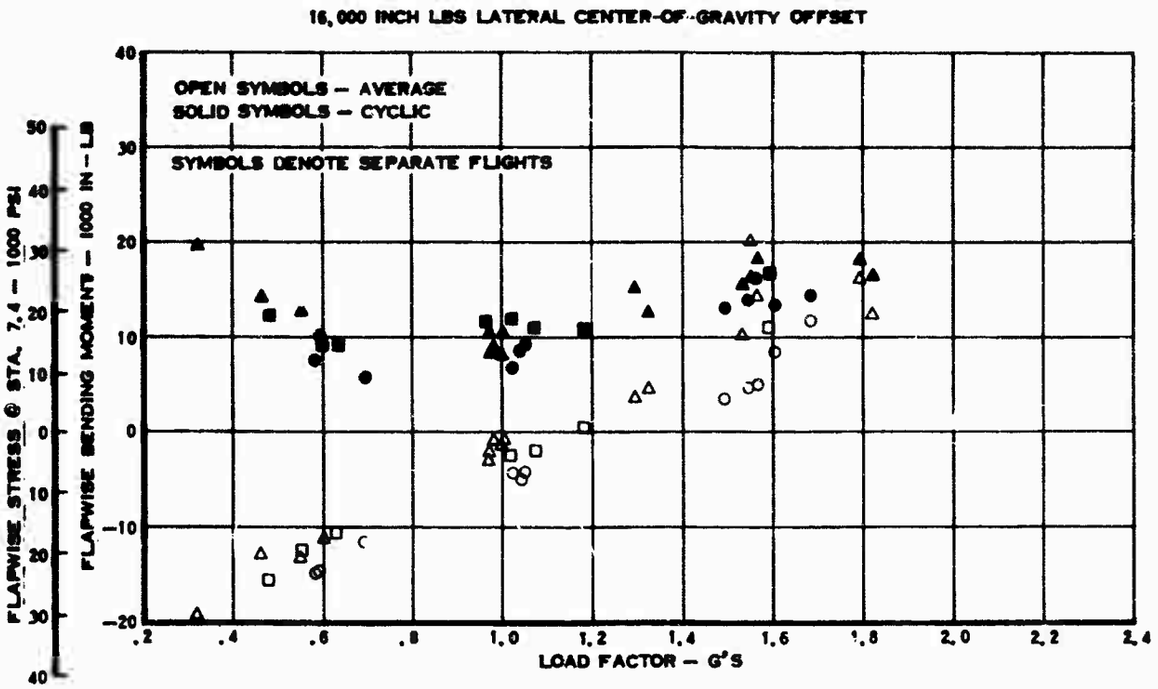

Figure 52. Flapwise Bending Moment at Station 6 Versus Load Factor - Three-Blade Rotor.

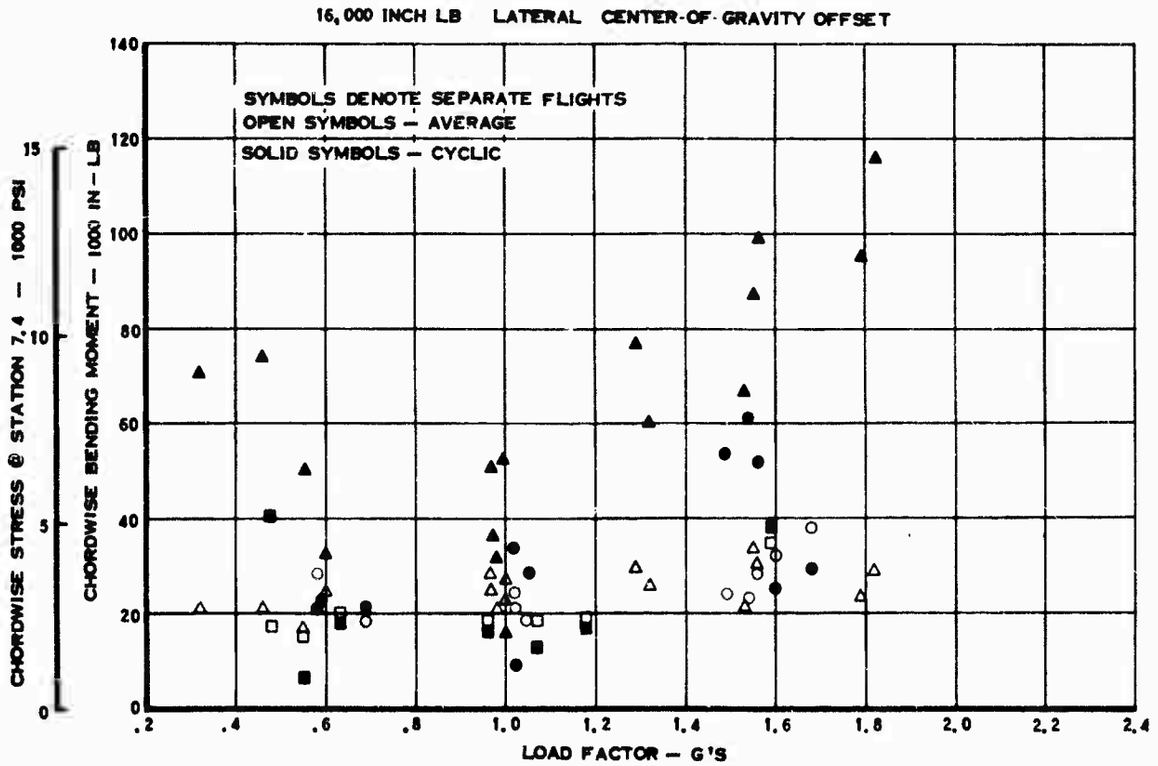

Figure 53. Chordwise Bending Moment at Station 6 Versus Load Factor - Three-Blade Rotor.

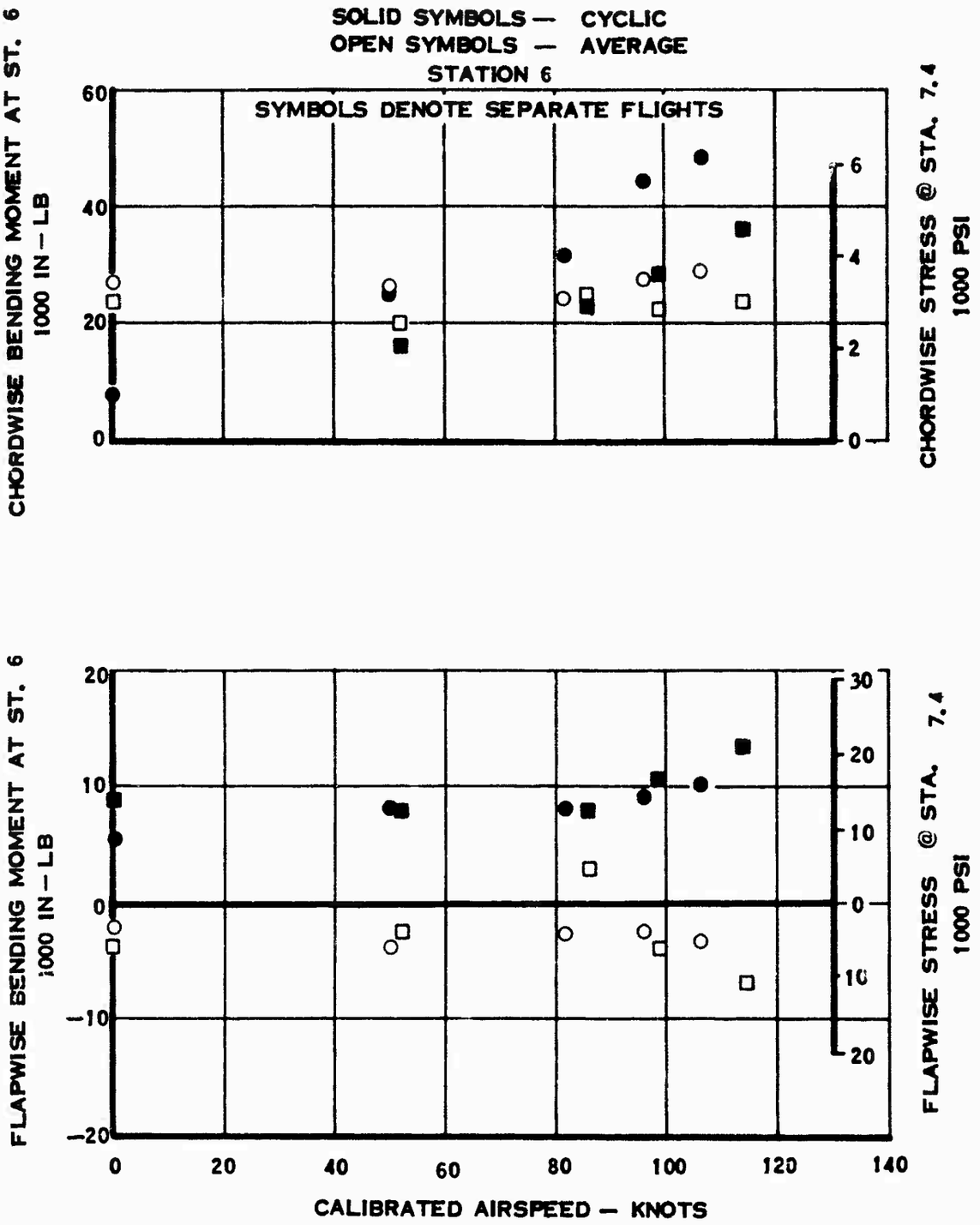

Figure 54. Blade Loads Versus Calibrated Airspeed - 10,000 Inch-Pounds Lateral Center-of-Gravity Offset - Three-Blade Rotor.

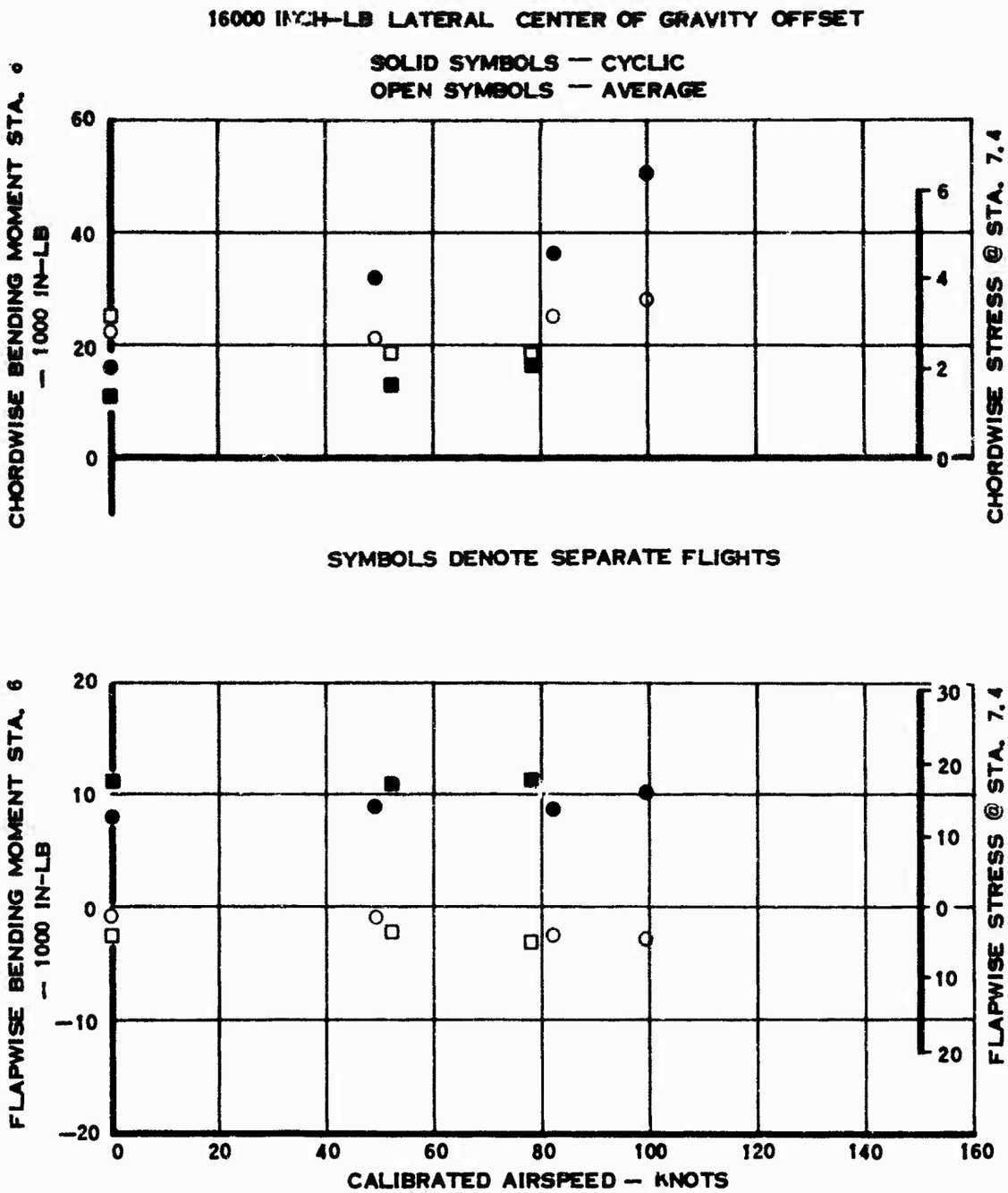

Figure 55. Blade Loads Versus Calibrated Airspeed - 16,000 Inch-Pound Lateral Center-of-Gravity Offset - Station 6 - Three-Blade Rotor.

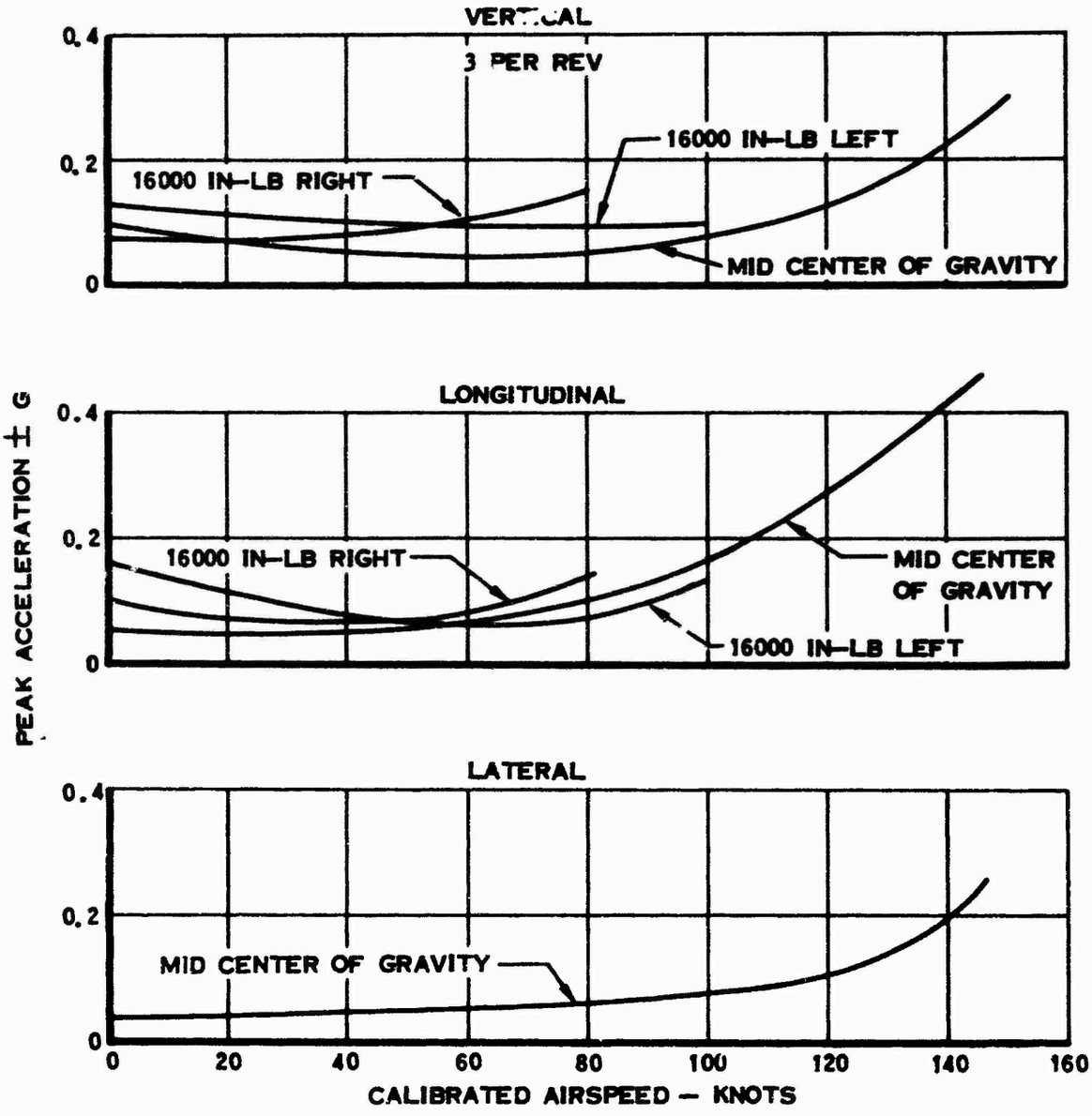

Figure 56. Effect of Lateral Center-of-Gravity Offset on Pilot Seat Vibration Levels - Three-Blade Rotor.

B. FOUR-BLADE-ROTOR FLIGHT TESTS - PHASE III

During the preparation for and execution of the Phase II flight tests, a four-blade rotor system was designed, fabricated and ground tested in preparation for the Phase III flight tests. The four-blade rotor system was installed on XH-51A BUNO 151262 following completion of the three-blade tests. Ground and flight tests were conducted in this configuration to establish an initial base line of data with the four-blade rotor. These data were used for comparison with the three-blade system and for verification of the selection of the four-blade system in the compound helicopter.

During the Phase III flight tests, 49 flights were made during 14.9 flight hours.

The major problem areas encountered during this portion of the research flight program consisted of excessive structural loads in the main rotor system and excessive cabin vibration levels. The results of development efforts directed against these problems are discussed in the following paragraphs.

Table 10 summarizes the performance goals and other flight conditions which were reached during the Phase III flight testing with the four-blade-rotor system.

Performance

Performance tests during Phase III were limited to hover tests in ground effect and out of ground effect and a level flight speed-power polar. The results of these tests are shown on Figures 57 and 58.

The hover performance is compared with the three-blade-rotor configuration hover data and indicates that the four-blade system requires approximately 30 additional horsepower to hover out of ground effect.

Level flight performance of the three-blade and four-blade configurations is shown on Figure 58. A direct comparison of the performance shown on this figure is not possible, due to the fact that external tuning weights were attached to each blade of the four-blade rotor at the 5-foot radius. The additional drag of these external weights

TABLE 10
SUMMARY OF PHASE III TEST CONDITIONS

Maximum True Airspeed (level flight)	135.5 kts
Maximum True Airspeed (rapid descent)	172 kts (198 mph)
Maximum Calibrated Airspeed (level flight)	132.5 kts
Maximum Altitude	4300 ft
Maximum Lateral C.G. Offset	0.72 in
Maximum Longitudinal C.G. Offset	2.15 aft, 1.63 fwd
Maximum Bank Angle	65°
Maximum Load Factor	2.71g (hover)
	2.52g (120 kts)
Maximum Gross Weight	4036 lb
Maximum Shaft Horsepower	435 hp

has not been computed since they are not representative of a production installation but were merely used as a research tool.

Flying Qualities

As discussed in a previous section of this report, one of the advantages of the four-blade rotor was expected to be an improvement in the maneuvering stability (or stick force per g). Figure 59 presents the maneuvering stability for speeds up to 100 knots. This curve, when compared with the Phase II results, shows that the anticipated improvement was realized. In addition to the quantitative results shown on Figure 59, the pilots have reported that the maneuvering forces remain comfortably strong over the entire flight envelope. Thus, the unsatisfactory condition reported for the three-blade rotor has been entirely eliminated by the installation of the four-blade rotor. This improvement was a strong factor verifying the selection of the four-blade rotor system for the Phase IV compound helicopter program.

Figure 67 is the maneuvering envelope for the four-blade rotor system. At a center of gravity of 1.5 inches forward, the envelope is substantially 2.5 to 0.2g up to 120 knots calibrated airspeed with reducing normal acceleration out to 165 knots calibrated airspeed. The aft envelope was opened up in only three or four flights, and no specific attempt was made to exceed the Phase II envelope. While it was felt that there would be little point in extending the hover beyond the 0.15 to 2.7g demonstrated, no structural, performance, or stability limits were encountered in forward flight.

Control power both laterally and longitudinally with the four-blade rotor installed is similar to that for the three-blade configuration, except the strong increase in longitudinal control effectiveness which was characteristic of the three-blade system at high speeds has been eliminated. This further indicates the improved maneuvering stability associated with the four-blade configuration. Figures 60 and 61 reflect the results of the control power testing of the four-blade system.

Static longitudinal stability and control motion characteristics are shown on Figures 62 and 63. The first figure indicates that the control motion for trim has a positive slope for the four-blade system. More than adequate control is available for maneuvering at all speeds within the demonstrated envelope. Control cross coupling of the four-blade system is stronger than on the three-blade system. This factor, although annoying, had no adverse effect on the conduct or the results of the Phase III testing, and, therefore, no corrective action to reduce or eliminate cross coupling was warranted.

Stick-fixed and stick-free static longitudinal stability, shown on

Figure 63, varies from lightly positive at low and intermediate speeds to neutral at high speed. Several simple design changes can be incorporated, such as aerodynamic shaping of the gyro arms or activation of the speed sensor, if stronger stability is desired. Neither of these changes was incorporated during Phase III since strong static stability was not one of the program objectives. The ability of the helicopter to return to trim following an off-trim release of the controls is indicative of the low friction level of the cyclic control system.

A number of autorotation entries were made at speeds of from 60 to 120 knots. A typical time history of a 120-knot entry is shown on Figure 64 (sheets 1 and 2). The slight nose-down trim shift accompanying the collective reduction was easily corrected by the pilot and required less than 1 inch of cyclic stick travel. No adverse characteristics were noted during any of these maneuvers.

Rotor rpm control during autorotation as a function of normal load factor was investigated at a speed of approximately 80 knots, as shown on Figure 65. The purpose of this test was to provide base line data for comparison with the compound helicopter autorotation characteristics and to develop piloting techniques for the very high speed autorotation entries anticipated in the compound helicopter flight test program.

The results of this test indicate that control of airspeed and rotor speed during the initial stages of autorotation entry at flight speeds beyond normally accepted rotary wing limits is more readily attainable by holding the collective in a nearly fixed position while regulating rotor speed with load factor application and airspeed with descent rate. Control by use of both collective and cyclic control while attempting to keep rotor speed within prescribed limits and reducing airspeed to an appropriate range is less readily attainable.

Cyclic and collective blade angle variations in level flight are shown on Figure 66. These data indicate that no blade angle limits are approached over the flight envelope investigated during Phase III.

Structures

Structural loads recorded during Phase III testing included loads in the main rotor hub and blades, gyro control arms, main rotor pitch link, tail rotor and tailplane. To assure continued flight safety, an incremental approach was employed during the tests, flight records being examined prior to each additional envelope expansion.

Rotor Stresses

A review of all structural data indicates that, for the four-way hub, station 7.0 is the critical fatigue section of the rotor. Assuming a stress concentration of 3, the endurance limit stress is 26,000 psi. The strain calibrations were effected in terms of bending moment rather than stress because the bending moment curve along the span of hub and blade is predictable. The conversion of bending moment to stress at station 7.0 is as follows:

Flapwise bending moment @ station 6.0 x 1.42	= station 7.0 stress
Chordwise bending moment @ station 6.0 x 0.152	= station 7.0 stress

Figure 68 shows that during the initial flights the chordwise bending stress was 40% lower than that in the three-blade, but the flapping stress was up by 80% to 90%. At this stage, the vibration was very high, and a series of changes in transmission suspension springs was initiated to reduce both vibration and stress. The pitch spring rate was varied first; the range covered was 6,400 pounds per inch to solid while both vertical and lateral remained solid. From the structural loads and vibration results, 11,000 pounds per inch was selected as the pitch spring rate to be held constant during vertical spring variations. The vertical spring range covered was from solid links down to as soft as 4,000 pounds per inch. A spring rate of 6,000 pounds per inch was selected from the results of this test series.

Harmonic analysis of the cyclic flapwise bending at station 6 during forward flight and flare showed relatively high content of three per revolution (3P) and five per revolution (5P) loads superimposed on the one per revolution (1P) loads. Blade natural frequencies in the second flapwise bending mode and the third flapwise bending mode were quite close to and slightly below the 3P and 5P forcing frequencies. Flight tests conducted at rotor speeds below and above normal 100% rated speed indicated reduced blade bending response at the higher rotor speed where the forcing frequencies were further separated from the blade natural frequencies. The 3P bending moments were reduced 45% and the 5P moments 55% below the previous levels.

Based on the results of these tests, external 13-pound weights were mounted on each blade at station 60 near the anti-nodes of the second and third flapwise modes to lower the natural frequencies of these modes. With the weights installed, at 100 knots the 3P bending moment was reduced from 4,090 inch-pounds to 2,400 inch-pounds and the 5P moment was reduced from 1.960 inch-pounds to 740 inch-pounds. With reduced bending moments, the 3P and 5P driving forces which produce the 4P pitching and rolling moments in the fuselage were reduced. Only slight

reduction was afforded in the fuselage, however.

In an effort to reduce the vibration levels further, a transmission mounting spring with a rate of 19,000 pounds per inch was installed to provide softness in transmission roll. A slight reduction in vibration resulted but there was no further change in structural loads. Figure 69 shows the main rotor structural loads and stresses following the configuration changes described above.

The flight data showed the 1P flapwise bending to be increasing with increased flight speed in a phase relationship to produce nose-down pitching, or to resist fuselage nose-up pitching. These data indicated that the horizontal stabilizer incidence was excessively negative and should be reset for longitudinal trim at higher speeds. Accordingly, the tailplane incidence was changed from -5-1/2 degrees to -3 degrees. Figure 70 shows the reduction in the flapwise bending moment increase with increasing flight speed following the incidence change.

Figures 71 and 72 show the effect of load factor on the flapwise bending moment at station 6 for two center-of-gravity positions. The average moment increases toward up bending with increased load factor, and down bending is recorded at 1.0g due to the precone angle of the hub. The smaller precone angle of the three-blade rotor and the 30% greater lift per blade resulted in the different levels of average flapwise bending moment.

Four-blade rotor cyclic chordwise stresses, Figure 73, at the aft center-of-gravity were of the order of 10% lower than those in the three-blade rotor at a mid center-of-gravity. At the forward center-of-gravity, Figure 74, the cyclic chordwise stresses were about 30% lower than with the three-blade rotor at mid center-of-gravity.

Chordwise average and cyclic bending moments in maneuvers were 50% lower than in the three-blade rotor except at high load factors where the reduction in average moment was approximately 10%. The cyclic flapwise and chordwise stresses at station 6 as shown are the maximum that occurred during the maneuvers and do not necessarily coincide with the maximum load factor.

Vibration

Vibration level in the cabin was measured for speeds up to 132 knots calibrated airspeed in level flight and up to 165 knots calibrated airspeed in descent. Vertical, fore and aft, and lateral measurements were made on the cabin floor at the pilot's seat. The data obtained are shown on Figure 75. The high vibration level remaining at the termination of Phase III was the only problem of any significance and was the factor which limited the speeds attainable.

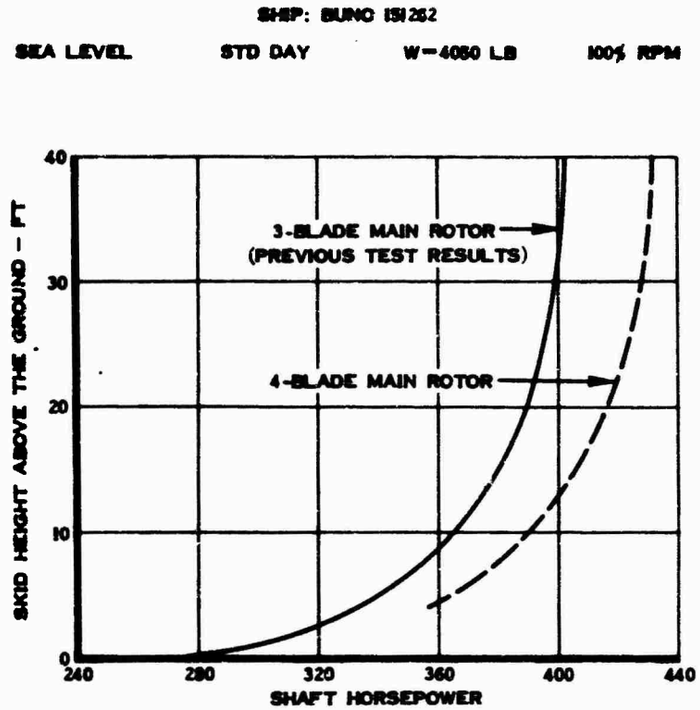

Figure 57. Comparison of Three-Blade and Four-Blade Rotor Hover Performance.

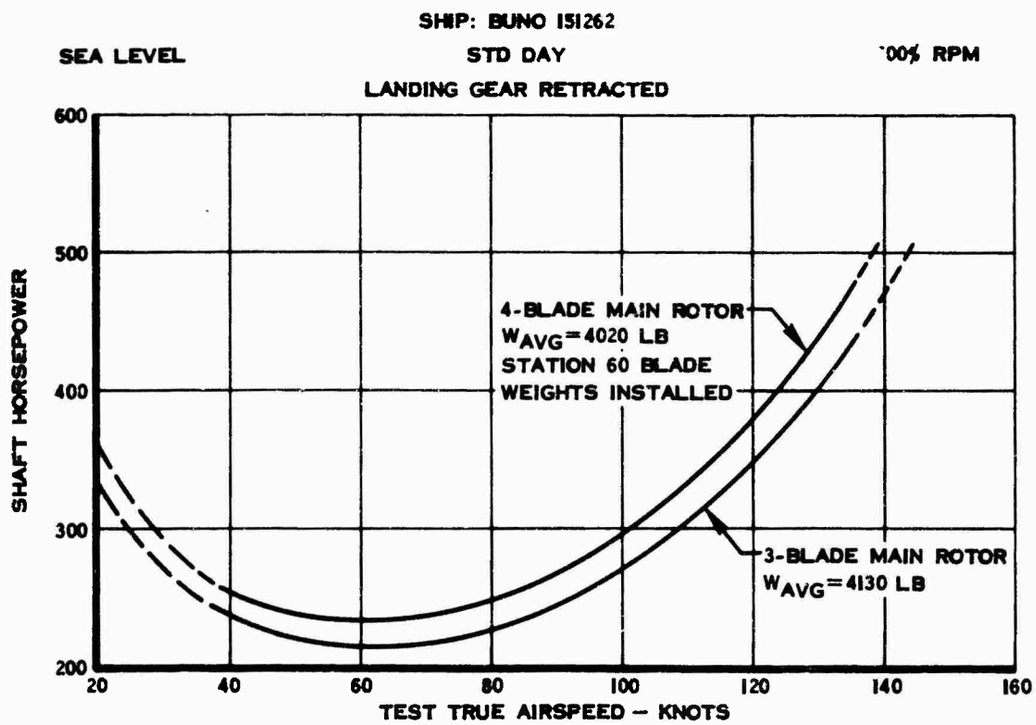

Figure 58. Level Flight Performance - Comparison of Three-Blade and Four-Blade Performance.

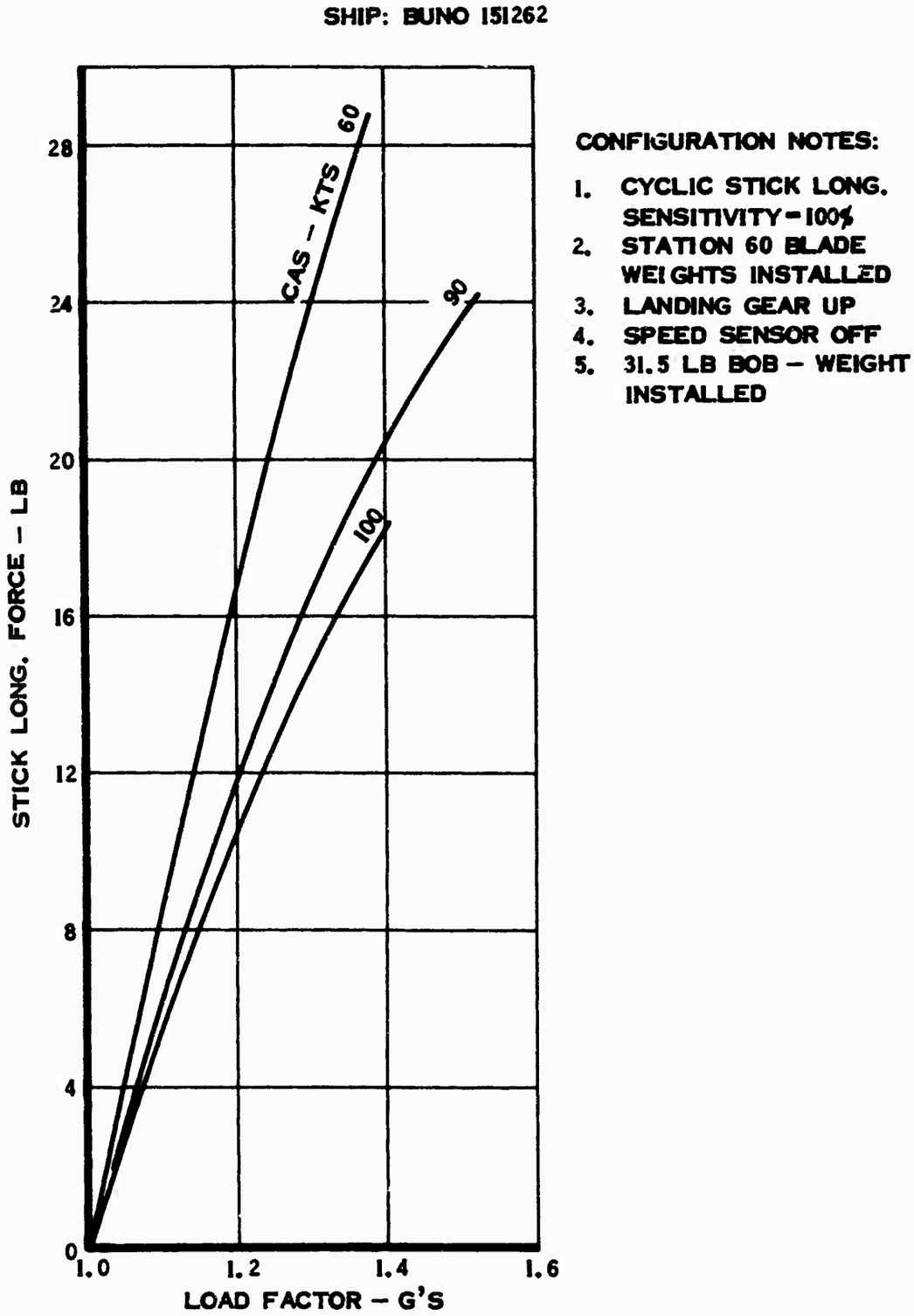

Figure 59. Maneuvering Stability, Forward Center-of-Gravity Location - Four-Blade Rotor.

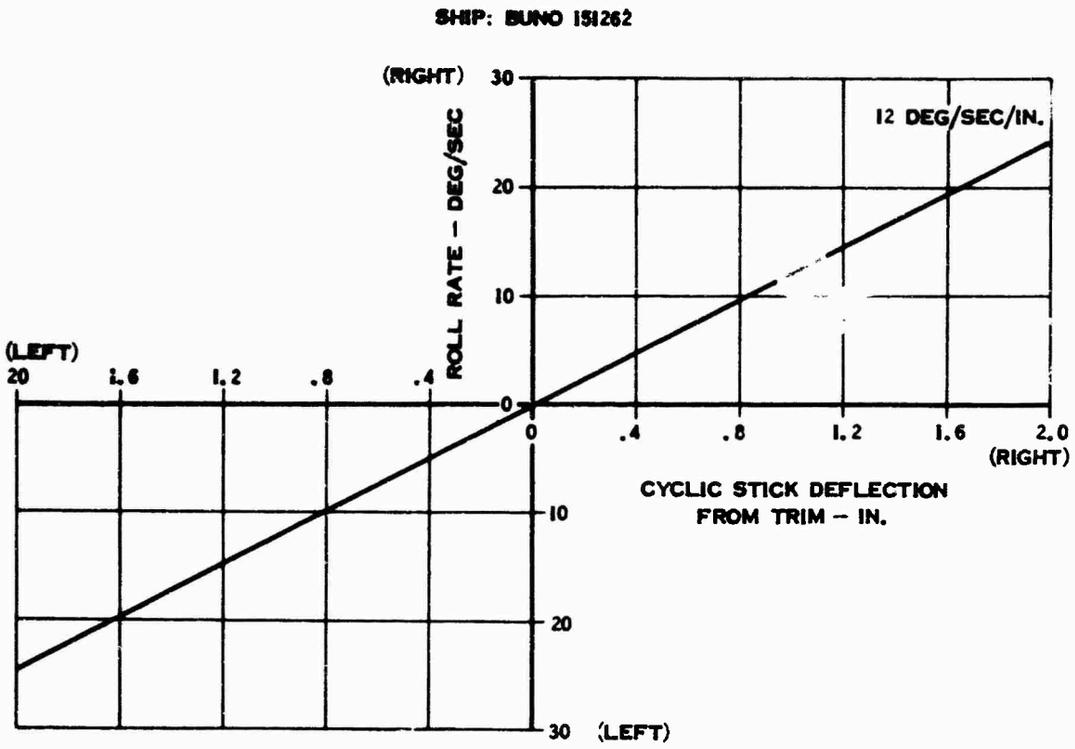

Figure 60. Lateral Control Power - Four-Blade Rotor.

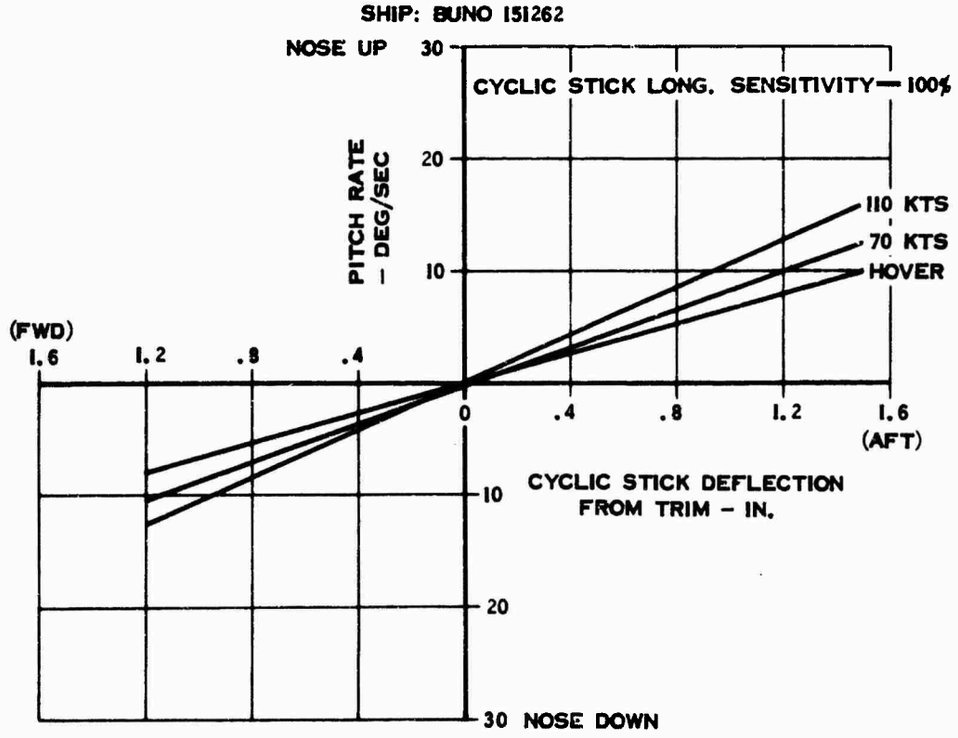

Figure 61. Longitudinal Control Power - Four-Blade Rotor.

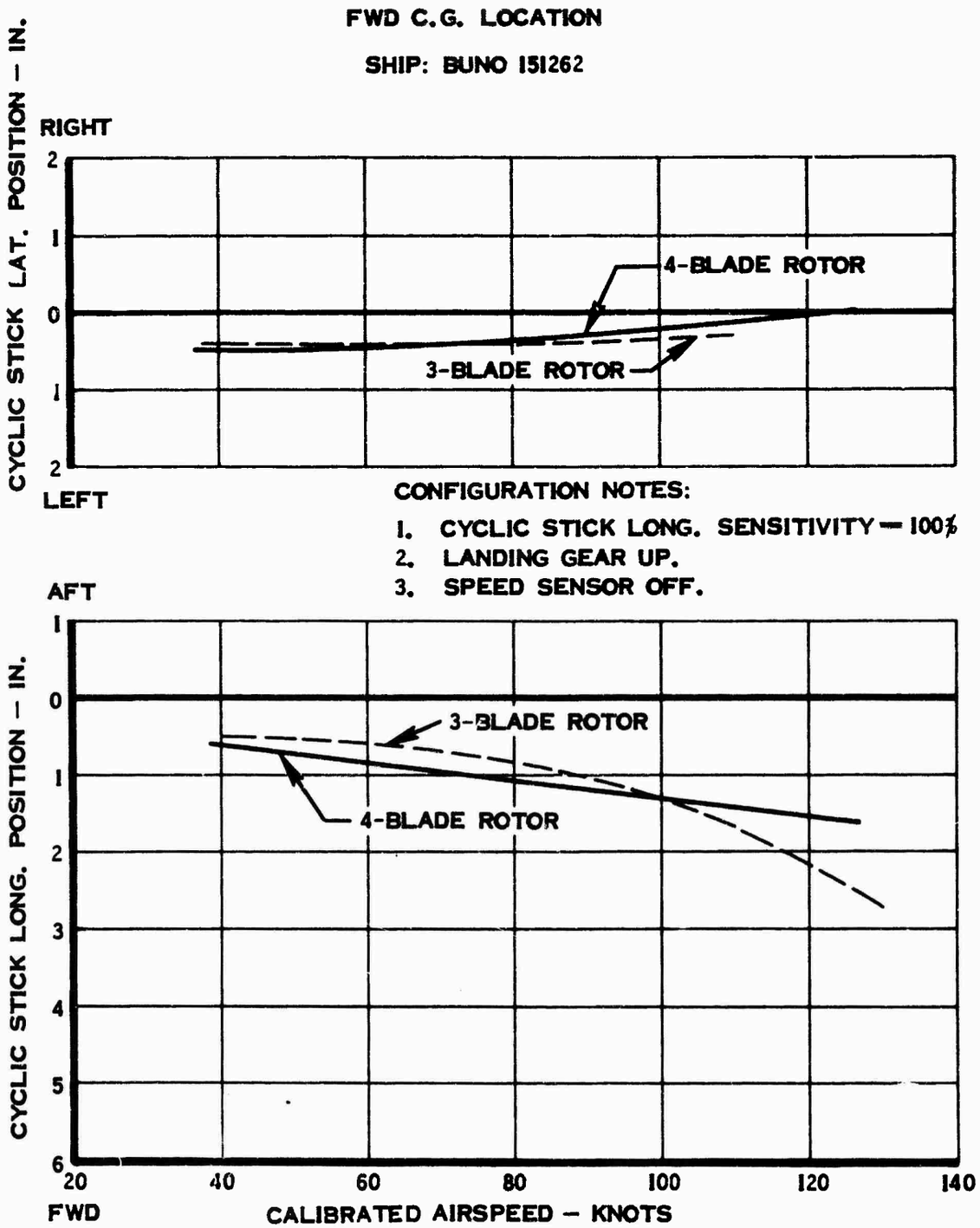

Figure 62. Cyclic Control Positions in Level Flight - Four-Blade Rotor.

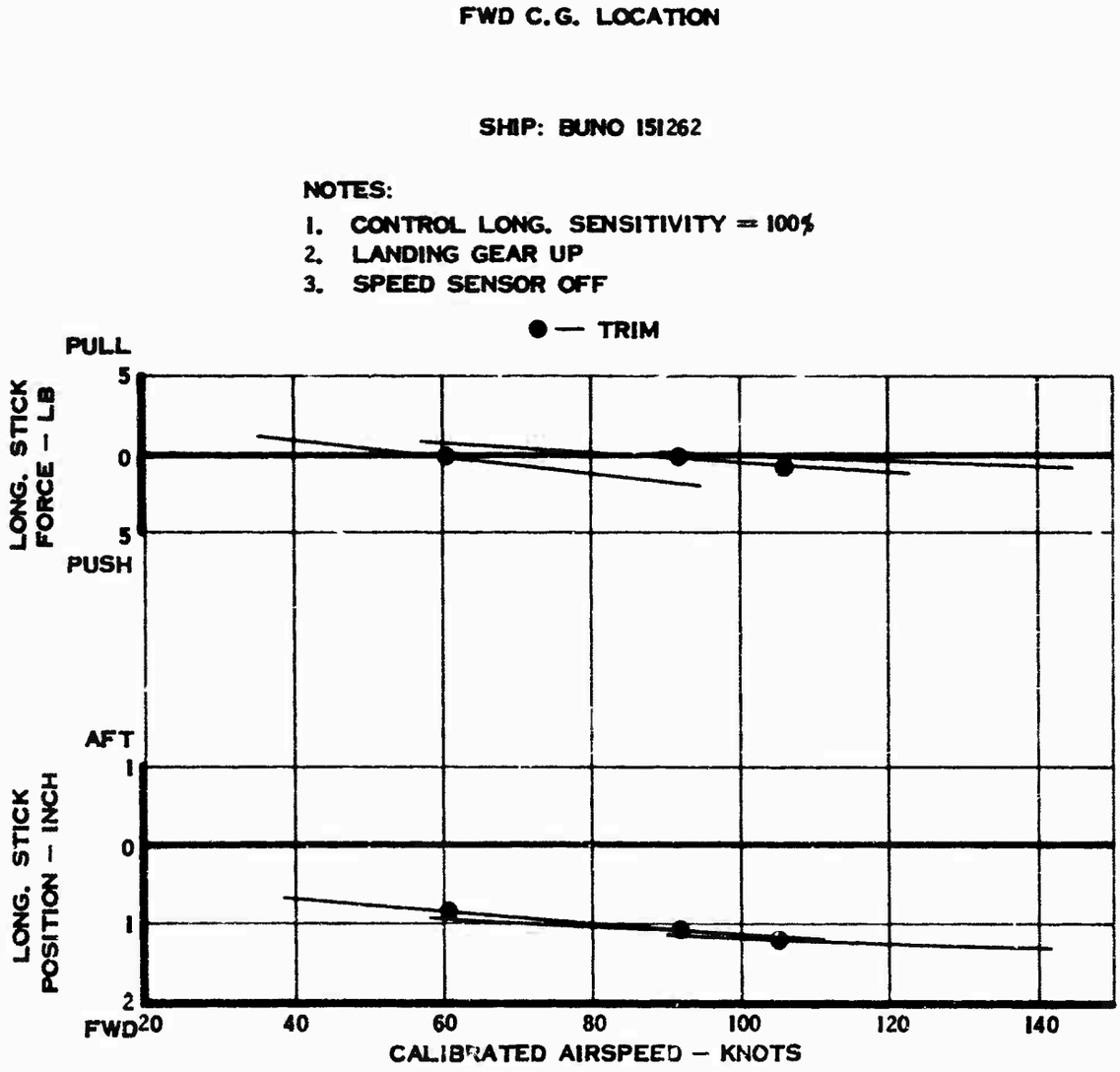

Figure 63. Static Longitudinal Stability - Four-Blade Rotor.

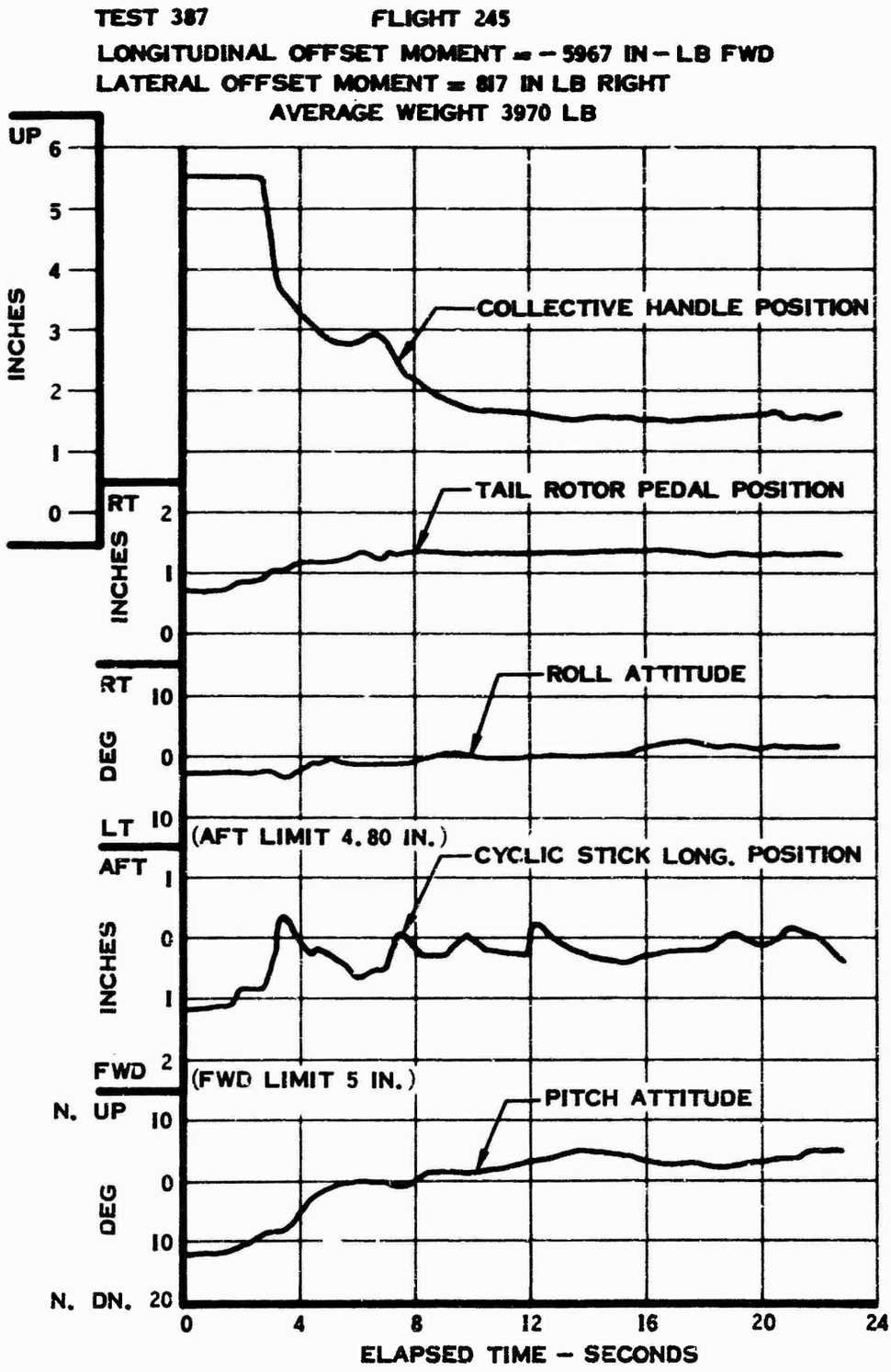

Figure 64 (Sheet 1 of 2). Time History of Autorotation Entry and Descent - Four-Blade Rotor.

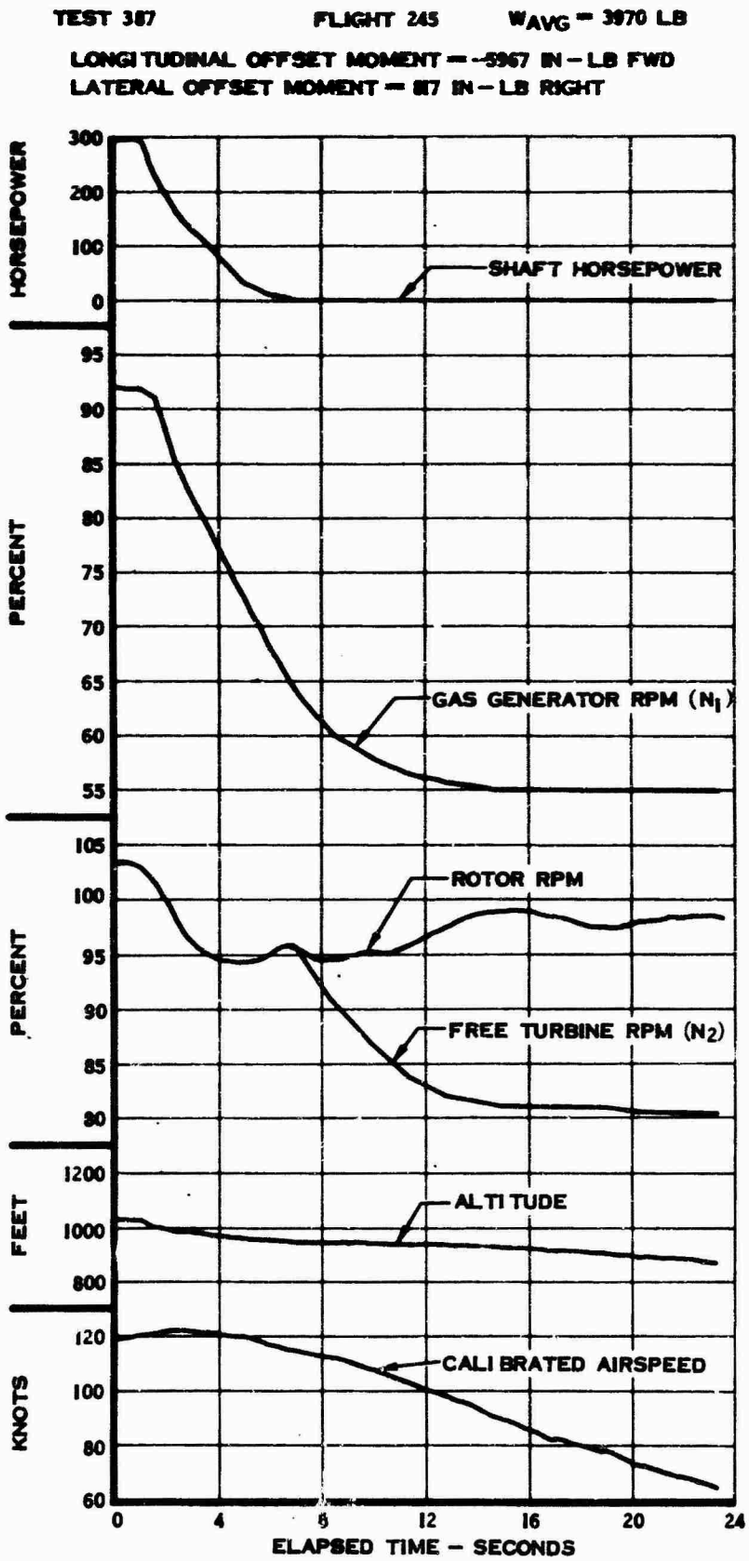

Figure 64 (Sheet 2 of 2). Time History of Autorotation Entry and Descent - Four-Blade Rotor.

SHIP: BUNO 151262

W=4000 LB

TEST 383, FLIGHT 241

NOTES:

1. STATION 60 BLADE WEIGHTS INSTALLED.
2. LANDING GEAR RETRACTED.
3. AIRSPEED — 76±2 KNOTS, CAS.
4. LOAD FACTORS DEVELOPED IN RIGHT TURNS.
5. COLLECTIVE BLADE ANGLE — 6° (BLADE STATION 0).

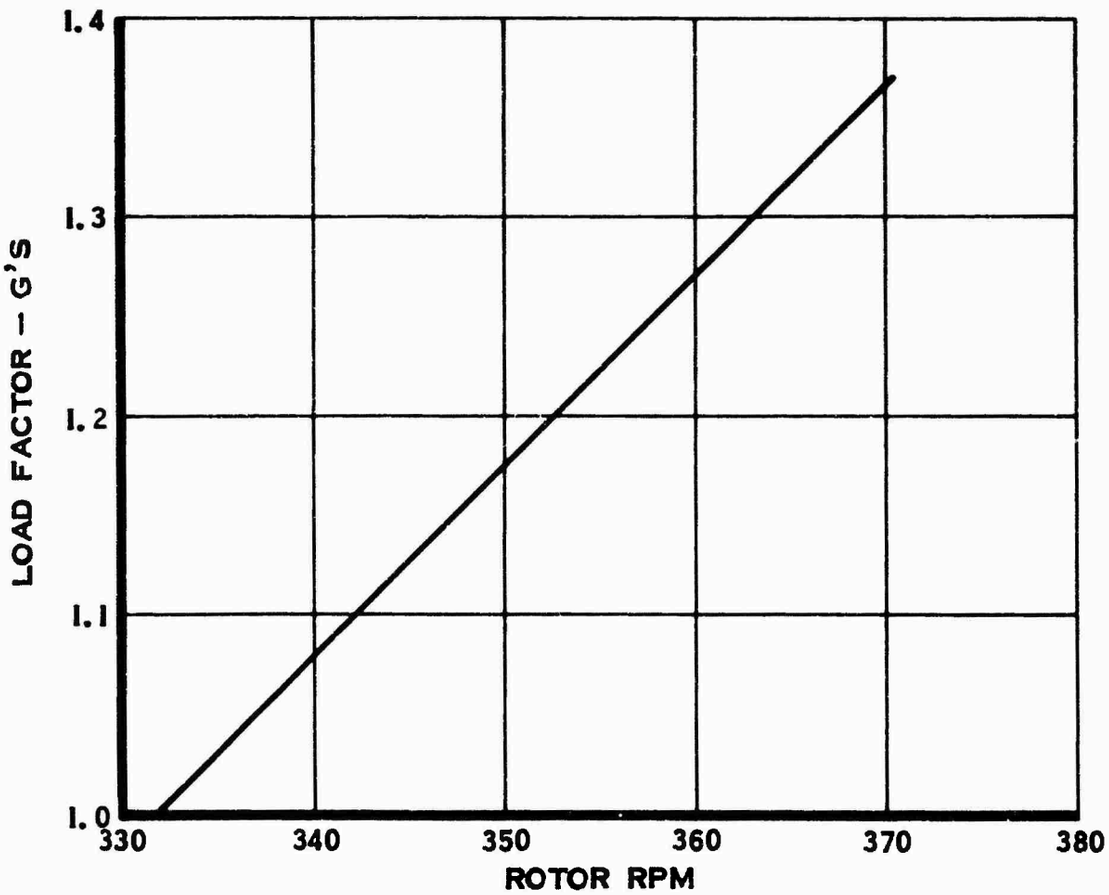

Figure 65. Load Factor Required to Maintain a Given Rotor RPM in Autorotation - Four-Blade Rotor.

FWD C.G. LOCATION

SHIP: BUNO 151262

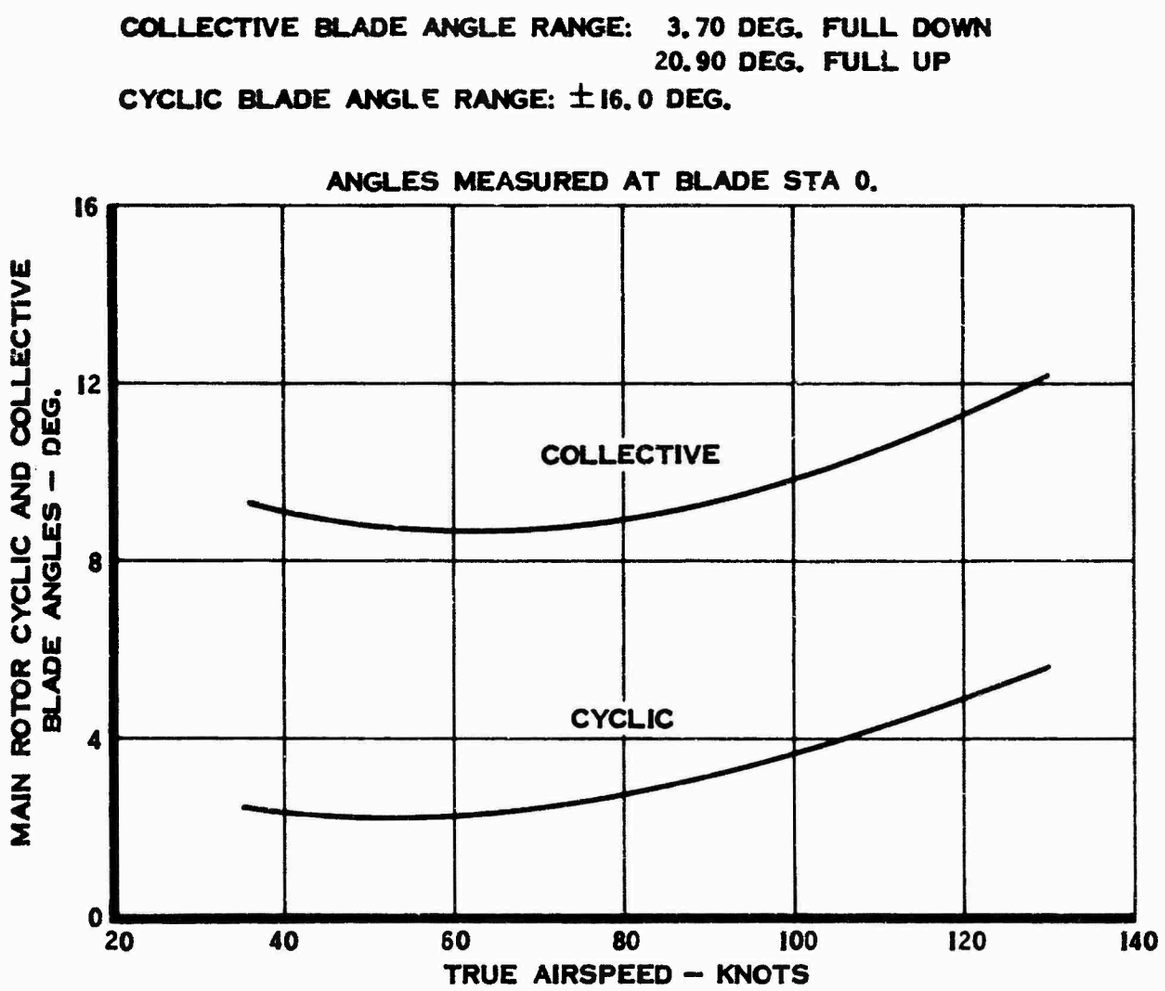

Figure 66. Cyclic and Collective Blade Angle Variation in Level Flight - Four-Blade Rotor.

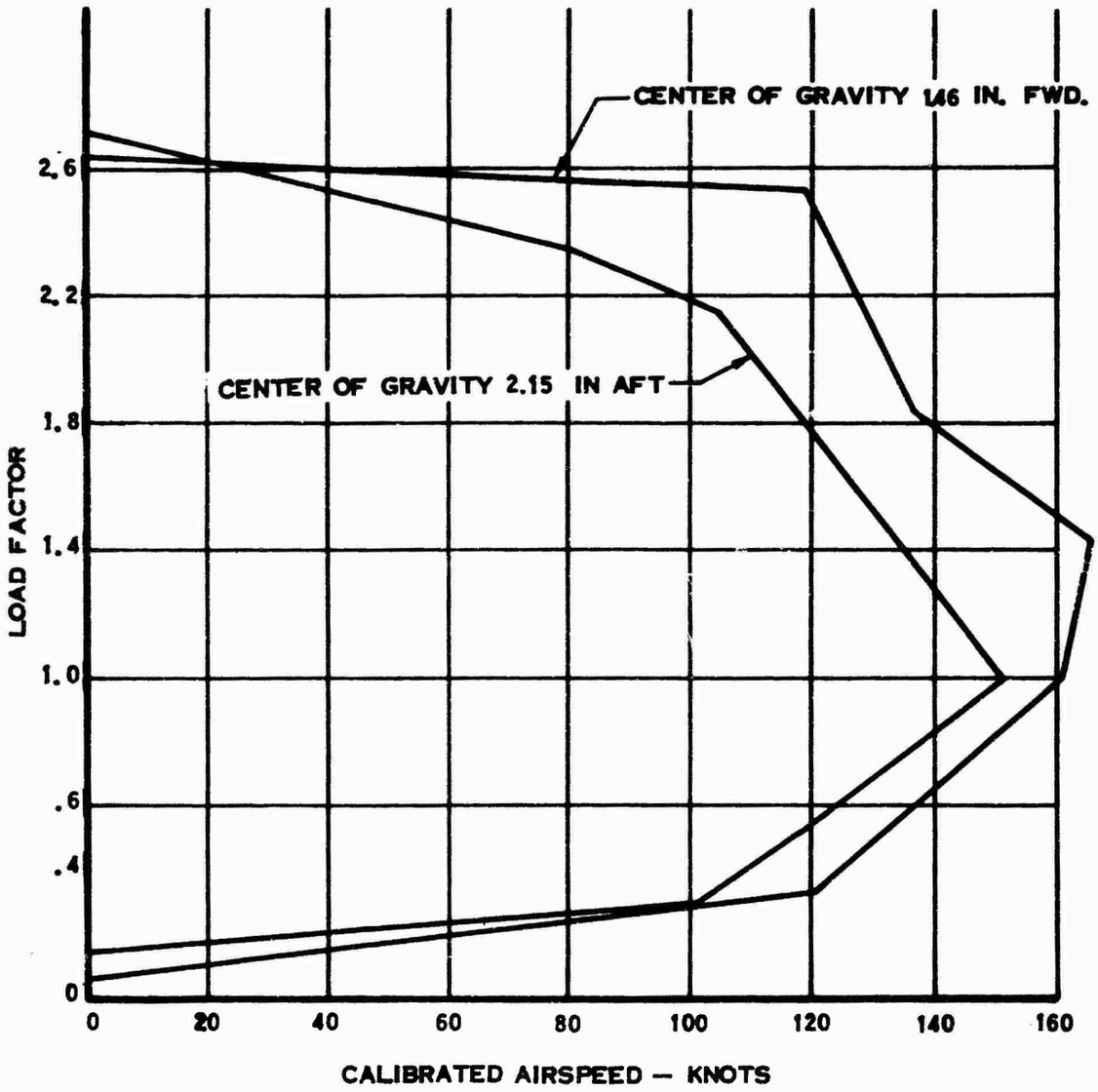

Figure 67. Maneuvering Envelope - Four-Blade Rotor.

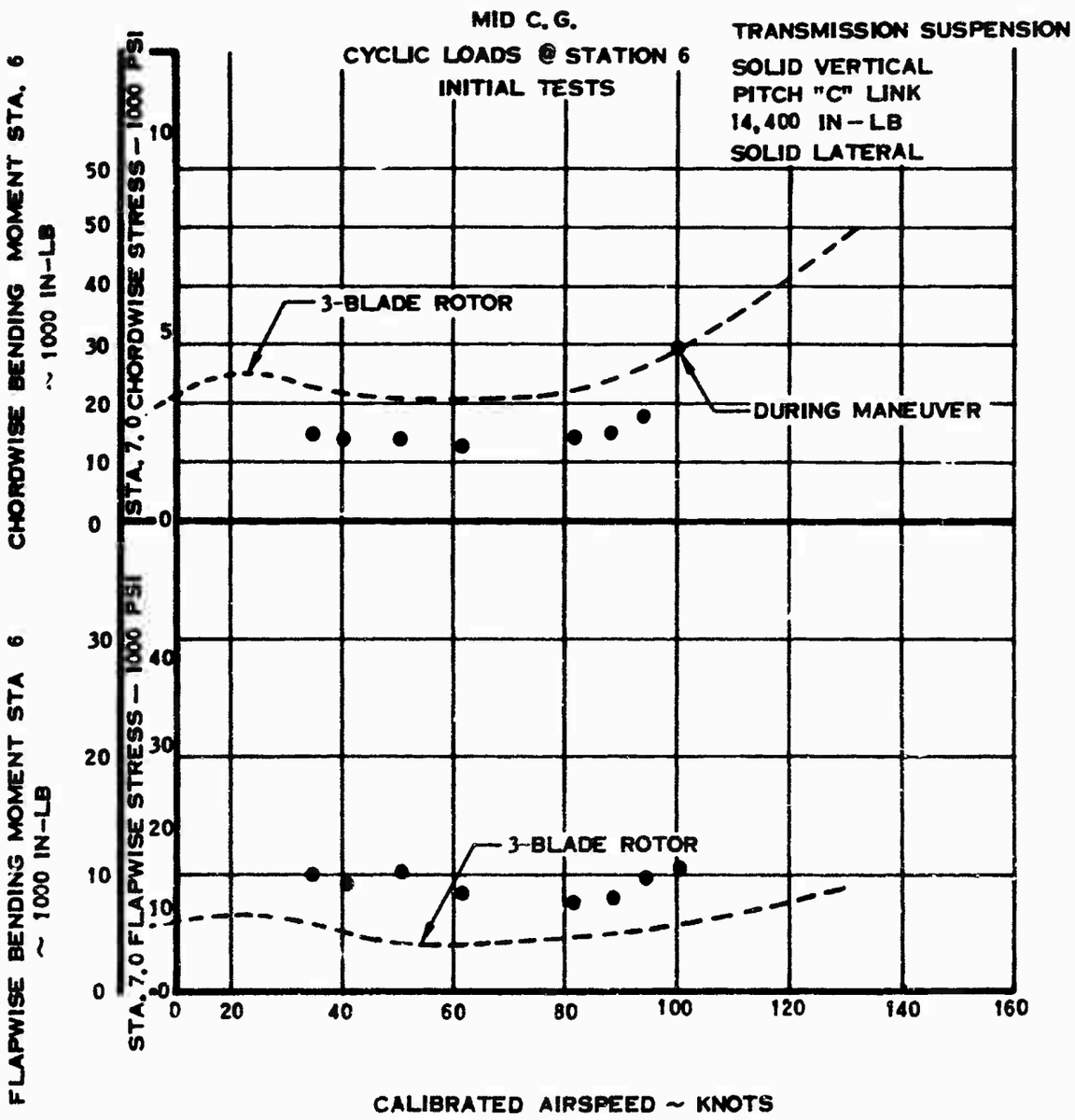

Figure 68. Four-Blade Rotor Loads Versus Calibrated Airspeed.

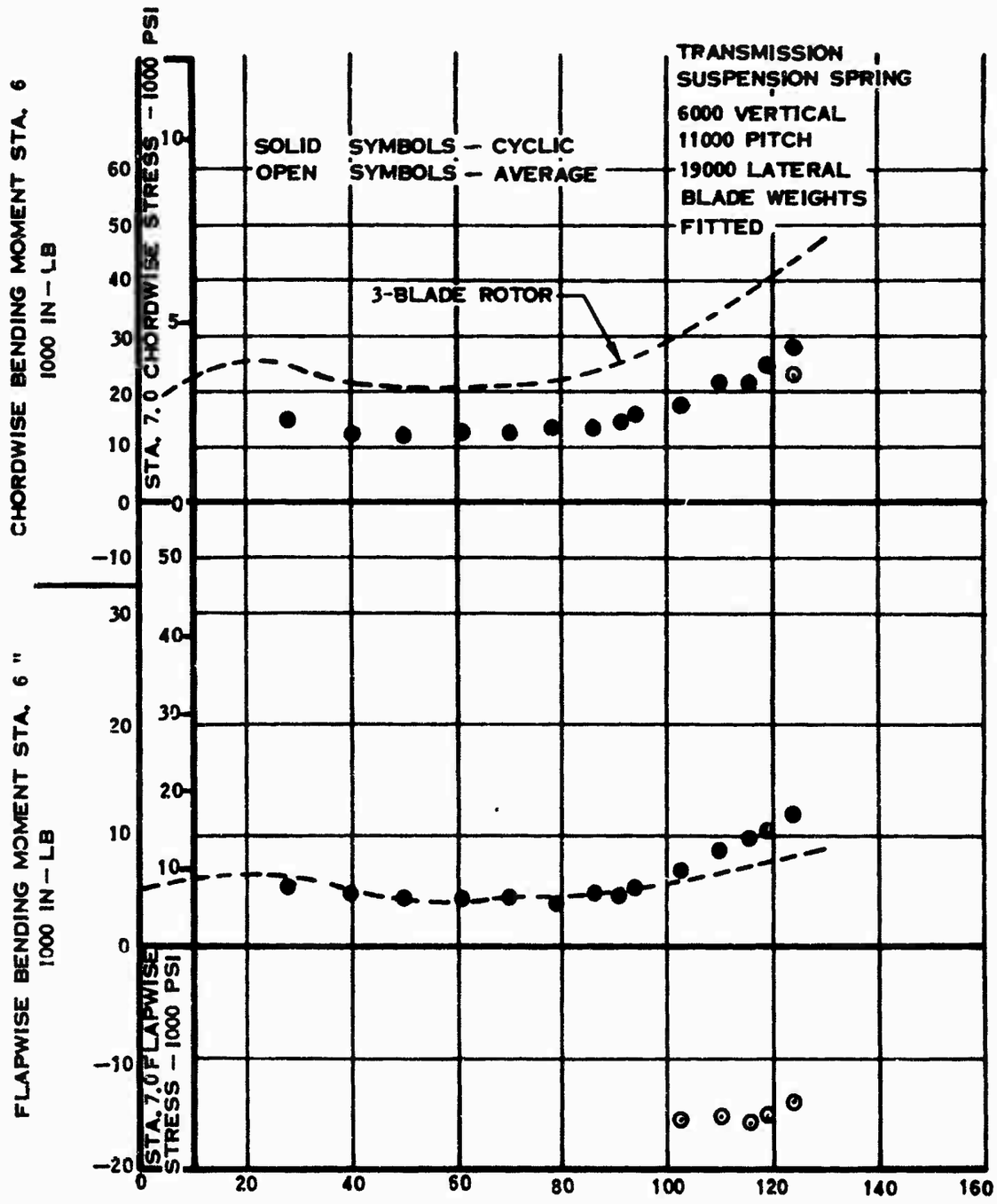

Figure 69. Four-Blade Rotor Loads Versus Calibrated Airspeed Horizontal Stabilizer Incidence - 5.5 Degrees.

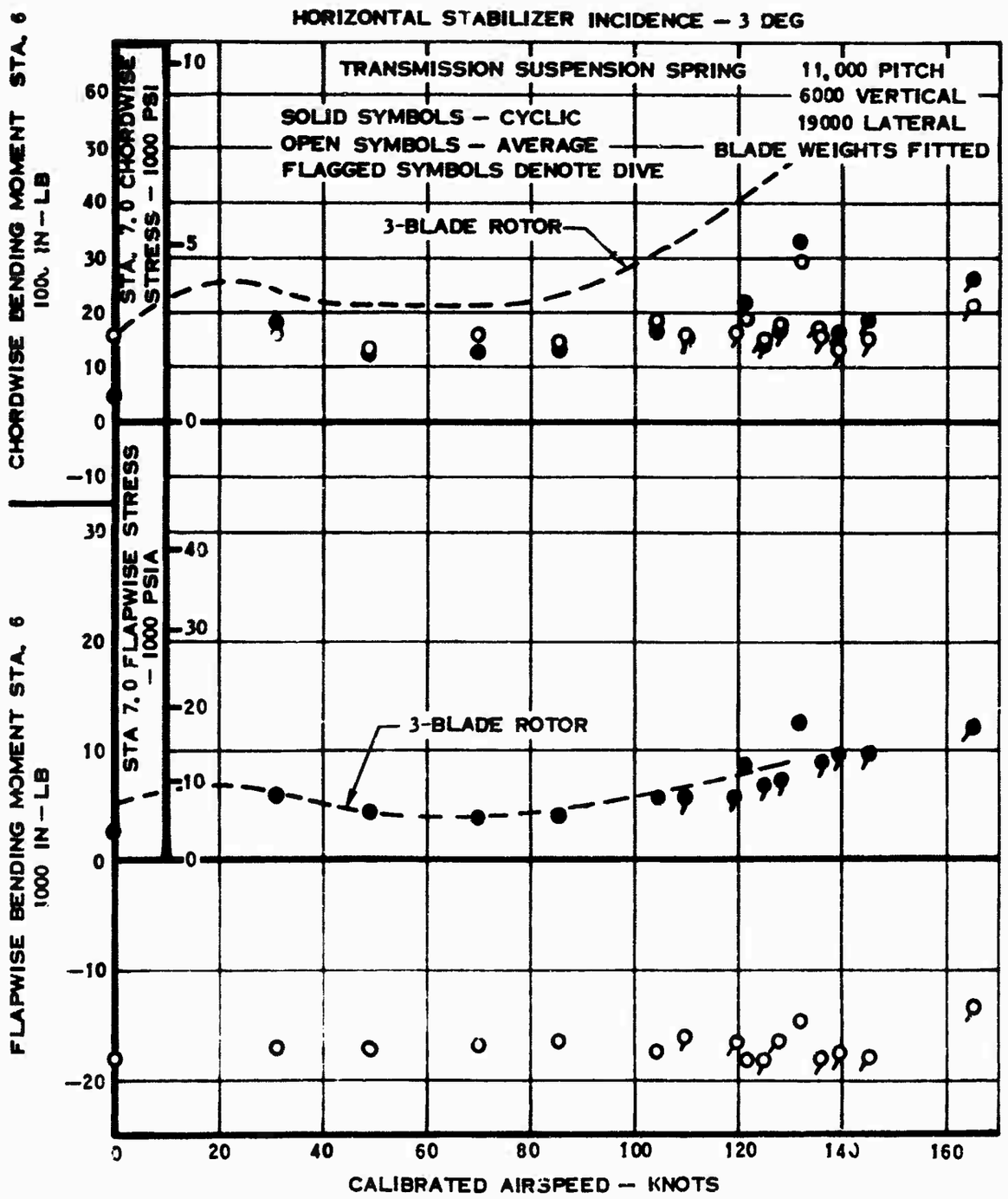

Figure 70. Four-Blade Rotor Load Versus Calibrated Airspeed.

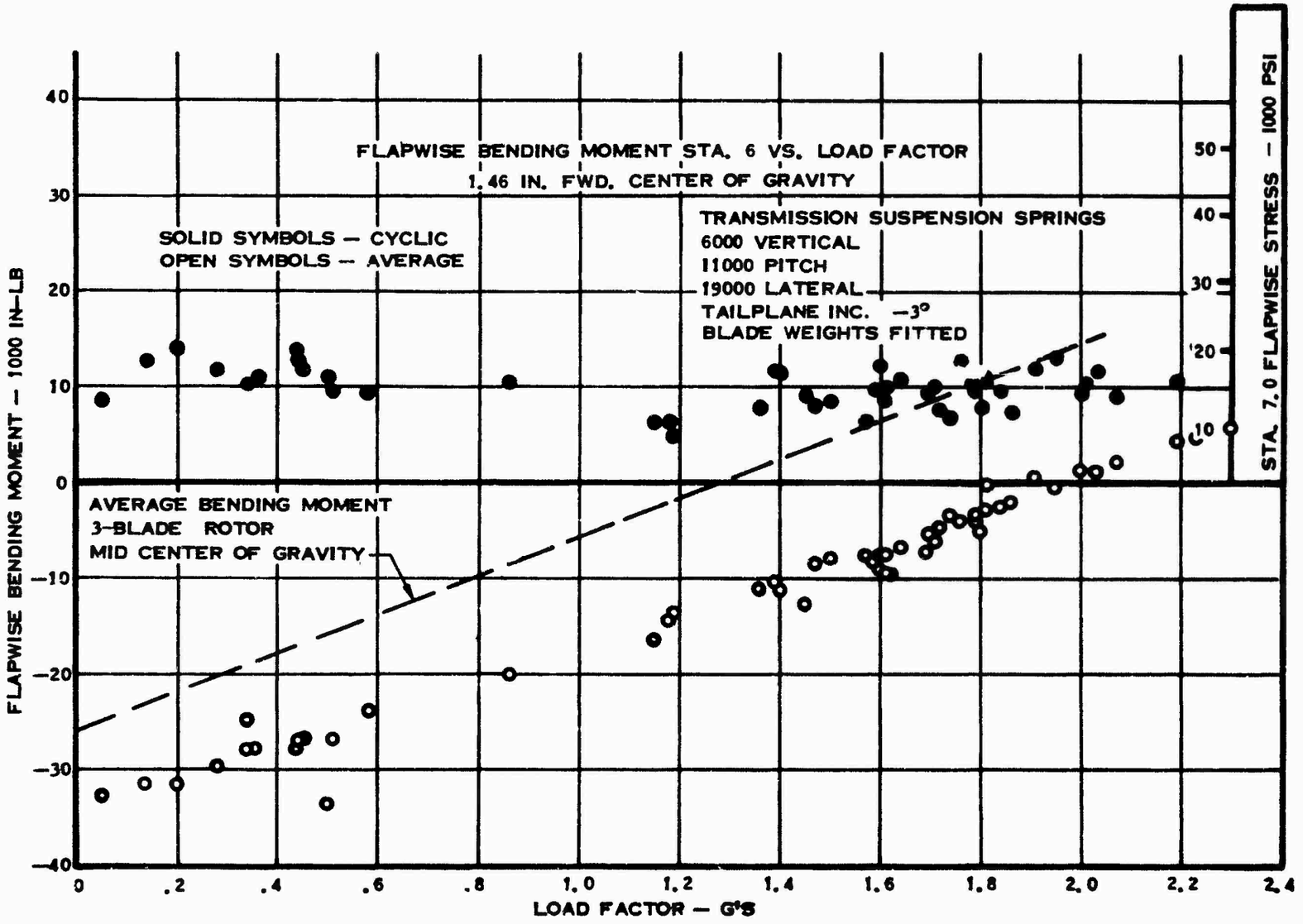

Figure 71. Flapwise Bending Moment Station 6 Versus Load Factor - Four-Blade Rotor.

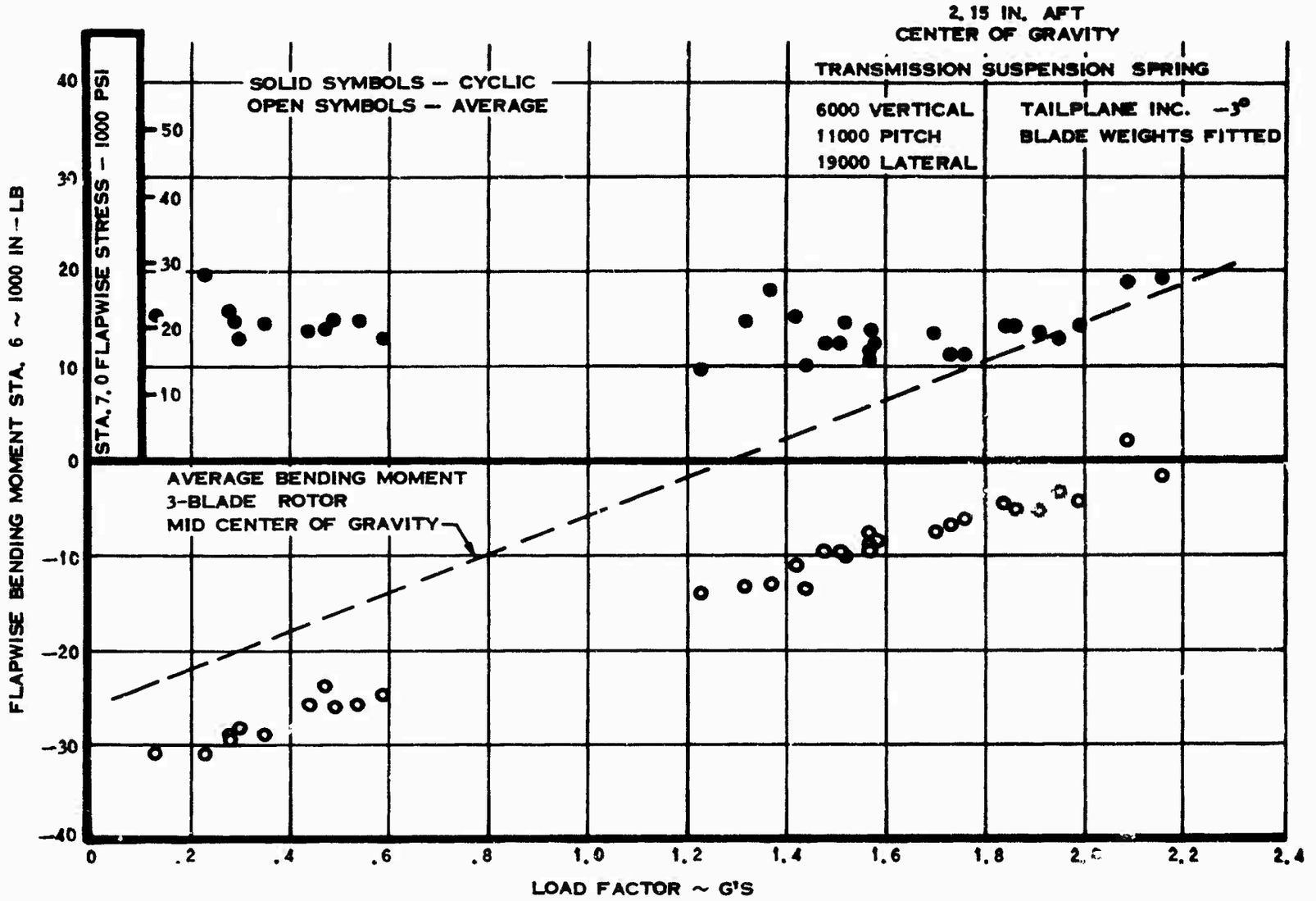

Figure 72. Flapwise Bending Moment Station 6 Versus Load Factor - Four-Blade Rotor.

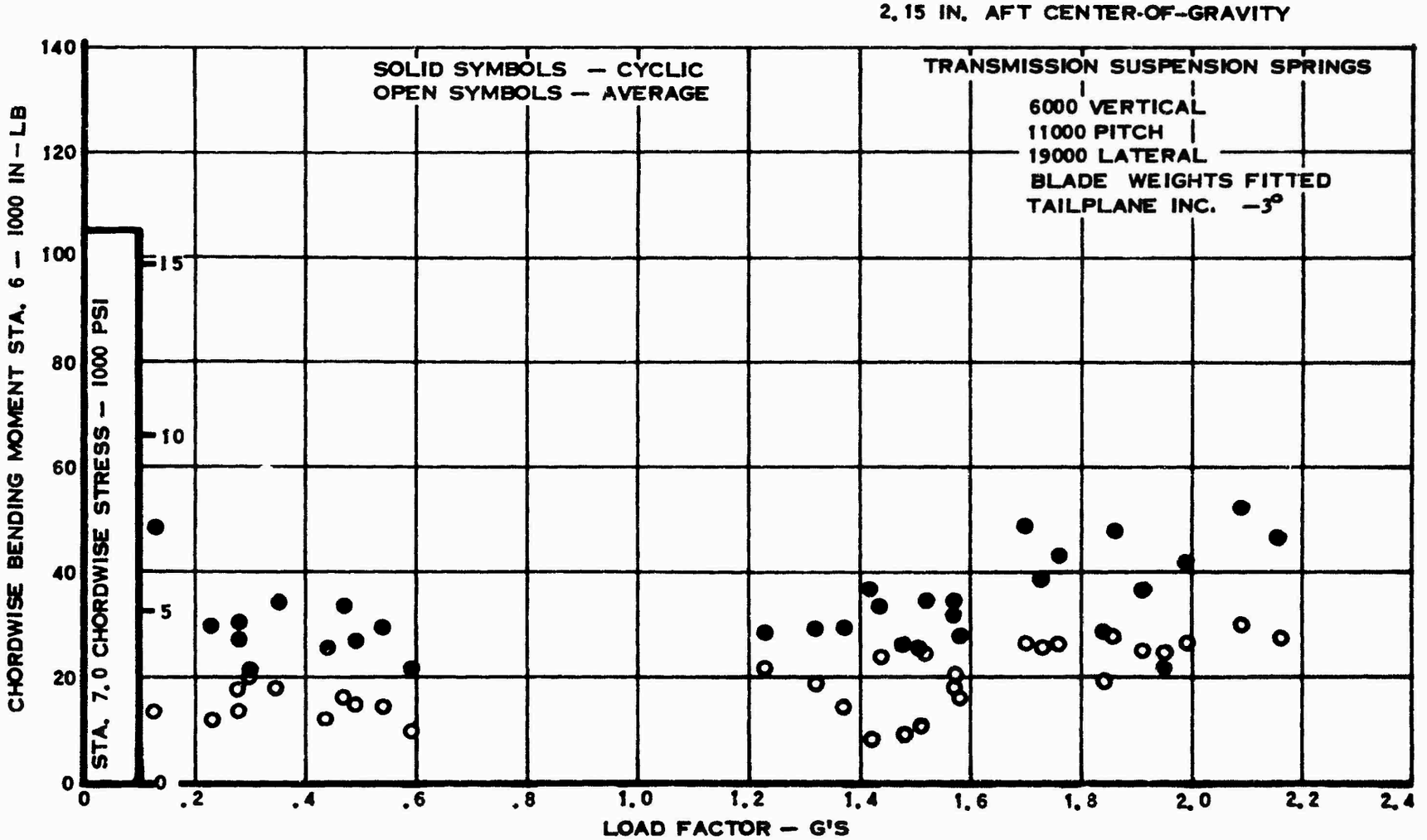

Figure 73. Chordwise Bending Station 6 Versus Load Factor - Four-Blade Rotor.

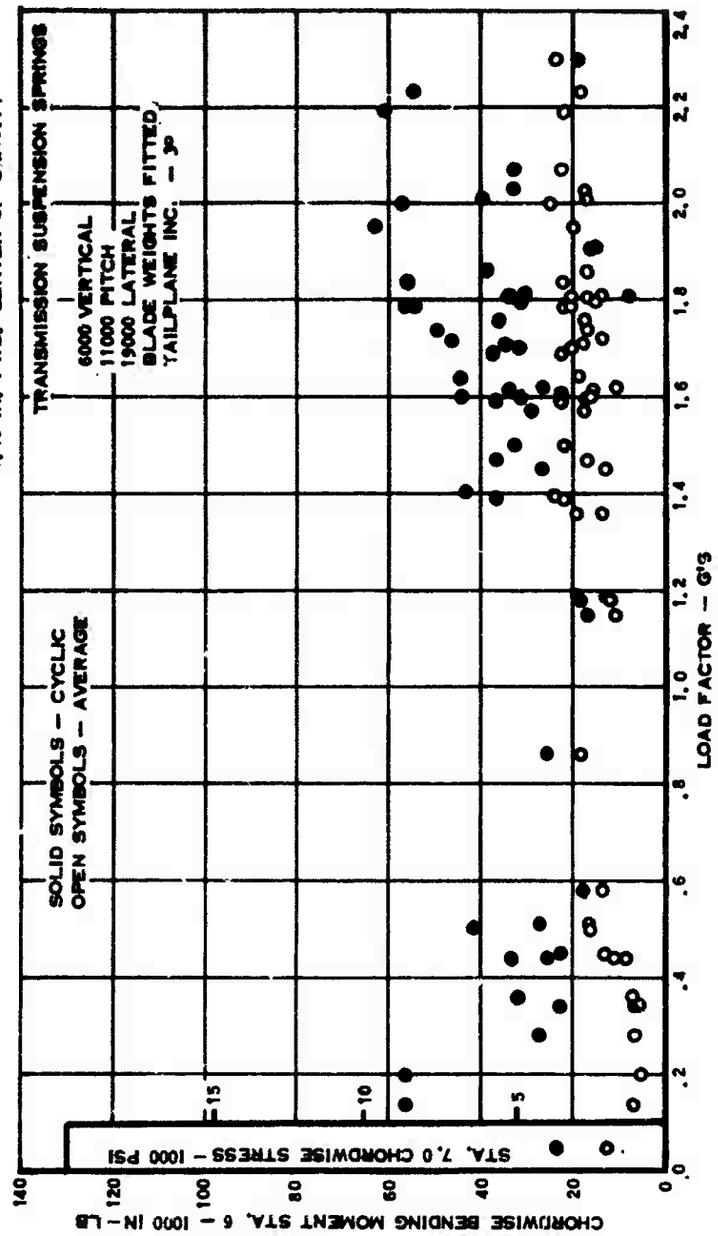

Figure 74. Chordwise Bending Station 6 Versus Load Factor - Four-Blade Rotor.

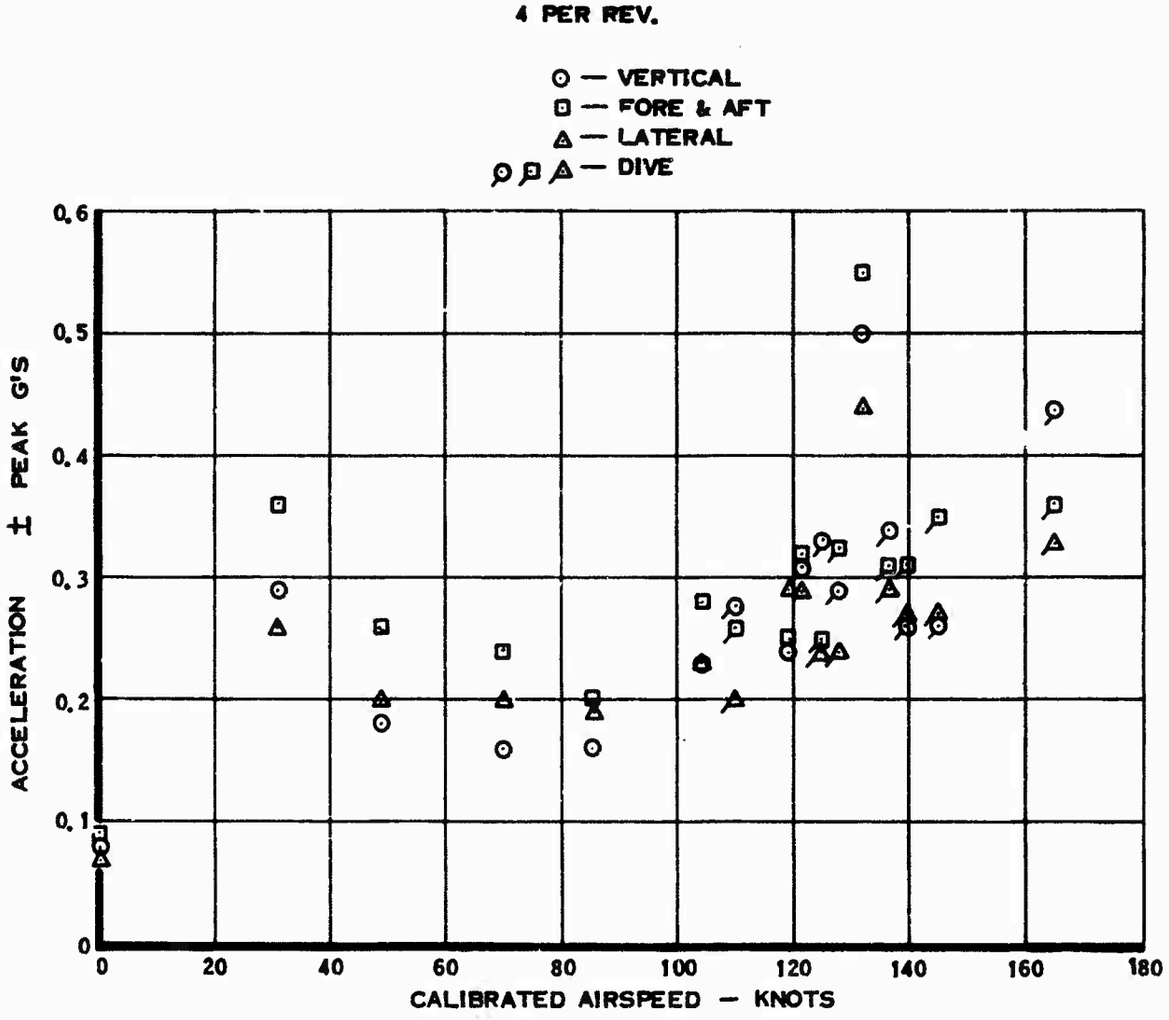

Figure 75. Cabin Vibrations at Pilot's Station Versus Calibrated Airspeed - Four-Blade Rotor.

C. COMPOUND HELICOPTER FLIGHT TESTS

Research flight tests were conducted with the XH-51A helicopter modified to incorporate a wing for lift augmentation and a jet engine for thrust augmentation. The primary objective of these tests was to attain a level flight speed of 200 knots. This goal was reached and exceeded.

Other objectives were concerned with the determination of the effects of lift and thrust sharing between the rotor and the wing and jet engine, rotor-wing interference, structural characteristics, stability, control, general handling qualities, performance, power loss and autorotation entry, and vibration.

These subjects were investigated during the course of the flight program and the data is presented in this section of the report.

As the speed envelope was extended, several problem areas became evident. The most serious problem was associated with increasingly negative static longitudinal stability with increased speed. This problem was solved by the installation of a horizontal tail of increased area.

At approximately 170 knots, the forward portion of the windshield deflected inward approximately 3 inches. This was accompanied by moderate buffetting due to the changed airflow pattern. Structural reinforcement of this portion of the windshield provided adequate strength for further speed increases.

Above approximately 170 knots, an unusual noise was heard by the pilot which was described as sounding like rotating interference. An inspection of all rotating components disclosed no evidence of rubbing, wear, or internal faults in any of the rotating equipment. Additional flights were conducted to determine the exact nature and, if possible, the source of the noise. Recordings of ambient sound in the cabin were made and analyzed for harmonic content. The unusual noise which had been reported was determined to be primarily 470 cycles per second with its second harmonic of 940 cycles per second also present. The third harmonic (1410 cps), if present, was masked by the general noise levels which were predominant at 1400 cps and above.

Study of the frequencies of the rotating equipment including the PT-6 gas generator and free turbine, the J-60 compressor, transmission and gear tooth frequencies and beat frequencies between these items did not indicate that any of these were the probable source of the noise.

The helicopter was treated with balsa and tape fairings, gap seals, a boot closing the top of the mast fairing, and the size and shape of the engine compartment were changed by removal of the oil cooler fan inlet shroud inside the engine compartment.

The nature of the sound was altered and on a subsequent flight was determined to be primarily 1350 cycles per second and was predominant over a small airspeed range while accelerating above 170 knots.

During the Phase IV tests, 65 flights totaling 17.7 hours were made. Performance goals and other test conditions which were attained in Phase IV are summarized in Table II.

Performance

Performance evaluation of the compound helicopter was predominately level flight performance in the compound mode. A minimum of testing in the pure helicopter mode was conducted.

Early in the program, it was established that two of the most important parameters, insofar as performance and flying qualities were concerned, were airspeed and angle of attack. To provide the most accurate indication of these quantities, a specially instrumented boom was installed which sensed total and static pressure, angle of attack, and sideslip angle. The fact that the boom-mounted vane senses local flow rather than true angle of attack in no way alters its validity as an analysis tool since changes in flow direction are the important factors in such analyses. For consistency, a fixed reference was used to relate the sensed angle of attack to the longitudinal axis of the helicopter. The conventional fuselage reference line (FRL) was selected for this purpose.

Airspeed Calibration. The boom airspeed system had been calibrated during previous testing of a pure helicopter at speeds up to 140 knots. For the initial compound testing, therefore, the calibration remained valid over the same range of speeds. At the higher speeds represented by the program goal, simple extrapolation of the calibration curve was inadvisable. In view of the restricted flight endurance of the compound helicopter, a representative airspeed system calibration would be exceedingly difficult, if not impossible, to accomplish. Accordingly, a pacer calibration was done using a light twin-engine aircraft as the pacer. The pacer aircraft airspeed system was first modified to include a sensitive, laboratory-calibrated airspeed indicator. The system error (position error) was then established by the altimeter depression method

TABLE 11
SUMMARY OF PHASE IV TEST CONDITIONS

Maximum Calibrated Airspeed (level flight)	201.5 kts
Maximum True Airspeed (level flight)	210 kts (242 mph)
J-60 Thrust Required at V_{max}	1,400 lb
PT6 Power Required at V_{max}	165 hp
Test Altitude at V_{max}	2,200 ft
Test Free Air Temperature at V_{max}	18°C
Maximum Gross Weight	4,800 lb
Maximum J-60 Thrust Used In Flight	1,500 lb
Maximum and Minimum Load Factors	1.8g at 106 kts
	0.64g at 154 kts
	1.21g at 190 kts
	0.80g at 190 kts
Maximum Longitudinal C.G. Offset	1.9 in fwd
	.5 in aft
Maximum Lateral C.G. Offset	4.80 in (left)

over the entire speed envelope of the airplane - 80 knots to 190 knots. The results of this calibration are shown on Figure 76. A check with the Western Region of FAA revealed that this calibration agrees favorably with the official FAA test results on this type aircraft. The same airplane was used to "chase" the helicopter during all subsequent high speed testing. Using the data obtained during such chase flights, the boom airspeed system of the helicopter was calibrated at high speeds. This calibration is shown on Figure 77. Good agreement was found to exist between the earlier calibration and the current pacer calibration.

Level Flight Performance: A summary of the level flight performance results are shown on Figure 78. This figure indicates the trade-off between collective setting and auxiliary thrust over the airspeed envelope. The build-up testing was accomplished by starting with the J-60 at idle, and with a fairly high collective setting. Then, holding speed and altitude constant, the collective was progressively lowered while the J-60 thrust was increased as required. This procedure was repeated at a number of airspeeds up to approximately 150 knots. At this speed, a collective pitch angle, $\theta_o = 3.4°$ to $3.8°$, provided the lowest level of blade stresses and vibration. This setting therefore was held constant for the remainder of the speed expansion tests through V_{max}. Figure 78 indicates that this collective setting essentially unloads the main rotor as far as lift is concerned at speeds of 200 knots and beyond. One final factor influenced this collective selection. Autorotation build-up testing at high speed indicated that this setting provided entirely satisfactory entry characteristics requiring no collective manipulation until the helicopter had decelerated to conventional helicopter autorotation airspeeds.

In the analysis of the level flight performance, Figure 79 was prepared. The lower half of this figure represents the relationship between calibrated airspeed and angle of attack at constant values of collective setting. The fairings are conventionally shaped and vary in the anticipated manner. The upper fairing is interesting in that the J-60 thrust coefficient (C_{Δ}) varies essentially linearly with angle of attack and is independent of airspeed or collective setting. Since C_{Δ} is identically equal to the total drag coefficient (C_D) in level unaccelerated flight, providing that the rotor is either at zero lift or is not inclined to the flight path, the linearity is the result of changes in rotor lift and inclination which are associated with the angle of attack changes. This relationship provides a simple and reliable method for performance extrapolation to speeds beyond the limits of the test program.

Figure 80 presents the variation of shaft horsepower with airspeed for various levels of auxiliary thrust. These data are corrected to sea level, standard day conditions. As anticipated, the power required in the pure helicopter mode is much greater than that of the conventional four-blade rotor. Comparison of the pure helicopter mode data with that with the J-60 engine at idle indicates that the parasite drag is increased by as much as 50% when the J-60 engine is not operating.

At high thrust settings, the shaft horsepower required was reduced to 90 SHP at 110 knots and 178 SHP at 210 knots. At the 110-knot condition, the shaft horsepower required was reduced by 70% as the J-60 was advanced from idle to the high thrust condition. The variation of thrust with airspeed, corrected to sea level standard day conditions, is shown on Figure 81 for the J-60 at idle and at high thrust.

The addition of jet thrust has a marked effect on rotor and wing lift characteristics. Figure 82 presents the variation of rotor lift for the pure helicopter mode, the J-60 at idle thrust, and the J-60 at high thrust for sea level standard day conditions. In the pure helicopter mode the rotor supplies all of the propulsive force to move the vehicle and a large percentage of the lift. The propulsive requirement is very high due to the large parasite drag of this configuration and results in a strong nose-down attitude change with increasing speed. In this condition, the wing is relatively ineffective since it only carries a small percentage of lift over the 50- to 80-knot speed range, starts to lose lift above 80 knots because of angle of attack changes, and eventually becomes a downlifting surface which puts an even greater demand on the main rotor.

With the addition of idle thrust, parasite drag is reduced (primarily by more favorable wing-nacelle-fuselage interference effects), and the aircraft operates with a higher angle of attack which decreases less rapidly with increasing speed. The higher angle of attack produces more wing lift over a larger speed range and unloads the rotor by approximately 13% at 110 knots when compared to the pure helicopter mode.

At high thrust settings the aircraft operates at still higher nose-up attitudes and the wing produces lift over the entire speed range. The data shown on Figure 82 indicate that the rotor is 95% unloaded at 210 knots.

Wing/Body Lift Characteristics: Figure 83 shows the wing/body lift characteristics of the helicopter. The lift data, which are plotted in conventional coefficient form, were obtained from strain gages attached to two of the transmission support links. This method

provides a more accurate indication of the total auxiliary lift than would be provided by any alternative procedure, such as measuring wing shear and bending. The lift-curve slope obtained from these data agrees quite well with the wind tunnel test results obtained prior to the start of flight testing.

These measured lift characteristics were used to compute the line of zero rotor lift shown on Figure 78. Also taken into account in computing the zero lift line was the vertical thrust component of the J-60 engine.

Flying Qualities

Conventional rotor systems, which rely on large changes in the rotor thrust vector to produce longitudinal and lateral control, experience a strong reduction in control power when they are aerodynamically unloaded. This tends to limit the amount of unloading which can be tolerated, with the result that generally high rotating system stress levels are unavoidable if strong wing/body aerodynamic moments are present. The alternative in such cases is to equip the helicopter with aircraft-type control systems, such as elevators and ailerons to provide trim and control.

Cyclic control power of the rigid rotor remains virtually unaffected by the magnitude of rotor lift which is being generated. This system therefore eliminates the need for complicated control systems and is well suited to compound helicopter applications. In this section of the report, the pitch and roll trim moments which the rotor system produces over a full lift spectrum are discussed.

Static Longitudinal Stability: Wing/body pitch and roll moments were measured directly during the flight test program using a procedure developed during previous helicopter programs. The advantage of this procedure is that it provides the test engineer with measurements of actual stability to supplement the potentially misleading apparent stability which may be indicated to the pilot by control motions and forces.

Figure 84 is the result of early testing in the Phase IV program. The upper fairings show two effects. First, the slope of the lines define the level of stability in conventional terms ($dCm/d\alpha$). Second, the variation shown for different thrust coefficients, C_{Δ}, represents the trim shift which occurs as a result of auxiliary thrust changes. A study of these data indicates that this trim shift is the result of thrust-induced lifting forces acting on the nacelle. Other possible

causes, such as changes in the local flow velocity at the stabilizer, or induced changes in the wing downwash field, were ruled out on the basis of the combined pitch and roll moment data. Similarly, the vertical component of the auxiliary thrust vector (+7°) is such that no pitching moment is produced, and only a slight roll moment occurs even at the maximum thrust used to date.

The lower fairing of Figure 84 represents a change in trim with dynamic pressure, q. This effect was established empirically by selecting and analyzing data which were obtained at constant values of C_{Δ} and α. A study of these and similar data obtained during Phase IV revealed that the "q-effect" was, in reality, the result of a change in the angle of attack of the horizontal stabilizer due to the effects of rotor downwash. The data on this figure indicate that the helicopter, in the noted configuration, is on the order of 8-10% longitudinally unstable ($C_{m_{\alpha}} = +.006$). In view of its research mission, this is not a particularly high level of instability and therefore the helicopter was tested to speeds of up to 150 knots with no difficulty. Before proceeding to higher speeds, it was felt that for dynamic stability reasons, and to assist the pilot in the event of an engine failure or other emergency, it would be advisable to alter the configuration to provide a positive level of longitudinal stability.

This was accomplished by increasing the area of the horizontal tail from 7.5 square feet to 24.3 square feet. The larger tail, when installed, produced the desired effect. The upper fairing at Figure 85 shows that the static stability margin with the larger tail is on the order of 15% ($C_{m_{\alpha}} = -.011$). This is a comfortable margin and, in fact, may be somewhat higher than is necessary. In view of the strong interplay of the stability parameters, additional study and test experience is required before a final definition of an optimum stabilizer size is possible.

The trim change with C_{Δ} is the same for this tail configuration as it was for the smaller horizontal tail (Figure 84). This supports the theory that the moment is associated with forces acting on the engine and nacelle and not with those acting on the horizontal stabilizer. In a similar vein, note that the downwash effect (q-effect) is magnified by the installation of the larger tail. This, of course, would be expected considering the large change in tail area. Further verification of the downwash theory is seen in the shape of the pitching moment coefficient versus q family. As the speed increases, the effect becomes considerably lessened. At dynamic pressures above 160-180 psf, the downwash effect is nil because as speed increases, the rotor contribution to total lift becomes less and the "blow-back" of the rotor downwash field increases with forward speed. The fact that

this trend was not apparent on Figure 84 is largely due to the lack of high speed data in that configuration. However, the correlation between these two sets of stability data is sufficiently good to warrant their use in extrapolating the flight envelope beyond the limits of the current test program. In this respect, the pitching moment data not only define the longitudinal stability of the vehicle, but because the rotor system is used to trim out the body moments, these data also indicate the station six 1-P flapwise bending moments in the rotor. This is done by using the following simple relationship:

$$F_{6P} = K \times C_{mR}$$

where:

$K = 3640\ q/2.65$

C_{m_R} = pitching moment coefficient

$q = 1/2\ \rho\ V_T^2$ - psf

F_{6P} = pitching component of station 6 flap bending moment - inch-pound

Lateral Trim Requirements: A similar analysis procedure was used to evaluate the rolling moment characteristics. Figure 86 shows the roll trim requirements in terms of rolling moment coefficient ($C_{\ell\ R}$) versus angle of attack. These data indicate that the lift characteristics remain symmetrical with angle of attack and no roll trim shift occurs. Thrust changes, as discussed briefly in the longitudinal stability section, have an effect on lateral trim. The direction and magnitude of this trim shift correlate well with the pitch trim data. The "q-effect" on this figure is not the result of rotor downwash, but appears to be due to aerodynamic forces acting on the highly cambered vertical stabilizer. The cambered surface provides a near-optimum balance of the yawing moments produced by the combination of thrust and rotor torque, but introduces a small right roll tendency at high speeds. The rolling moment produced by the cambered fin is not large enough to be disturbing to the pilot. Although the J-60 engine installation results in a lateral unbalance of nearly 20,000 inch-pounds, the net rolling moment remains relatively low for forward flight conditions as a result of the asymmetric wing design - the wing being shifted 5 inches to the left of the vehicle centerline.

Handling Characteristics: The preceding data reflect the actual level of stability of the helicopter. Handling characteristics, however, are more associated with an apparent level of stability since the pilot

is generally aware only of control motions and forces. Figure 87 is a plot of the cyclic control motion as a function of calibrated airspeed. With the control gyro arms set at an angle of 30 degrees, the stick-fixed stability (control motion versus speed) is positive. When the gyro arm angle was reduced to 5 degrees, however, the apparent level of stability became negative. Aerodynamic forces acting on the control gyro arms in forward flight result in a rolling moment acting on the gyro. This rolling moment must be reached by the pilot to prevent precession of the gyro. If the gyro arms have positive incidence, the rolling moment becomes stronger with increased forward speed, requiring additional pilot control deflection and force to prevent gyro precession and to maintain level flight. This is sensed by the pilot as positive static longitudinal stability. Increase in the positive incidence angle of the gyro arms will steepen the gradient of gyro rolling moment with speed and will appear to the pilot as stronger static longitudinal stability.

Negative control motion with speed variation occurs with the low incidence gyro arms. Figure 78 indicates that as speed increases with collective held constant, the angle of attack decreases slightly. Also, although the jet thrust increases, the rotor thrust coefficient actually decreases. Figure 85 shows that the combined effect of the changes in angle of attack, rotor thrust coefficient, and rotor downwash result in a fairly strong nose-down change in pitching moment with speed. This moment must be balanced by an aft motion of the cyclic stick if the q-sensitive gyro precessional forces are not high enough to provide the required compensation.

Stick-free longitudinal stability (control force versus speed) may be determined from Figure 87 by multiplying the control displacement noted thereon by the longitudinal force gradient of 5.0 pounds per inch. The forces are not excessive over the speed range tested to date even assuming that intermediate trimming is not employed.

The lateral cyclic control motion shown on this figure indicates essentially no cross coupling, and only a slight trim requirement with speed.

Both sets of data, longitudinal and lateral, indicate that adequate control exists for maneuvering capability over the entire flight envelope.

Directional Characteristics: For satisfactory high-speed operation, it is essential to reduce the tail rotor load to the lowest possible level. Figures 88 and 89 show that this objective was successfully met due to the camber in the vertical stabilizer and the 6-inch chord extension which was added to the trailing edge of this surface.

The displacement between the two fairings of Figure 88 at the same airspeed is because the tradeoff between rotor thrust and auxiliary thrust favors the latter insofar as total yawing moment is concerned. The combined yawing moment from rotor torque and auxiliary thrust at low collective and high jet thrust is approximately 80% of the moment at high collective and idle jet. The slope of these fairings is indicative of the fact that the cambered tail does not quite balance these propulsive moments. The amount of unbalance had no adverse effect on the Phase IV testing.

Maneuvering Stability: Maneuvering stability at high speeds was qualitatively evaluated and was comfortably positive. In view of previous testing in this area, this is a characteristic which unloading of the rotor system was expected to provide. On Figure 90, maneuvering stability at speeds up to 140 knots is seen to be positive even though the rotor is only partially unloaded. At this point the rotor, in 1g flight, is supplying approximately 35% of the net lift. Maneuvering capabilities at higher speeds and with the rotor system supplying smaller percentages of lift is an area which is worthy of additional study and flight testing.

Autorotation Entries: Safe autorotation entries and descents formed an important part of the Phase IV speed extension testing. The basic problem in this regard was to arrive at an operational procedure which, in the event of engine failure at very high speed, would be simple to perform and would provide the necessary rotor rpm control during the deceleration to conventional autorotational flight speeds.

The procedure which evolved from the build-up testing consists simply of deploying the wing spoilers and entering a right climbing turn as soon as a failure of the main engine is sensed. During this maneuver, load factors (g's) is modulated by the pilot with cyclic control to control rotor rpm to the desired level. With the rotor autorotating, the higher the load factor, the higher will be the rotor rpm for any given flight speed. The collective handle remains at the pre-failure setting until the helicopter has decelerated to the speed range of 100-120 knots at which point conventional autorotational characteristics exist. During the deceleration, the jet engine should remain operating; however, the thrust may be reduced to idle to facilitate the deceleration.

The purpose of the spoilers is to permit the attainment of the high angles of attack required for autorotation without attendant high or excessive load factors. Trim shifts when the spoilers are actuated are moderate and in the nose-up direction. This is favorable, since a higher angle of attack is desired, and is probably the result of lift forces continuing to act on the J-60 nacelle.

No problems were encountered during any of the autorotation testing which included entries up to approximately 150 knots. Spoiler deployment resulted in buffetting of the horizontal stabilizer, but controllability was not affected.

The autorotation testing conducted during Phase IV was of limited scope and oriented specifically to the task of assuring safety of flight during the speed envelope expansion testing. Optimization of techniques and exploration of other procedures did not form a part of these investigations. This is an area where additional testing should be focused. For example, the effect of wide variations in jet thrust and forward speed during autorotation should be explored, including the capability of the vehicle to perform in the autogyro mode.

Wing Stall Effects: Because of the asymmetry of wing design and nacelle placement, roll moments produced during stall and post-stall flight were investigated. A study of wind tunnel data was conducted to determine the magnitude of the roll moments which would be produced. These data indicated that as the stall is approached, the helicopter would first experience a roll moment to the left followed shortly thereafter by a right roll moment. The reason for this progression is that the wing and nacelle on the left-hand side are not as aerodynamically clean as the right-hand wing. This produces the left rolling tendency as the angle of attack is increased to high values. At some angle of attack, however, the flow over the right-hand wing separates abruptly, which causes the rolling moment to the right.

The magnitude of these moments, even considering the trim change from left to right, were well within previously demonstrated rotor control moments. Subsequent to this study, flight tests were performed wherein the wing was intentionally stalled. The pilot reported that the control displacements during these maneuvers were small and control was entirely satisfactory.

Structural Loads

Structural loads were measured during the Phase IV compound helicopter flight research program to determine the magnitude of loads and maintain safety of flight. Measurements that were included during the testing are the main rotor hub and blade loads, control gyro arm loads, main rotor pitch link axial load, tail rotor loads, horizontal stabilizer loads, wing bending, and main rotor lift.

Hub bending moment measurements were obtained at station 6 and are converted to stress at station 7 in the same manner as during the Phase III tests. This steel section at station 7 has an estimated endurance limit cyclic stress of 26,000 psi assuming a stress concentration factor of 3.

Level Flight: The compound helicopter was initially flown without the auxiliary J-60 jet engines operating. These tests were conducted from hover to a forward speed of 96 knots CAS. The structural loads with the J-60 off are shown in Figures 91 and 92. The structural loads on these plots are essentially the same as the conventional XH-51A helicopter loads extrapolated to the weight and center-of-gravity of the compound helicopter.

The next series of tests were conducted with the J-60 at idle (approximately 200 pounds of thrust). The structural loads with the J-60 at idle are shown in Figures 91 and 93. These plots show that the main rotor hub loads decrease with the added thrust from the J-60 at idle. With the thrust increased as required to maintain level flight, tests were conducted to determine the optimum collective pitch angle setting for the higher speeds. The structural loads are plotted versus collective blade angle for the various speeds and collective pitch settings up to 158 knots CAS, Figures 94 through 97. From these tests the optimum collective blade angle setting from a blade loads standpoint was determined to be approximately 4.5 degrees. The main rotor hub loads for this collective blade angle setting are also plotted versus calibrated airspeed on Figure 91.

The area of the horizontal stabilizer was then increased from 7.57 square feet to 24.2 square feet to increase the static longitudinal stability of the helicopter. Tests were conducted at 120 knots with variations in collective blade angle settings with this larger horizontal stabilizer. From the pitching moment plot, Figure 98, it was determined that a change in the incidence angle of the horizontal stabilizer from 2.0 degrees nose down to 0.0 degrees was desirable to relieve the pitching moment.

With the 0.0 degree horizontal stabilizer setting, tests were conducted at 120 knots and 140 knots with variations in collective to determine the effect of collective blade angle setting. The data from these tests are plotted in Figures 99 through 102. With the new stabilizer setting, the pitch moment component has been reduced considerably at the low collective blade angles. Extrapolation of these data to the higher speed conditions indicated that a collective setting of approximately 3.8 degrees would be a satisfactory compromise angle for proceeding to high speeds with a constant collective blade angle.

The speed was built up to 201.5 knots CAS in approximately 10-knot increments with the collective blade angle held at approximately 3.8 degrees. The data from these tests are plotted versus airspeed in Figures 103 through 107.

The main rotor blade flapwise cyclic bending at station 6, shown in Figure 103, increased almost linearly with speed to a maximum value of 15,300 inch-pounds at 201.5 knots. As can be seen in Figure 107, the majority of this moment was caused by the one-per-revolution pitch and roll components of the blade bending. Further adjustments in stabilizer size or incidence setting and adjusting the flexible tabs in the wing trailing edge could be accomplished to reduce the pitch and roll components for flight to higher speeds.

The cyclic flapwise bending at station 6 of 15,300 inch-pounds converts to a cyclic stress of 21,700 psi at station 7. The cyclic chordwise moment at station 6 of 18,200 inch-pounds converts to a stress of 2,800 psi at station 7. The sum of the two results in a maximum possible cyclic stress of 24,500 psi as compared to an estimated endurance limit of 26,000 psi.

A harmonic analysis was run on the wave form of the flapwise bending moment at station 6 to determine the one-per-revolution through six-per-revolution components. The one-per-revolution component was then resolved into a roll component and pitch component as shown in Figure 107. The two-per-revolution and three-per-revolution components from the harmonic analysis are plotted in Figure 108. The two- and three-per-revolution components are both reduced when the main rotor is unloaded as evidenced by the abrupt change in slope of both sets of curves and the pronounced displacement of the three-per-revolution curve as the rotor is unloaded, that is, as it goes from condition (A) to condition (B).

Main rotor pitch link axial loads are shown in Figure 105. The maximum cyclic loads are only 137 pounds as compared to an estimated endurance limit of 1,400 pounds. Note that there has been no tendency for the loads to increase rapidly with speed increase although at the highest speeds reached, advancing tip Mach numbers were approximately 0.9, well into the critical Mach range for the airfoil section. Since the blades are operating at low angles of attack, center of pressure shift with increasing Mach does not result in large blade pitching moments, as would be the case with a more heavily loaded rotor. The blade feathering and torsion loads have increased only very gradually with increase in airspeed.

Gyro arm flap and chord bending loads also are shown in Figure 105. At speeds above 170 knots, the gyro arm incidence angle setting was reduced from 30 degrees to 5 degrees. This had negligible effect on the cyclic chordwise loads, but did reduce the cyclic flapwise loads. The incidence angle was changed to reduce the steady torsion load on the gyro drive shaft. The cyclic loads measured are well below the estimated endurance limit of the gyro arms.

Measurements of tail rotor flapwise bending at station 19.5 were ob-

tained at speeds above 170 knots. These are shown in Figure 106. Analysis of data obtained during previous tests with the three-blade main rotor had shown that station 19.5 was the most critical bending station on the tail rotor. The cyclic loads fall somewhat below what might be expected by extrapolating the measurements as a regular helicopter; however, they are approaching the estimated endurance limit of 790 inch-pounds. Linear extrapolation of the data indicates that the endurance limit would be reached at a speed somewhere between 230 and 240 knots CAS.

Measured horizontal stabilizer bending loads are shown in Figure 104. There is a difference between the average load on the left and right sides, indicating an apparent swirl in the air flow in that area. The static loads are well under the limit static strength. The cyclic loads obtained are reasonably high, and the frequency of motion is at tail rotor rotational frequency. The symmetrical first-bending mode of the stabilizer, as determined by ground shake tests, is 30.5 cps. The tail rotor rotational frequency is 35 cps, and apparently the two frequencies are close enough together to provide a reasonable amount of excitation to the stabilizer. To help alleviate this, cable guy wires were strung from the stabilizer tips to the fuselage, top and bottom, at the stabilizer. These helped keep the oscillatory amplitude from building up too rapidly. The estimated endurance limit for the stabilizer is 3,200 inch-pounds. This was exceeded by 22% for a few minutes of flight time in the runs at speeds above 180 knots. For future tests to higher speeds, changes in the stabilizer will be required to reduce the cyclic loads.

Autorotation Entries: Structural loads during the transition from powered flight to autorotation and during the autorotation are usually less than experienced in powered level flight.

Maneuvering Conditions: The load factors obtained at various airspeeds are shown in the maneuvering envelope on Figure 109. The maximum speed obtained with jet off was 134 knots CAS and the maximum load factor was 1.51g with the minimum load factor of 0.4g. With the jet engine operating, the maximum load factor obtained was 1.8g and the minimum 0.64g. All load factors are corrected to a weight of 4,300 pounds.

Main rotor flapwise and chordwise bending moments at station 6 and flapwise bending moment at station 157 are plotted versus sustained and transient load factor in Figures 110, 111, and 112. With the jet engine on and the collective blade angle lowered, the flapwise average bending moments at station 6 are more negative due to the reduced rotor lift. The cyclic loads scatter considerably and do not appear to have any significant trend with either load factor or rotor lift. With reduced

rotor lift, the chordwise loads, both average and cyclic, are reduced considerably at all load factors. At station 157, the flapwise cyclic bending loads appear to be somewhat smaller with a reduced collective blade angle (jet engine on), whereas the average loads appear to be relatively unaffected by the collective blade angle.

The flapwise and chordwise cyclic loads are the maximum loads that occurred during the maneuver and do not necessarily occur at the time of the maximum load factor.

Vibration: Cabin vibration was monitored throughout the compound helicopter flight research program. Vibration levels were strongly affected by the amount of rotor loading. This is reflected in high levels of vibration in the pure helicopter mode shown in Figure 92 and also in slightly lower levels with the J-60 engine at idle, Figure 93. These figures show the amplitude of the four-per-revolution vibration in the vertical, lateral, and longitudinal direction at the pilot's station.

During subsequent high-speed flights with J-60 engine thrust as required for these speeds, vertical vibration was the only one recorded due to the lower levels apparent and the shortage of oscillograph channels. The combined levels of four-per-revolution and higher frequencies in the vertical mode are shown on Figure 113. The four-per-revolution vertical mode amplitudes for J-60 off and J-60 idle from Figures 92 and 93 are also shown here for reference.

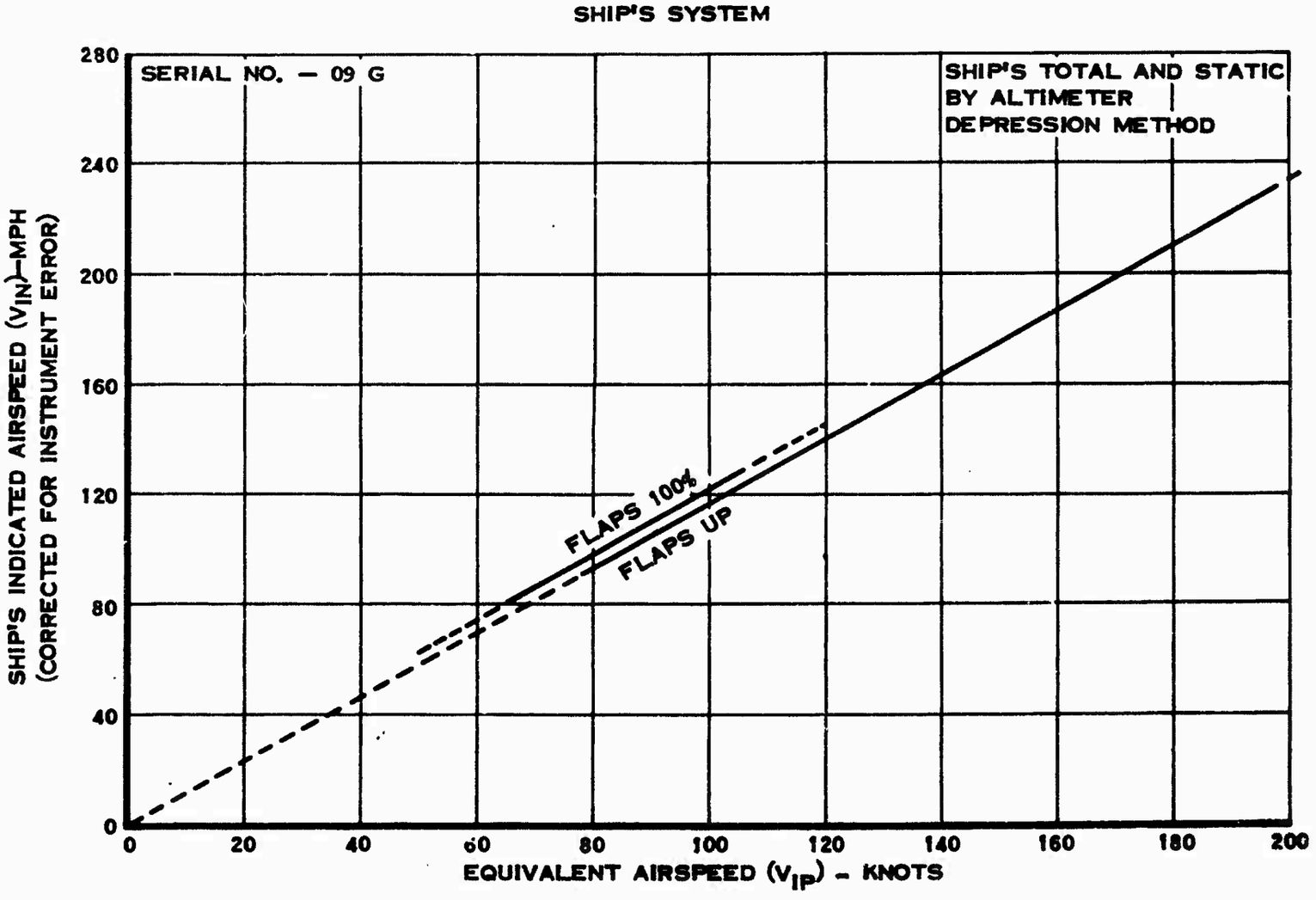

Figure 76. Pacer Aircraft Airspeed Calibration.

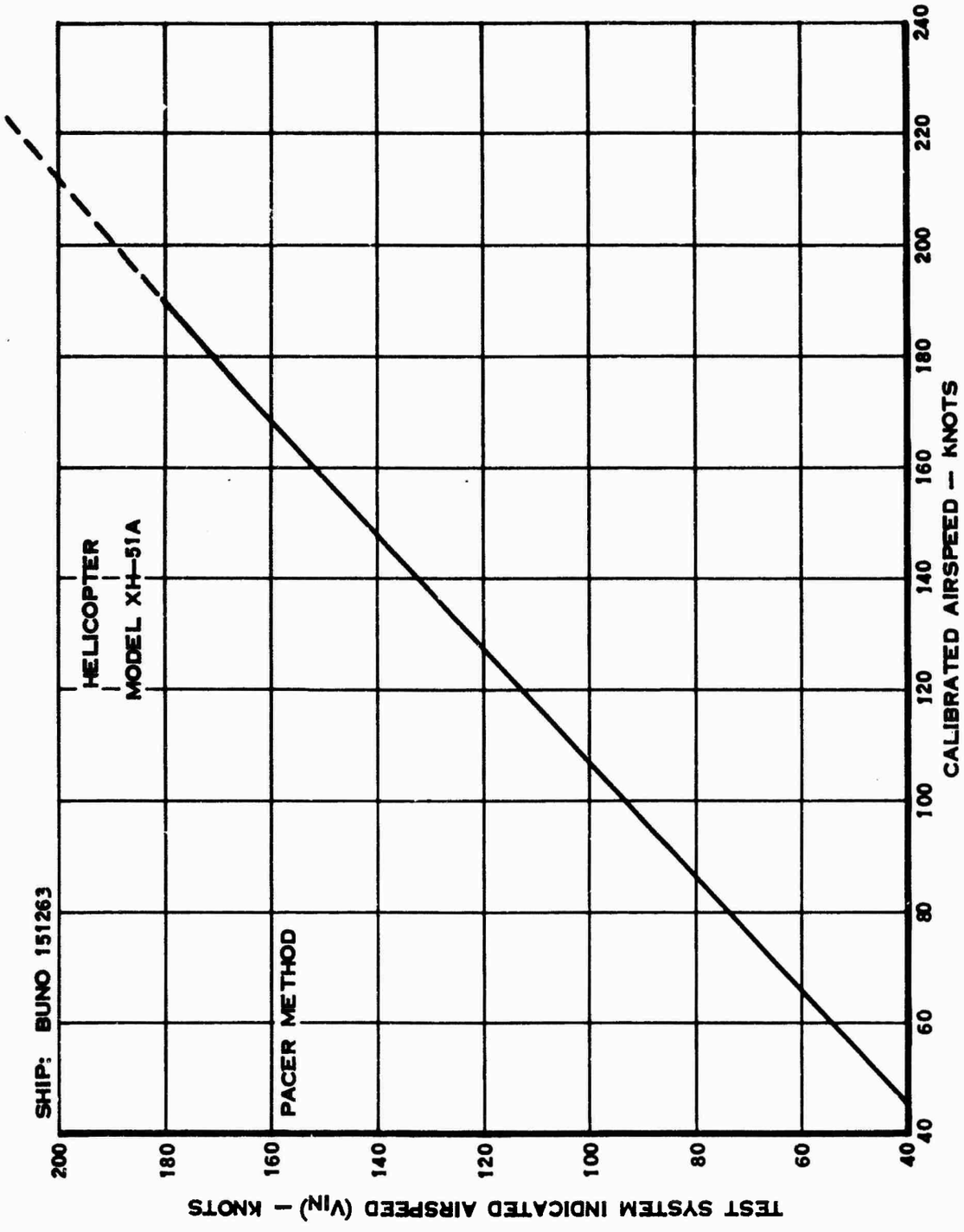

Figure 77. Airspeed Calibration Test System.

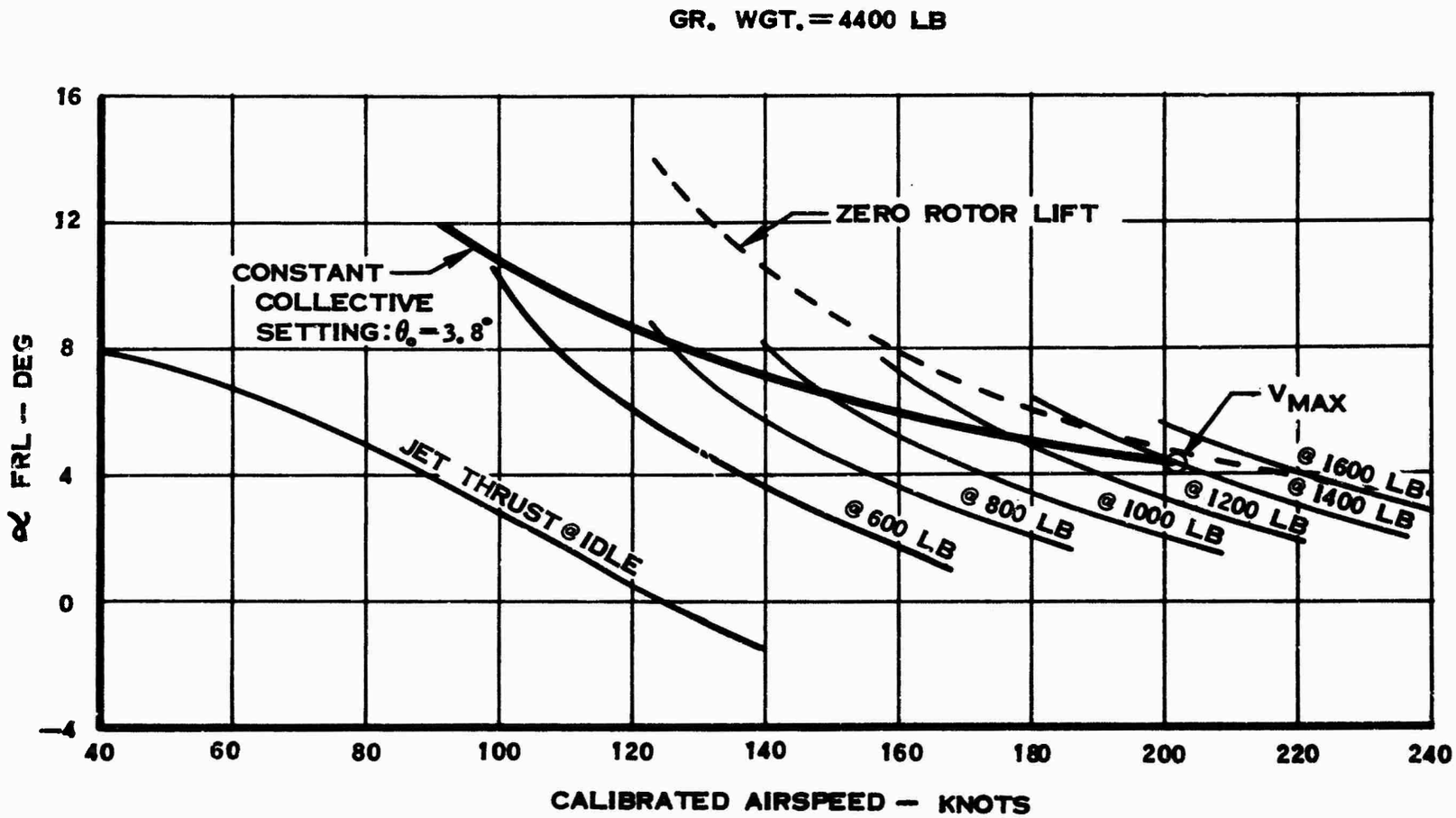

Figure 78. Level Flight Performance Versus Angle of Attack and Jet Thrust - Compound Helicopter.

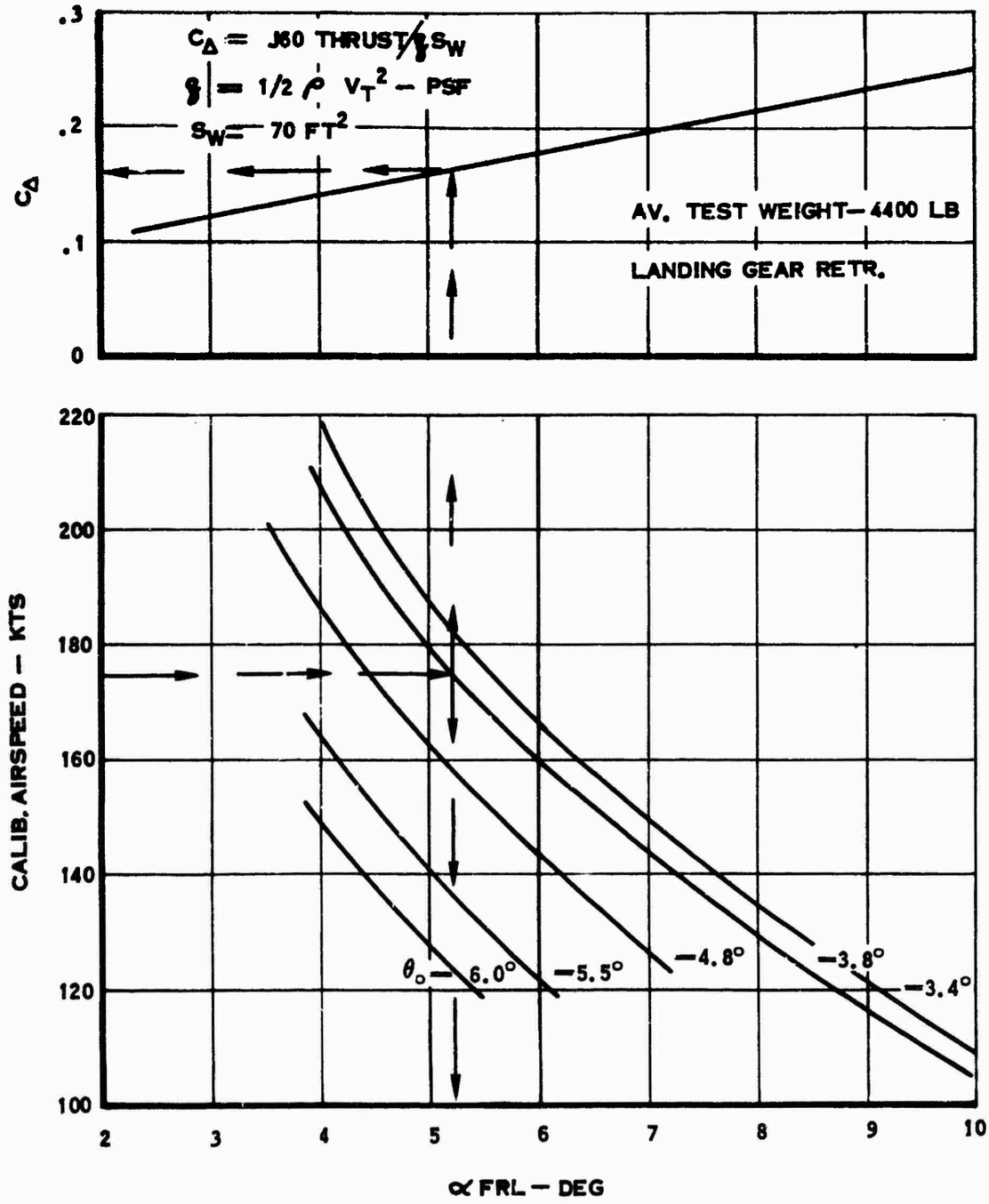

Figure 79. Collective Pitch Blade Angle and Auxiliary Thrust Requirements - Compound Helicopter.

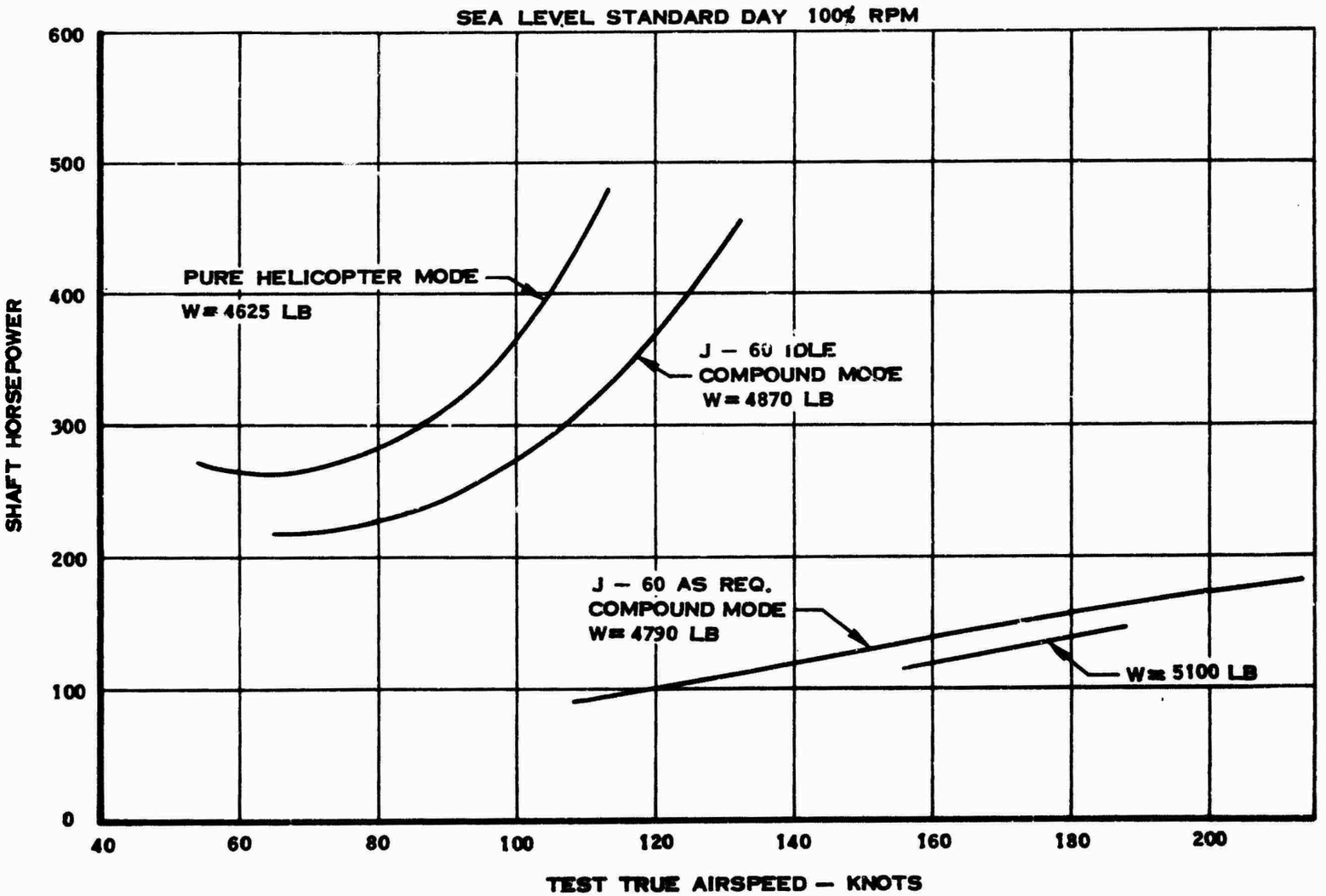

Figure 80. Level Flight Performance - Variation of Shaft Horsepower - Compound Helicopter.

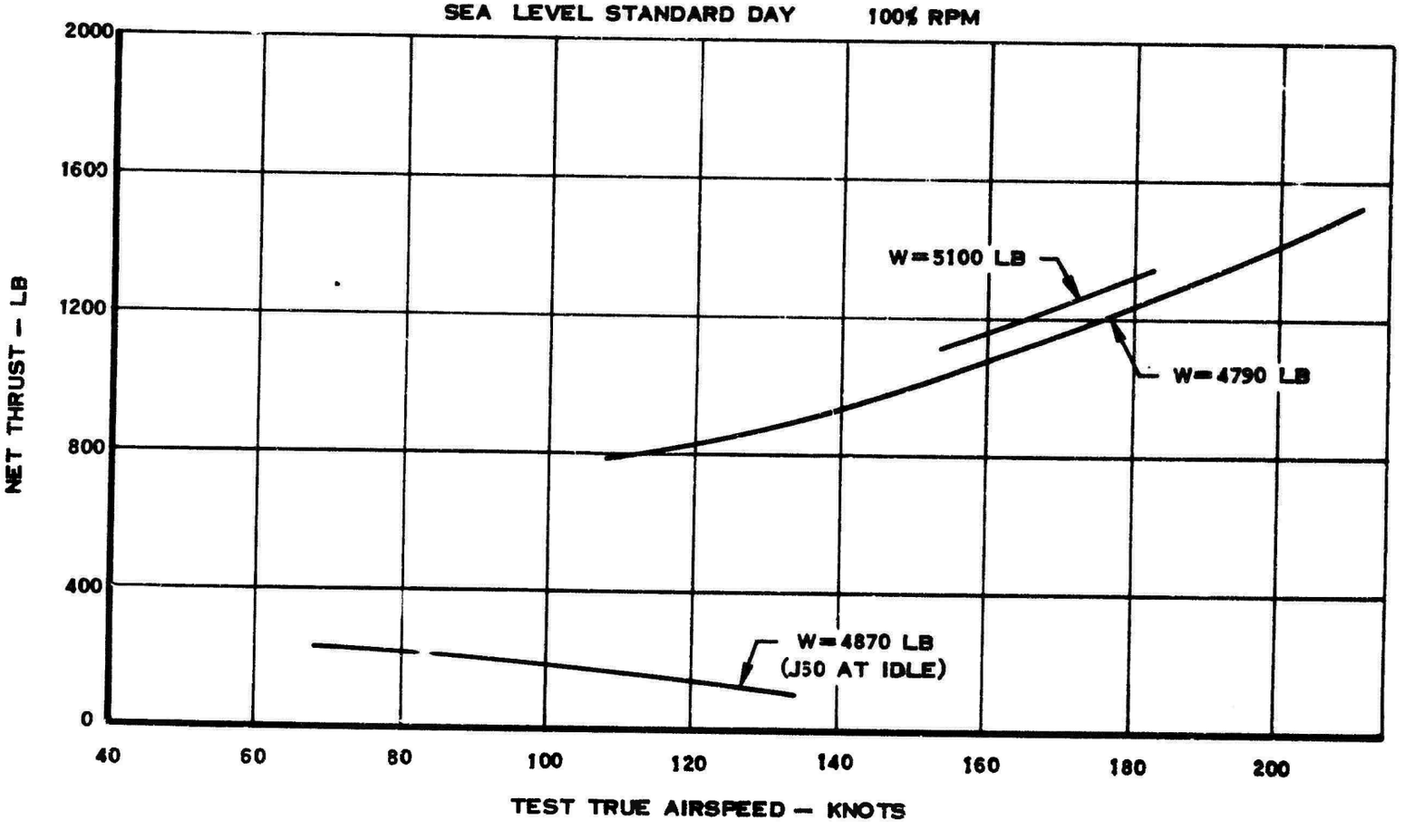

Figure 81. Level Flight Performance - Variation of Net Jet Thrust - Compound Helicopter.

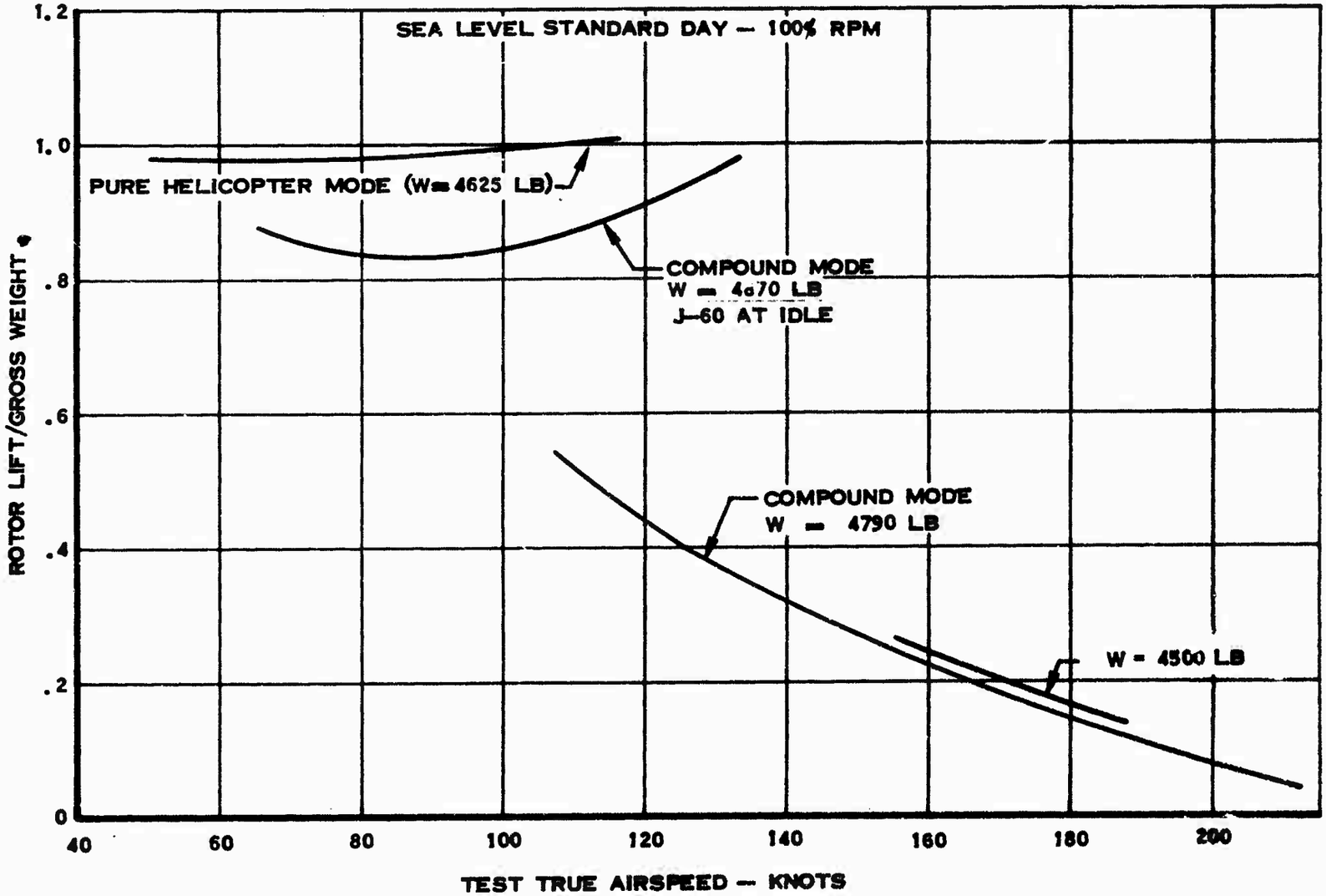

Figure 82. Level Flight Performance - Variation of Rotor Lift - Compound Helicopter.

$C_L = LIFT/q\ S_W$

$q = 1/2\ \rho V^2$

$S_W = 70\ FT^2$

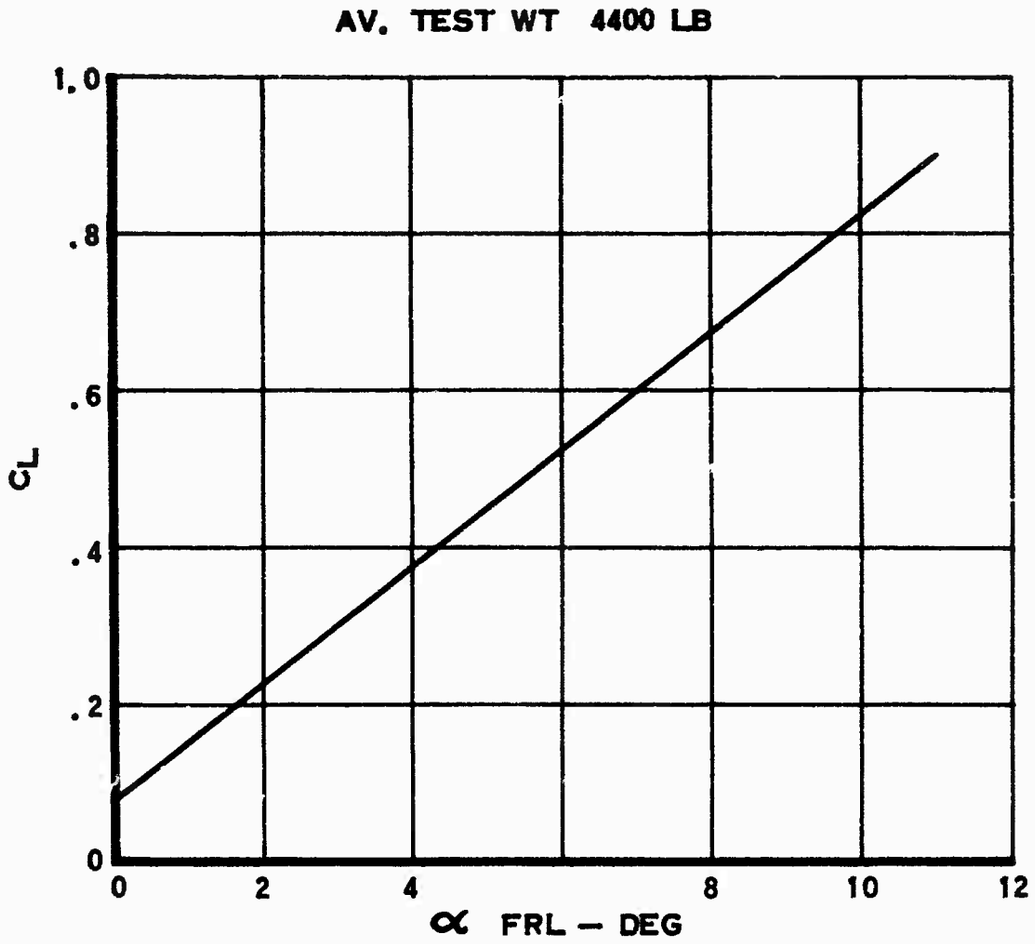

Figure 83. Wing-Body Lift Coefficient Versus Angle of Attack - Compound Helicopter.

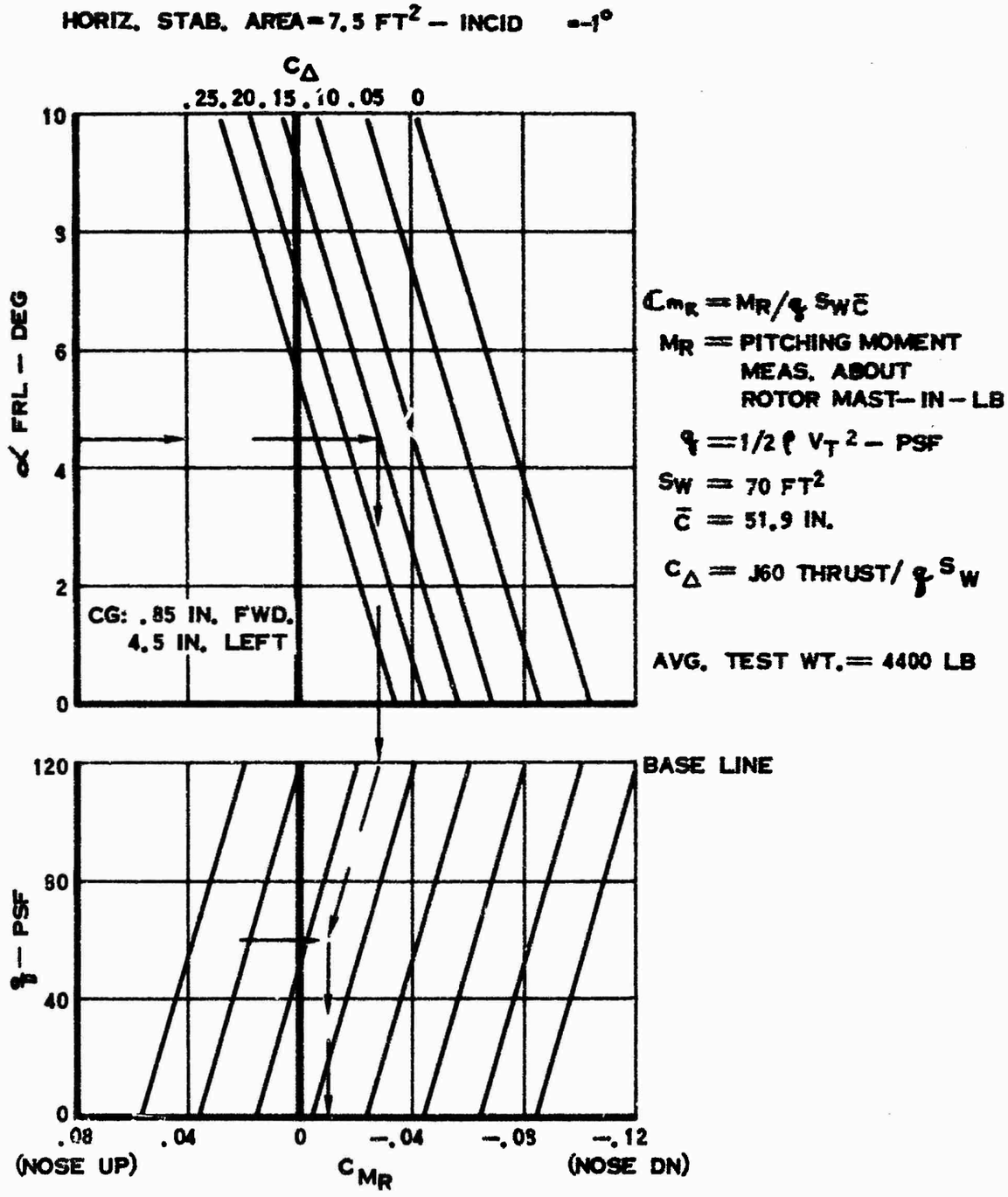

Figure 84. Static Longitudinal Stability and Trim Requirements - Compound Helicopter.

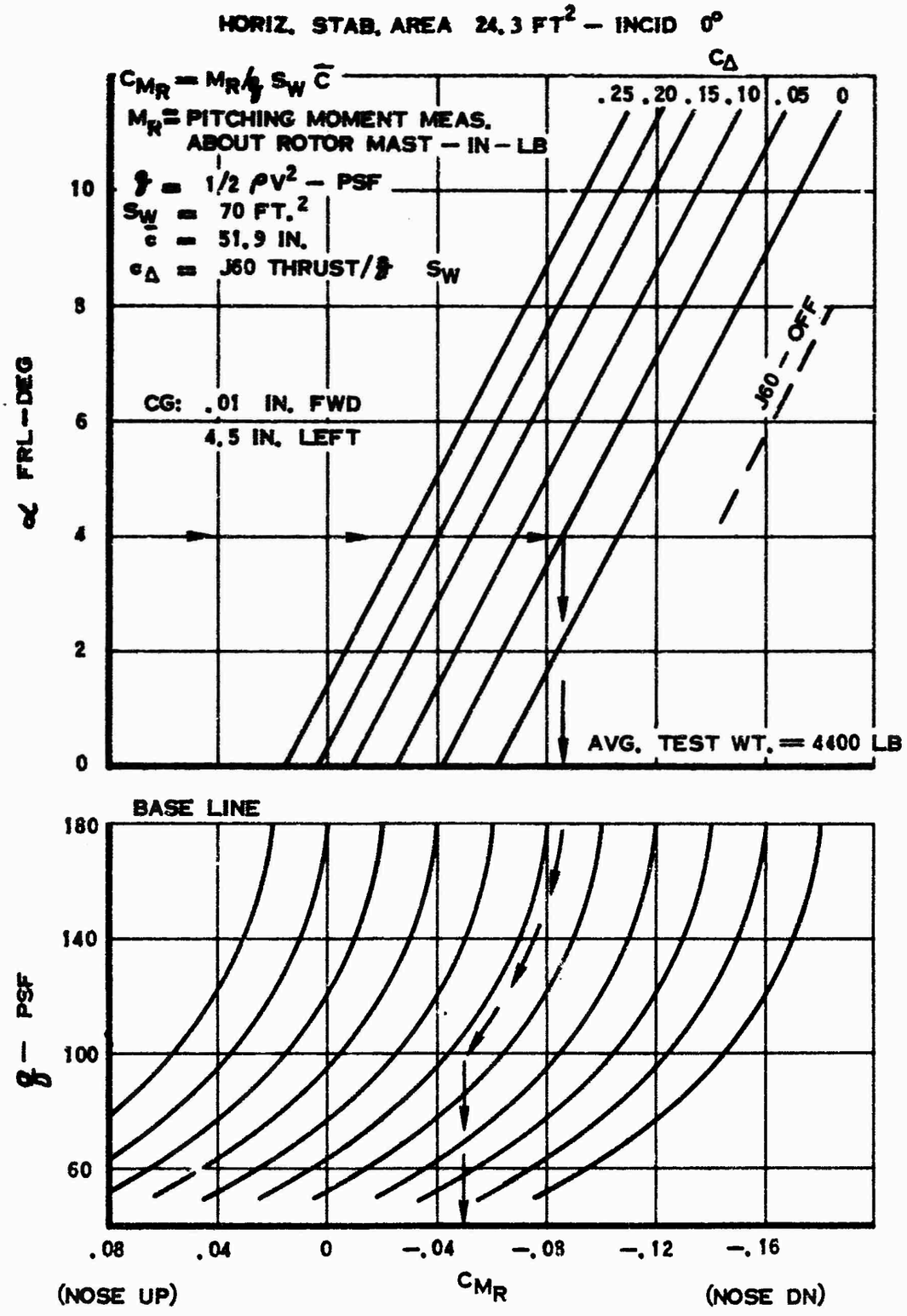

Figure 85. Static Longitudinal Stability and Trim Requirements - Compound Helicopter.

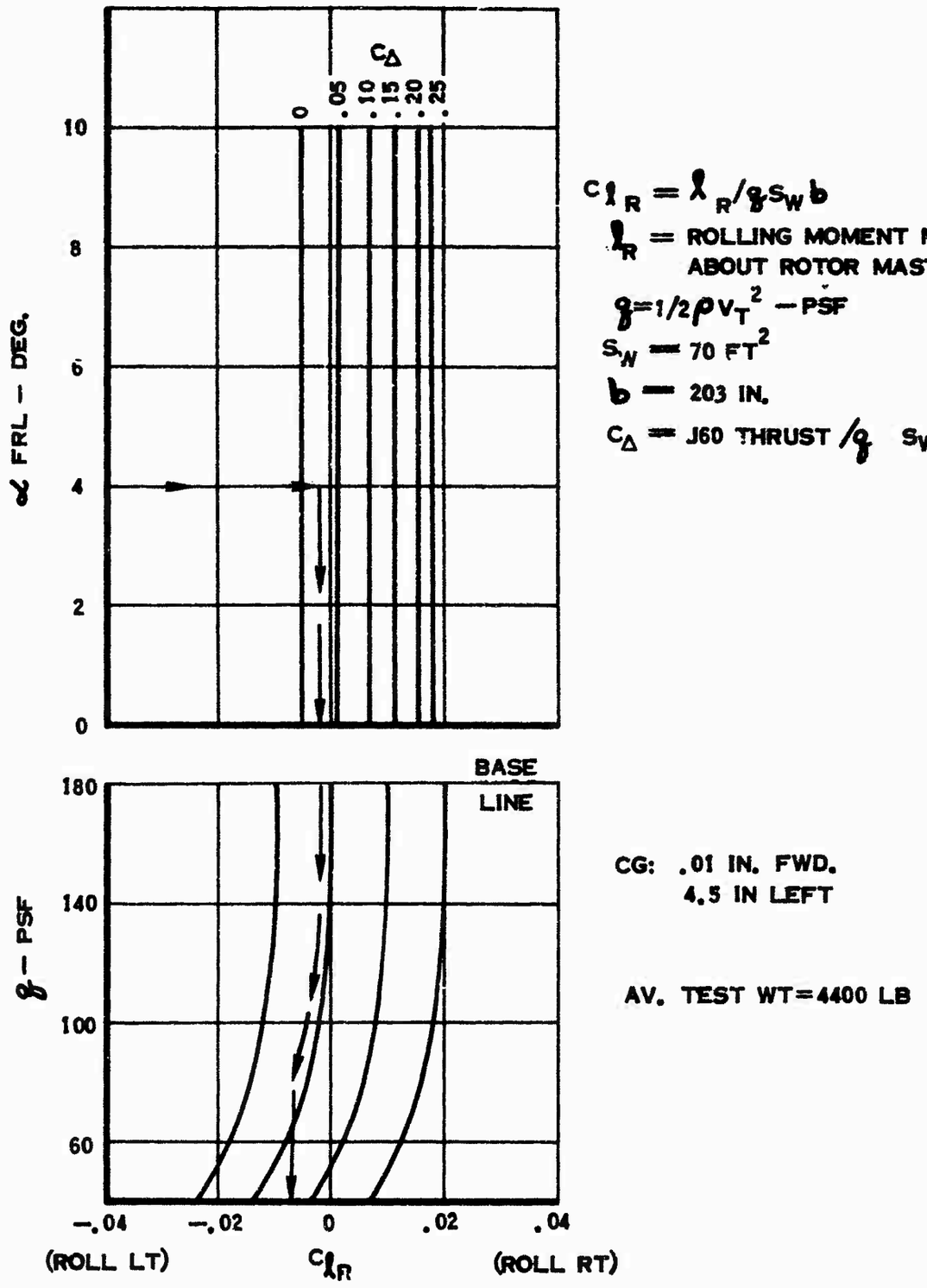

Figure 86. Lateral Trim Requirements - Compound Helicopter.

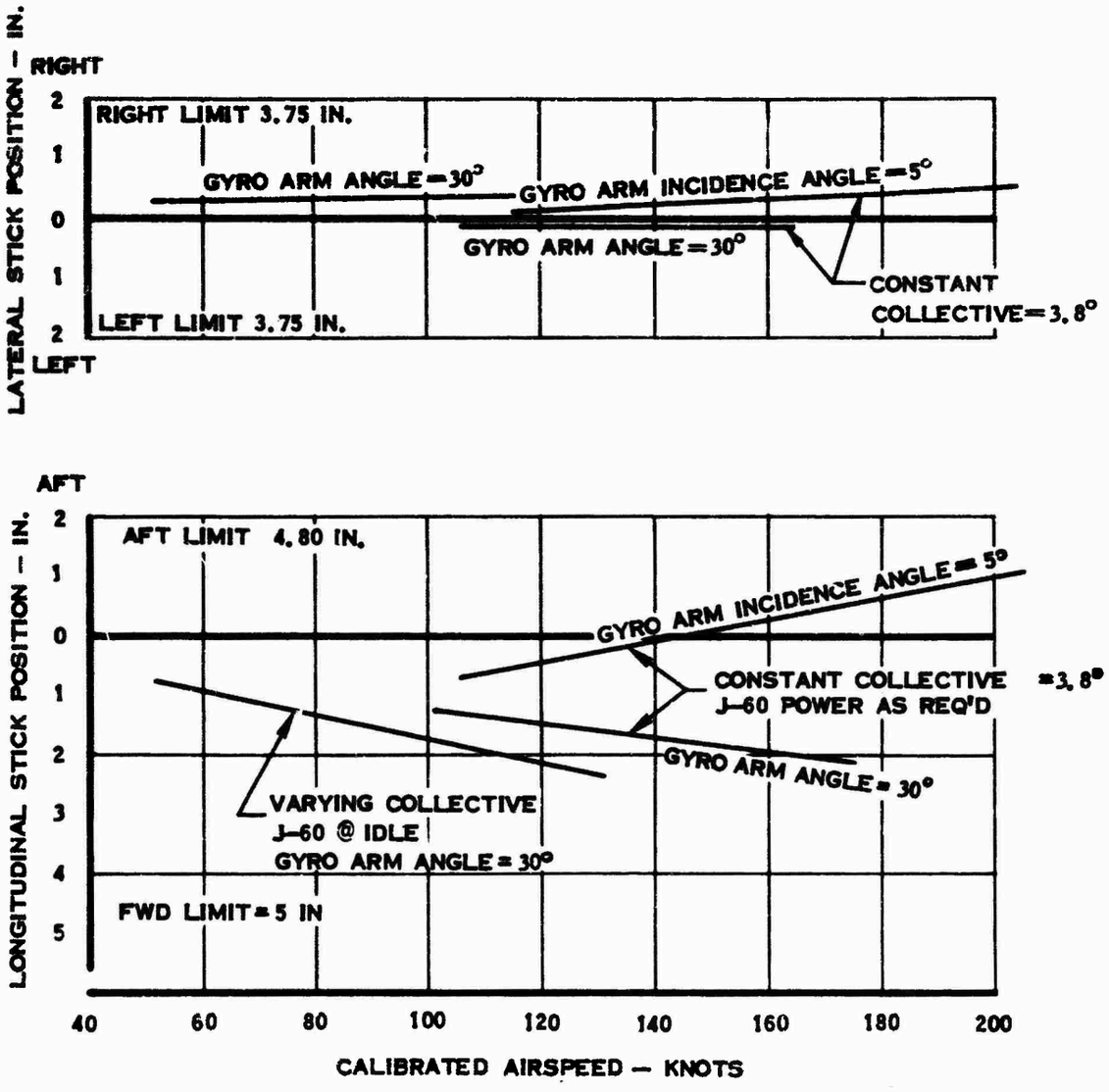

Figure 87. Cyclic Pitch Control Stick Positions in Level Flight - Compound Helicopter.

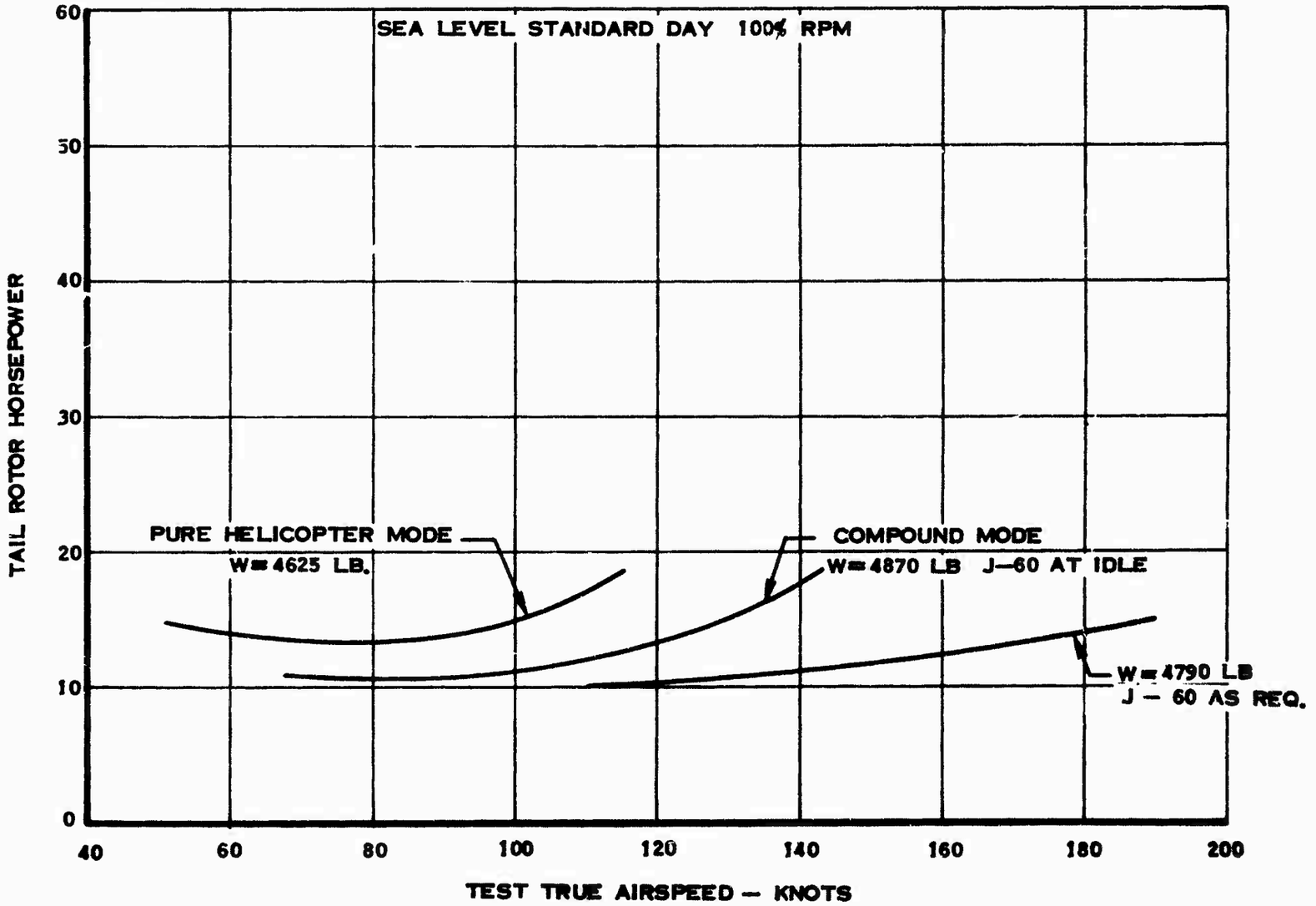

Figure 88. Level Flight Performance - Variation of Tail Rotor Horsepower - Compound Helicopter.

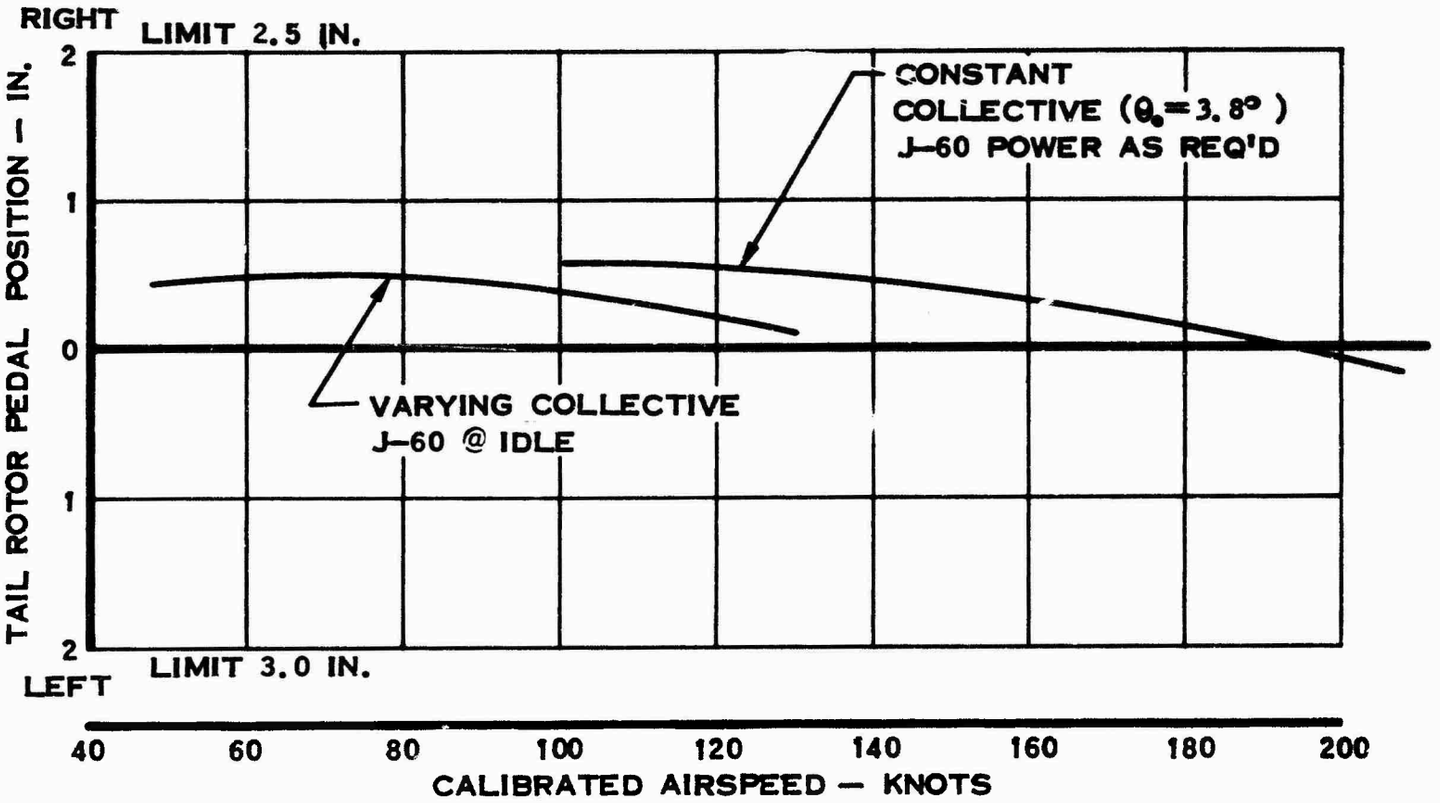

Figure 89. Tail Rotor Pedal Position in Level Flight - Compound Helicopter

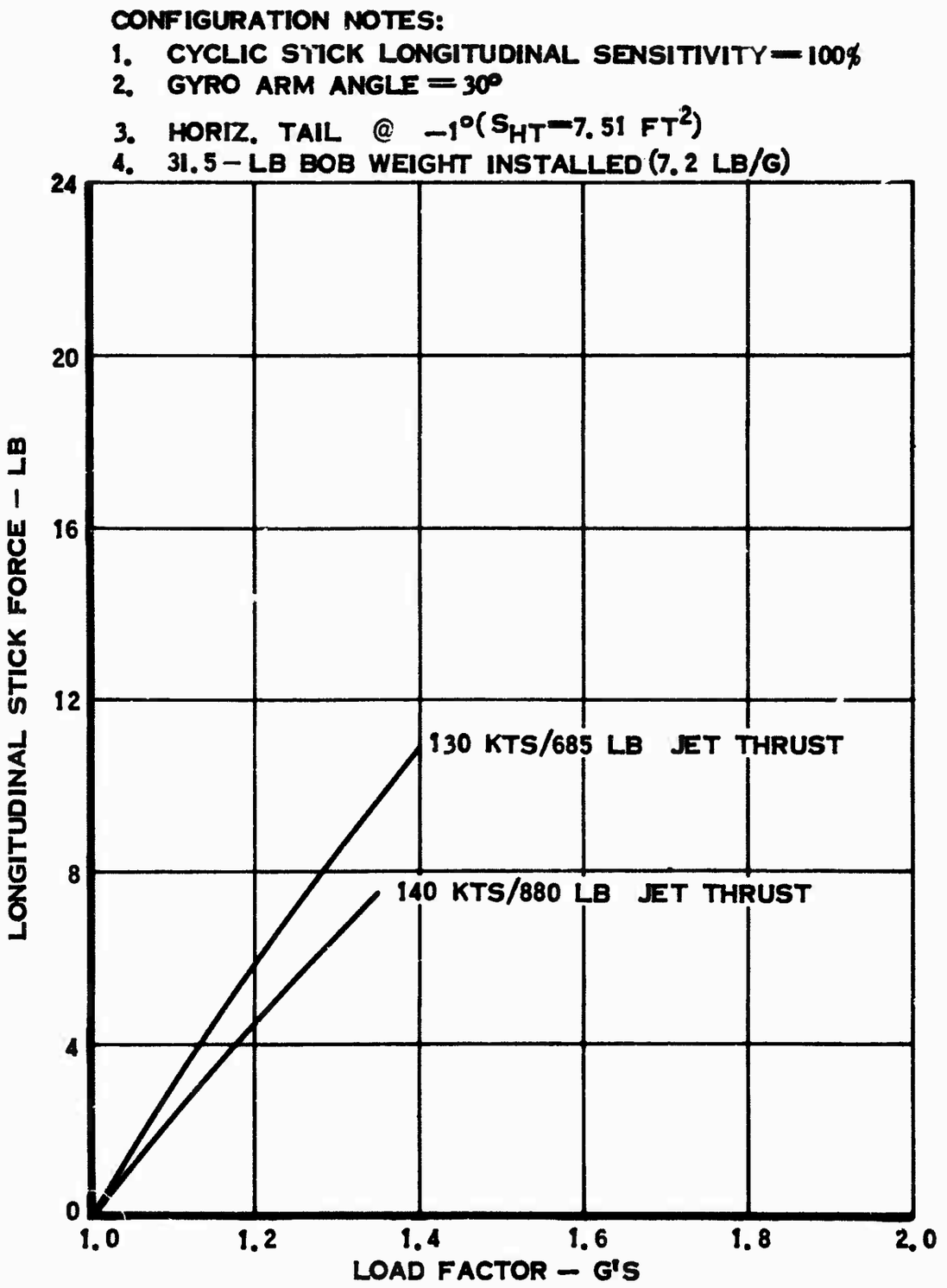

Figure 90. Maneuvering Stability With J-60 Engine Operating - Compound Helicopter

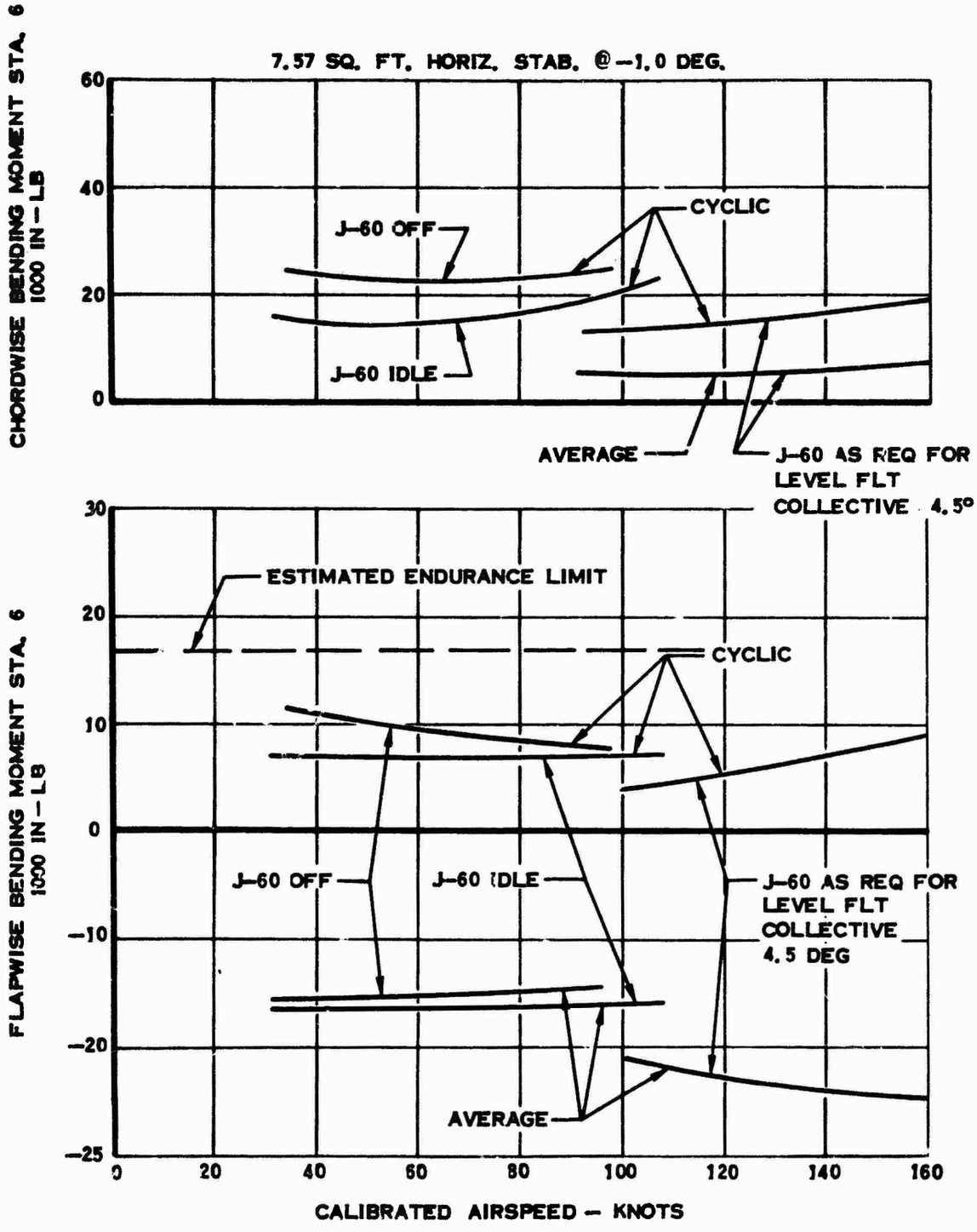

Figure 91. Main Rotor Loads Versus Calibrated Airspeed - Compound Helicopter.

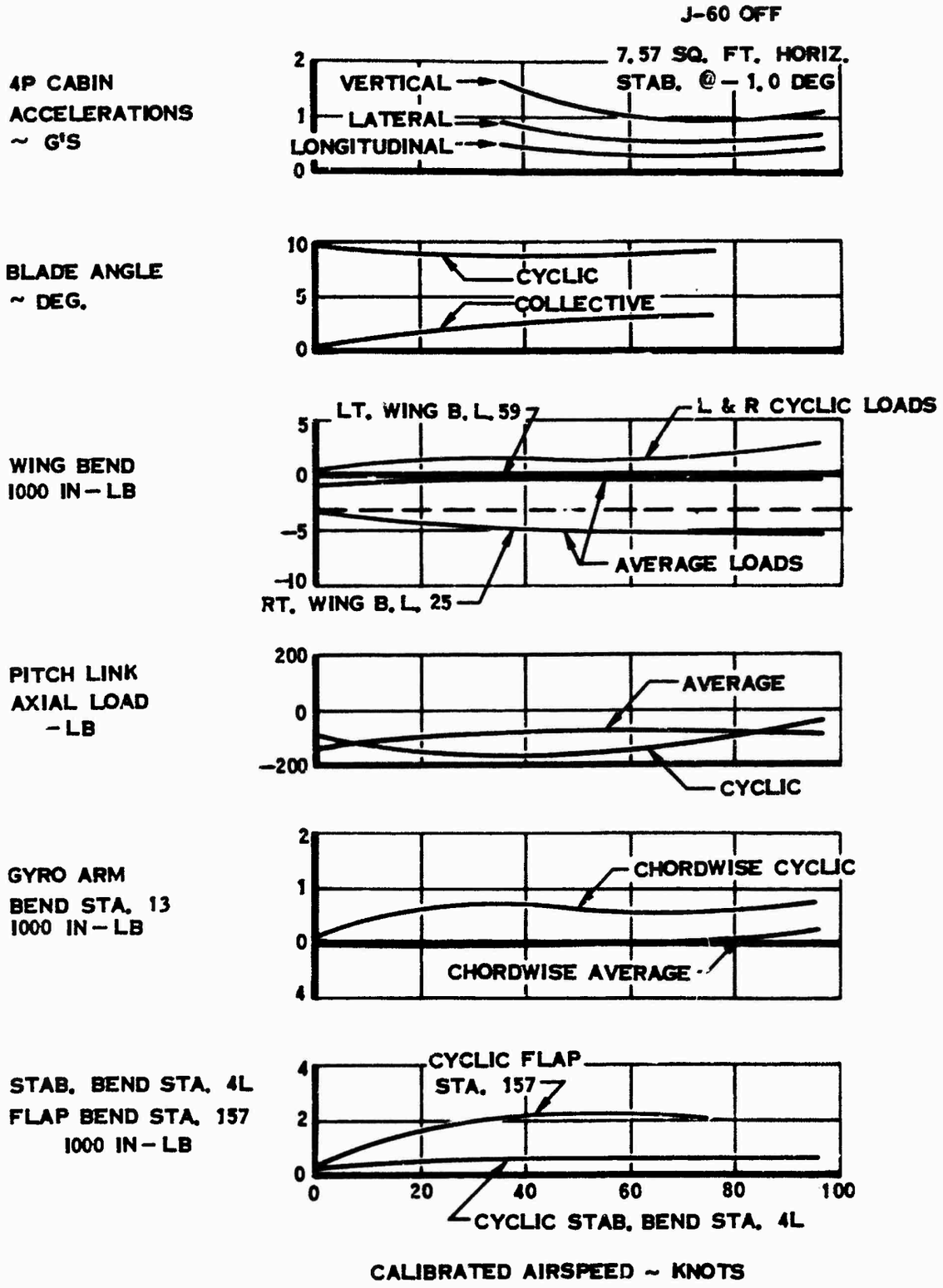

Figure 92. Loads and Accelerations Versus Calibrated Airspeed - Compound Helicopter.

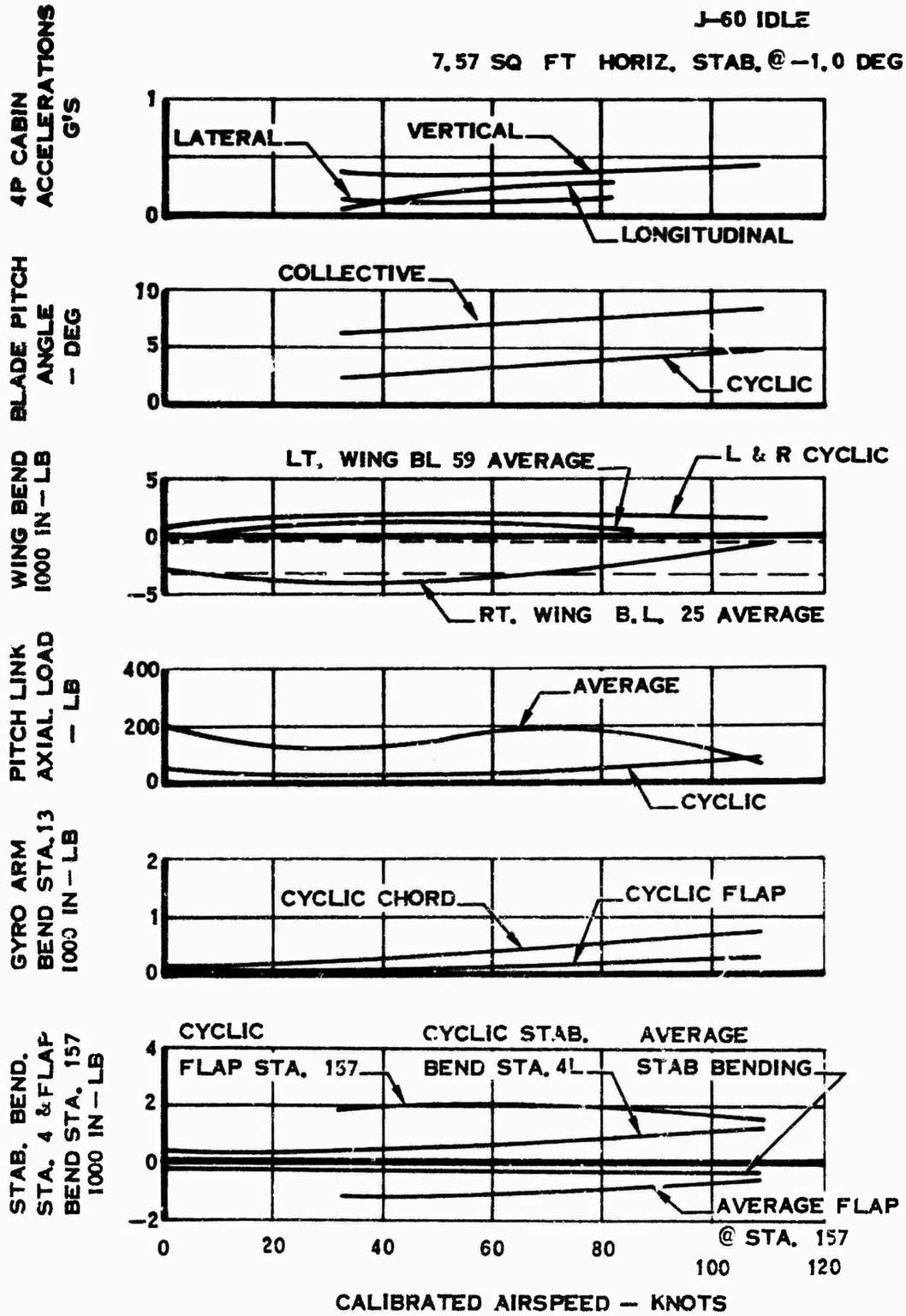

Figure 93. Loads and Accelerations Versus Calibrated Airspeed - Compound Helicopter.

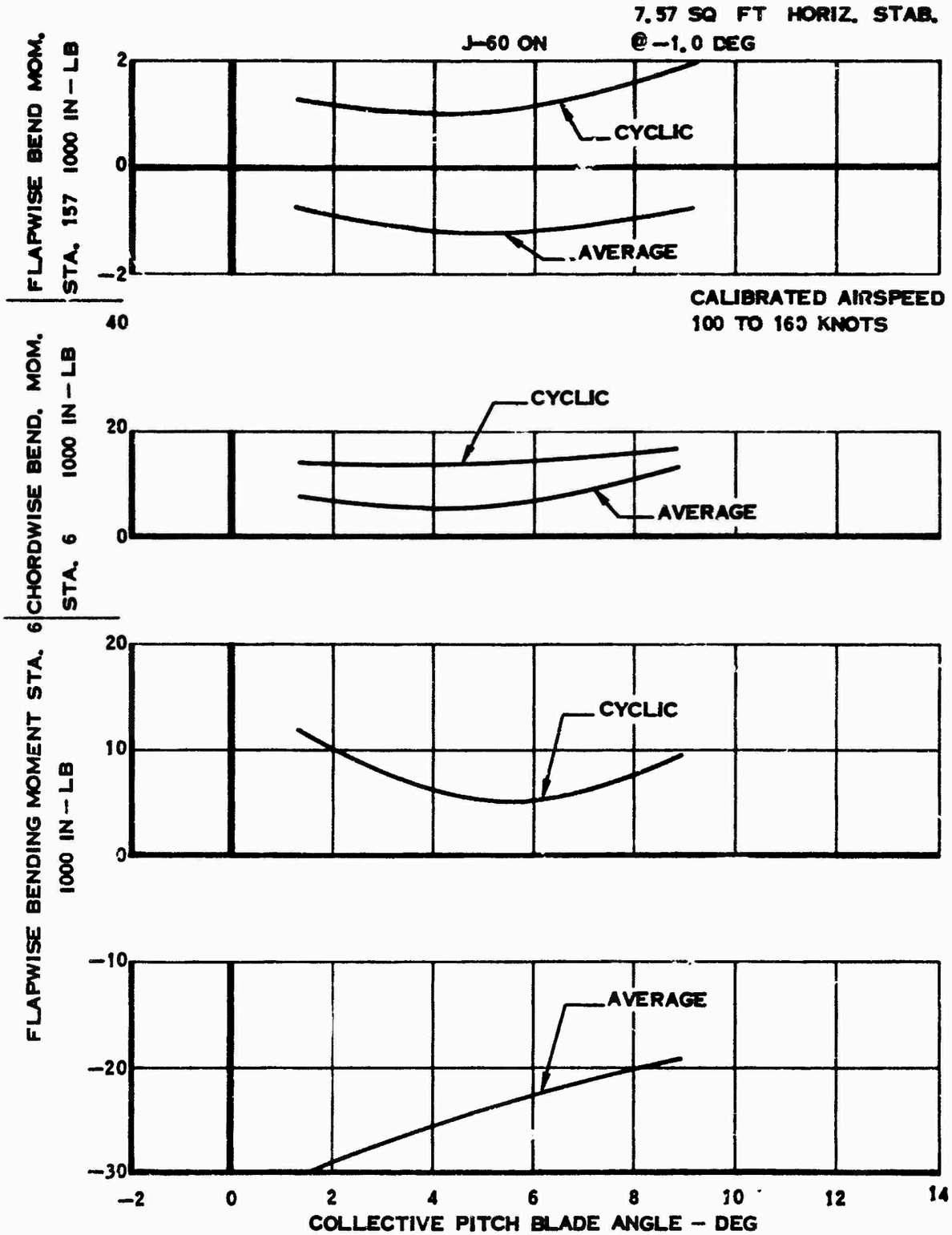

Figure 94. Main Rotor Loads Versus Collective Pitch Blade Angle - Compound Helicopter.

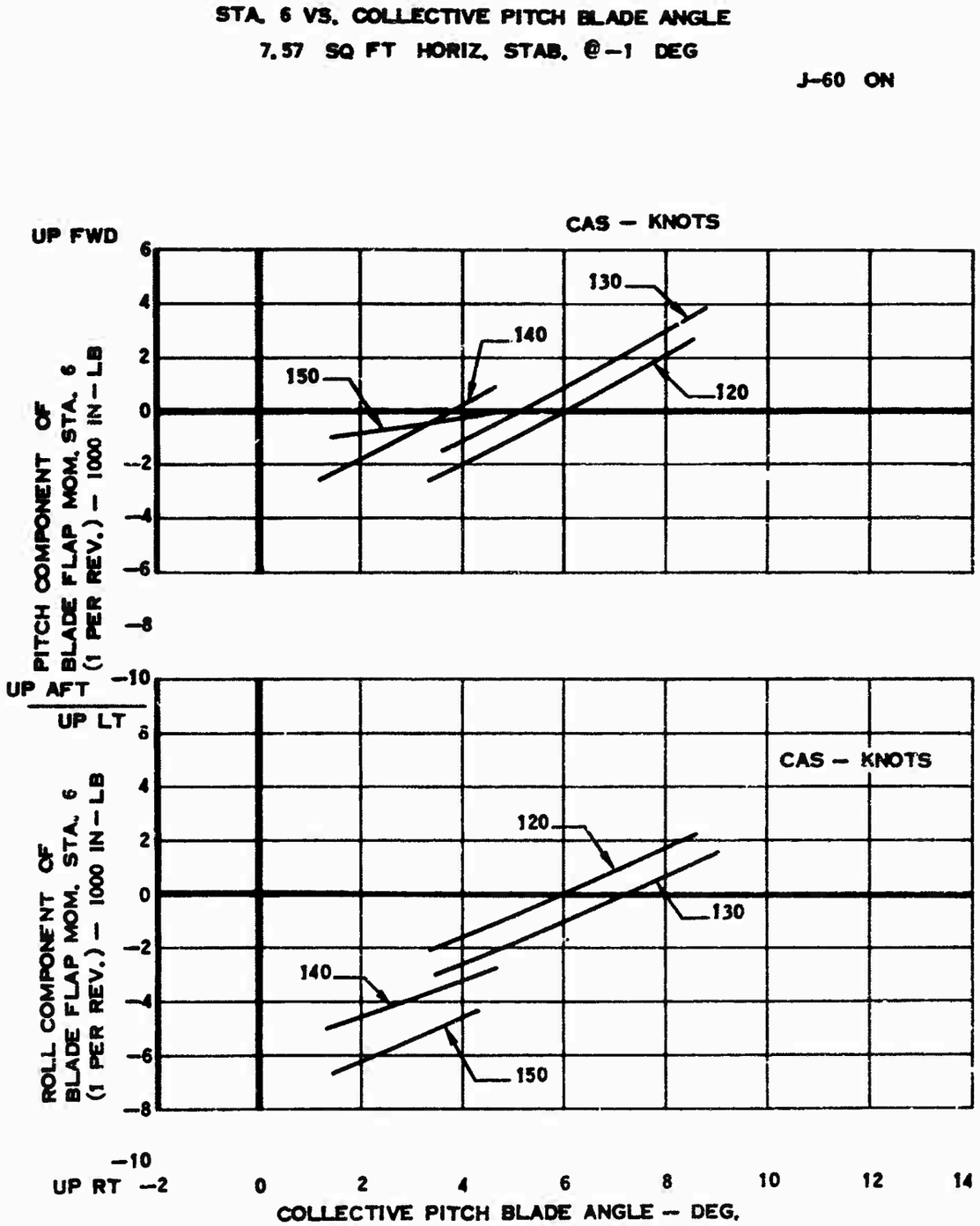

Figure 95. Pitch and Roll Component of Flapwise Bending Moment - Compound Helicopter.

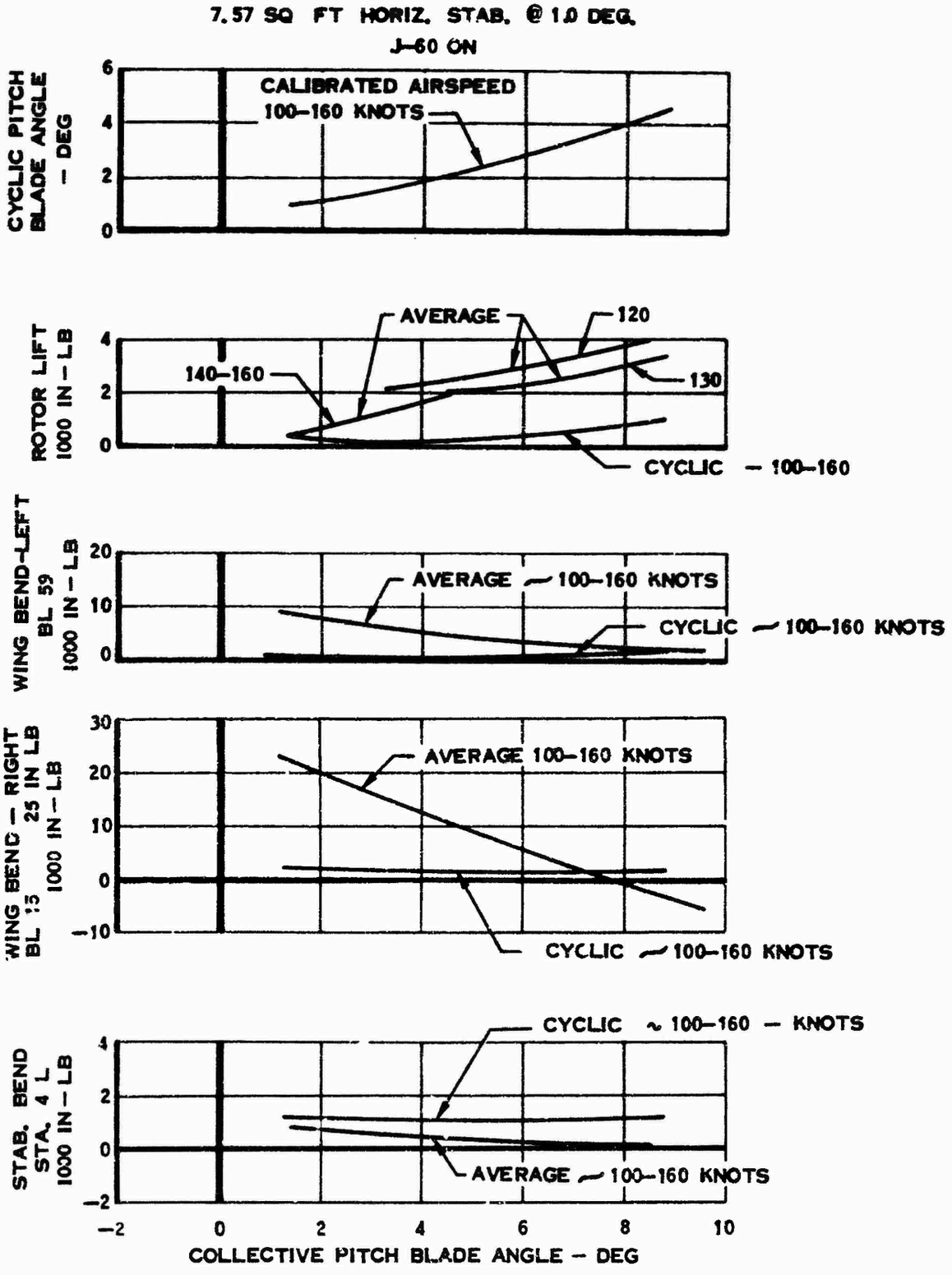

Figure 96. Loads Versus Collective Pitch Blade Angle - Compound Helicopter.

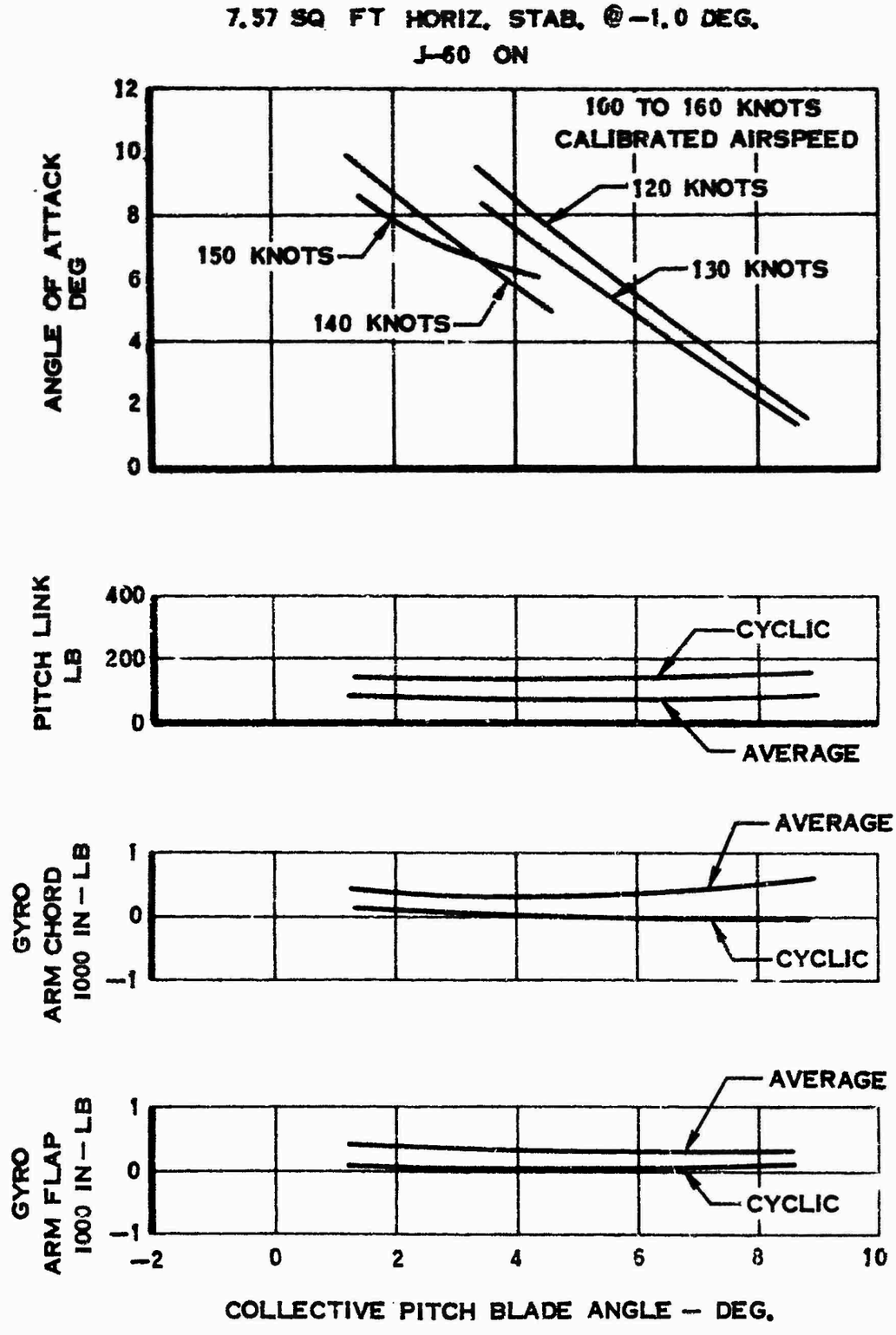

Figure 97. Loads Versus Collective Pitch Blade Angle - Compound Helicopter.

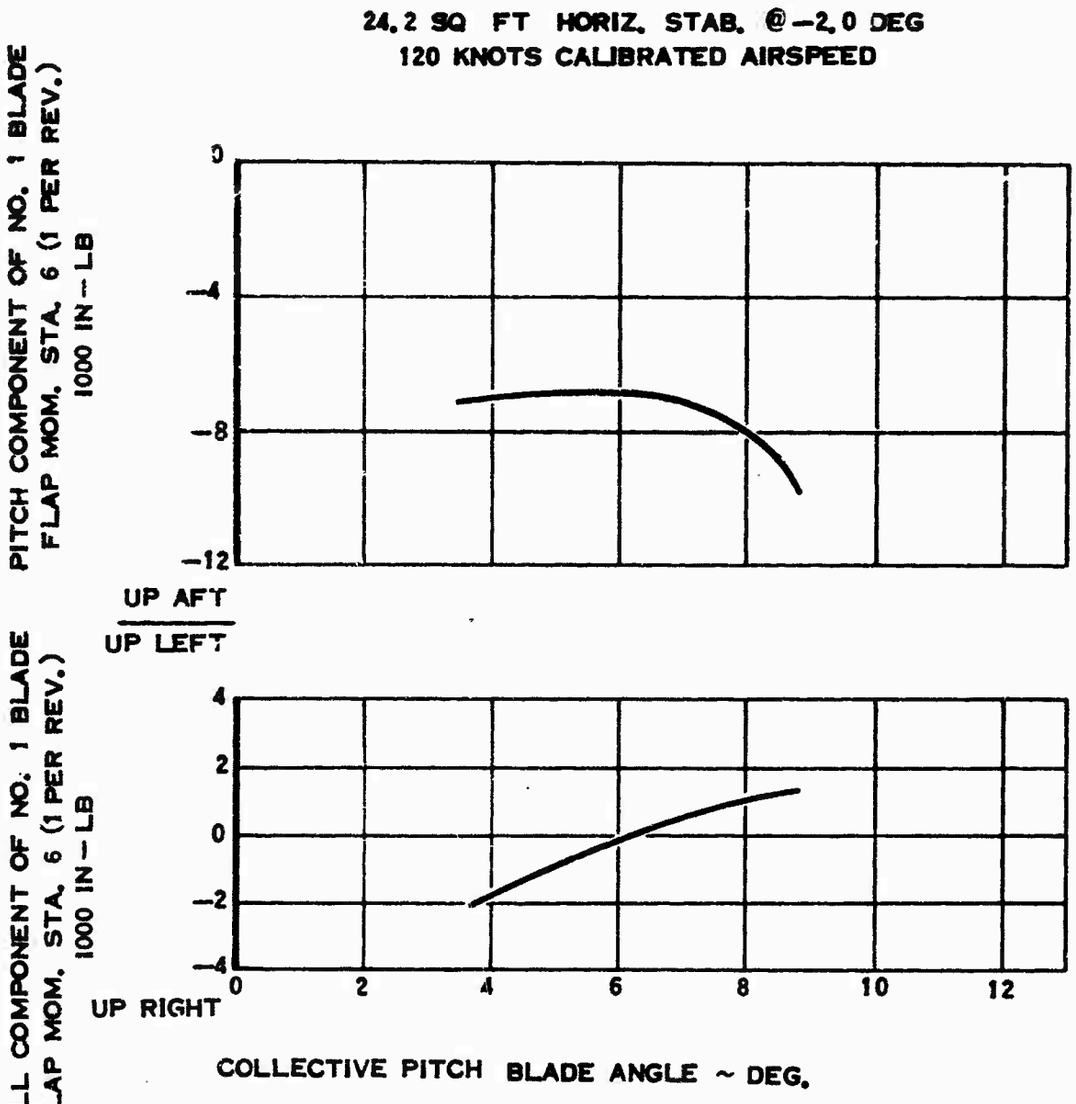

Figure 98. Roll Component and Pitch Component Versus Collective Pitch Blade Angle J-60 On - Compound Helicopter.

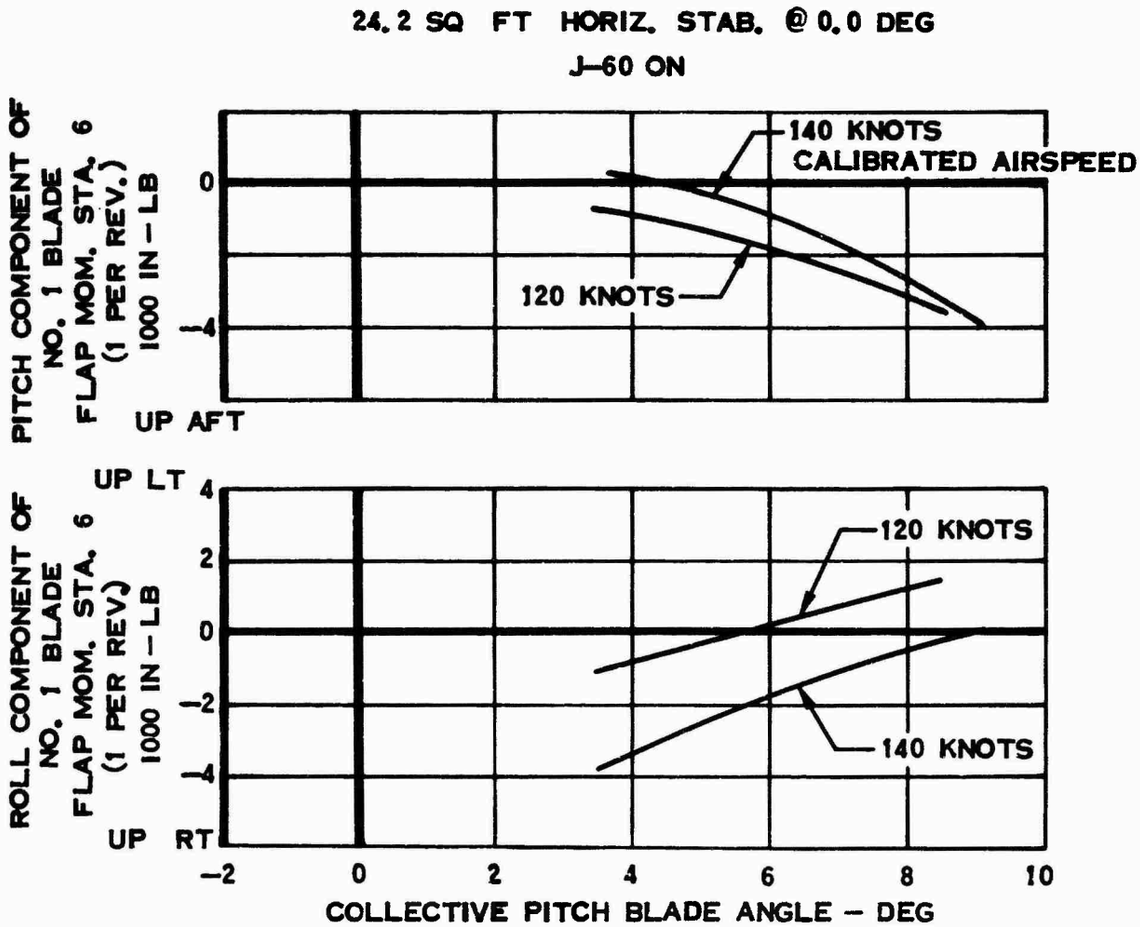

Figure 99. Roll Component and Pitch Component Versus Collective Pitch Blade Angle - Compound Helicopter.

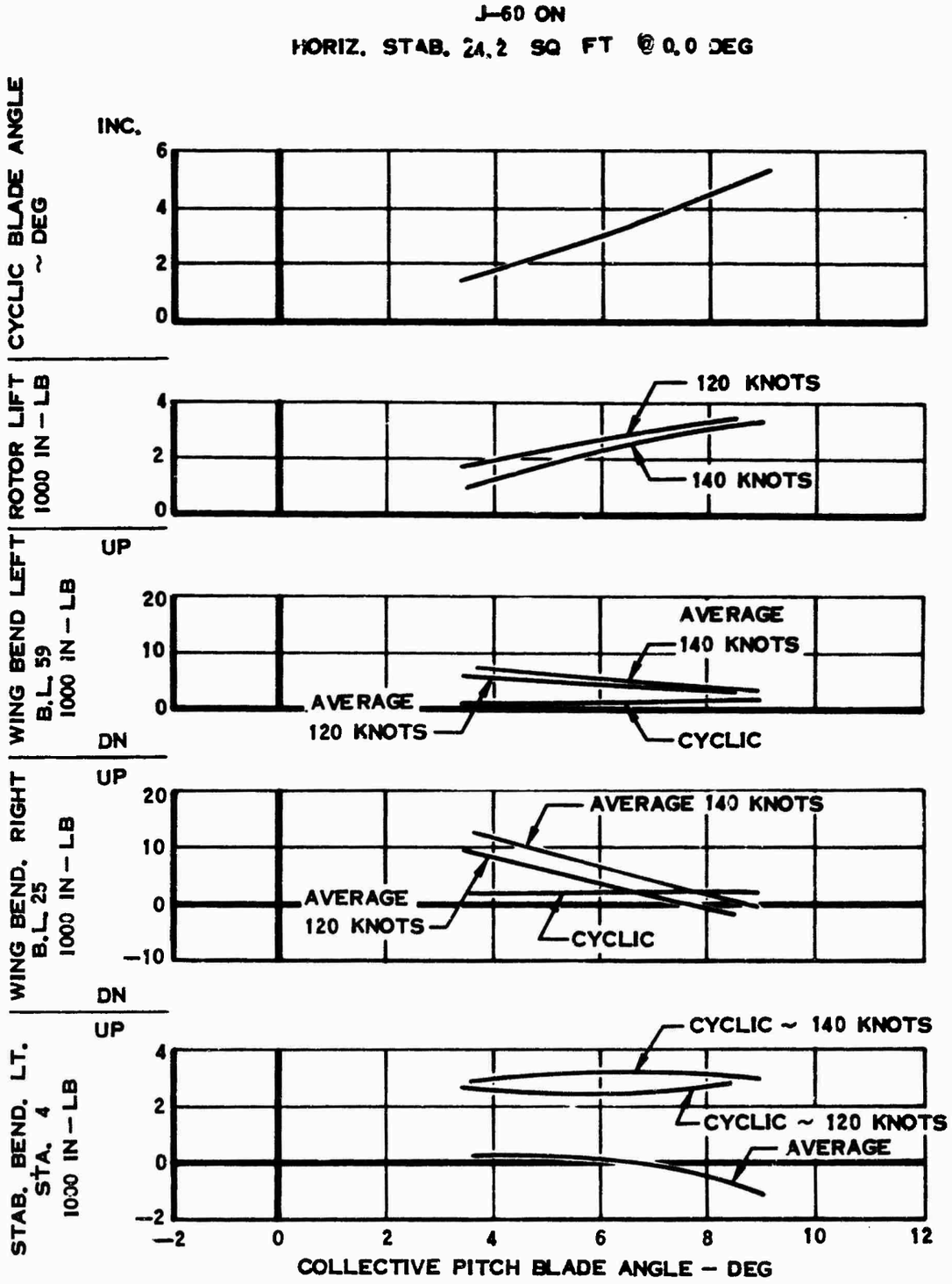

Figure 100. Load Versus Collective Pitch Blade Angle - Compound Helicopter.

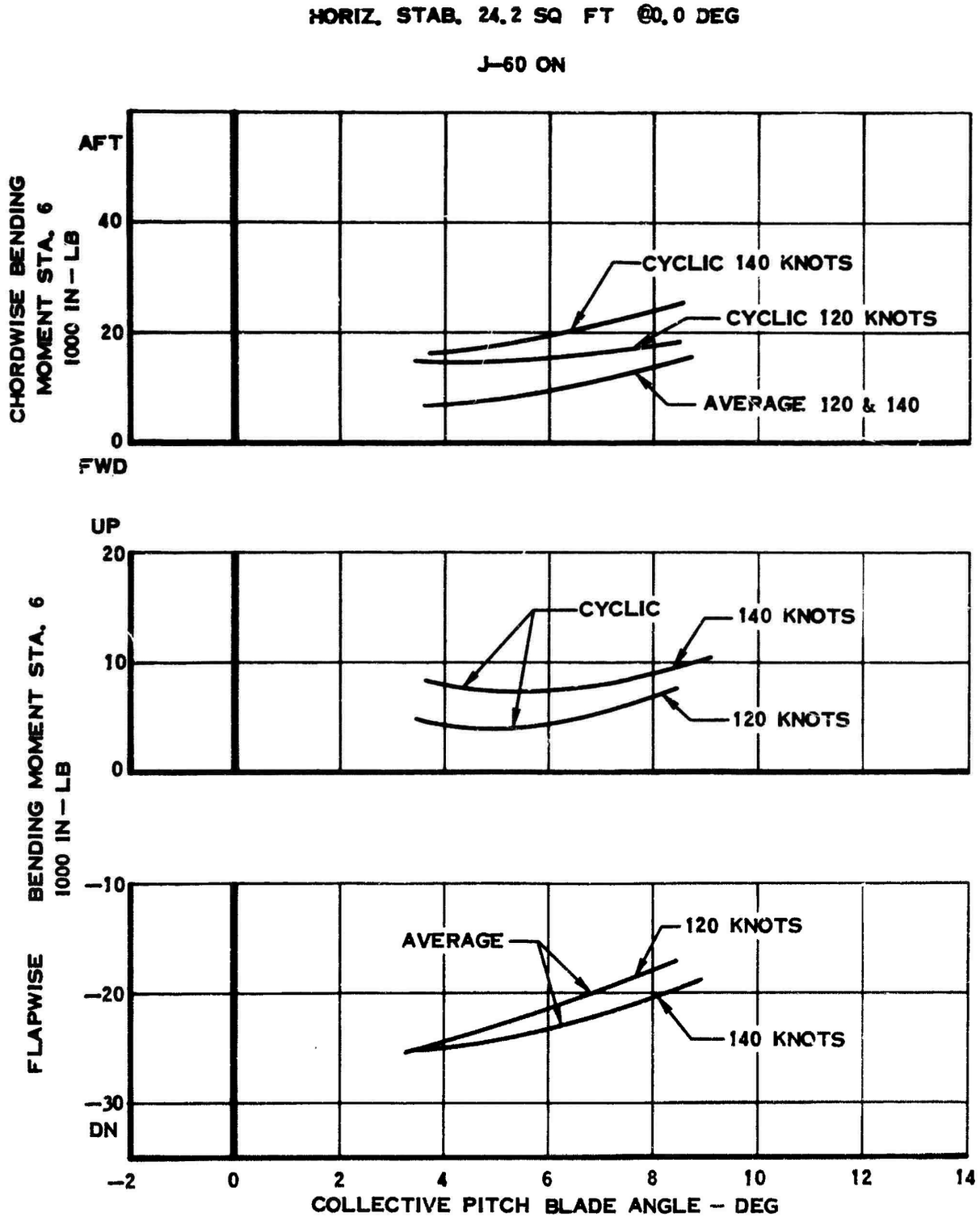

Figure 101. Main Rotor Loads Versus Collective Pitch Blade Angle - Compound Helicopter.

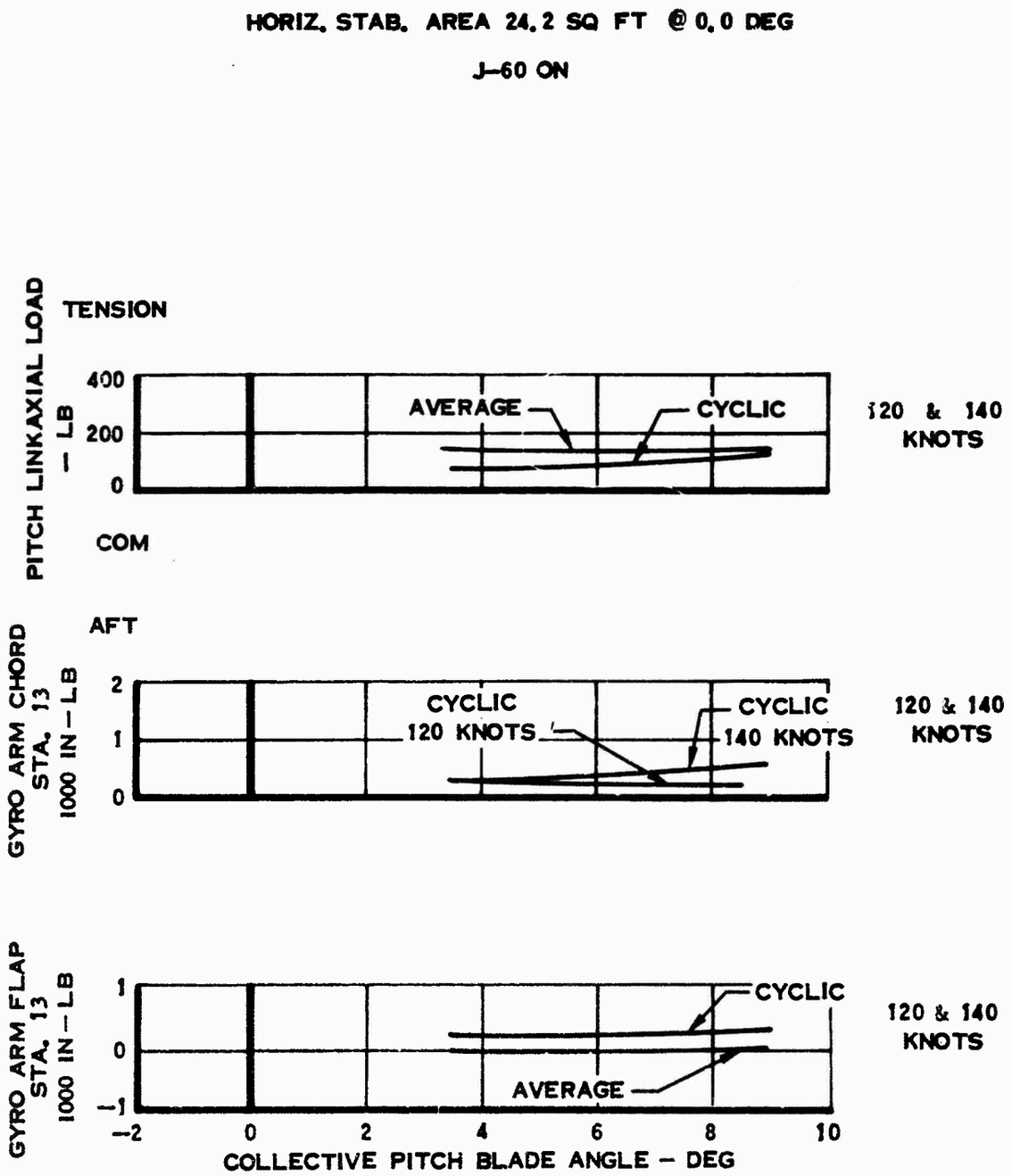

Figure 102. Load Versus Collective Pitch Blade Angle - Compound Helicopter.

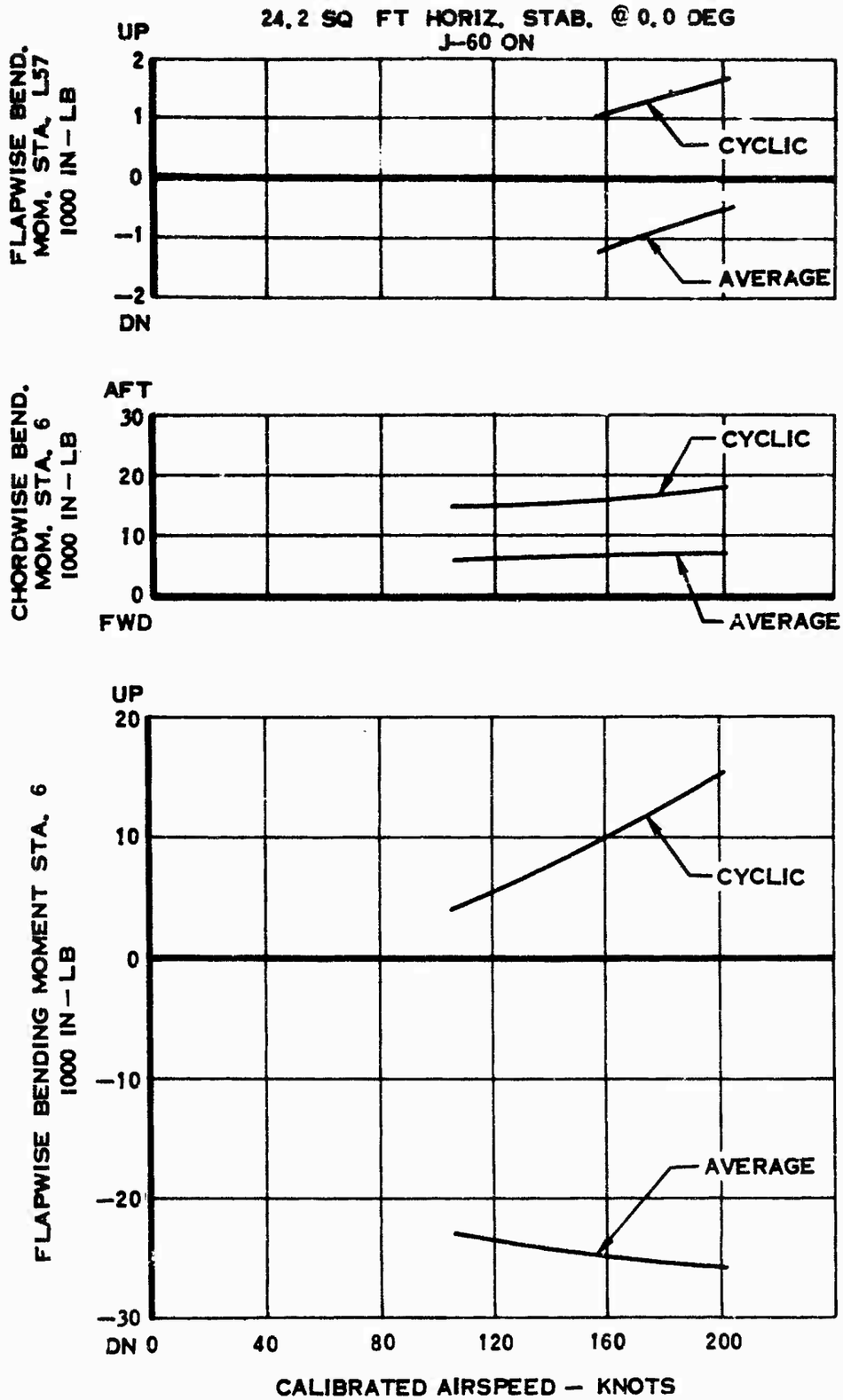

Figure 103. Main Rotor Loads Versus Calibrated Airspeed - Compound Helicopter.

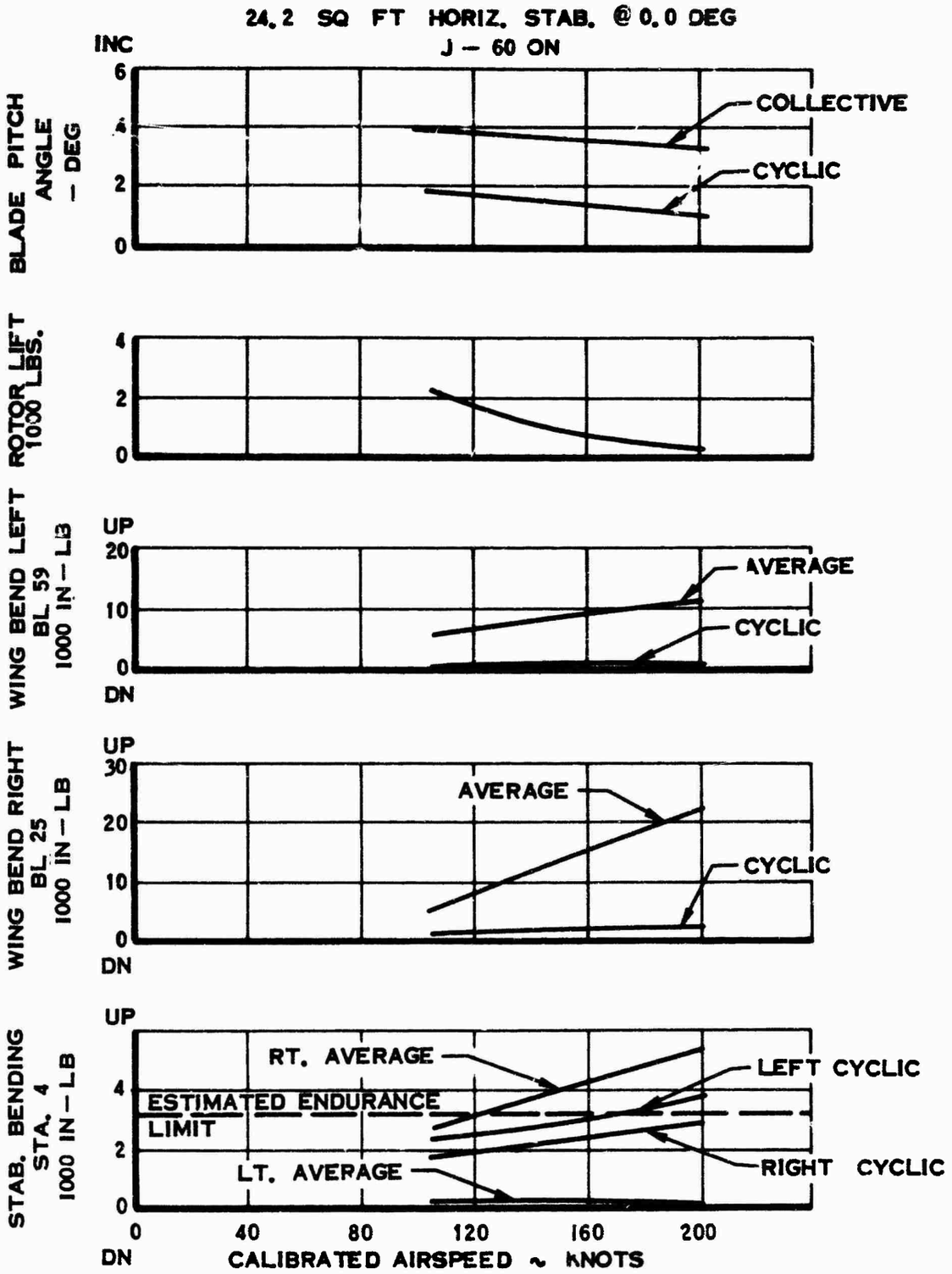

Figure 104. Main Rotor Loads Versus Calibrated Airspeed - Compound Helicopter.

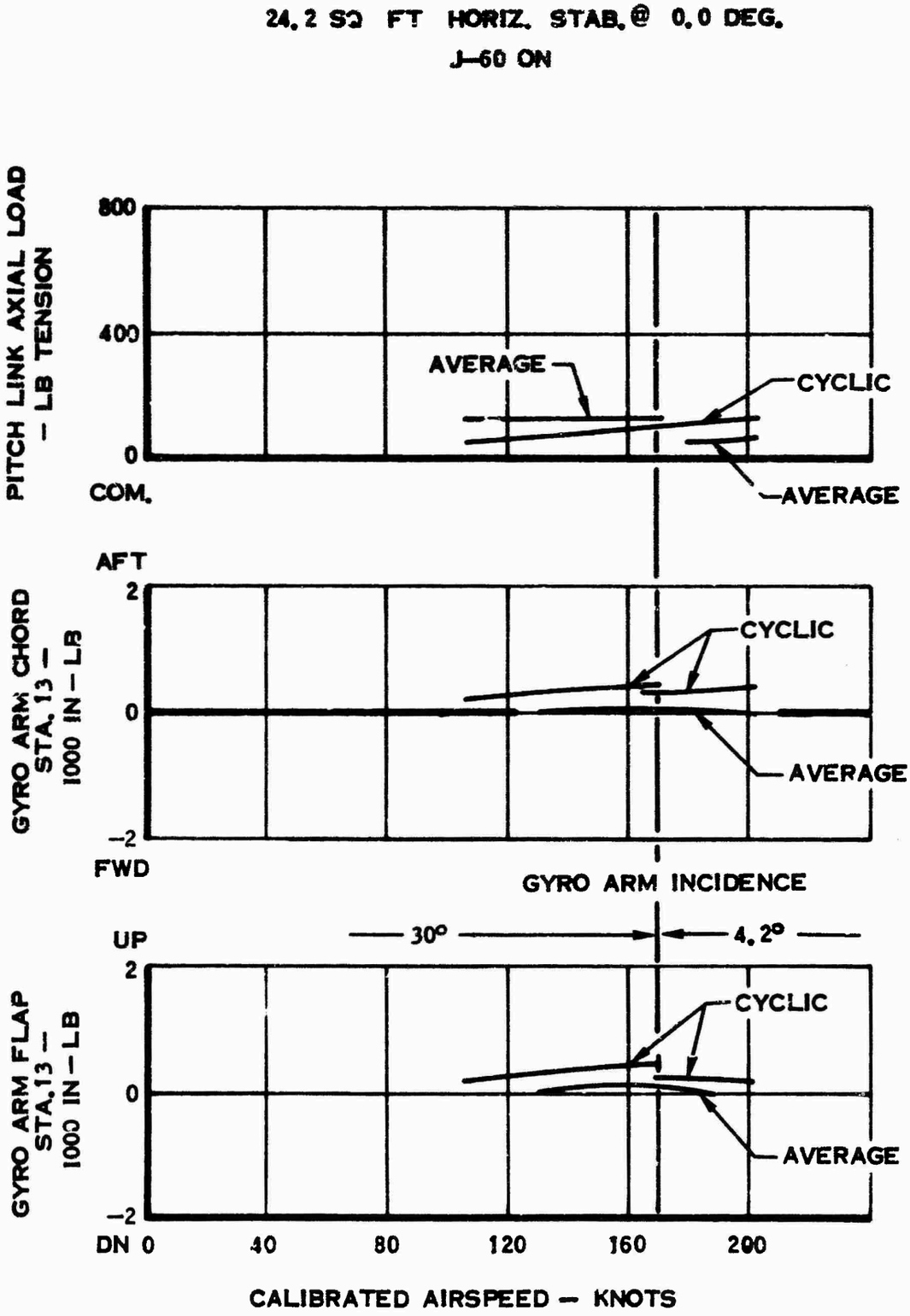

Figure 105. Load Versus Calibrated Airspeed - Compound Helicopter.

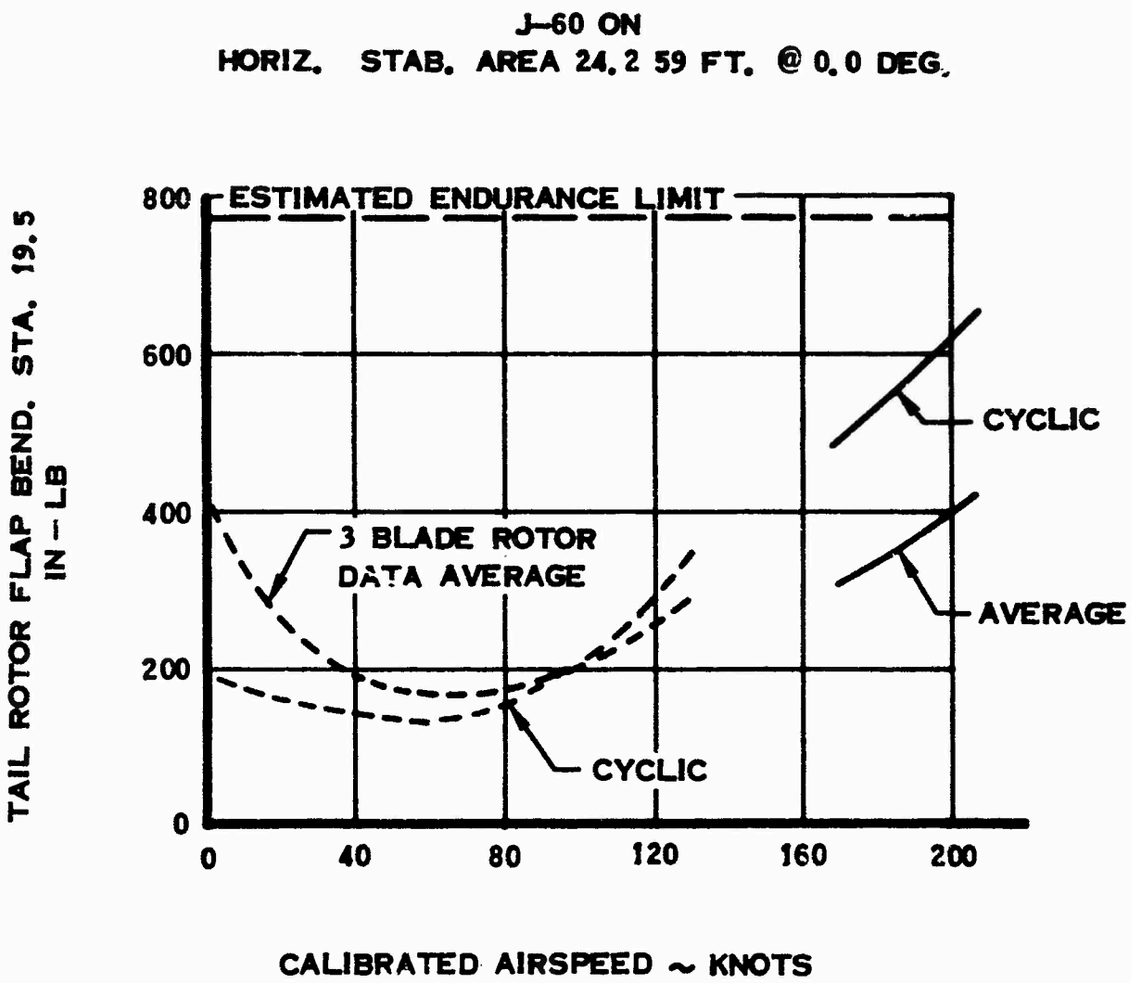

Figure 106. Tail Rotor Flap Bending Station 19.5 Versus Calibrated Airspeed - Compound Helicopter.

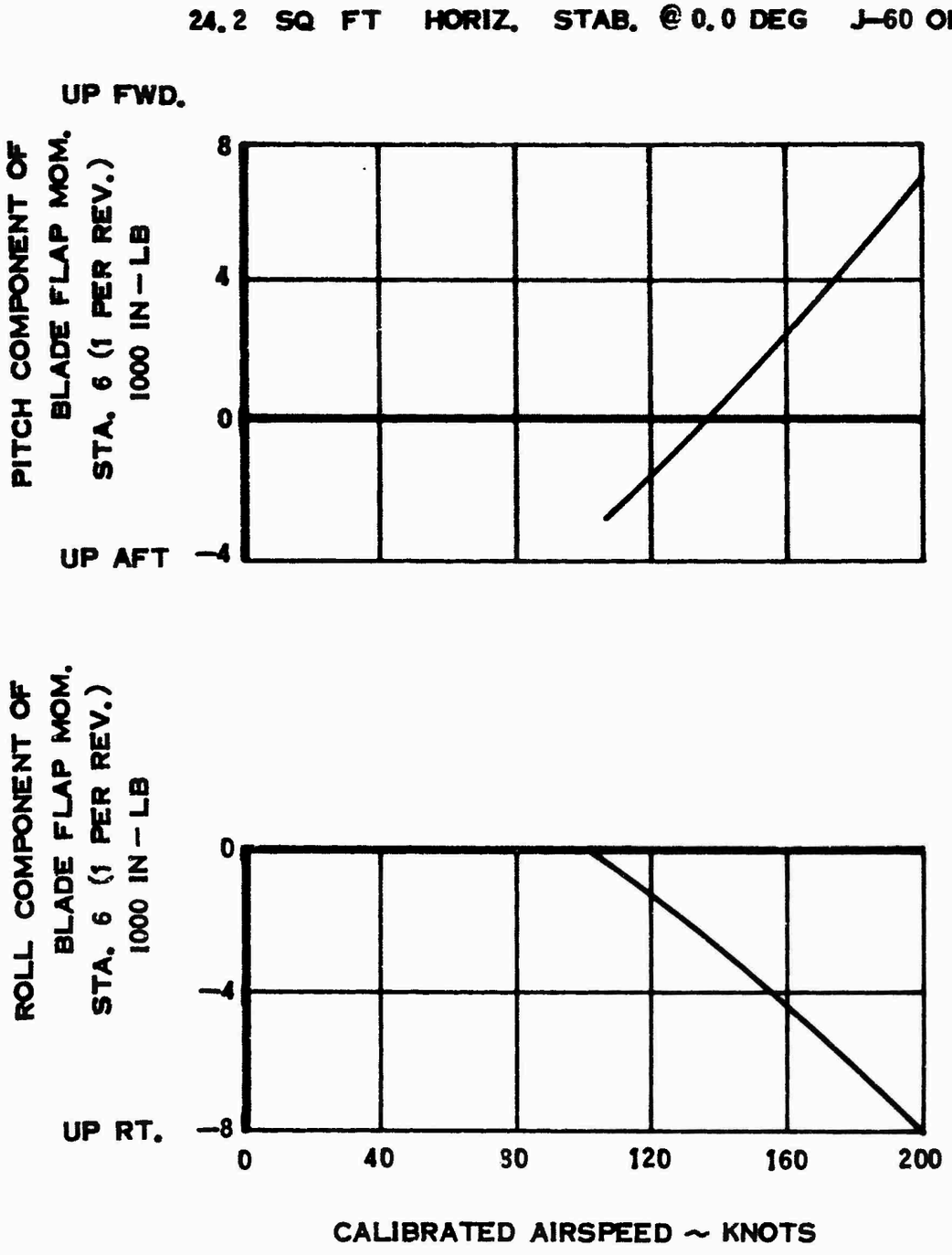

Figure 107. Roll and Pitch Component Versus Calibrated Airspeed - Compound Helicopter.

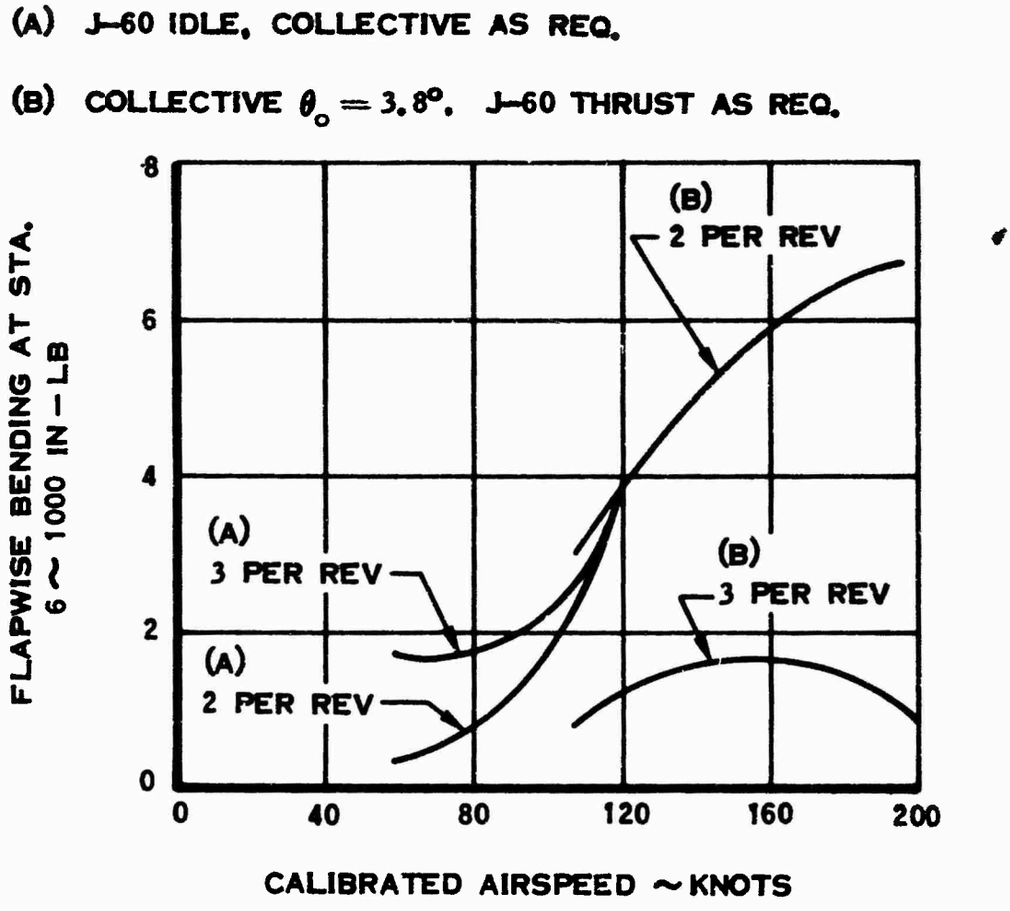

Figure 108. Flapwise Bending Versus Calibrated Airspeed, 2P and 3P Content - Compound Helicopter.

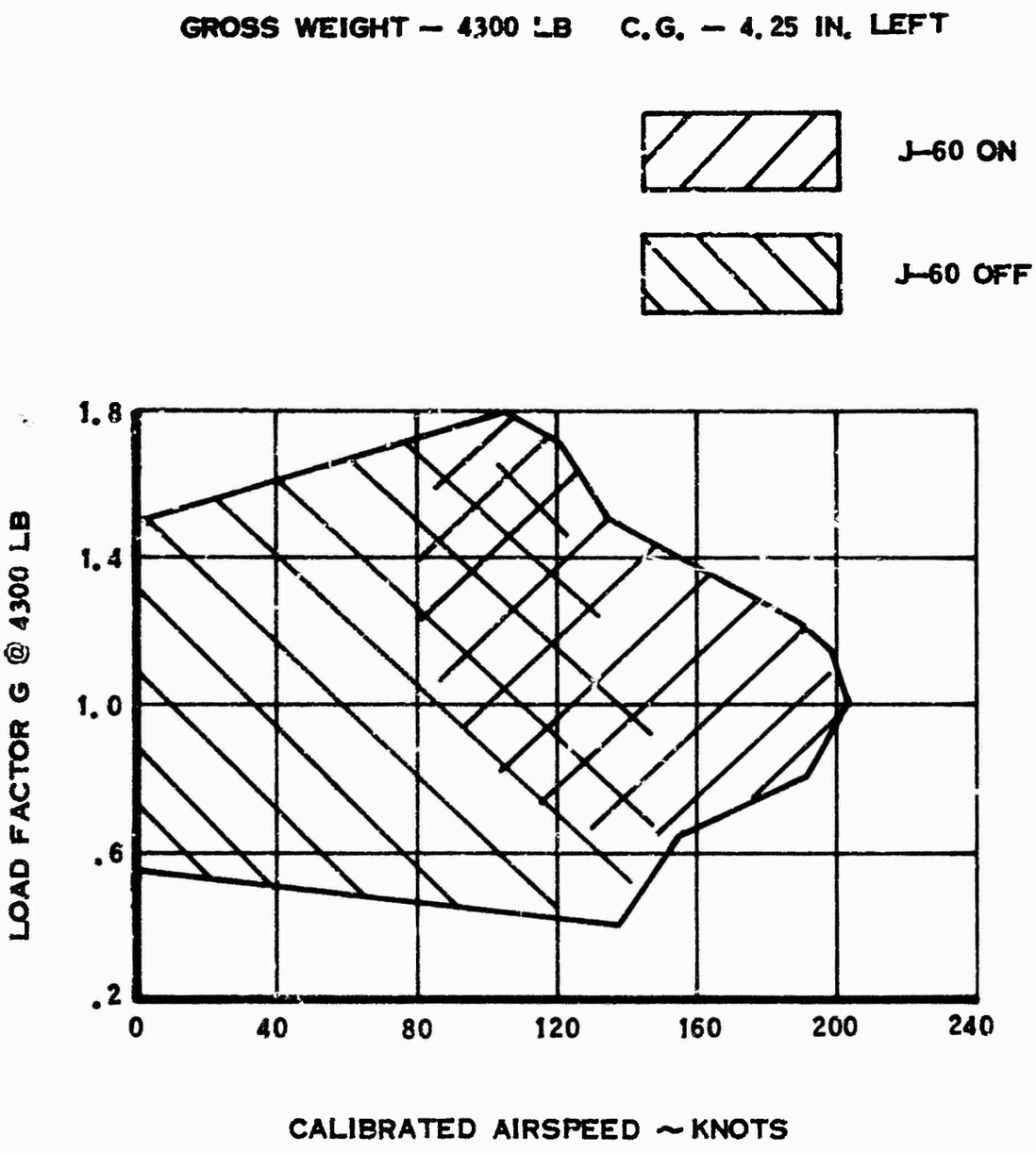

Figure 109. Maneuvering Envelope - Compound Helicopter.

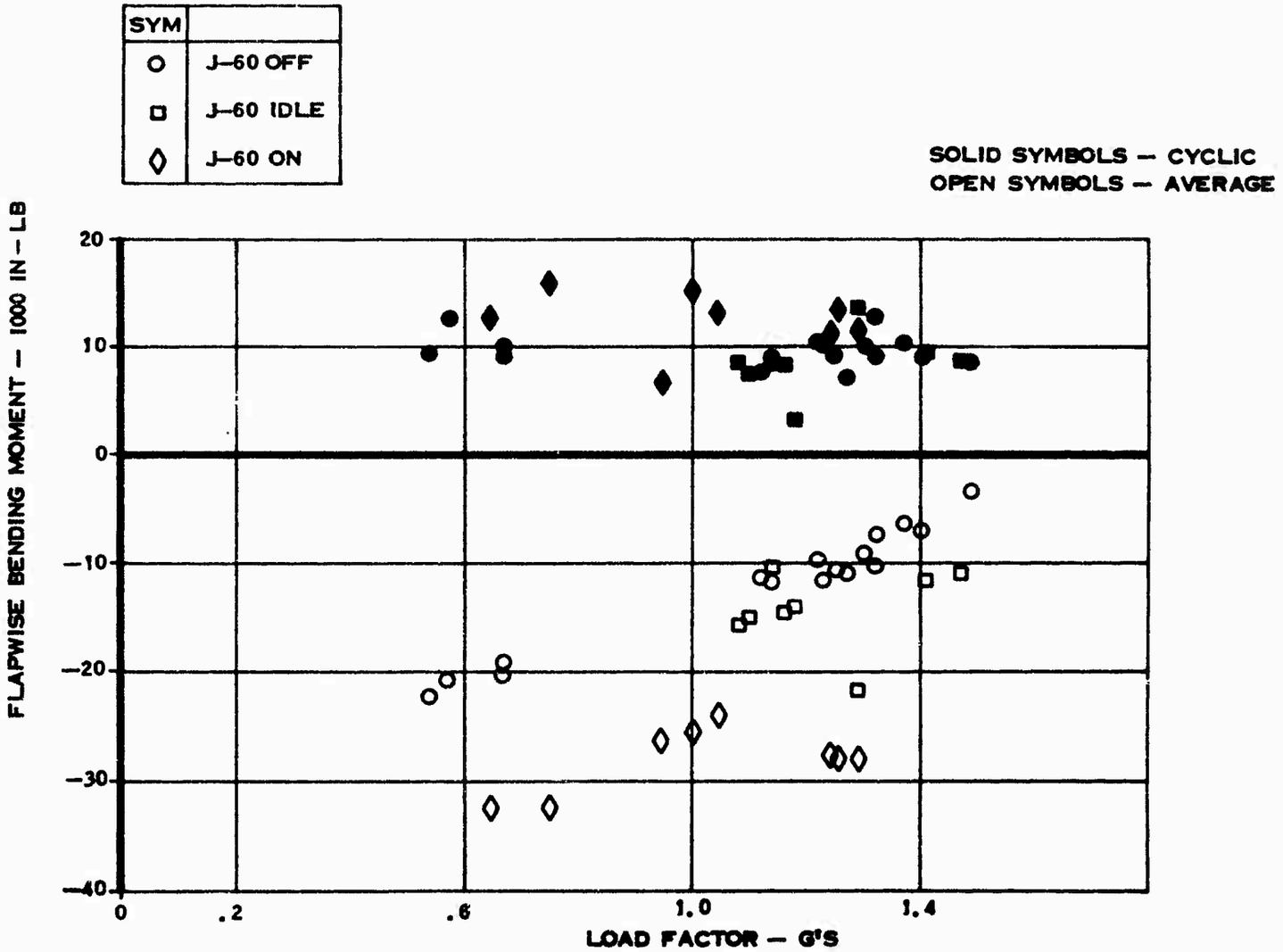

Figure 110. Main Rotor Flapwise Bending Moment at Station 6 Versus Load Factor - Compound Helicopter.

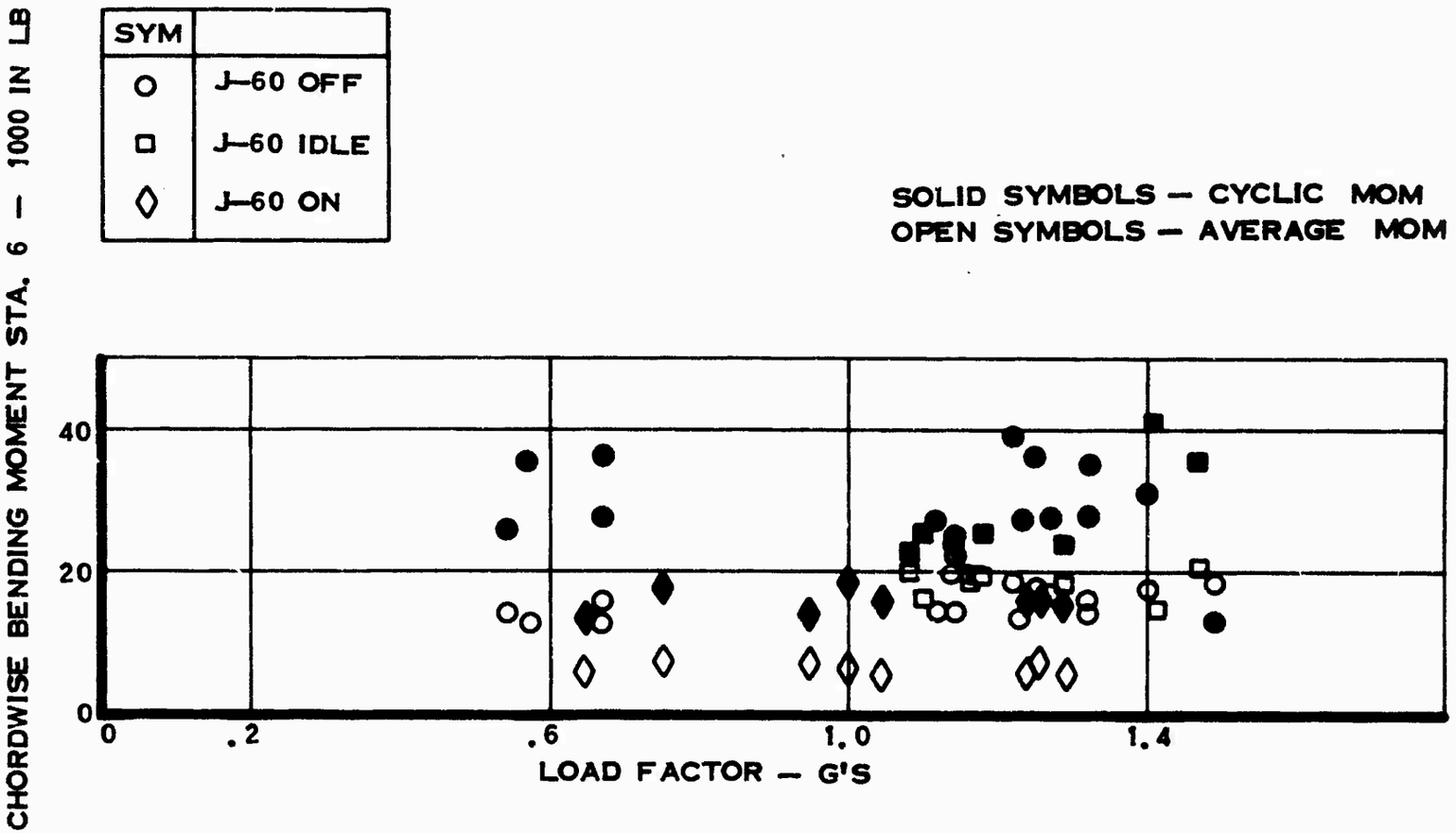

Figure 111. Main Rotor Chordwise Bending Moment at Station 6 Versus Load Factor - Compound Helicopter.

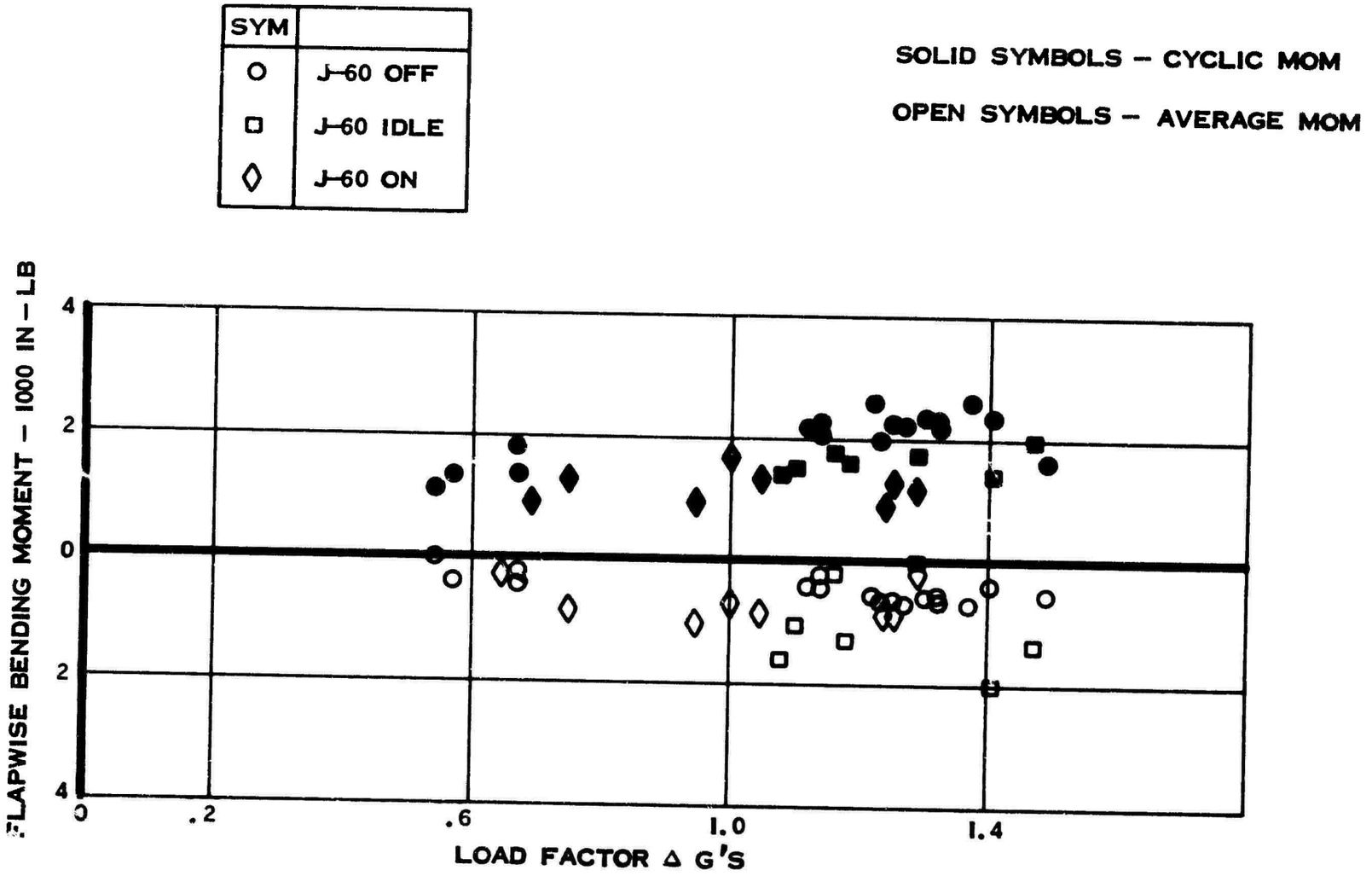

Figure 112. Main Rotor Flapwise Bending Moment at Station 157 Versus Load Factor - Compound Helicopter.

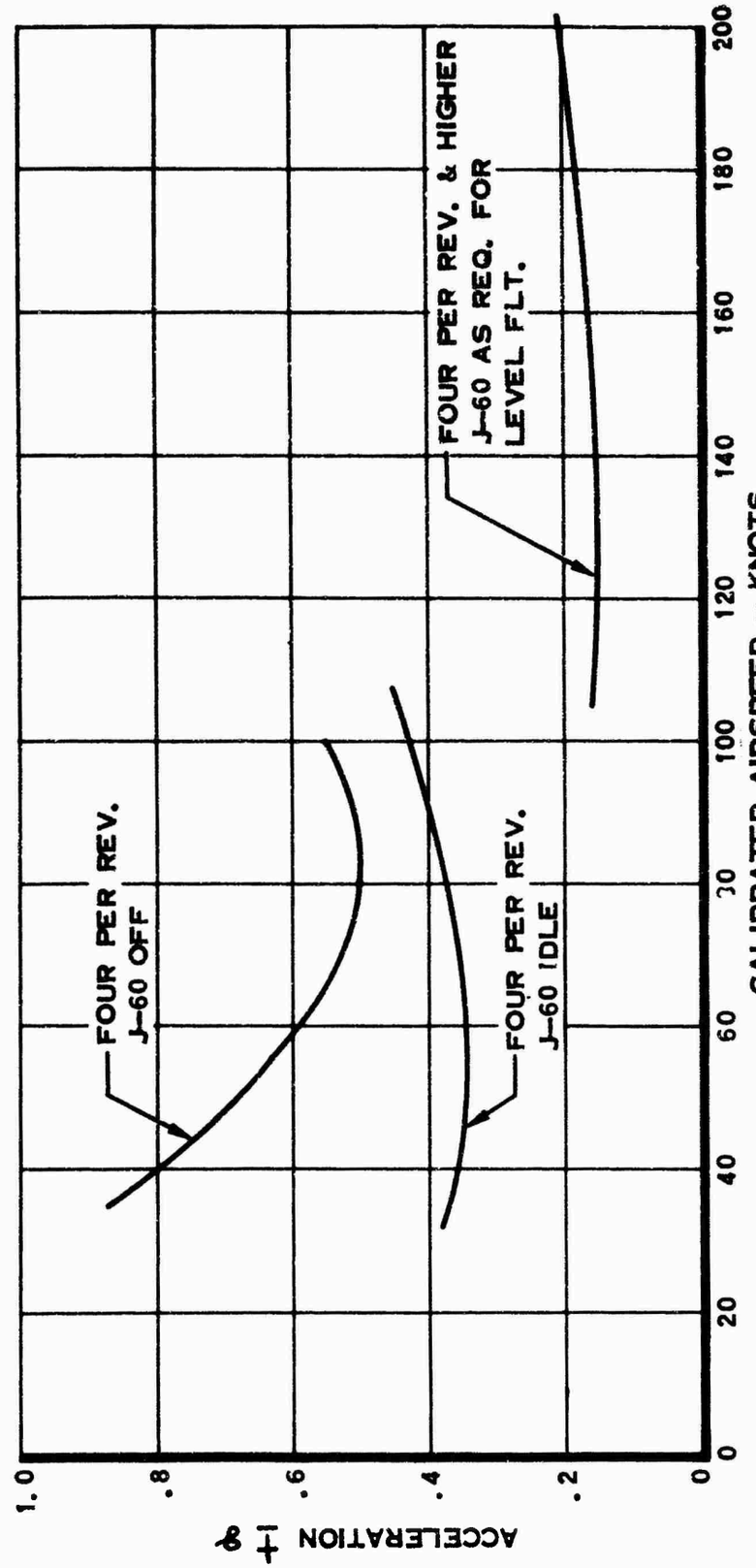

Figure 113. Cabin Vertical Vibration Versus Calibrated Airspeed - Compound Helicopter.

BIBLIOGRAPHY

Reference

1. Contract DA 44-177-AMC-150(T), Model XH-51A, Safety of Flight Procedures for Experimental Research Vehicles Operated by Contractor on Test Program, LAC/432579, 22 October 1964.

2. Structural Design Criteria and Loads for Modifications to the XH-51A Helicopter for the Compound Version, Lockheed Report 18066, 9 August 1964.

3. Structural Design Criteria and Loads - Part I, Structural Design Criteria, Lockheed Report 15992, 5 June 1962.

   Structural Design Criteria and Loads - Part II, Structural Design Loads, Lockheed Report 15992, 16 July 1962.

4. Structural Analysis of Modifications to the XH-51A Helicopter for the Compound Version, Lockheed Report 18067, 10 August 1964.

5. Fatigue Substantiation of XH-51A and XH-51A Compound for 150 Hours Flight, Lockheed Report 18309, 30 October 1964.

The following items were used in the preparation of this report but are not referenced in the text.

Fatigue Strength Summary of Lockheed Rigid Rotor, Lockheed Report 17984, 29 June 1964.

Spec. MIL-F-8785, Flying Qualities of Piloted Airplanes

Structural Analysis of the Four-Bladed Rotor on the XH-51A Helicopter, Lockheed Report 18011, 14 July 1964.

Contract DA 44-177-AMC-150(T), Model XH-51A Compound Configuration, LAC/425756, 22 May 1964.

Final Summary Report - Model XH-51A Rigid Rotor Helicopter Program (Preliminary Draft), Lockheed Report 17545, 3 February 1964.

MIL-S-8698, Structural Design Requirements, Helicopters (ASG).

Federal Aviation Administration Civil Aeronautics Manual 6, Rotorcraft Airworthiness Normal Category, June 1962.

North American Aviation Report NA-62-776, Nacelle Stress Analyses for T-39 Series

Pre-Military Research Evaluation Conference Report - Model XH-51A Rigid Rotor Helicopter, Lockheed Report 16933, 6 June 1963.

Contract No. DA-44-177-AMC-150(T), Model XH-51A Helicopter, Structural Test Plan for the Compound Helicopter Static Proof Tests, Lockheed Report 18021, 20 July 1964.

Ground Test Results on the XH-51A Compound Helicopter, Lockheed Report 18261, 7 October 1964.

Fatigue Tests of XH-51A and XH-51A Compound, Lockheed Report 18310, 30 October 1964.

Ground Vibration Tests - Model XH-51A High Speed Compound Four-Bladed Rigid Rotor System Helicopter, Lockheed Report 18182, 24 September 1964.

Results of Ground Tests on the XH-51A Four-Bladed Rigid Rotor System, Lockheed Report 18128, 29 August 1964.

Report of Progress on Model XH-51A Exploration of High Speed Flight for June 1964, Lockheed Report 17995, 8 July 1964.

Static Proof Test, Lockheed Report 18022, 24 August 1964.